DIVERSITÉ ET FONCTIONS DES PHAGOCYTES MONONUCLÉÉS DANS LES MALADIES CARDIOMÉTABOLIQUES.

Emmanuel Gautier

UNIVERSITE PIERRE ET MARIE CURIE – PARIS VI

Mémoire en vue de l'obtention de l'

HABILITATION A DIRIGER DES RECHERCHES

Présenté par

Emmanuel GAUTIER

DIVERSITE ET FONCTIONS DES PHAGOCYTES MONONUCLEES. DANS LES MALADIES CARDIOMETABOLIQUES.

Soutenue le 18 Février 2021

Jury :

Christophe Combadière	Président du jury
Giuseppina Caligiuri	Rapportrice
Thierry Tordjmann	Rapporteur
Bruno Fève	Examinateur
Julie Helft	Examinatrice

SOMMAIRE

A- CURRICULUM VITAE.

1 – Positions held.

Jan 2015 - …	INSERM - Researcher at INSERM UMR_S 1166, Pitié-Salpétrière Hospital in Paris, France.
Oct 2013 - Dec 2014	INSERM - Researcher at INSERM UMR_S 939, Pitié-Salpétrière Hospital in Paris, France.
Jan 2012 - Oct 2013	Research instructor. Washington University School of Medicine in St Louis, USA (Pr Gwendalyn J. Randolph).
Jan 2008 - Dec 2011	Post-doctoral fellow. Mount Sinai School of Medicine in New York, USA (Pr Gwendalyn J. Randolph).
Oct 2003 - Jan 2008	PhD fellow. INSERM U551, Pitié-Salpétrière Hospital in Paris (Dr Philippe Lesnik and Dr John Chapman).
Oct 2002 - Jul 2003	Master internship. INSERM U572, Lariboisière Hospital in Paris (Dr Jane-Lyse Samuel, Dr Catherine Chassagne).

2 – Education and training.

2003-2007	PhD in Cellular & Molecular Physiopathology, Pierre & Marie Curie University, Paris.
2003	Master's degree in Cellular & Molecular Physiopathology, Pierre & Marie Curie University, Paris.
2002	MSI in Cell Biology & Physiology (Molecular and Cellular Genetics), Rennes I University, Rennes.
1999-2001	BS in Cell Biology & Physiology, Rennes I University, Rennes.
1999-1997	University degree of technology in Biological Sciences, Rennes I University, Rennes.

3 – Prizes and honors.

2010 - 2012	Two-years post-doctoral fellowship from the American Heart Association (AHA, USA).
2009	Thesis prize from the French Society of Atherosclerosis (NSFA, France).
2007	One-year doctoral fellowship from the Medical Research Foundation (FRM, France).
2003 - 2007	Three-years doctoral Fellowship from the French Ministry of Education, Research and Technology (MERT funding).

4 – Publications (chronological order).

1. Gautier EL, Huby T, Ouzilleau B, Doucet C, Saint-Charles F, Gremy G, Chapman MJ, Lesnik P. Enhanced immune system activation and arterial inflammation accelerates atherosclerosis in lupus-prone mice. *Arterioscler Thromb Vasc Biol. 2007 Jul;27(7):1625-31. (IF 2007 = 7)*
2. Gautier EL, Huby T, Saint-Charles F, Ouzilleau B, Chapman MJ, Lesnik P. Enhanced dendritic cell survival attenuates lipopolysaccharide-induced immunosuppression and increases resistance to lethal endotoxic shock. *J Immunol. 2008 May 15;180(10):6941-6. (IF 2008 = 6)*

3. Gautier EL, Huby T, Witztum JL, Ouzilleau B, Miller ER, Saint-Charles F, Aucouturier P, Chapman MJ, Lesnik P. Macrophage apoptosis exerts divergent effects on

atherogenesis as a function of lesion stage. *Circulation. 2009 Apr 7;119(13):1795-804. (IF 2009 = 14.8)*

4. Gautier EL, Huby T, Saint-Charles F, Ouzilleau B, Pirault J, Deswaerte V, Ginhoux F, Miller ER, Witztum JL, Chapman MJ, Lesnik P. Conventionnal dendritic cells at the crossroads between immunity and cholesterol homeostasis in atherosclerosis. *Circulation, 2009 May 5;119(17):2367-75. (IF 2009 = 14.8)*

5. Gautier EL, Jakubzick C, Randolph GJ. Regulation of the migration and survival of monocyte subsets by chemokine receptors and its relevance to atherosclerosis. *Arterioscler Thromb Vasc Biol. 2009 Oct;29(10):1412-8. (IF 2009 = 7.2)*

6. Ingersoll MA, Spanbroek R, Lottaz C, Gautier EL, Frankenberger M, Hoffmann R, Lang R, Haniffa, M, Collin M, Tacke F, Habenicht AJR, Ziegler-Heitbrock, L, Randolph GJ. Comparison of gene expression profiles between human and mouse monocyte subsets. *Blood. 2010 Jan 21;115(3):e10-9. (IF 2010 = 10.6)*

7. Yvan-Charvet L[#], Pagler T[#], Gautier EL, Avagyan S, Siry RL, Han S, Welch CL, Wang N, Randolph GJ, Snoeck HW, Tall AR. ATP-Binding Cassette Transporters and HDL Suppress Hematopoietic Stem Cell Proliferation. *Science. 2010 Jun 25;328(5986):1689-93* (# Equal contributors). *(IF 2010 = 31.4)*

8. Feig JE, Pineda-Torra I, Sanson M, Bradley MN, Vengrenyuk Y, Bogunovic D, Gautier EL, Rubinstein D, Hong C, Liu J, Wu C, Van Rooijen N, Bhardwaj N, Garabedian MJ, Tontonoz P, Fisher EA. LXR promotes the maximal egress of monocyte-derived cells from mouse aortic plaques during atherosclerosis regression. *J Clin Invest. 2010;120(12):4415–4424. (IF 2010 = 14.2)*

9. Gautier EL and Yvan-Charvet L. HDL and its transporters ABCA1 and ABCG1 regulate innate immunity and hematopoietic stem cell proliferation. *Med Sci (Paris). 2011 Feb;27(1):9-11.*

10. Potteaux S, Gautier EL, Hutchison SB, van Rooijen N, Rader DJ, Randolph GJ. Suppressed monocyte recruitment accounts for macrophage removal from mouse atherosclerotic lesions during plaque stabilization. *J Clin Invest. 2011 May 2;121(5):2025-36. (IF 2011 = 13.1)*

11. Desch AN, Randolph GJ, Murphy K, Gautier EL, Kedl RL, Lahoud MH, Caminschi I, Shortman K, Henson PM, Jakubzick CV. CD103^{+} pulmonary dendritic cells preferentially acquire and present apoptotic cell–associated antigen. *J Exp Med. 2011. Aug 29;208(9):1789-97. (IF 2011 = 13.9)*

12. Shearn AI[#], Deswaerte V[#], Gautier EL, Saint-Charles F, Pirault J, Rucker EB, Beliard S, Chapman MJ, Jessup W, Huby T, Lesnik P. Bcl-x inactivation in macrophages accelerates progression of advanced atherosclerotic lesions in Apoe-/- mice. *Arterioscler Thromb Vasc Biol. 2012 May;32(5):1142-9* (# Equal contributors). *(IF 2012 = 6.3)*

13. Malhotra D, Fletcher AL, Astarita J, Lukacs-Kornek V, Tayalia P, Gonzalez SF, Elpek KG, Chang SK, Knoblich K, Hemler ME, Brenner MB, Carroll MC, Mooney DJ, Turley

SJ; the Immunological Genome Project Consortium, Zhou Y, Shinton SA, Hardy RR, Bezman NA, Sun JC, Kim CC, Lanier LL, Miller J, Brown B, Merad M, Fletcher AL, Elpek KG, Bellemare-Pelletier A, Malhotra D, Turley SJ, Narayan K, Sylvia K, Kang J, Gazit R, Garrison B, Rossi DJ, Jojic V, Koller D, Jianu R, Laidlaw D, Costello J, Collins J, Cohen N, Brennan P, Brenner MB, Shay T, Regev A, Kim F, Rao TN, Wagers A, Gautier EL, Jakubzick C, Randolph GJ, Monach P, Best AJ, Knell J, Goldrath A, Heng T, Kreslavsky T, Painter M, Mathis D, Benoist C. Transcriptional profiling of stroma from inflamed and resting lymph nodes defines immunological hallmarks. *Nat Immunol. 2012 Apr 1;13(5):499-510*. *(IF 2012 = 26.2)*

14. Narayan K, Sylvia KE, Malhotra N, Yin CC, Martens G, Vallerskog T, Kornfeld H, Xiong N, Cohen NR, Brenner MB, Berg LJ, Kang J; The Immunological Genome Project Consortium, Zhou Y, Shinton SA, Hardy RR, Bezman NA, Sun JC, Kim CC, Lanier LL, Miller J, Brown B, Merad M, Fletcher A, Elpek K, Bellemare-Pelletier A, Malhotra D, Turley S, Narayan K, Sylvia K, Kang J, Gazit R, Garrison B, Rossi DJ, Jojic V, Koller D, Jianu R, Laidlaw D, Costello J, Collins J, Cohen N, Brennan P, Brenner M, Shay T, Regev A, Kim F, Rao TN, Wagers A, Gautier EL, Jakubzick C, Randolph GJ, Monach P, Best AJ, Knell J, Goldrath A, Heng T, Kreslavsky T, Painter M, Mathis D, Benoist C. Intrathymic programming of effector fates in three molecularly distinct γδ T cell subtypes. *Nat Immunol. 2012 Apr 1;13(5):511-8*. *(IF 2012 = 26.2)*

15. Greter M, Helft J, Chow A, Hashimoto D, Mortha A, Agudo-Cantero J, Bogunovic M, Gautier EL, Miller J, Leboeuf M, Lu G, Aloman C, Brown BD, Pollard JW, Xiong H, Randolph GJ, Chipuk JE, Frenette PS, Merad M. GM-CSF controls nonlymphoid tissue dendritic cell homeostasis but Is dispensable for the differentiation of inflammatory dendritic cells. *Immunity. 2012 Jun 29;36(6):1031-46. (IF 2012 = 19.8)*

16. Miller JC, Brown BD, Shay T, Gautier EL, Jojic V, Cohain A, Pandey G, Leboeuf M, Elpek KG, Helft J, Hashimoto D, Chow A, Price J, Greter M, Bogunovic M, Bellemare-Pelletier A, Frenette PS, Randolph GJ, Turley SJ, Merad & the Immunological Genome Consortium. Deciphering the transcriptional network of the dendritic cell lineage. *Nat Immunol. 2012 Jul 15;13(9):888-899. (IF 2012 = 26.2)*

17. Gautier EL, Chow A, Spanbroek R, Marcelin G, Greter M, Jakubzick C, Bogunovic M, Leboeuf M, van Rooijen N, Habenicht AJ, Merad M, Randolph GJ. Systemic analysis of PPARγ in mouse macrophage populations reveals marked diversity in expression with critical roles in resolution of inflammation and airway immunity. *J Immunol. 2012 Sep 1;189(5):2614-24. (IF 2012 = 5.5)*

18. Gautier EL, Shay T, Miller J, Chow A, Davis S, Helft J, Greter M, Jakubzick C, Bogunovic M, Benoist C, Merad M, Randolph GJ; The Immunological Genome Project Consortium. Gene-expression profiles and transcriptional regulatory pathways that underlie the identity and diversity of mouse tissue macrophages. *Nat Immunol. 2012 Sep 30;13(11):1118-1128. (IF 2012 = 26.2)*

19. Cohen NR, Brennan PJ, Shay T, Watts GF, Brigl M, Kang J, Brenner MB; ImmGen Project Consortium, Monach P, Shinton SA, Hardy RR, Jianu R, Koller D, Collins J, Gazit R, Garrison BS, Rossi DJ, Narayan K, Sylvia K, Kang J, Fletcher A, Elpek K, Bellemare-Pelletier A, Malhotra D, Turley S, Best AJ, Knell J, Goldrath A, Jojic V, Koller D, Shay T,

Regev A, Cohen N, Brennan P, Brenner M, Kreslavsky T, Bezman NA, Sun JC, Kim CC, Lanier LL, Miller J, Brown B, Merad M, Gautier EL, Jakubzick C, Randolph GJ, Kim F, Rao TN, Wagers A, Heng T, Painter M, Ericson J, Davis S, Ergun A, Mingueneau M, Mathis D, Benoist C. Shared and distinct transcriptional programs underlie the hybrid nature of iNKT cells. *Nat Immunol. 2013 Jan;14(1):90-9. (IF 2013 = 25)*

20. Gautier EL, Westerterp M, Neha Bhagwat N, Cremers S, Shih A, Abdel-Wahab O, Lütjohann D, Randolph GJ, Levine RL, Tall AR, Yvan-Charvet L. HDL and Glut1 inhibition reverse a hypermetabolic state in mouse models of myeloproliferative disorders. *J Exp Med. 2013 Feb 11;210(2):339-53. (IF 2013 = 13.9)*

21. Best JA, Blair DA, Knell J, Yang E, Mayya V, Doedens A, Dustin ML, Goldrath AW; Immunological Genome Project Consortium, Monach P, Shinton SA, Hardy RR, Jianu R, Koller D, Collins J, Gazit R, Garrison BS, Rossi DJ, Narayan K, Sylvia K, Kang J, Fletcher A, Elpek K, Bellemare-Pelletier A, Malhotra D, Turley S, Best JA, Knell J, Goldrath AW, Jojic V, Koller D, Shay T, Regev A, Cohen N, Brennan P, Brenner M, Kreslavsky T, Bezman NA, Sun JC, Kim CC, Lanier LL, Miller J, Brown B, Merad M, Gautier EL, Jakubzick C, Randolph GJ, Kim F, Rao TN, Wagers A, Heng T, Painter M, Ericson J, Davis S, Ergun A, Mingueneau M, Mathis D, Benoist C. Transcriptional insights into the CD8(+) T cell response to infection and memory T cell formation. *Nat Immunol. 2013 Apr;14(4):404-12. (IF 2013 = 25)*

22. Martel C, Li WJ, Fulp B, Platt AM, Gautier EL, Westerterp M, Bittman R, Tall AR, Chen SH, Thomas MJ, Kreisel D, Swartz M, Sorci-Thomas M, Randolph GJ. Macrophage reverse cholesterol transport in mice relies on the lymphatic vasculature. *J Clin Invest. 2013 Apr 1;123(4):1571-9. (IF 2013 = 13.8)*

23. Malhotra N, Narayan K, Cho OH, Sylvia KE, Yin C, Melichar H, Rashighi M, Lefebvre V, Harris JE, Berg LJ, Kang J; Immunological Genome Project Consortium, Monach P, Shinton SA, Hardy RR, Jianu R, Koller D, Collins J, Gazit R, Garrison BS, Rossi DJ, Narayan K, Sylvia K, Kang J, Fletcher A, Elpek K, Bellemare-Pelletier A, Malhotra D, Turley S, Best JA, Knell J, Goldrath AW, Jojic V, Koller D, Shay T, Regev A, Cohen N, Brennan P, Brenner M, Kreslavsky T, Bezman NA, Sun JC, Kim CC, Lanier LL, Miller J, Brown B, Merad M, Gautier EL, Jakubzick C, Randolph GJ, Kim F, Rao TN, Wagers A, Heng T, Painter M, Ericson J, Davis S, Ergun A, Mingueneau M, Mathis D, Benoist C. A network of high-mobility group box transcription factors programs innate interleukin-17 production. *Immunity. 2013 Apr 18;38(4):681-93. (IF 2013 = 19.7)*

24. Randolph GJ, Gautier EL. Emerging roles of neural guidance molecules in atherosclerosis: sorting out the complexity. *Arterioscler Thromb Vasc Biol. 2013 May;33(5):882-3. (IF 2013 = 5.5)*

25. Jojic V, Shay T, Sylvia K, Zuk O, Sun X, Kang J, Regev A, Koller D; the Immunological Genome Project Consortium, Best AJ, Knell J, Goldrath A, Jojic V, Koller D, Shay T, Regev A, Cohen N, Brennan P, Brenner M, Kim F, Rao TN, Wagers A, Heng T, Ericson J, Rothamel K, Ortiz-Lopez A, Mathis D, Benoist C, Bezman NA, Sun JC, Min-Oo G, Kim CC, Lanier LL, Miller J, Brown B, Merad M, Gautier EL, Jakubzick C, Randolph GJ, Monach P, Blair DA, Dustin ML, Shinton SA, Hardy RR, Laidlaw D, Collins J, Gazit R, Rossi DJ, Malhotra N, Sylvia K, Kang J, Kreslavsky T, Fletcher A, Elpek K, Bellemare-Pelletier A,

Malhotra D, Turley S. Identification of transcriptional regulators in the mouse immune system. *Nat Immunol. 2013 Apr 28;14(6):633-643. (IF 2013 = 25)*

26. Mingueneau M, Kreslavsky T, Gray D, Heng T, Cruse R, Ericson J, Bendall S, Spitzer M, Nolan G, Kobayashi K, von Boehmer H, Mathis D, Benoist C; the Immunological Genome Consortium, Best AJ, Knell J, Goldrath A, Jojic V, Koller D, Shay T, Regev A, Cohen N, Brennan P, Brenner M, Kim F, Rao TN, Wagers A, Heng T, Ericson J, Rothamel K, Ortiz-Lopez A, Mathis D, Benoist C, Bezman NA, Sun JC, Min-Oo G, Kim CC, Lanier LL, Miller J, Brown B, Merad M, Gautier EL, Jakubzick C, Randolph GJ, Monach P, Blair DA, Dustin ML, Shinton SA, Hardy RR, Laidlaw D, Collins J, Gazit R, Rossi DJ, Malhotra N, Sylvia K, Kang J, Kreslavsky T, Fletcher A, Elpek K, Bellemare-Pelletier A, Malhotra D, Turley S. The transcriptional landscape of αβ T cell differentiation. *Nat Immunol. 2013 May 5;14(6):619-632. (IF 2013 = 25)*

27. Ergun A, Doran G, Costello JC, Paik HH, Collins JJ, Mathis D, Benoist C; ImmGen Consortium (Best AJ, Knell J, Goldrath A, Jojic V, Koller D, Shay T, Regev A, Cohen N, Brennan P, Brenner M, Kim F, Rao TN, Wagers A, Heng T, Ericson J, Rothamel K, Ortiz-Lopez A, Mathis D, Benoist C, Bezman NA, Sun JC, Min-Oo G, Kim CC, Lanier LL, Miller J, Brown B, Merad M, Gautier EL, Jakubzick C, Randolph GJ, Monach P, Blair DA, Dustin ML, Shinton SA, Hardy RR, Laidlaw D, Collins J, Gazit R, Rossi DJ, Malhotra N, Sylvia K, Kang J, Kreslavsky T, Fletcher A, Elpek K, Bellemare-Pelletier A, Malhotra D, Turley S). Differential splicing across immune system lineages. *Proc Natl Acad Sci U S A*. 2013 Aug 27;110(35):14324-9. *(IF 2013 = 9.8)*

28. Gautier EL, Ivanov S, Lesnik P, Randolph GJ. Local apoptosis mediates clearance of macrophages from resolving inflammation in mice. *Blood*. 2013 Oct 10;122(15):2714-2722*. (IF 2013 = 9.8)*

29. Jakubzick C, Gautier EL, Gibbings SL, Sojka DK, Schlitzer A, Johnson TE, Ivanov S, Duan Q, Bala S, Condon T, Van Rooijen N, Grainger JR, Belkaid Y, Ma'ayan A, Riches DWH, Yokoyama WM, Ginhoux F, Henson PM, Randolph GJ. Minimal differentiation of classical monocytes as they survey steady state tissues and transport antigen to lymph nodes. *Immunity.* 2013 Sep 19;39(3):599-610*. (IF 2013 = 19.7)*

30. Epelman S, Lavine KJ, Beaudin AE, Sojka DK, Carrero JA, Calderon B, Brija T, Gautier EL, Ivanov S, Satpathy AT, Schilling JD, Schwendener R, Sergin I, Razani B, Forsberg EC, Yokoyama WM, Unanue ER, Colonna M, Randolph GJ, Mann DL. Embryonic and Adult-Derived Resident Cardiac Macrophages Are Maintained through Distinct Mechanisms at Steady State and during Inflammation. *Immunity*. 2014 Jan 16;40(1):91-104. *(IF 2013 = 19.7)*

31. Gautier EL, Ivanov S, Williams JW, Huang SC, Marcelin G, Fairfax K, Wang PL, Francis JS, Leone P, Wilson DB, Artyomov MN, Pearce EJ, Randolph GJ. Gata6 regulates aspartoacylase expression in resident peritoneal macrophages and controls their survival. *J Exp Med*. 2014 Jul 28;211(8):1525-31. *(IF 2013 = 13.8)*

32. Nascimento M, Huang SC, Smith A, Everts B, Lam W, Bassity E, Gautier EL, Randolph GJ, Pearce EJ. Ly6Chi Monocyte Recruitment Is Responsible for Th2 Associated

Host-Protective Macrophage Accumulation in Liver Inflammation due to Schistosomiasis. *PLoS Pathog*. 2014 Aug 21;10(8):e1004282. *(IF 2013 = 8.1)*

33. Mostafavi S, Ortiz-Lopez A, Bogue MA, Hattori K, Pop C, Koller D, Mathis D, Benoist C; The Immunological Genome Consortium, Blair DA, Dustin ML, Shinton SA, Hardy RR, Shay T, Regev A, Cohen N, Brennan P, Brenner M, Kim F, Rao TN, Wagers A, Heng T, Ericson J, Rothamel K, Ortiz-Lopez A, Mathis D, Benoist C, Kreslavsky T, Fletcher A, Elpek K, Bellemare-Pelletier A, Malhotra D, Turley S, Miller J, Brown B, Merad M, Gautier EL, Jakubzick C, Randolph GJ, Monach P, Best AJ, Knell J, Goldrath A, Jojic V, Koller D, Laidlaw D, Collins J, Gazit R, Rossi DJ, Malhotra N, Sylvia K, Kang J, Bezman NA, Sun JC, Min-Oo G, Kim CC, Lanier LL. Variation and Genetic Control of Gene Expression in Primary Immunocytes across Inbred Mouse Strains. *J Immunol*. 2014 Nov 1;193(9):4485-96. *(IF 2013 = 5.4)*

34. Ericson JA, Duffau P, Yasuda K, Ortiz-Lopez A, Rothamel K, Rifkin IR, Monach PA; ImmGen Consortium, Best AJ, Knell J, Goldrath A, Jojic V, Koller D, Shay T, Regev A, Cohen N, Brennan P, Brenner M, Kim F, Rao TN, Wagers A, Heng T, Ericson J, Rothamel K, Ortiz-Lopez A, Mathis D, Benoist C, Bezman NA, Sun JC, Min-Oo G, Kim CC, Lanier LL, Miller J, Brown B, Merad M, Gautier EL, Jakubzick C, Randolph GJ, Monach P, Blair DA, Dustin ML, Shinton SA, Hardy RR, Laidlaw D, Collins J, Gazit R, Rossi DJ, Malhotra N, Sylvia K, Kang J, Kreslavsky T, Fletcher A, Elpek K, Bellemare-Pelletier A, Malhotra D, Turley S. Gene expression during the generation and activation of mouse neutrophils: implication of novel functional and regulatory pathways. PLoS One. 2014 Oct 3;9(10):e108553. *(IF 2013 = 3.5)*

35. Gautier EL, Yvan-Charvet L. Understanding macrophage diversity at the ontogenic and transcriptomic levels. *Immunol Rev*. 2014. Nov;262(1):85-95. *(IF 2013 = 12.9)*

36. Bouchareychas L, Pirault J, Saint-Charles F, Deswaerte V, Le Roy T, Jessup W, Giral P, Le Goff W, Huby T, Gautier EL*, Lesnik P*. (*co-senior author). Promoting macrophage survival delays progression of established atherosclerotic lesions through macrophage-derived apoE. *Cardiovasc Res.* 2015 Oct 1;108(1):111-23. (*IF 2015 = 5.9*)

37. Sarrazy V, Sore S, Viaud M, Rignol G, Westerterp M, Ceppo F, Tanti JF, Guinamard R, Gautier EL, Yvan-Charvet L. Maintenance of macrophage redox status by ChREBP limits inflammation and apoptosis and protects against advanced atherosclerotic lesion formation. *Cell Rep.* 2015 Oct 6;13(1):132-44. *(IF 2015 = 7.9)*

38. Tussiwand R, Gautier EL. Transcriptional Regulation of Mononuclear Phagocyte Development. *Front Immunol*. 2015 Oct 19;6:533. *(IF 2015 = 3.4)*

39. Sarrazy V*, Viaud M*, Westerterp M, Ivanov S, Giorgetti-Peraldi S, Guinamard R, Gautier EL, Thorp EB, De Vivo DC, Yvan-Charvet L. Disruption of Glut1 in Hematopoietic Stem Cells Prevents Myelopoiesis and Enhanced Glucose Flux in Atheromatous Plaques of ApoE-/- Mice. Transcriptional Regulation of Mononuclear Phagocyte Development. *Circ Res*. 2016. Apr 1;118(7):1062-77. (* Equal contributors). *(IF 2016 = 11.6)*

40. Ivanov S, Scallan JP, Kim KW, Werth K, Johnson MW, Saunders BT, Wang PL, Kuan EL, Straub AC, Ouhachi M, Weinstein EG, Williams JW, Briseño C, Colonna M, Isakson BE, Gautier EL, Förster R, Davis MJ, Zinselmeyer BH, Randolph GJ. CCR7 and IRF4-dependent dendritic cells regulate lymphatic collecting vessel permeability. *J Clin Invest*. 2016 Apr 1;126(4):1581-91. *(IF 2016 = 12.6)*

41. Kim KW, Williams JW, Wang YT, Ivanov S, Gilfillan S, Colonna M, Virgin HW, Gautier EL, Gwendalyn J. Randolph GJ. MHC II^+ resident peritoneal and pleural macrophages rely on IRF4 for development from circulating monocytes. *J Exp Med*. 2016 Sep 19;213(10):1951-9. *(IF 2016 = 12)*

42. Buttgereit A, Lelios I, Yu X, Vrohlings M, Krakoski NR, Gautier EL, Nishinakamura R, Becher B, Greter M. Sall1 is a transcriptional regulator defining microglia identity and function. *Nat Immunol*. 2016 Dec;17(12):1397-1406. *(IF 2016 = 21.5)*

43. Menezes S, Melandri D, Anselmi G, Perchet T, Loschko J, Dubrot J, Patel R, Gautier EL, Hugues S, Longhi MP, Henry JY, Quezada SA, Lauvau G, Lennon-Dumenil AM, Gutierrez-Martinez E, Bessis A, Gomez-Perdiguero E, Jacome-Galarza CE, Garner H, Geissmann F, Golub R, Nussenzweig MC, Guermonprez P. The heterogeneity of Ly6Chi monocytes controls their differentiation into iNOS+ macrophages or monocyte-derived dendritic cells. *Immunity*. 2017 Dec 20;45(6):1205-1218. *(IF 2016 = 22.8)*

44. Calippe B*, Augustin S*, Beguier F, Messance HC, Poupel L, Conart JB, Hu S, Lavalette S, Fauvet A, Rayes J, Levy O, Raoul W, Fitting C, Denèfle T, Pickering MC, Harris C, Jorieux S, Sullivan PM, Sahel JA, Karoyan P, Paques M, Sapieha P, Guillonneau X, Gautier EL, Sennlaub F. Complement factor H inhibits CD47-mediated resolution of inflammation. *Immunity*. 2017 Feb 21;46(2):261-272. *(IF 2016 = 22.8)*

45. Marcelin M, Ferreirra A, Liu Y, Atlan M, Aron-Wisnewsky J, Pelloux V, Botbol Y, Ambrosini M, Fradet M, Rouault C, Hénégar C, Mutel S, Hulot JS, Poitou C, Torcivia A, Nail Barthelemy R, Bichet JC, Gautier EL, Clement K. PDGFR□-mediated switch to $CD9^{high}$ progenitors controls fibrotic adipose tissue alteration in obesity. *Cell Metab*. 2017 Mar 7;25(3):673-685. *(IF 2016 = 18.2)*

46. Westerterp M, Gautier EL, Ganda A, Molusky MM, Wang W, Fotakis P, Wang N, Randolph GJ, D'Agati VD, Yvan-Charvet L, Tall AR. Cholesterol Accumulation in Dendritic Cells Links the Inflammasome to Acquired Immunity. *Cell Metab*. 2017 Jun 6;25(6):1294-1304. *(IF 2016 = 18.2)*

5 – Meeting presentations.

Invited speaker

2015 49th Annual Scientific Meeting of the European Society for Clinical Investigation (ESCI). Cluj-Napoca, Romania.

2014 European Association for Vision and Eye Research (EVER) Congress. Nice, France.

2014 Physiology, Pharmacology and Therapeutics (P2T) Congress. Poitiers, France.

2013 New York Academy of Sciences Symposia "Harnessing New Players in Atherosclerosis to Treat Heart Disease". New York, USA.
2012 European Atherosclerosis Society Congress, Milan, Italy.

Selected oral and poster presentations

2013 Keystone Symposia. Myeloid Cells: Regulation and Inflammation. Keystone, USA. Poster presentation.
2012 Arteriosclerosis, Thrombosis and Vascular Biology Annual Conference, Chicago, USA. Poster presentation.
2011 Gordon Research Conference on Atherosclerosis. Newport, USA. Poster presentation.
2010 Keystone symposia joint meeting "Advances in Molecular Mechanisms of Atherosclerosis / The Macrophage: Intersection of Pathogenic and Protective Inflammation". Banff, Canada. Poster presentation.
2009 Gordon Research Conference on Atherosclerosis. Tilton, USA. Poster presentation.
2009 Arteriosclerosis, Thrombosis and Vascular Biology Conference, Washington, USA. Poster presentation.
2008 European Atherosclerosis Society Congress, Istanbul, Turkey. Selected oral communication.
2007 French Atherosclerosis Society Congress, Biarritz, France. Selected oral communication.
2007 European Atherosclerosis Society Congress, Helsinki, Finland. Selected oral communication.
2007 Arteriosclerosis, Thrombosis and Vascular Biology Conference, Chicago, USA. Selected oral communication.
2006 European Congress of Immunology, Paris, France. Selected oral communication.
2006 French Atherosclerosis Society Congress, Biarritz, France. Poster presentation.
2006 International Symposium on Atherosclerosis, Rome, Italy. Selected oral communication.

6 - Funding.

- Agence Nationale pour la Recherche (ANR, JCJC), Projet TARGETKC "Maintenance and role of Kupffer cells in steatohepatitis" (2018-2022) as a project leader.
- Agence Nationale pour la Recherche (ANR, PRC), Projet CAPTOR "Controlling fate determination of Adipose tissue-derived Progenitors to improve obesity- related metabolic disorders." (2018-2022) as a partner (leader: Karine Clément).
- Agence Nationale pour la Recherche (ANR, PRC), Projet MACLEAR "Mononuclear phagocyte clearance in immune- and non-immune-privileged sites" (2015-2019) as a partner (leader: Florian Sennlaub).
- Fondation de France, Projet "Rôles des cellules dendritiques CD11b+ dans le développement de la plaque d'athérome et la réponse à la vaccination athéroprotectrice" (2015-2018)
- Agence Nationale pour la Recherche (ANR, PRC), Projet LIPOCAMD "LIPA as a promising target to fight cardiometabolic diseases" (2014-2018) as a partner (leader: Laurent Yvan-Charvet).

- Nouvelle Société Française d'Athérosclérose (NSFA) : one-year PhD fellowship (2015)

7 – Training and supervision.

Oct 2017 - … Supervision of a PhD Student (Adélaïde Gélineau). INSERM UMR_S 1166, Paris, France. Adélaïde Gélineau is working under my supervision on the the gut/liver axis and how Kupffer cells are involved in its regulation. She obtained a fellowship from the French government.

May 2017 – June 2017 A master 1 student (Charlene Delmas) worked under my supervision on the role of macrophages in atherosclerosis.

Jan 2017 – July 2017 A Master 2 student (Eva Hernandez Rodriguez) worked under my supervision on how dietary fat impacts on the intestinal immune system.

Jan 2016 – July 2016 A Master 2 student (Alexandra Cousin) worked on the impact of dietary cholesterol on T lymphocytes activation in mouse models of atherosclerosis. She is now working as an ARC (Attaché de Recherche Clinique) trainee at the Gustave Roussy Hospital (Villejuif)

Nov 2015 - … Supervision of a PhD Student (Sophie Tran). INSERM UMR_S 1166, Paris, France. Sophie Tran is working under my supervision on the maintenance of liver macrophages (Kupffer cells) and the physiopathological role they play in the context of metabolic diseases (obesity and steatohepatitis). Her salary is covered by the ANR grant MACLEAR.

Jan 2015 – July 2015 A Master 2 student (Sophie Tran) worked under my supervision on developing new mouse models allowing for the specific depletion of liver macrophages.

Jan 2015 - … Supervision of a PhD Student (Melissa Ouhachi). INSERM UMR_S 1166, Paris, France. Melissa Ouhachi is working under my supervision on the role of CD11b+ dendritic cells in the physiopathology of atherosclerosis and diet-induced obesity. Her salary is covered by the ANR grant LIPOCAMD, the Fondation de France "Programme Maladies Cardiovasculaires" as well as a 1-year fellowship we obtained from the Nouvelle Société Française d'Athérosclérose (NSFA).

Jan 2014 – July 2014 A Master 2 student (Melissa Ouhachi) worked under my supervision on the role of CD11c+ dendritic cells in atherosclerosis.

Jan 2014 – July 2014 A Master 2 student (Thi Bich Hong Nguyen) worked under my supervision on defining macrophages subsets and their origin in adipose tissue during obesity.

Oct 2013 - Oct 2014 Co-supervisor of a PhD student (Laura Bouchareychas). INSERM UMR_S 1166, Paris, France. Laura Bouchareychas worked on the impact of macrophage lifespan on atherosclerotic plaque stabilization and the regulation of plasma cholesterol levels in conditions of atherosclerosis regression. I was her co-supervisor and as such I am co-senior author on the article she published during a thesis

(article number 36 in the list presented above). She is now doing a post-doctoral fellowship in Iannis Adamopoulos laboratory at UC Davis (Sacramento, USA).

B- EXPOSE DES TRAVAUX DE THESE ET DU STAGE POST-DOCTORAL.

1 - Thèse de Doctorat.

a - Présentation générale.

Mes travaux de thèse (2004 - 2008) ont porté sur l'impact de l'apoptose des macrophages sur le statut inflammatoire, le développement et la progression de la plaque d'athérome ; le rôle des cellules dendritiques dans le processus d'athérogénèse ainsi que l'impact de l'auto-immunité sur la progression de la plaque d'athérome. Parallèlement, j'ai également développé un projet qui avait pour objectif de déterminer l'impact de la survie des cellules dendritiques sur la résistance au choc endotoxique. Ces travaux, détaillés ci-dessous, ont donné lieu à la publication de 5 articles scientifiques dans des revues internationales à comité de lecture ainsi qu'à diverses présentations orales ou affichées dans des congrès nationaux et internationaux, ainsi qu'à un prix de thèse par la Nouvelle Société Française d'Athérosclérose (NSFA).

b - Descriptif des travaux de thèse.

Dans cette section, les projets associés à une publication en premier auteur dans une revue internationale à comité de lecture seront décris dans l'ordre chronologique de publication. Ces travaux seront présentés séparément du fait de la diversité des thèmes abordés.

Projet #1 : Impact de l'auto-immunité sur la progression des plaques d'athérome.

Publication issue du projet. Enhanced immune system activation and arterial inflammation accelerates atherosclerosis in lupus-prone mice. Gautier EL et *al. Arterioscler Thromb Vasc Biol. 2007*. (Article disponible en annexe).

Contexte scientifique, méthodologie et résultats obtenus. Les patients atteints de lupus érythémateux présentent un risque cardiovasculaire dramatiquement accru associé à une prévalence accrue de plaques d'athérome[1]. Toutefois, les mécanismes sous-jacents sont méconnus. Dans ce cadre, j'ai développé un modèle de souris auto-immunes susceptibles au développement de l'athérosclérose afin d'évaluer l'impact de l'auto-immunité sur la progression de la plaque d'athérome et les mécanismes

impliqués. Nous avons utilisé le modèle de souris mutante *gld* qui développe une maladie lymphoproliferative de type auto-immune dont les caractéristiques sont semblables au tableau clinique des patients atteints de lupus. L'auto-immunité a été transférée dans des souris Ldl-$r^{-/-}$ susceptibles à l'athérosclérose en utilisant une approche de transplantation de moelle osseuse. Nos résultats ont montré que :

- Le développement des plaques d'athérome est accéléré chez les souris auto-immunes.
- Les taux plasmatiques de cholestérol ne sont pas modifiés par l'auto-immunité dans notre modèle.
- Le système immunitaire est suractivé chez les souris auto-immunes : élévation des taux d'anticorps dirigés contre les LDL modifiées (activation des lymphocytes B) et augmentation du nombre de lymphocytes T (LTs) $CD4^+$ activés.
- Les plaques d'athérome de souris auto-immunes présentent un profil inflammatoire exacerbé dû à une plus forte accumulation de cellules apoptotiques, de LTs $CD4^+$ et de Mϕ.

Contribution à l'avancée des connaissances. Ce travail a permis de montrer que les aspects immuno-inflammatoires liés au lupus pouvaient expliquer à eux seuls (indépendamment d'une dyslipidémie) l'accélération de la progression des plaques d'athérome dans un modèle murin d'athérosclérose accélérée due au lupus. Ces données suggèrent que dans un cadre préventif, contrôler les aspects inflammatoires s'avère aussi important que traiter la dyslipidémie afin de faire diminuer leur risque cardiovasculaire des patients atteints de lupus.

Projet #2 : Impact de la survie des cellules dendritiques sur la résistance au choc endotoxique.

***Publication issue du projet*.** Enhanced dendritic cell survival attenuates lipopolysaccharide-induced immunosuppression and increases resistance to lethal endotoxic shock. Gautier EL et *al. J Immunol. 2008*. (Article disponible en annexe).

Contexte scientifique, méthodologie et résultats obtenus. Le nombre de cellules dendritiques (CDs) est diminué au cours de la septicémie et du choc endotoxique[2], induisant un état d'immunodépression. De plus, après un choc septique, la production d'IL-12 par les CDs, une cytokine impliquée dans l'initiation des réponses immunitaires de type Th1, est fortement diminuée[3]. Dans ce cadre, Il a été proposé que l'immunodépression due à la mort cellulaire des leucocytes impliqués dans l'initiation

(CDs) et le maintien (LTs et LBs) des réponses immunitaires serait délétère pour la résistance au choc septique ou endotoxique. Nous nous sommes donc attachés à déterminer l'impact de la survie des CDs sur l'immunodépression due à un choc endotoxique non-létal ainsi que sur la mortalité suite au choc endotoxique létal. Afin de répondre à cette question, nous avons développé une lignée de souris transgénique surexprimant la protéine anti-apoptotique Bcl-2 sous le contrôle d'un promoteur court du gène CD11c ciblant les CDs (souris CD11c-Bcl2) et nous avons étudié la réponse de ces souris à l'immunodépression consécutive à l'injection d'une dose sous-létale de lipopolysaccharides (LPS). Ensuite, nous avons mesuré la survie de ces souris en réponse à une dose létale de LPS. Cette étude a démontré que :

- Les souris CD11c-Bcl2 naïves présentent une accumulation de CDs dans la rate qui est associée à une augmentation du nombre de LTs activés.
- La déplétion des CDs de la rate, suite à une injection non-létale de LPS, est atténuée chez les souris CD11c-Bcl2 et s'accompagne d'une augmentation de l'expression de cytokines immuno-stimulatrices (IL-12p40, IL23p19, IL-15), une meilleure activation des LTs (polarisés vers la voie Th1) et des LBs.
- Les souris CD11c-Bcl2 ont une meilleure survie en réponse à une dose létale de LPS.

Contribution à l'avancée des connaissances. Nos données montrent que les CDs, acteur central de l'immunité, sont une cible privilégiée au cours du choc endotoxique. En effet, le choc endotoxique altère la fonction des CDs ce qui explique au moins en partie l'immunodépression qui lui est associée. Notre étude suggère que l'augmentation de la survie des CDs pourrait représenter une cible thérapeutique dans le cadre du choc septique.

Projet #3 : Impact de la mort par apoptose des macrophages lésionnels sur le statut inflammatoire, le développement et la progression de la plaque d'athérome.

***Publication issue du projet*.** Macrophage apoptosis exerts divergent effects on atherogenesis as a function of lesion stage. Gautier EL et *al*. *Circulation. 2009*. (Article disponible en annexe).

Contexte scientifique, méthodologie et résultats obtenus. Le macrophage (Mϕ) est le type cellulaire le plus touché par l'apoptose au sein de la plaque d'athérome. Toutefois, bien que l'élimination des cellules apoptotiques est connue pour jouer un rôle anti-

inflammatoire dans l'athérosclérose, peu de données permettaient jusqu'ici d'incriminer la mort par apoptose du Mϕ comme un événement pouvant moduler la progression des lésions. Afin de moduler de manière spécifique l'apoptose du Mϕ et d'en étudier l'impact sur la progression des lésions, nous avons créé un modèle de souris transgénique surexprimant la protéine anti-apoptotique Bcl-2 sous le contrôle du promoteur macrophagique CD68 (CD68-hBcl-2). Cette nouvelle lignée transgénique a été croisée en fond ApoE$^{-/-}$. Par ailleurs, nous avons utilisé la lignée transgénique CD11c-DTR (expression du récepteur à la toxine diphtérique, normalement absent chez la souris, sous le contrôle du promoteur CD11c), que nous avons croisé en fond ApoE$^{-/-}$. L'injection de toxine diphtérique à ces souris permet d'induire l'apoptose de Mϕ/cellules dendritiques au sein de la plaque d'athérome et d'étudier ainsi la réponse à l'induction de l'apoptose au sein des lésions d'athérome. Nos travaux ont montré que :

- L'apoptose du Mϕ est pro-athérogène dans les phases précoces et anti-athérogène dans les phases avancées de développement des plaques.
- L'induction de l'apoptose dans les plaques d'athérome favorise l'accumulation de débris cellulaires du fait de leur mauvaise élimination, augmente le statut inflammatoire de la plaque d'athérome et favorise le recrutement des monocytes circulants.

Contribution à l'avancée des connaissances. Ces travaux ont montré pour la première fois que l'impact de l'apoptose des Mϕ lésionnels sur le développement de l'athérosclérose dépend du stade de développement de la plaque. Nous montrons un rôle protecteur de l'apoptose des macrophages sur le développement des plaques dans les stades précoces de l'athérogénèse. A l'inverse, lorsque les plaques atteignent un stade avancé l'apoptose des macrophages s'avère délétère. Notre étude révèle également que l'accumulation de corps apoptotiques dans les lésions augmente l'inflammation et favorise le recrutement des monocytes circulants. Ce travail peut servir de base au développement de stratégies thérapeutiques visant à bloquer l'apoptose dans les plaques avancées de manière à diminuer l'état inflammatoire de la plaque, ralentir sa progression et les complications associées (rupture, thrombose,…).

Projet #4 : Rôle des cellules dendritiques dans le processus d'athérogénèse.

***Publication issue du projet*.** Conventional dendritic cells at the crossroads between immunity and cholesterol homeostasis in atherosclerosis. Gautier EL et *al*. *Circulation. 2009*. (Article disponible en annexe).

Contexte scientifique, méthodologie et résultats obtenus. Les cellules dendritiques (CDs) sont des cellules présentatrices d'antigènes spécialisées dans l'initiation des réponses immunitaires. Elles ont la capacité d'activer les lymphocytes T naïfs et de les polariser selon les voies d'activation Th1, Th2 ou Th17. Par ailleurs, les CDs jouent un rôle dans l'établissement de la tolérance périphérique. De par son rôle de régulateur central des réponses immunitaires, les CDs pourraient jouer un rôle majeur dans le développement de la plaque d'athérome, processus dépendant de mécanismes immuno-inflammatoires. Cependant, aucune étude n'avait jusqu'ici permis de positionner les CDs comme un acteur clé de l'athérosclérose. Nous avons donc cherché à moduler la demi-vie des CDs, permettant ainsi d'augmenter leur nombre et leur capacité à induire des réponses immunitaires, afin d'évaluer leur rôle dans le développement de l'athérosclérose. Afin de répondre à cette question, nous avons utilisé la lignée de souris transgénique CD11c-Bcl2 (présentée ci-dessus, Projet #2) qui a été croisée avec des souris susceptibles au développement de l'athérosclérose (Ldl-r $^{-/-}$, ApoE $^{-/-}$). Ce travail a montré que l'augmentation de la demi-vie de la CD est associée :

- À une augmentation du nombre de CDs dans les organes lymphoïdes.
- À une élévation des niveaux d'expression de cytokines impliquées dans la stimulation des LTs, se traduisant par une augmentation de LTs activés polarisés suivant les voies Th1 et Th17.
- À une élévation des taux d'anticorps dirigés contre les lipoprotéines modifiées de type IgG2c (indicatif d'une réponse humorale de type Th1).
- À une baisse du taux plasmatique de cholestérol, contrebalançant l'hyperactivation du système immunitaire d'où l'absence d'effet net sur la taille des plaques.

Contribution à l'avancée des connaissances. Ce travail, qui pour la première fois dans le domaine de l'athérosclérose, cible de manière spécifique les CDs, a permis d'établir que la CD joue un rôle central dans la modulation des réponses immunitaires pro-athérogènes ainsi que dans la régulation du taux plasmatique de cholestérol.

2 - Stage post-doctoral.

a - Présentation générale.

Afin d'acquérir une plus grande expertise en immunologie, j'ai effectué mon stage post-doctoral au sein du laboratoire du Dr Gwendalyn J. Randolph, reconnue dans le domaine de la migration et la fonction des phagocytes mononucléés (monocytes, Mϕ et

CDs). Mes travaux ont porté sur la diversité et la fonction des phagocytes mononucléés dans des modèles expérimentaux d'inflammation aiguë et chronique.

b - Descriptif des travaux de post-doctorat.

La majeure partie des projets de recherches réalisés au cours de mon stage post-doctoral, bien que se regroupant autour du thème commun du macrophage, touchent à différents aspects de cette cellule clé de l'immunité. Aussi, chaque projet sera décrit séparément afin de pouvoir clairement poser le contexte et établir les objectifs de chacun des projets. De plus, seuls les principaux projets seront présentés.

Projet #1: Spécificité de l'expression de PPARγ au sein de certaines populations de macrophages: impact sur l'homéostasie tissulaire, la résolution de l'inflammation et la réponse à l'infection.

Publication issue du projet. Systemic analysis of PPARγ in mouse macrophage populations reveals marked diversity in expression with critical roles in resolution of inflammation and airway immunity. Gautier EL et *al. J Immunol. 2012*. (Article disponible en annexe).

Contexte scientifique, méthodologie et résultats obtenus. Le récepteur nucléaire PPARγ est connu pour ses propriétés anti-inflammatoires au sein du Mϕ et l'utilisation d'agonistes de PPARγ comme approche thérapeutique dans les maladies inflammatoires est envisagée. Cependant, de nombreuses questions restent en suspens concernant le rôle de PPARγ au sein du Mϕ *in vivo*, comme la nature des populations de Mϕ exprimant PPARγ *in vivo*, ou comment l'expression de PPARγ au sein du Mϕ participe à l'homéostasie tissulaire, l'initiation et la résolution de l'inflammation. Enfin, le rôle de PPARγ au sein du Mϕ dans la réponse à l'infection est méconnu. Afin de répondre à ces questions, nous avons tout d'abord établi le profil d'expression de PPARγ parmi de nombreuses populations de Mϕ, puis nous avons étudié les souris déficientes en PPARγ dans les Mϕ (LysM-cre x PPARγ$^{fl/fl}$). Les tissus d'intérêt ont été étudiés à l'état basal et dans des modèles d'inflammation résolutive (péritonite induite par injection de thioglycollate) et d'infection des poumons (pneumocoque). Ce travail a permis de mieux comprendre comment l'expression de PPARγ par des populations spécifiques de Mϕ régule l'homéostasie tissulaire, la résolution de l'inflammation ainsi que la réponse à l'infection par pneumocoque. Nous montrons ainsi *in vivo* que :

- PPARγ est exprimé dans les Mϕ résidents des poumons et de la rate, mais est absent dans les Mϕ résidents du péritoine, du cerveau, de l'intestin et du cerveau, dans les monocytes Ly-6C$^+$, les neutrophiles et les CDs.
- Les Mϕ pulmonaires déficients en PPARγ accumulent des lipides intracellulaires et présentent des changements profonds de leur transcriptome.
- La délétion de PPARγ dans les Mϕ résidents des poumons induit un état inflammatoire chronique mais modéré alors que sa délétion dans les Mϕ de la rate est sans effet à l'état basal.
- La réponse à l'infection par pneumocoque est altérée dans les souris LysM-cre x PPARγ$^{fl/fl}$ du fait d'une moindre capacité des Mϕ déficients en PPARγ à éliminer l'agent pathogène.
- PPARγ est induit lors de la différentiation des monocytes Ly-6C$^+$ en Mϕ inflammatoires, et sa délétion au sein de ces Mϕ limite la résolution de la réponse inflammatoire sans modifier son initiation.

Contribution à l'avancée des connaissances. Ces données permettent une meilleure compréhension du rôle de PPARγ au sein du Mϕ dans l'homéostasie des tissues dont les Mϕ expriment PPARγ, la résolution de l'inflammation et la réponse à l'infection. Ce travail suggère que les agonistes de PPARγ pourraient être utilisé afin de favoriser la résolution de pathologies inflammatoires chroniques ainsi que les infections pulmonaires.

Projet #2 : Analyse de la diversité des macrophages résidents et établissement d'une signature macrophagique universelle.

***Publication issue du projet*.** Gene expression profiles and transcriptional regulatory pathways underlying tissue macrophage identity and diversity. Gautier EL et al. *Nat immunol* 2012. (Article disponible en annexe).

Contexte scientifique, méthodologie et résultats obtenus. Les Mϕ et les CDs sont des phagocytes parfois difficiles à identifier du fait de leurs nombreuses ressemblances (marqueurs de surface communs comme CD11c, MHC-II, etc …). De plus, alors que la diversité phénotypique et fonctionnelle des CDs a été énormément documentée ces dernières années, la diversité des populations de Mϕ *in vivo* est méconnue. En prenant part au projet « Immunological Genome » qui a consisté à trier par cytométrie et

analyser par micro-array des centaines de populations de cellules immunitaires, nous avons apporté un certain nombre de réponses à ces questions. En tandem avec le groupe de Miriam Merad à Mount Sinai (New York), nous avons trié par cytométrie des dizaines de populations de CDs et de Mϕ. Les données ont été traitées en utilisant des méthodes d'analyses classiques ainsi que des outils bioinformatiques permettant de générer des modules de gènes co-régulés et de déterminer les facteurs de transcription régulant ces modules. Notre analyse a permis de :

- Mettre en valeur la grande hétérogénéité des populations de Mϕ tissulaires par comparaison à l'hétérogénéité observée entre les sous-populations de CDs.
- Déterminer une signature de gènes spécifiques pour chaque population de Mϕ étudiée.
- Établir une signature macrophagique globale par comparaison au CDs.

Contribution à l'avancée des connaissances. Pour la première fois nous montrons que les Mϕ tissulaires sont d'une grande hétérogénéité. Nous avons aussi pu mettre en valeur une signature spécifique pour chaque population de Mϕ étudiée ainsi que les fonctions associées à ces gènes. Ces données permettent de mieux comprendre l'adaptation des Mϕ résidents à leur environnement et leurs spécialisations fonctionnelles. Nous avons également pu déterminer une signature macrophagique globale par comparaison au CDs ainsi que l'identification de nouveaux facteurs de transcription pouvant jouer un rôle dans le développement et/ou la fonction des Mϕ.

Projet #3: Rôle des cellules myéloïdes dans l'homéostasie du glucose et la cachexie du tissu adipeux dans les maladies myéloproliferatives.

Publication issue du projet. Gautier EL et al. Neha Bhagwat N, Cremers S, Shih A, Abdel-Wahab O, Lütjohann D, Randolph GJ, Levine RL, Tall AR and Yvan-Charvet L. Glucose consumption in proliferating and inflammatory myeloid cells contributes to adipose loss in myeloproliferative disorders. *J Exp Med. 2012.* (Article disponible en annexe).

Contexte scientifique, méthodologie et résultats obtenus. La perte de masse au niveau musculaire ainsi que du tissu adipeux est associée aux syndromes néoplasiques. Toutefois, très peu de données permettent de comprendre dans quelle mesure survient la perte de masse adipeuse, alors que la perte de muscle est plus documentée. En partant de l'observation que les souris déficientes en ABCA1 et ABCG1 (récepteurs au HDL) dans les leucocytes présentent un syndrome myéloprolifératif et une atrophie marquée du tissu adipeux, nous avons cherché à déterminer les mécanismes sous-jacents. Nous

avons montré que les cellules en prolifération s'adaptent de manière à capter plus efficacement le glucose environnant afin de l'utiliser comme substrat nécessaire à leur division. De plus, les cellules myéloïdes infiltrées dans le tissu adipeux produisent des médiateurs inflammatoires qui induisent une insulino-resistance locale, limitant la capacité du tissue adipeux à capter le glucose circulant. Ces 2 phénomènes, en détournant l'utilisation du glucose par le tissu adipeux, sont à l'origine de son atrophie. Mécanistiquement, nous montrons que la myéloprolifération et l'inflammation dépendent du glucose transporteur Glut1 qui permet l'entrée de glucose dans les cellules fournissant ainsi l'énergie nécessaire à la prolifération et à la synthèse de cytokine inflammatoires. L'inhibition de Glut1 par shRNA bloque ainsi la myéloprolifération et l'atrophie du tissu adipeux. Nous montrons enfin que les HDL restaurent ces défauts dans des modèles de leucémie. L'inhibition de Glut1 et les HDL pourraient être des voies thérapeutiques de choix dans le traitement des syndromes prolifératifs.

Contribution à l'avancée des connaissances. Pour la première fois, ces travaux suggèrent comment les cellules en prolifération s'adaptent et modifient leur environnement afin de favoriser leur multiplication. Ce travail montre également que les HDL pourraient représenter une voie thérapeutique dans d'autres contextes pathologiques que les maladies cardiovasculaires

Projet #4 : Mécanismes cellulaires à l'origine de l'élimination des macrophages du site inflammatoire au cours de la résolution de l'inflammation.

***Publication issue du projet*.** Macrophage clearance from resolving inflammation depends on apoptosis rather than migration to lymph nodes. Gautier EL et *al*. *Blood*. *2013*. (Article disponible en annexe).

Contexte scientifique, méthodologie et résultats obtenus. La phase de résolution de l'inflammation est une étape clé du retour à un état homéostatique après l'initiation d'une réponse inflammatoire. Son échec conduit à une réponse inflammatoire chronique qui favorise le développement et la progression de nombreuses pathologies (cancer, diabète/obésité, athérosclérose). Il a été proposé que la migration via les vaisseaux lymphatiques serait à l'origine de la disparition des Mϕ du site inflammatoire au cours de la résolution, bien que cette étude ne soit pas quantitative[4]. Cependant, les mécanismes cellulaires conduisant à la résolution restent dans l'ensemble méconnus.

Nous avons donc entrepris d'évaluer l'importance de la migration dans le processus de résolution (élimination des Mϕ inflammatoires) ainsi qu'explorer le rôle d'un mécanisme alternatif, la mort cellulaire par apoptose de ces Mϕ. Nous avons étudié le modèle de péritonite induite par injection de thioglycollate, modèle précédemment utilisé pour montrer un rôle de la migration[4]. Par ailleurs, des lignées de souris transgéniques, des techniques de compétition et de migration par transfert adoptif ainsi que la cytométrie en flux ont été utilisés afin de répondre à cette question. Nous montrons que :

- L'accumulation des macrophages inflammatoires dans les nœuds lymphatiques drainant le site inflammatoire s'opère suivant une cinétique et des proportions (nombre de cellules) incompatibles avec un rôle prépondérant de la migration via les vaisseaux lymphatiques comme mécanisme majeur de l'élimination des macrophages durant la résolution.
- Bloquer la migration des Mϕ inflammatoires a un effet mineur sur la résolution de l'inflammation.
- Limiter l'apoptose des Mϕ inflammatoires favorise leur accumulation au sein du site inflammatoire au cours de la résolution.

Contribution à l'avancée des connaissances. Nos données remettent en question l'idée établie selon laquelle la résolution de l'inflammation dépend de la migration des Mϕ inflammatoires vers les nœuds lymphatiques. En effet, nos résultats démontrent une absence de corrélation dans le temps entre la phase de migration des Mϕ vers les nœuds lymphatiques et la phase de résolution. De plus, bloquer la migration des Mϕ n'a qu'un très faible impact sur leur élimination du site inflammatoire au cours de la résolution. L'étude des mécanismes impliqués montre que l'apoptose, dans un contexte où l'élimination des cellules apoptotiques est optimale, est le déterminant majeur de la résolution. Ces résultats inattendus vont permettre de proposer de nouvelles pistes pour favoriser la résolution de l'inflammation notamment dans l'athérosclérose.

Projet #5: Le facteur de transcription Gata6 contrôle la survie des macrophages résidents du péritoine.

***Publication issue du projet*.** Gautier EL, Ivanov S, Williams JW, Huang SC, Marcelin G, Fairfax K, Wang PL, Francis JS, Leone P, Wilson DB, Artyomov MN, Pearce EJ, Randolph GJ. Gata6 regulates aspartoacylase expression in resident peritoneal macrophages and controls their survival. *J Exp Med. 2014*. (Article disponible en annexe).

Contexte scientifique, méthodologie et résultats obtenus. Nous avions précédemment définies les signatures transcriptomiques caractérisant un certain nombre de populations de macrophage résidents[5]. Cette étude nous avait alors permit de montrer que le facteur de transcription Gata6 n'était exprimé que par une seule population de cellules du système immunitaire, les macrophages F4/80^{hi} résidents du péritoine. De plus, Gata6 était prédit pour réguler une large partie des gènes constituant la signature spécifique de ces macrophages. Nous avons obtenus des souris dont le gène Gata6 est « floxé » et nous les avons croisé avec des souris exprimant la recombinase cre dans les macrophages (Lyz2-cre). Les souris Lyz2 x Gata6$^{flox/flox}$ présentent une forte baisse du nombre de macrophages F4/80^{hi} résidents du péritoine, sans que d'autres populations tissulaires de macrophages résidents ne soient altérées. Nous avons pu montré que la délétion de Gata6 limitait la survie des macrophages résidents du péritoine, de même que leur capacité à s'auto-renouveler par prolifération locale du fait d'un défaut de cytokinèse. Le défaut de survie est du à la perte d'expression d'une enzyme nécessaire à la production d'acetyl-CoA, l'aspartoacylase, en l'absence de Gata6. Les souris invalidées pour l'aspartoacylase présentent également une baisse du nombre de macrophages résidents dans le péritoine.

Contribution à l'avancée des connaissances. Nos données montrent comment un unique facteur de transcription peut réguler le devenir, et ce de manière très spécifique, d'une seule population de cellules immunitaires. Gata6 est donc le régulateur spécifique de la maintenance des macrophages résidents du péritoine. Des données publiées au même moment par un groupe de Yale ont montré que l'expression de Gata6 dans cette population de macrophage est dictée par l'environnent du péritoine et est sous le contrôle de l'acide rétinoïque produit localement. Ces travaux permettent de mieux comprendre comment les macrophages résidents se maintiennent de manière tissu-spécifique, selon des déterminants issus de l'environnement tissulaire.

c- Expertise développée au cours de mon stage post-doctoral.

Les projets que j'ai développé au cours de mon stage post-doctoral m'ont amené à étudier le phénotype, la migration et la fonction des populations de monocytes, de macrophages et de cellules dendritiques à l'état basal mais également au cours de l'inflammation chronique (athérosclérose, leucémie) et aigüe (péritonite, infection bactérienne). Mon stage post-doctoral, au sein de mon laboratoire mais également au

contact du laboratoire voisin du Dr Miriam Merad (spécialiste de l'étude des sous-populations de CDs, de leur développement et de leurs fonctions), m'a permis d'approfondir mon expertise dans le domaine de l'immunologie et des cellules dendritiques. Cet apprentissage m'a servit de base afin de développer des projets axés sur la diversité des phagocytes et leurs rôles fonctionnels dans les maladies cardio-métaboliques.

C- THÉMATIQUE DE RECHERCHE DEVELOPPÉE : DIVERSITÉ DES POPULATIONS DE PHAGOCYTES MONONUCLÉES ET LEURS RÔLES RESPECTIFS DANS LES MALADIES CARDIOMÉTABOLIQUES.

Les maladies cardiométaboliques (obésité, diabète, athérosclérose,...) représentent un important problème de santé publique dans les pays industrialisés mais elles sont également en plein essor dans les pays en développement ou en voie de développement (www.who.int). Au niveau mondial, on parle ainsi de syndrome en ce qui concerne l'obésité au vu de la forte croissance de la part de la population touchée par cette pathologie. L'athérosclérose en tant que complication cardio-vasculaire observée chez le patient obèse, mais dont la prévalence est également élevée en absence d'obésité, représente également un enjeu majeur en terme de santé publique.

Bien que n'étant pas directement à l'origine du développement de ces pathologies, l'activation du système immunitaire, en maintenant un état immuno-inflammatoire chronique, semble être impliqué dans la progression et la perpétuation des désordres métaboliques et vasculaires. Si l'existence d'une composante immuno-inflammatoire caractérisant les maladies cardiométaboliques est communément admise, il reste de nombreuses zones d'ombres sur le rôle intégré de chacun des acteurs du système immunitaire, la manière dont ils sont activés ainsi que les stratégies à développer pour contrer les réponses immuno-inflammatoires délétères ou, à l'inverse, renforcer celles qui révèrent une caractère bénéfique.

Aussi, nous étudions le rôle des phagocytes dans ces contextes physiopathologiques avec pour but de mieux identifier la source des médiateurs de la réponse immunitaire innée, notamment en discriminant les macrophages tissulaires résidents des macrophages inflammatoires issus des monocytes recrutés. Nous cherchons également à

établir si les cellules dendritiques, cellules qui sont nécessaires à l'initiation d'une réponse immunitaire acquise, relayée par les lymphocytes, jouent un rôle physiopathologique dans l'athérosclérose et l'obésité.

Ces projets ont nécessité le développement de modèles animaux transgéniques qui permettent de cibler spécifiquement certaines sous-populations de phagocytes mononucléés, et qui nous permettront ainsi d'étudier de manière plus spécifique leurs rôles respectifs. L'étude du rôle des cellules dendritiques CD11b$^+$ dans le développement de l'athérosclérose, de l'obésité et du diabète est ainsi en cours. L'ensemble de ces travaux précliniques nous permettra de mieux comprendre comment réguler la fonction des macrophages et des cellules dendritiques afin de limiter leurs impacts néfastes ou favoriser leurs fonctions protectrices au cours des maladies cardiométaboliques.

D- EXEMPLE DE PROJET DE RECHERCHE : RÔLES DES CELLULES DENDRITIQUES CD11b$^+$ DANS LE DÉVELOPPEMENT DE LA PLAQUE D'ATHÉROME ET LA RÉPONSE A LA VACCINATION ATHÉROPROTECTRICE.

1 - Contexte scientifique, objectifs et axes de recherche.

L'athérosclérose est une maladie inflammatoire chronique se développant sur un terrain de dyslipidémie, facteur de risque majeur de cette pathologie. Toutefois, il est maintenant établi que le développement de l'athérosclérose dépend également de l'activation du système immunitaire, que ce soit de ces composantes innée ou adaptative[6,7]. Les plaques d'athérome contiennent ainsi des infiltrats inflammatoires constitués, entre autres, de macrophages (réponse innée), de cellules dendritiques (CDs) et de lymphocytes T (LTs) (réponse adaptative)[6,7]. De nombreuses composantes de la réponse immunitaire acquise exercent une influence sur l'initiation et la progression de la plaque[8,9]. Ainsi, les LTs CD4$^+$ conventionnels[10], les lymphocytes NK[11] et NKT[12] ainsi que les lymphocytes B (LBs) conventionnels de type B2[13] favorisent le développement des plaques, alors que le rôle des LTs CD8$^+$ n'a jusqu'ici pu être clairement établi. À l'inverse, les LT CD4$^+$ régulateurs, qui contrôlent l'activation des LTs CD4$^+$ conventionnels, freinent le processus athérogène[14]. Il a également été montré qu'au niveau des LTs CD4$^+$ conventionnels, la voie de polarisation Th1 est pro-athérogène[15,16], alors que le rôle des voies Th17 et Th2 reste toujours ambiguë à ce jour. Dans ce contexte, et en complément des approches thérapeutiques visant à contrôler les taux de

LDL-cholestérol plasmatique, il est maintenant envisagé de moduler les réponses immunitaires pro- et anti- athérogènes à des fins thérapeutiques. Notamment, les approches de vaccinations, effectuées à l'aide de particules LDL modifiées par oxydation ou de peptides correspondant à une portion de l'apolipoprotéine B100 (ApoB100 ; apolipoprotéine majeure des LDL), ont montré un potentiel thérapeutique intéressant chez l'animal[17,18] et motivé la proposition de développement d'un vaccin contre l'athérosclérose[17]. Toutefois, les mécanismes cellulaires et moléculaires par lesquels la vaccination induit un effet athéroprotecteur restent largement méconnus.

Récemment, les cellules dendritiques (CDs) ont été identifiées dans le système vasculaire et les lésions d'athérosclérose[19,20]. Les CDs sont des cellules présentatrices d'antigènes capables d'activer et de polariser les LTs naïfs[21], permettant ainsi d'initier la réponse immunitaire et d'établir la mémoire immunitaire. Elles jouent également un rôle dans l'induction de la tolérance périphérique[22,23] et la génération de LTs $CD4^+$ régulateurs[24]. Toutefois, les CDs ne sont pas homogènes d'un point de vue phénotypique et fonctionnel. Ainsi, les CDs plasmacytoïdes (pCDs) représentent un acteur clé de la réponse antivirale[25,26] et leur rôle pro-athérogène a récemment été mis en évidence[27]. Les CDs conventionnelles (cCDs) $CD11b^+$ sont spécialisées dans la présentation d'antigènes aux LTs $CD4^+$ conventionnels[28,29] et l'induction des voies de polarisation Th2[30] et Th17[31,32]. Leur développement dépend, entre autres, des facteurs de transcription Notch2 et IRF4[25,26]. Enfin, les cCDs $CD8^+/CD103^+$ sont spécialisées dans la présentation d'antigènes aux LTs $CD8^+$[28,33]. Les facteurs de transcription Batf3 et Id2 ont été impliqués dans leur développement[25,26]. Le rôle des CDs $CD8^+/CD103^+$ dans l'athérosclérose semble peu évident au vu de l'absence de phénotype des souris $Batf3^{-/-}$ en fond $Ldl\text{-}r^{-/-}$[34,35], alors que le rôle des CDs $CD11b^+$ reste inconnu à ce jour.

Nos travaux ont permis de positionner la cCD comme un potentiel régulateur clé de l'immunité dans l'athérosclérose[36]. En développant une lignée de souris transgénique dont les CDs ont une demi-vie augmentée, menant à une augmentation du nombre de cDCs $CD8^+/CD103^+$ et $CD11b^+$ CDs, et une immunogénicité accrue (souris CD11c-Bcl2), nous avons pu montrer que les cCDs modulent l'activation des LTs $CD4^+$ et leur polarisation suivant les voies Th1 et Th17, ainsi que l'activation des lymphocytes B dans des modèles murins d'athérosclérose[36]. Cette étude a également révélé que l'augmentation du nombre de cCDs entraîne une diminution du taux de cholestérol plasmatique[36]. Les cCDs modulent donc à la fois l'immunité et l'homéostasie du

cholestérol dans l'athérosclérose. Il est important de noter que les effets dépendant des CDs dans notre modèle CD11c-Bcl-2 sont uniquement dus aux cCDs car les pCDs ne sont pas ciblées par notre approche de transgénèse[36]. En conséquence, nous nous intéressons maintenant à mieux comprendre le rôle des sous-populations de cCDs dans le processus athérogène.

Aussi, au vu du rôle central des CDs CD11b$^+$ dans la présentation d'antigènes aux LTs CD4$^+$[29] ainsi que sur leur polarisation[30–32], l'objectif de ce projet sera d'évaluer le rôle des cCDs CD11b$^+$ sur l'induction et la polarisation des réponses immunitaires adaptatives au cours de l'athérosclérose, et in fine sur le développement de la plaque d'athérome. Nous concentrerons nos efforts sur l'étude de l'axe cCDs CD11b$^+$ / LTs CD4$^+$ et de son impact sur le développement de la plaque d'athérome, sans toutefois omettre d'évaluer l'activation d'autres populations effectrices (LBs, NK, NKT). Dans un second, nous chercherons à déterminer si les effets athéroprotecteurs de la vaccination anti-ApoB100 dépendent des cCDs CD11b$^+$.

L'objectif principal de ce projet est d'établir le rôle des cCDs CD11b$^+$ dans le processus athérogène, et le(s) mécanisme(s) sous-jacent à leur action. Ce projet permettra d'évaluer pour la première fois si les cCDs CD11b$^+$ pourraient représenter une potentielle cible thérapeutique dans l'athérosclérose. Nous chercherons également à déterminer si l'effet athéroprotecteur de la vaccination à l'aide de peptides de l'ApoB100 dépend des cCDs CD11b$^+$.

Notre projet sera développé suivant les 3 axes de recherche suivants :

Axe 1: Déterminer le rôle des cCDs CD11b$^+$ dans le développement de la plaque d'athérome.

Axe 2 : Déterminer le(s) mécanisme(s) par le(s)quel(s) les cCDs CD11b$^+$ influe(nt) sur le développement des plaques.

Axe 3 : Déterminer si l'effet anti-athérogène de la vaccination anti-apoB100 dépend des cCDs CD11b$^+$.

2 – Méthodologie et données préliminaires.

Axe 1 : Déterminer le rôle des cCDs CD11b$^+$ dans le développement de la plaque d'athérome.

Afin d'éliminer spécifiquement les cCDs CD11b$^+$, nous avons récemment développé une lignée de souris présentant une déficience spécifique d'Irf4 dans les CDs

(souris CD11c-cre x Irf4$^{flox/flox}$ ou IRF4$^{\Delta DC}$). L'analyse des souris IRF4$^{\Delta DC}$ montre une quasi totale absence des CDs CD4$^+$/CD11b$^+$ dans la rate, les poumons, les ganglions lymphatiques, le tissu adipeux et l'intestin. Afin de déterminer le rôle des CDs CD11b$^+$ dans le processus athérogène, la moelle osseuse de souris IRF4$^{\Delta DC}$ a été transplantée chez des souris Ldl-r$^{-/-}$ préalablement irradiées. Après 4 semaines de reconstitution, les souris ont été nourries avec un régime enrichi en cholestérol (1% cholestérol) pendant 8 semaines. En parallèle, les souris IRF4$^{\Delta DC}$ ont été croisées avec des souris Ldl-r$^{-/-}$ afin d'étudier le rôle des CDs CD11b$^+$ en absence d'irradiation. Les paramètres suivant sont évalués :

- Lipoprotéines et lipides plasmatiques

- La taille des plaques d'athérome et leur composition cellulaire (macrophages, cellules musculaires lissses, ...).

- Le statut d'activation du système immunitaire :

  * Le nombre de CDs CD11b$^+$ (CD11c^{hi} MHC-II$^+$ CD4$^+$ CD8$^-$) et CD8$^+$/CD103$^+$, le nombre et l'activation des LTs conventionnels CD4$^+$ et CD8$^+$ (TCRβ$^+$ CD4$^+$ ou CD8$^+$ CD44$^+$ CD62L$^-$ CD69$^+$), le nombre de lymphocytes NK (TCRαβ$^-$ NK1.1$^+$) et NKT (TCRαβ$^+$ NK1.1$^+$) et le nombre de LT régulateurs (TCRβ$^+$ CD4$^+$ CD25$^+$ Foxp3$^+$) dans les organes lymphoïdes.

  * La polarisation de la réponse immunitaire (Th1, Th2, Th17) par restimulation (PMA/Ionomycine pendant 4 heures ou anti-CD3 pendant 6 heures) ex vivo des LTs CD4$^+$ provenant de la rate et/ou des ganglions lymphatiques. La production des cytokines IL-10, IFNγ, IL-4, IL-13 et IL-17 se fera par marquage intracellulaire ou par dosage des cytokines dans le surnageant de culture par ELISA. Les aortes seront analysées par qPCR afin de détecter la présence de ces cytokines en local.

  * L'activation du pool de LBs, notamment le nombre de LBs associés aux centres germinatifs (B220$^+$ GL7$^+$ CD95$^+$) et de plasmocytes (B220^{low} CD19^{low} CD138$^+$) sera déterminé par cytométrie en flux.

  * Les taux d'anticorps (IgM, IgG1, 2a et 2b) totaux et ceux dirigés contre les lipoprotéines modifiées (MDA-LDL) par ELISA.

- Le statut inflammatoire de la plaque d'athérome par analyse d'expression de gènes(molécules d'adhésion, chimiokines, interleukines, ..) par PCR quantitative en temps réel.

Nos données préliminaires montrent que le nombre de cCDs CD11b$^+$ CD4$^+$ (qui représentent la grande majorité des cCDs CD11b$^+$ dans la rate) est très fortement diminué chez les souris Ldl-r$^{-/-}$ transplantées avec de la moelle osseuse de souris IRF4$^{\Delta DC}$, sans que les CDs CD8$^+$ soient touchées. Cette forte baisse des cCDs CD11b$^+$ n'influence toutefois pas le nombre de lymphocytes T CD4$^+$, CD8$^+$, de lymphocytes NK et NKT, ni de lymphocytes B (B1 et B2). Toutefois, une augmentation de la capacité des LT CD4$^+$ à produire de l'IFNγ (voie Th1) est observée ainsi qu'une baisse des LT CD4$^+$ producteur d'IL-17 (Th17). Le pourcentage de LT CD8$^+$ producteurs d'IFNγ reste inchangé. Nous n'avons pu mesurer la production des cytokines Th2 (IL-4, IL-13 et IL-5) par marquage intracellulaire et allons maintenant procéder via l'analyse du surnageant de LT CD4$^+$ restimulés *in vitro* par ELISA. En conclusion, nous observons une baisse d'IL-17 ainsi qu'une augmentation de la voie Th1. Les voies Th1 et Th2 étant connues pour s'inhiber mutuellement, ce biais Th1 pourrait s'expliquer par le défaut de polarisation Th2 précédemment décrit chez les animaux IRF4$^{\Delta DC}$ [30].

A ce stade, nous devons maintenant analyser la taille des plaques d'athérome dans nos expériences de transplantation de moelle osseuse. Par ailleurs, des groupes de souris IRF4$^{\Delta DC}$ croisées avec des souris Ldl-r$^{-/-}$ ont été mis sous régime athérogène afin d'évaluer l'impact des cCDs CD11b$^+$ dans un modèle ne nécessitant pas d'irradiation. L'ensemble des paramètres décrits ci-dessus sera également analysé dans ce modèle.

Axe 2 : Déterminer le(s) mécanisme(s) par le(s)quel(s) les cCDs CD11b$^+$ influent sur le développement des plaques.

Nous allons chercher à démontrer s'il existe une causalité entre le défaut d'induction de la réponse Th2[30] et le développment de l'athérosclérose chez les souris IRF4$^{\Delta DC}$. Pour cela, nous allons développer plusieurs stratégies :

1/ Inhibition de la voie Th1 par un anticorps bloquant anti-IFNγ.

Nous testerons ici si la neutralisation de l'IFNγ, la cytokine produite par les LT CD4 polarisés Th1, permet de moduler la taille des plaques chez les souris IRF4$^{\Delta DC}$. Pour cela des souris Ldl-r$^{-/-}$ transplantées avec de la moelle osseuse de souris contrôles IRF4$^{flox/flox}$ (CTRL) ou IRF4$^{\Delta DC}$ seront réparties en 4 groupes : CTRL + isotype ; CTRL + anti-IFNγ ; IRF4$^{\Delta DC}$ + isotype ; IRF4$^{\Delta DC}$ + anti-IFNγ. Nous utiliserons l'anticorps neutralisant anti-IFNγ (clone H22, BioXcell) par injection intrapéritonéale une fois par semaine pendant 8

semaines (500µg à la première injection puis 250 µg chaque semaine) comme décrit précédemment[37]. Les paramètres décritss dans l'Axe 1 seront analysés dans les groupes de souris cités ci-dessus.

2/ Utilisation d'un modèle de souris où seule la capacité des cDCs à polariser suivant la voie Th2 est altérée.

Nous obtiendrons auprès du groupe du Dr Roxane Tussiwand de l'Université de Bâle un modèle de souris dont les CDs ont été invalidées pour le facteur de transcription KLF4 ($KLF4^{\Delta DC}$). Ce modèle présente une perte sélective de la capacité à polariser les LT $CD4^+$ suivant la voie Th2, sans affecter la polarisation suivant les voies Th1 et Th17[39]. La moelle osseuse de ces souris sera injectée dans des souris Ldl-$r^{-/-}$ préalablement irradiées et l'analyse de leur phénotype s'effectuera comme décrit dans l'Axe 1.

Ces approches permettront donc d'évaluer si la balance Th1/Th2 influence le développment de l'athérosclérose dans notre modèle de souris $IRF4^{\Delta DC}$. De plus, l'utilisation d'un modèle de souris ayant un incapacité sélective à monter une réponse Th2 permettra d'impliquer de manière directe la voie Th2 dans le processus athérogène.

<u>Axe 3</u> : Déterminer si l'effet anti-athérogène de la vaccination anti-apoB100 dépend des cCDs $CD11b^+$.

La vaccination de souris susceptibles à l'athérosclérose par des LDL oxydées ou des peptides de l'ApoB100 freine le développement de l'athérosclérose[17,18]. De manière intéressante, les protocoles de vaccination utilisés nécessitent des adjuvants qui ont un effet anti-athérogène propre[40], c'est à dire indépendant de la co-injection d'un antigène. Toutefois, la présence de l'antigène augmente l'effet athéroprotecteur. Les effets des adjuvants sont associées à un biais de la réponse immunitaire suivant la voie Th2[40]. Ainsi, les vaccinations anti-athérosclérose sont associées à une polarisation de type Th2 mais l'importance de cette voie sur l'effet anti-athérogène n'est pas connue. Aussi, dans le dernier axe du projet, nous allons tester l'importance de la polarisation Th2 sur l'efficacité de la vaccination anti ApoB100 à l'aide des modèles animaux décrits ci dessus et qui présentent une incapacité à développer une réponse Th2. La moelle osseuse de souris $IRF4^{\Delta DC}$, $KLF4^{\Delta DC}$ et leurs contrôles seront injectées dans des souris Ldl-$r^{-/-}$ préalablement irradiées. Après 4 semaines de reconstitution, les souris seront vaccinées à l'aide des peptides ApoB100(3501–3516) or ApoB100(978–993) émulsifiés dans de

l'adjuvant de Freund complet pour la phase d'immunisation puis dans du Freund incomplet pour le phase de « booster » comme décrit précédemment[41]. Les souris seront soumises à un régime enrichi en cholestérol pendant 8 semaines et les paramètres cités dans l'Axe 1 seront analysés. La réponse humorale sera étudiée en détail ainsi que la polarisation des LT $CD4^+$ et le nombre de LT régulateurs. Cet axe de recherche nous permettra de comprendre l'importance de la voie Th2 dans l'effet athéroprotecteur de la vaccination, et d'envisager de nouvelles méthodes basées sur la modulation des cCDs pour augmenter l'efficacité de cette approche thérapeutique.

3 - Conclusions - Perspectives.

Ce projet de recherche pose de nouvelles questions concernant la relation entre l'immunité, et son acteur central la cCD, et l'athérosclérose. Ce projet vise à mieux comprendre le rôle des cCDs $CD11b^+$ dans le processus athérogène afin d'en moduler les fonctions pour reprogrammer la réponse immunitaire et la rendre athéroprotectrice. De plus, dans un contexte de recherche d'un vaccin contre l'athérosclérose, comprendre le rôle des cCDs au cours de la vaccination anti-ApoB100 protectrice s'avère essentiel. Ce projet servira de base au développement de nouvelles stratégies thérapeutiques à tester dans des modèles murins précliniques.

D- BIBLIOGRAPHIE.

1. Roman MJ, Shanker B-A, Davis A, et al. Prevalence and correlates of accelerated atherosclerosis in systemic lupus erythematosus. N Engl J Med 2003;349:2399–2406.
2. Efron PA, Martins A, Minnich D, et al. Characterization of the systemic loss of dendritic cells in murine lymph nodes during polymicrobial sepsis. J Immunol Baltim Md 1950 2004;173:3035–3043.
3. Flohé SB, Agrawal H, Schmitz D, et al. Dendritic cells during polymicrobial sepsis rapidly mature but fail to initiate a protective Th1-type immune response. J Leukoc Biol 2006;79:473–481.
4. Bellingan GJ, Caldwell H, Howie SE, et al. In vivo fate of the inflammatory macrophage during the resolution of inflammation: inflammatory macrophages do not die locally, but emigrate to the draining lymph nodes. J Immunol Baltim Md 1950 1996;157:2577–2585.
5. Gautier EL, Shay T, Miller J, et al. Gene-expression profiles and transcriptional regulatory pathways that underlie the identity and diversity of mouse tissue macrophages. Nat Immunol 2012;13:1118–1128.
6. Libby P, Lichtman AH, Hansson GK. Immune effector mechanisms implicated in atherosclerosis: from mice to humans. Immunity 2013;38:1092–1104.
7. Hansson GK, Hermansson A. The immune system in atherosclerosis. Nat Immunol 2011;12:204–212.

8. Hansson GK, Libby P. The immune response in atherosclerosis: a double-edged sword. Nat Rev Immunol 2006;6:508–519.
9. Weber C, Zernecke A, Libby P. The multifaceted contributions of leukocyte subsets to atherosclerosis: lessons from mouse models. Nat Rev Immunol 2008;8:802–815.
10. Zhou X, Nicoletti A, Elhage R, et al. Transfer of CD4(+) T cells aggravates atherosclerosis in immunodeficient apolipoprotein E knockout mice. Circulation 2000;102:2919–2922.
11. Whitman SC, Rateri DL, Szilvassy SJ, et al. Depletion of natural killer cell function decreases atherosclerosis in low-density lipoprotein receptor null mice. Arterioscler Thromb Vasc Biol 2004;24:1049–1054.
12. Tupin E, Nicoletti A, Elhage R, et al. CD1d-dependent activation of NKT cells aggravates atherosclerosis. J Exp Med 2004;199:417–422.
13. Ait-Oufella H, Herbin O, Bouaziz J-D, et al. B cell depletion reduces the development of atherosclerosis in mice. J Exp Med 2010;207:1579–1587.
14. Ait-Oufella H, Salomon BL, Potteaux S, et al. Natural regulatory T cells control the development of atherosclerosis in mice. Nat Med 2006;12:178–180.
15. Laurat E, Poirier B, Tupin E, et al. In vivo downregulation of T helper cell 1 immune responses reduces atherogenesis in apolipoprotein E-knockout mice. Circulation 2001;104:197–202.
16. Buono C, Binder CJ, Stavrakis G, et al. T-bet deficiency reduces atherosclerosis and alters plaque antigen-specific immune responses. Proc Natl Acad Sci U S A 2005;102:1596–1601.
17. Shah PK, Chyu K-Y, Dimayuga PC, et al. Vaccine for atherosclerosis. J Am Coll Cardiol 2014;64:2779–2791.
18. Witztum JL, Lichtman AH. The influence of innate and adaptive immune responses on atherosclerosis. Annu Rev Pathol 2014;9:73–102.
19. Cybulsky MI, Jongstra-Bilen J. Resident intimal dendritic cells and the initiation of atherosclerosis. Curr Opin Lipidol 2010;21:397–403.
20. Choi J-H, Do Y, Cheong C, et al. Identification of antigen-presenting dendritic cells in mouse aorta and cardiac valves. J Exp Med 2009;206:497–505.
21. Guermonprez P, Valladeau J, Zitvogel L, et al. Antigen presentation and T cell stimulation by dendritic cells. Annu Rev Immunol 2002;20:621–667.
22. Hawiger D, Inaba K, Dorsett Y, et al. Dendritic cells induce peripheral T cell unresponsiveness under steady state conditions in vivo. J Exp Med 2001;194:769–779.
23. Luckashenak N, Schroeder S, Endt K, et al. Constitutive crosspresentation of tissue antigens by dendritic cells controls CD8+ T cell tolerance in vivo. Immunity 2008;28:521–532.
24. Darrasse-Jèze G, Deroubaix S, Mouquet H, et al. Feedback control of regulatory T cell homeostasis by dendritic cells in vivo. J Exp Med 2009;206:1853–1862.
25. Satpathy AT, Wu X, Albring JC, et al. Re(de)fining the dendritic cell lineage. Nat Immunol 2012;13:1145–1154.
26. Merad M, Sathe P, Helft J, et al. The dendritic cell lineage: ontogeny and function of dendritic cells and their subsets in the steady state and the inflamed setting. Annu Rev Immunol 2013;31:563–604.
27. Sage AP, Murphy D, Maffia P, et al. MHC Class II-restricted antigen presentation by plasmacytoid dendritic cells drives proatherogenic T cell immunity. Circulation 2014;130:1363–1373.
28. Dudziak D, Kamphorst AO, Heidkamp GF, et al. Differential antigen processing by

dendritic cell subsets in vivo. Science 2007;315:107–111.
29. Vander Lugt B, Khan AA, Hackney JA, et al. Transcriptional programming of dendritic cells for enhanced MHC class II antigen presentation. Nat Immunol 2014;15:161–167.
30. Gao Y, Nish SA, Jiang R, et al. Control of T helper 2 responses by transcription factor IRF4-dependent dendritic cells. Immunity 2013;39:722–732.
31. Persson EK, Uronen-Hansson H, Semmrich M, et al. IRF4 transcription-factor-dependent CD103(+)CD11b(+) dendritic cells drive mucosal T helper 17 cell differentiation. Immunity 2013;38:958–969.
32. Schlitzer A, McGovern N, Teo P, et al. IRF4 transcription factor-dependent CD11b+ dendritic cells in human and mouse control mucosal IL-17 cytokine responses. Immunity 2013;38:970–983.
33. Hildner K, Edelson BT, Purtha WE, et al. Batf3 deficiency reveals a critical role for CD8alpha+ dendritic cells in cytotoxic T cell immunity. Science 2008;322:1097–1100.
34. Legein B, Janssen EM, Theelen TL, et al. Ablation of CD8α(+) dendritic cell mediated cross-presentation does not impact atherosclerosis in hyperlipidemic mice. Sci Rep 2015;5:15414.
35. Gil-Pulido J, Cochain C, Lippert MA, et al. Deletion of Batf3-dependent antigen-presenting cells does not affect atherosclerotic lesion formation in mice. PloS One 2017;12:e0181947.
36. Gautier EL, Huby T, Saint-Charles F, et al. Conventional dendritic cells at the crossroads between immunity and cholesterol homeostasis in atherosclerosis. Circulation 2009;119:2367–2375.
37. Koebel CM, Vermi W, Swann JB, et al. Adaptive immunity maintains occult cancer in an equilibrium state. Nature 2007;450:903–907.
38. Finkelman FD, Madden KB, Morris SC, et al. Anti-cytokine antibodies as carrier proteins. Prolongation of in vivo effects of exogenous cytokines by injection of cytokine-anti-cytokine antibody complexes. J Immunol Baltim Md 1950 1993;151:1235–1244.
39. Tussiwand R, Everts B, Grajales-Reyes GE, et al. Klf4 expression in conventional dendritic cells is required for T helper 2 cell responses. Immunity 2015;42:916–928.
40. Khallou-Laschet J, Tupin E, Caligiuri G, et al. Atheroprotective effect of adjuvants in apolipoprotein E knockout mice. Atherosclerosis 2006;184:330–341.
41. Tse K, Gonen A, Sidney J, et al. Atheroprotective Vaccination with MHC-II Restricted Peptides from ApoB-100. Front Immunol 2013;4:493.

D- ANNEXES (PUBLICATIONS ASSOCIEES AUX TRAVAUX PRESENTES DANS CE MEMOIRE).

Enhanced Immune System Activation and Arterial Inflammation Accelerates Atherosclerosis in Lupus-Prone Mice

Emmanuel L. Gautier, Thierry Huby, Betty Ouzilleau, Chantal Doucet, Flora Saint-Charles, Guilaine Gremy, M. John Chapman, Philippe Lesnik

Objective—Premature atherosclerosis is a characteristic feature of systemic lupus erythematosus, a prototypic autoimmune disease. The principle cellular and molecular mechanisms which underlie such accelerated atherosclerosis are indeterminate.

Methods and Results—The pathophysiology of lupus-mediated atherogenesis was evaluated in a novel animal model involving transplantation of bone marrow cells from the lupus prone strain *gld* into *Ldl-r*$^{-/-}$ mice. Diet-induced atherogenesis in lethally-irradiated *Ldl-r*$^{-/-}$ mice transplanted with *gld* bone marrow cells resulted in accelerated atherosclerosis (+65%) as compared with control mice transplanted with wild-type marrow cells. Enhanced atherogenesis was associated with enhanced activation of both B and T lymphocytes and with arterial inflammation involving endothelial cell activation, monocyte recruitment, and accumulation of apoptotic debris, macrophages, and CD4 T cells, but was independent of plasma lipid levels and renal function.

Conclusions—Our data support the contention that despite the absence of both disturbed cholesterol homeostasis and renal dysfunction in autoimmune *gld*→*Ldl-r*$^{-/-}$ mice, lupus disease induces enhanced activation of the immune system and acts locally on the vasculature to induce inflammation, together with accumulation of apoptotic debris, macrophages, and CD4 T cells, thereby accelerating plaque progression. **(*Arterioscler Thromb Vasc Biol*. 2007;27:1625-1631.)**

Key Words: atherosclerosis ■ lupus ■ arterial inflammation ■ immune system ■ apoptotic cells

The risk of cardiovascular disease (CVD) is significantly increased in the prototypic autoimmune disease, systemic lupus erythematosus (SLE).[1,2] The mechanisms underlying premature CVD in SLE may be related to accelerated atherosclerosis.[3,4] Such accelerated atherosclerosis potentially involves a combination of autoimmune-specific mechanisms and traditional cardiovascular risk factors (dyslipidemia, renal failure, and inflammation), although the central mechanisms involved are indeterminate.[2] Moreover, as most SLE patients are on active therapy (corticosteroids and other pharmacological agents), such agents might interfere with the atherogenic process[5] and lead to confounding findings. Therefore, identification of the mechanisms that contribute to disease progression might allow optimization of therapeutic approaches for prevention of CVD in SLE patients. In this setting, development of murine models may facilitate evaluation of the specific impact of autoimmunity on atherosclerosis progression and of the underlying mechanisms involved.

Genetic studies of various strains of lupus-prone mice have identified at least 30 chromosomal regions of interest reflecting the multifactorial aspect of SLE.[6] In this context the use of various strains of lupus-prone mice and the study of their impact on atherogenesis may highlight the key molecular mechanisms that promote autoimmune-accelerated atherosclerosis. Mouse strains defective for the *Fas*/*Fas L* pathway (*gld*, *lpr*) present lupus-like autoimmune disorders comparable to those of human SLE.[6,7] Indeed, these mice are characterized by a deficit in apoptotic cell clearance[8] which induces the production of a repertoire of autoantibodies directed against neoantigens derived from apoptotic cells (nucleosome, dsDNA). In addition, these mice progressively develop renal dysfunction with age.[6,7]

When *gld* mice are crossed with atherosclerosis-susceptible *Apoe*$^{-/-}$ animals, they develop accelerated atherogenesis associated with defective phagocytosis of apoptotic cells in lymph nodes and glomerulonephritis.[8] These findings suggest that defective apoptotic cell clearance, a feature of autoimmunity, might potentiate atherosclerosis. Impaired clearance of apoptotic cells is equally observed in *Apoe*$^{-/-}$ mice[9] and could synergize with the *gld* mutation to exacerbate both autoimmunity and atherogenesis. Moreover, the renal dysfunction observed in *gld Apoe*$^{-/-}$ mice might potentiate atherosclerosis as renal dysfunction is associated with accelerated atherogenesis in mice and humans.[10,11,12]

To further evaluate the relationship between autoimmune disease and accelerated atherogenesis, we generated an ath-

Original received October 26, 2006; final version accepted March 29, 2007.
From INSERM Unit 551, UPMC-Paris 6, Dyslipoproteinemia and Atherosclerosis Research Unit, Hôpital de la Pitié, Paris, France.
Correspondence to Dr Philippe Lesnik, INSERM U551, Hôpital de la Pitié, 83 Bd de l'hôpital, 75651 Paris 13, France. E-mail lesnik@chups.jussieu.fr

Arterioscler Thromb Vasc Biol. **is available at http://www.atvbaha.org** **DOI: 10.1161/ATVBAHA.107.142430**

erosclerosis-susceptible autoimmune mouse model by transfer of bone marrow cells from the *gld* strain to lethally irradiated *Ldl-r*$^{-/-}$. In this new murine model, we demonstrated both an enhanced activation of B and T cells and a vascular inflammatory profile that results in accelerated atherosclerosis. Such enhanced atherogenesis was independent of plasma lipid levels and renal dysfunction.

Materials and Methods

Please see the supplemental data section at http://atvb.ahajournals.org for detailed Methods.

Mice, Bone Marrow Transplantation, and Study Design

Ldl-r$^{-/-}$ and *gld* mice (*FasL*-deficient mice) on the C57BL/6J background were obtained from Jackson Laboratories. Males *Ldl-r*$^{-/-}$ mice (8- to 9-week-old) were subjected to medullar aplasia with 10 Gray lethal total body irradiation. The next day, femurs were isolated from donor *gld* or *wt* mice and 2.5×10^6 bone marrow cells were injected via the retrorbital vein into the irradiated mice to rescue their hematopoietic systems. Mice were housed in cages under air-filtered conditions for 4 weeks to allow the hematopoietic system to reconstitute, after which they were fed a diet consisting of 0.15% cholesterol and 20% saturated fat (SAFE) for 12 weeks.

Assessment of Chimerism and Analysis of Gene Expression by Q-Polymerase Chain Reaction (PCR)

Real time quantitative PCR was performed using a LightCycler PCR System (Roche) as previously described.[13] The specific primers are described in supplemental Table I available online at http://atvb.ahajournals.org

Plasma Lipid Analyses and Lipoprotein Profile

Blood samples were collected and analyzed as previously described.[13]

Flow Cytometry, Antibody Measurements, and Serum Cytokine Levels

Please see the supplemental data section at http://atvb.ahajournals.org for details.

Analysis of Atherosclerotic Plaques, Immunohistochemistry, and Terminal Deoxynucleotidyl Transferase-Mediated dUTP Nick End-Labeling (TUNEL) Staining

Atherosclerotic lesions quantification and Immunohistochemistry were performed as previously described.[13,14] TUNEL staining was performed according to the manufacturer's instructions (In situ Cell Death Detection Kit, Roche Applied Science)

Statistical Analysis

The statistical significance of the differences between groups was evaluated using the Mann–Whitney *U* test for unpaired comparisons. $P<0.05$ was considered significant. Values are expressed as mean±SEM.

Results

Generation of Chimeric Mice With *gld* or *wt* Bone Marrow–Derived Cells

Irradiated male *Ldl-r*$^{-/-}$ mice were reconstituted with bone marrow cells from *gld* mice (n=18) or wild-type controls (n=14). After 12 weeks of a Western-style diet, *Ldl-r*$^{-/-}$ mice which had received *gld* bone marrow cells displayed similar body weight as compared with those receiving *wt* marrows (21.6±1.0 versus 22.2±1.2 g, respectively). The hematocrit, leukocyte count, and relative levels of T cells, B cells, and monocytes were not significantly different between the two groups (data not shown). The efficacy of transplantation was attested by the significant splenomegaly observed in *gld*→*Ldl-r*$^{-/-}$, a feature of the *gld* model, and by the fact that we detected less than 5% of *FasL wt* alleles in bone marrow cells from these mice (supplemental Figure I, available online at http://atvb.ahajournals.org). Clearly, the chimerism for *FasL* in our *gld*→*Ldl-r*$^{-/-}$ was in the range of 95 to 100%.

Quantification of Atherosclerotic Lesions

As shown in Figure 1A, the surface of ORO-positive areas in the aortic root of *Ldl-r*$^{-/-}$ recipients reconstituted with *gld* marrow cells was significantly greater (+65%) than that observed for their *wt* reconstituted controls (170454±64391 versus 104134±31709 μm^2 respectively; $P<0.0005$).

Plasma Lipid and Lipoprotein Profile

To assess whether the effects of *gld* marrow cells on atherosclerosis in *Ldl-r*$^{-/-}$ mice were attributable to changes in lipid or lipoprotein metabolism, we analyzed serum lipids and lipoproteins. *Ldl-r*$^{-/-}$ mice transplanted with *gld* marrow cells displayed, as compared with controls, similar plasma total cholesterol (481±67 versus 511±99 mg/dL, respectively), free cholesterol (148±23 versus 150±24 mg/dL, respectively), and triglyceride (206±61 versus 227±64 mg/dL, respectively) levels. Analysis of plasma lipoproteins by gel filtration showed no difference in cholesterol distribution across the VLDL, LDL, and HDL lipoprotein classes between *gld*→*Ldl-r*$^{-/-}$ and *wt*→*Ldl-r*$^{-/-}$ mice (data not shown).

Systemic Autoimmunity in *gld*→*Ldl-r*$^{-/-}$

The spleen/body weight ratio in *gld*→*Ldl-r*$^{-/-}$ mice was increased almost 2-fold as compared with *wt*→ *Ldl-r*$^{-/-}$ mice (Table 1). The enhanced lymphoproliferation and autoimmunity seen both in *Fas* or *FasL*-deficient mice and *Fas* mutant human subjects is attributable predominantly to the expansion of an unusual T cell population of $CD3^+$ cells that lacks both CD4 and CD8 (double negative T cells, DNTC). Therefore, we performed quantitative analysis of DNTC in spleen and blood samples from each animal. Significant expansion of DNTC was seen in both spleen and blood of *gld*→*Ldl-r*$^{-/-}$ animals compared with their *wt*→*Ldl-r*$^{-/-}$ controls (Table 1). Lupus is associated with the appearance of specific subsets of autoantibodies directed against nuclear materials. Thus, we measured the levels of antibodies directed against double-strand DNA (dsDNA) and nuclear materials (ANA) and showed that they were significantly elevated in *gld*→*Ldl-r*$^{-/-}$ mice as compared with the *wt*→*Ldl-r*$^{-/-}$ animals (Table 1). Moreover, autoimmune *gld*→*Ldl-r*$^{-/-}$ mice presented a global hypergammaglobulinemia as observed by significantly increased serum IgG levels compared with controls. Therefore, these data demonstrated the development of autoimmune disease in *gld*→*Ldl-r*$^{-/-}$ mice.

Renal Function in Autoimmune Mice

As autoimmune disease is frequently associated with renal dysfunction, histological analysis was performed on renal

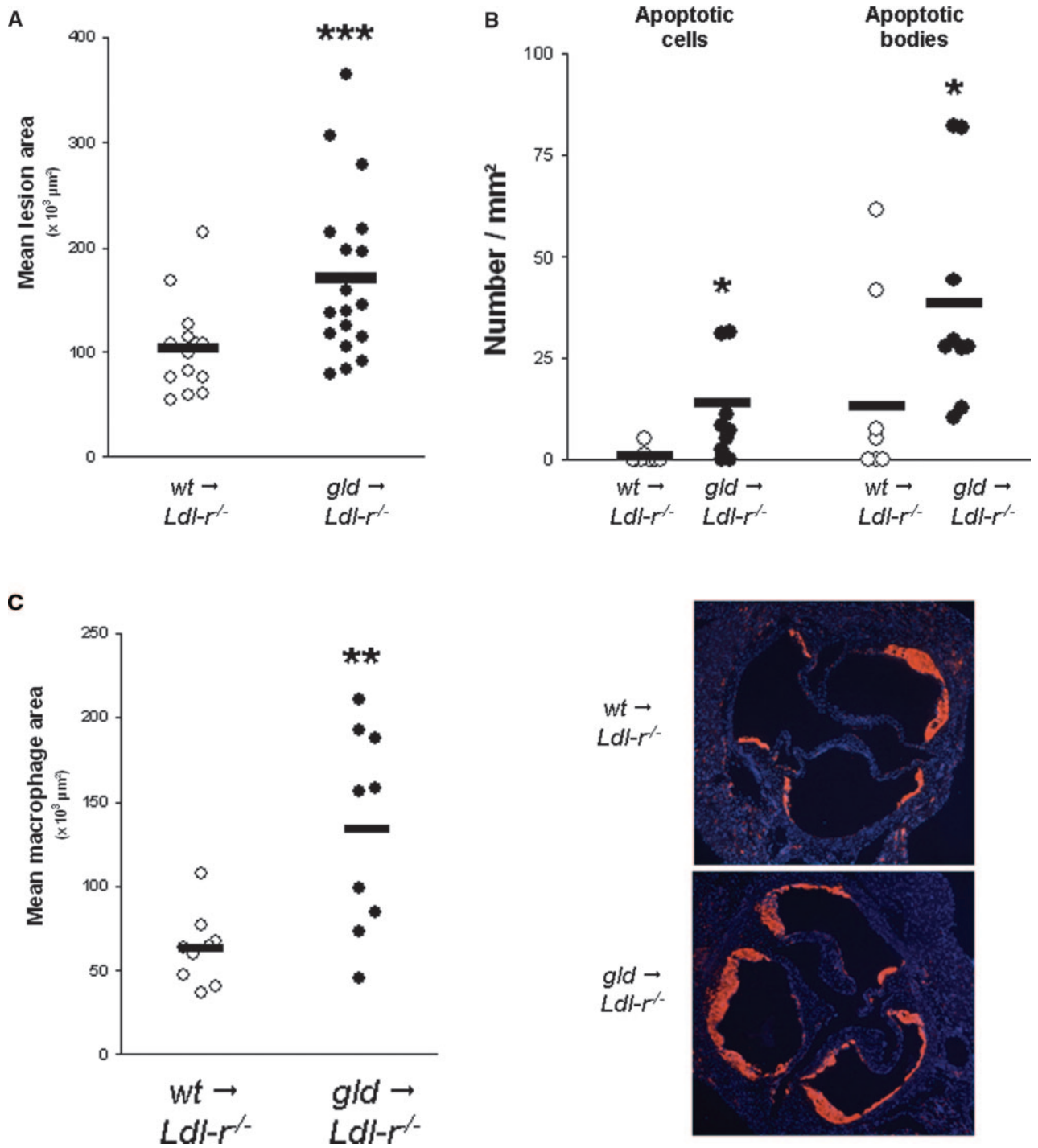

Figure 1. Increased atherosclerosis, apoptotic material deposition, and macrophage accumulation in *gld→Ldl-r*$^{-/-}$ mice as compared with *wt→Ldl-r*$^{-/-}$ mice. A, The degree of atherosclerosis was determined by ORO staining of aortic root sections. Each symbol represents the mean lesion area in a single mouse. The horizontal bar indicates the mean value for the respective group. B, Atherosclerotic lesions were stained by the TUNEL method and the number of apoptotic cells and bodies counted. The ratio of TUNEL-positive cells or bodies to ORO-positive staining was calculated for both groups. Each symbol represents the ratio for a single mouse. C, Atherosclerotic lesions were immunostained for the macrophage CD68 antigen and the degree of macrophage accumulation was determined. Each symbol represents the mean lesion area in a single mouse. Photomicrographs illustrate macrophage abundance in aortic root sections from both groups of mice (magnification ×100). Nuclei are visualized in blue with DAPI staining. *, **, and *** indicate statistically significant differences between the 2 groups: $P<0.05$, $P<0.01$, and $P<0.0005$, respectively.

tissue from both groups of mice. Glomerular cellularity in *gld→Ldl-r*$^{-/-}$ mice was similar to that observed in *wt→Ldl-r*$^{-/-}$ mice (data not shown). Accordingly, urinary protein and serum and urine creatinine levels were unchanged (Table 1). Moreover, at the time of sacrifice, kidney weight to body M_rs did not reveal differences between the two groups of mice (Table 1). Collectively, these data argue for the absence of specific renal impairment in autoimmune *gld→Ldl-r*$^{-/-}$ mice.

TABLE 1. Autoimmune Parameters and Renal Function in *wt→Ldl-r*$^{-/-}$ and *gld→Ldl-r*$^{-/-}$ Mice After 12 Weeks of Diet

	wt→Ldl-r$^{-/-}$	*gld→Ldl-r*$^{-/-}$	*P*
Spleen/body wt, mg/g	3.8±0.8	7.5±1.5	<0.0001
Blood DNTC, % of T cells	8.3±1.8	19.0±6.9	<0.0005
Spleen DNTC, % of T cells	8.3±2.5	16.8±3.7	<0.05
Serum IgG, μg/mL	15.9±11.8	49.3±28.9	<0.002
Serum ANA, μg/mL	29.7±12.7	58.4±15.0	<0.0001
Serum dsDNA, ng/mL	7.2±3.5	35.3±26.0	<0.0001
Serum creatinine, μmol/L	29.6±1.3	30.3±1.1	NS
Urinary creatinine, mmol/L	7.7±0.1	7.2±0.6	NS
Urinary protein, g/L	7.6±0.7	6.5±2.6	NS
Kidney/body wt, mg/g	6.0±0.3	5.9±0.7	NS

Systemic Inflammatory Cytokines

As immunoinflammatory cytokines play a significant role in atherosclerosis progression, we performed an exhaustive analysis of systemic cytokine profile. Serum levels of cytokines including interleukin (IL)-12, IFNγ, IL-1β, IL-2, IL-4, and IL-6 were significantly decreased (up to 9-fold) in *gld→Ldl-r*$^{-/-}$ mice as compared with *wt→Ldl-r*$^{-/-}$ mice (supplemental Table II). No significant changes were observed for IL-10, IL-1α, GM-colony stimulating factor (CSF), and tumor necrosis factor (TNF)-α between the two groups. This particular profile observed in *gld→Ldl-r*$^{-/-}$ mice was not associated with changes in IL-12p35, IL-1β, IL-4, nor in TNF-α mRNA levels in the spleen of these mice as compared with *wt→Ldl-r*$^{-/-}$ mice (data not shown), thereby indicating that tissues other than spleen might contribute to the circulating cytokine pool.

Anti-MDA LDL Antibody Levels, IgG2a/IgG1 Ratio, and B Cell Activation in Autoimmune Mice

As levels of antibodies directed against oxidized-LDL are correlated with lesion size,[15] we sought to associate the serum titers of anti–MDA-LDL antibodies with the increased extent of lesions in *gld→Ldl-r*$^{-/-}$ mice. Thus, we observed significantly elevated titers of IgG and IgM to MDA-LDL in *gld→Ldl-r*$^{-/-}$ mice (Figure 2A and 2B, respectively). Next, as an indicator of Th1 versus Th2 polarization, we measured the serum IgG2a to IgG1 ratio. As this ratio is similar in *wt→Ldl-r*$^{-/-}$ and *gld→Ldl-r*$^{-/-}$ mice, it revealed no bias toward a Th1 or a Th2 response (Figure 2C). Finally, B cell activation was revealed by a significant increase in the proportion of CD86-positive cells among the B cell population of *gld→Ldl-r*$^{-/-}$ mice as compared with controls (Figure 2D).

Activation of CD4 T Cells and Accumulation in Atherosclerotic Plaques

CD4-positive T cells are key players in both atherosclerosis and autoimmunity, and therefore we analyzed both their activation status and presence in atherosclerotic plaques. Analysis of splenic CD4 T cells demonstrated that *gld→Ldl-r*$^{-/-}$ mice displayed increased proportions of both activated CD69-positive T cells (Figure 3A, $P<0.005$) and memory CD44-positive T cells (Figure 3B, $P<0.005$); by contrast there was no change in regulatory CD25/Foxp3 double positive T cells (12.1±1.4 in *gld→Ldl-r*$^{-/-}$ mice versus 11.0±1.5 in *wt→Ldl-r*$^{-/-}$ control mice). The increase in the activated and memory phenotype of CD4 T cells observed in lupus-prone mice was associated with their increased accumulation within the lesions (Figure 3C, $P<0.05$).

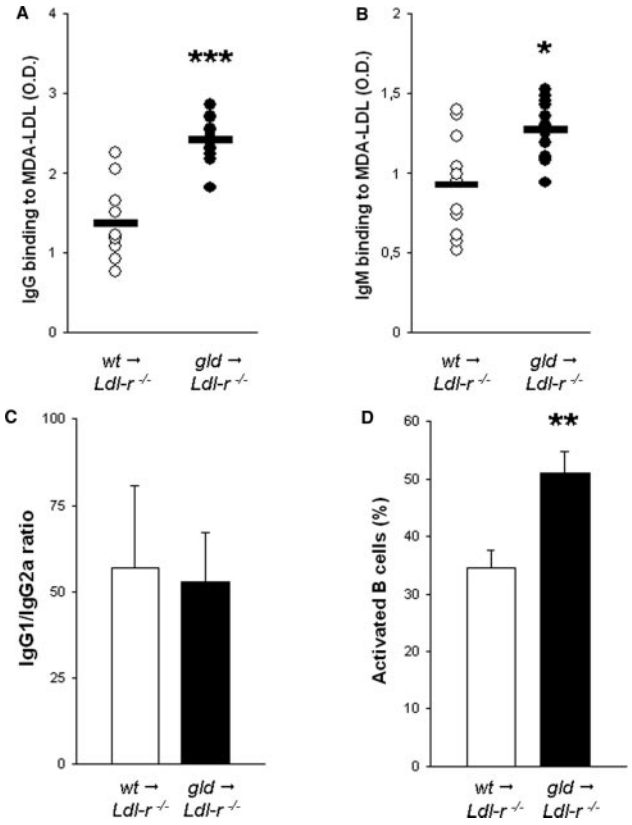

Figure 2. Increased anti–MDA-LDL antibody levels and B cell activation in autoimmune mice. Anti–MDA-LDL IgG (A) and IgM (B) levels were determined by ELISA in the serum of both *wt→Ldl-r*$^{-/-}$ and *gld→Ldl-r*$^{-/-}$ mice. The horizontal bar indicates the mean value from 12 animals per group. C, The IgG1 and IgG2a antibody subclass levels were determined by ELISA and the IgG1/IgG2a ratio is shown. Values represent the mean±SEM of 12 animals analyzed per group. D, Expression of the activation marker CD86 was determined on CD19-positive B cells by flow cytometry. *, **, and *** indicate statistically significant differences between the two groups: $P<0.05$, $P<0.005$, and $P<0.0001$, respectively.

Apoptotic Structures in Atherosclerotic Lesions

As defective apoptotic cell clearance is observed in lymphoid organs of autoimmune mice, we quantified the number of cells in terminal stages of apoptosis in the aortic sinus of both groups of mice. Late stage apoptotic cells and apoptotic bodies were stained by fluorescein isothiocyanate (FITC)-dUTP TUNEL whereas nuclei were counterstained with DAPI. Discrimination of apoptotic cells and apoptotic bodies by DAPI staining was based on nuclear size and morphology (normal or fragmented nuclei respectively). The frequencies of apoptotic cells and apoptotic bodies in aortic tissue were 15-fold and 3-fold higher in *gld→Ldl-r*$^{-/-}$ mice as compared with *wt→Ldl-r*$^{-/-}$ animals respectively (Figure 1B, $P<0.05$).

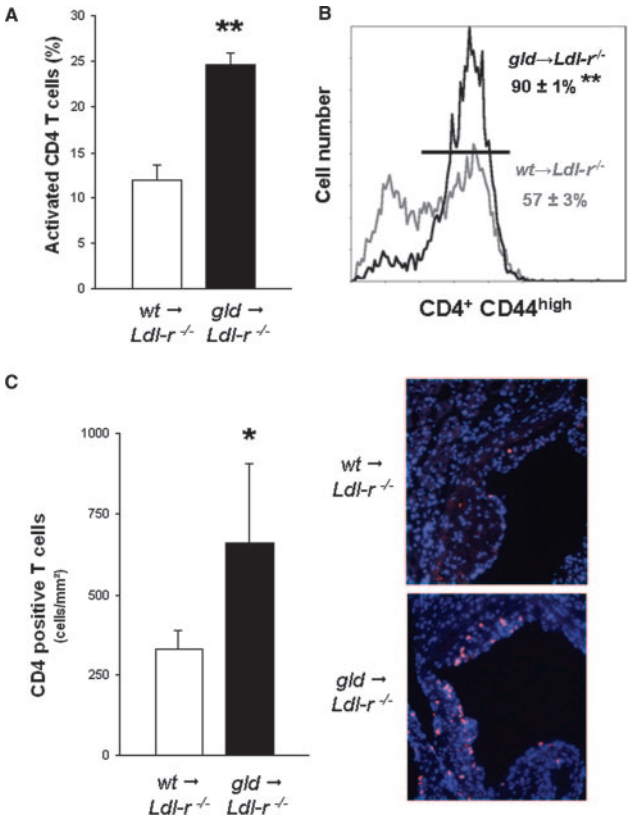

Figure 3. CD4 T cell activation and accumulation in atherosclerotic lesions. A, Expression of the activation marker CD69 was determined on CD4-positive T cells by flow cytometry. B, Expression of the memory marker CD44 was determined on CD4-positive T cells by flow cytometry. C, Atherosclerotic lesions were immunostained for the lymphocyte T CD4 antigen and the number of CD4 T cells per mm^2 was determined. Values represent the mean±SEM of 9 animals analyzed per group. Photomicrographs illustrate CD4 T cell abundance in aortic root sections from both groups of mice (magnification ×100). Nuclei are visualized in blue by DAPI staining. * and ** indicate statistically significant differences between the 2 groups: $P<0.05$ and $P<0.0001$, respectively.

Macrophage Accumulation and Recruitment of Monocytes in Atherosclerotic Lesions.

Aortic root sections from mice on the Western diet were stained with a macrophage-specific antibody directed against CD68. Quantitative analysis revealed a significant 2-fold increase in CD68-staining lesions of *gld→Ldl-r*$^{-/-}$ mice as compared with *wt→Ldl-r*$^{-/-}$ controls (Figure 1C, $P<0.01$). Macrophages were abundant in the subendothelial space of *gld→Ldl-r*$^{-/-}$ mice and constituted the majority of the cells in the lesion (Figure 1C). To further document macrophage accumulation in atherosclerotic lesions, we extracted mRNA from descending aortas of mice to perform quantitative real-time PCR. Levels of mRNA for CD68 and F4/80 were significantly elevated (2- and 4-fold respectively) in the arch and abdominal areas of the aorta in *gld→Ldl-r*$^{-/-}$ mice as compared with *wt→Ldl-r*$^{-/-}$ controls (Table 2). To investigate the potential molecular mechanisms underlying macrophage accumulation, we next evaluated expression of adhesion molecules and chemokines in the descending aorta. As shown in Table 2, the expression levels of MCP-1, P-selectin, and intercellular adhesion molecule-1 (ICAM-1) mRNA were significantly increased (3.5-, 1.5-, and 2.5-fold, respectively) in *gld→Ldl-r*$^{-/-}$ mice as compared with their *wt→Ldl-r*$^{-/-}$ controls, while the levels of vascular cell adhesion molecule (VCAM)-1 and CX3CL1 mRNA were comparable in both groups (Table 2). Concomitantly, we observed that expression of the monocyte-associated genes CD115, CD11b, and CCR2 was elevated (1.5-, 2.5-, and 4-fold, respectively) in *gld→Ldl-r*$^{-/-}$ aortas as compared with their *wt→Ldl-r*$^{-/-}$ controls, whereas CX3CR1 expression was also increased but did not reach statistical significance (Table 2).

TABLE 2. Gene Expression Profile in the Arterial Wall of *wt→Ldl-r*$^{-/-}$ and *gld→Ldl-r*$^{-/-}$ Mice After 12 Weeks of Diet

	wt→Ldl-r$^{-/-}$	*gld→Ldl-r*$^{-/-}$	*P*
MCP-1	2416±1430	8699±5526	<0.05
ICAM-1	843±202	1281±364	<0.05
VCAM-1	1209±297	2184±894	NS
P-selectin	212±89	560±233	<0.005
CX3CL1	185±72	158±73	NS
CCR2	500±162	1934±1443	<0.05
CX3CR1	712±471	1742±1252	NS
CD11b	87±52	217±152	<0.05
CD115	121±44	203±73	<0.05
F4/80	83±28	314±114	<0.05

Discussion

We have developed a new animal model susceptible to concomitant development of SLE and atherogenesis. SLE prone-mice exhibited accelerated progression of atherosclerosis, although plasma lipid levels, lipoprotein-cholesterol distribution, and renal function were similar to wild-type controls. Aortic lesions in autoimmune mice were characterized by accumulation of apoptotic cells, consistent with the defective apoptotic cell clearance associated with SLE.[16] In addition, enhanced immune system activation, arterial inflammation, and recruitment of both lymphocytes and monocytes were prominent aspects of accelerated atherosclerosis in *gld→Ldl-r*$^{-/-}$ lupus-prone animals. These data extend our comprehension of the mechanisms that can contribute to accelerated atherosclerosis in lupus patients as observed in prospective cohorts.[3,4]

Chronic renal dysfunction associated with glomerulonephritis develops in the course of lupus.[8,17] In addition, several studies have provided evidence that renal dysfunction promotes atherosclerosis in mice,[10,11] but equally represents an independent risk factor for atherogenesis in man.[12] However, as we did not observe renal dysfunction within the time frame of our study (creatinine levels and proteinuria were unchanged in *gld→Ldl-r*$^{-/-}$ mice), this mechanism does not appear to account for the accelerated atherosclerosis observed in our murine model.

Another prominent feature of autoimmunity in SLE patients concerns abnormal T and B-cell responses manifested by their activation status and the dysregulation in systemic cytokine profile.[18] In our mouse SLE model, serum levels of IL-12, IFN-γ (Th1 cytokines), IL-4 (Th2 cytokine), IL-1β,

IL-6 (inflammatory cytokines), and the T-cell growth factor IL-2 were significantly decreased whereas those of IL-10, TNF-α, and GM-CSF remained unchanged. These findings are consistent with clinical investigations in SLE patients, in which attenuated expression of IL-12,[19,20,21] IFN-γ,[19,22] IL-4,[19] and IL-2[22] have been documented. Similarly, in the lupus-prone autoimmune strain NZB/WF1, IL-12, IL-1, IL-2, IL-4, and IL-6 cytokine levels were decreased, whereas those of the antiinflammatory cytokine IL-10 and the proinflammatory cytokine TNF-α[18,23,24] were unchanged as equally observed in our model. Overall, the impact of reduced cytokine levels (ie, Th1 and inflammatory cytokines) might appear primarily antiatherogenic. Indeed, in mouse models of atherosclerosis, substantial data support a proatherogenic role for IFN-γ,[25,26] IL-12,[27,28] IL-4,[27,29] and IL-1β[30], whereas IL-10 plays an antiatherogenic role.[31]

Surprisingly, we observed an enhanced activation of the immune system consistent with increased B and T cell activation, increased memory phenotype of CD4 T cells, and concomitant elevation of anti–MDA-LDL IgG and IgM levels in *gld*→*Ldl-r*$^{-/-}$ mice as compared with controls. Similar findings concerning T cell activation were reported in a recent study based on transplantation of bone marrow cells from congenic mice expressing a susceptibility locus for SLE in *Ldl-r*$^{-/-}$ mice.[17] In addition, it is important to note that the proportion of atheroprotective type 1 regulatory T cells did not differ between *gld*→*Ldl-r*$^{-/-}$ and *wt*→*Ldl-r*$^{-/-}$ mice. In our model, despite lower proinflammatory cytokine levels, we report higher activation of both B and T cells. These results are not contradictory as a diminished threshold of activation for both T and B cells could favor the onset of autoimmunity. These defects appear to be key players in the accelerated atherosclerosis typical of lupus. In this setting, the elevated degree of CD4 T cell activation, and memory status in *gld*→*Ldl-r*$^{-/-}$ mice, which is associated with increased lesional T cell numbers could accelerate atherogenesis and is consistent with a highly inflammatory plaque phenotype.

Marked accumulation of apoptotic cells and bodies occurred in aortic sinus tissue of *gld*→*Ldl-r*$^{-/-}$ mice, thereby corroborating the observation that increased amounts of apoptotic material were deposited in the lymph nodes of *gld Apoe*$^{-/-}$ mice.[8] Several studies have demonstrated that the impaired clearance of apoptotic cells by macrophages is a feature of SLE,[16] and that a defective complement system may play an active role in this process.[32] However, we did not observe decreased mRNA expression of the main complement components C1q, C2, C3, and C4 in the liver of *gld*→*Ldl-r*$^{-/-}$ animals (data not shown). Additionally, the observed elevation in titers of autoantibodies to dsDNA and ANA directed against nuclear material suggest that elevated levels of circulating nucleosomes may occur in *gld*→*Ldl-r*$^{-/-}$ mice. Such nucleosomes may partly account for defective apoptotic cell clearance as suggested by Laderach and colleagues.[33] In this context, the accumulation of TUNEL-positive bodies in the aortic sinus is indicative of an ineffective clearance of primary apoptotic cells, ie, cells exposing phosphatidylserine in the outer plasma membrane leaflet, rather than the result of increased rates of apoptosis. Such defective apoptotic cell clearance observed in atherosclerotic lesions suggests that apoptotic cells evolve to necrotic cells, the latter triggering proinflammatory and immunostimulatory responses.[34,35] In turn, impaired clearance of dying cells may promote arterial inflammation and contribute to lesion development.[8,34,36]

In our model, plaque progression was potentiated by local inflammation in the arterial wall of *gld*→*Ldl-r*$^{-/-}$ mice as demonstrated by significant upregulation of mRNAs indicative of activation of endothelial cells (MCP-1, P-selectin, and VCAM-1) and macrophages (MCP-1) as compared with controls. This finding was associated with significantly elevated expression of mRNAs encoding genes associated with monocytes (CCR2, CD11b, and CD115) and macrophages (CD68 and F4/80) in the descending aorta of *gld*→*Ldl-r*$^{-/-}$ mice. Endothelial cell activation might be induced by elevated circulating IgG levels among which specific IgGs and/or specific immune complexes might interact with the endothelium to activate endothelial cells inducing endothelial dysfunction.[37,38,39,40] Elevated endothelial permeability typical of endothelium dysfunction facilitates enhanced lipoprotein access, retention, and deposition in the intimal space, a classical feature of fatty streak formation. In this setting, the adhesion molecules and chemokines whose expression is upregulated in the aortas of *gld*→*Ldl-r*$^{-/-}$ mice are known to be key players in the recruitment of monocytes into the subendothelial space, thus favoring lesion progression.[41,42] Indeed, increase in the expression of CD11b may reflect the entry of newly recruited monocytes,[9,14] thereby leading to the accumulation of macrophages in the arterial wall. However, we cannot exclude the possibility that macrophages with the *gld* mutation could display higher resistance to apoptosis, a feature equally reported in another mouse model for SLE,[43] and which, in turn, favors their accumulation in the aortic sinus of *gld*→*Ldl-r*$^{-/-}$ mice. Nevertheless, the similar proportions of splenic F4/80^{+} macrophages observed in *wt*→*Ldl-r*$^{-/-}$ and *gld*→*Ldl-r*$^{-/-}$ mice (4.8 ± 1.1 versus 3.3 ± 0.5%, respectively) suggest that the half life of *gld* macrophages is not affected and argues that higher resistance to apoptosis may not be operative in aortic lesions.

In our innovative *gld*→*Ldl-r*$^{-/-}$ mouse model, we provide new insight into the molecular mechanisms that may underlie accelerated atherosclerosis in autoimmune disease. Indeed, our experimental findings highlight enhanced activation of the immune system, aortic inflammation, and endothelial cell activation, together with lesional accumulation of apoptotic cells, macrophages, and CD4 T cells as being central to the development and progression of atherosclerosis in autoimmune mice. These findings may lead to development of innovative therapeutic strategies in SLE patients at high cardiovascular risk.

Acknowledgments

We are indebted to Dr B. Lelongt for technical assistance with renal morphology and Pr J.J. Mazeron and Dr G. Boisserie of the Radiotherapy Unit for advice with mouse irradiation.

Sources of Funding

This work was supported by INSERM and by an Award from The Fondation de France to P.L. E.G. was supported by a Fellowship from the Ministère de la Recherche and the Fondation pour la

Recherche Médicale. M.J.C. and P.L. gratefully acknowledge the award of a "Contrat d'Interface" by the Assistance Publique - Hôpitaux de Paris/INSERM.

Disclosures

None.

References

1. Urowitz MB, Bookman AA, Koehler BE, Gordon DA, Smythe HA, Ogryzlo MA. The bimodal mortality pattern of systemic lupus erythematosus. *Am J Med*. 1976;60:221–225.
2. Frostegard J. Atherosclerosis in patients with autoimmune disorders. *Arterioscler Thromb Vasc Biol*. 2005;25:1776–1785.
3. Roman MJ, Shanker BA, Davis A, Lockshin MD, Sammaritano L, Simantov R, Crow MK, Schwartz JE, Paget SA, Devereux RB, Salmon JE. Prevalence and correlates of accelerated atherosclerosis in systemic lupus erythematosus. *N Engl J Med*. 2003;349:2399–2406.
4. Asanuma Y, Oeser A, Shintani AK, Turner E, Olsen N, Fazio S, Linton MF, Raggi P, Stein CM. Premature coronary-artery atherosclerosis in systemic lupus erythematosus. *N Engl J Med*. 2003;349:2407–2415.
5. del Rincon I, O'Leary DH, Haas RW, Escalante A. Effect of glucocorticoids on the arteries in rheumatoid arthritis. *Arthritis Rheum*. 2004;50:3813–3822.
6. Liu K, Mohan C. What do mouse models teach us about human SLE? *Clin Immunol*. 2006;119:123–130.
7. Cohen PL, Eisenberg RA. Lpr and gld: single gene models of systemic autoimmunity and lymphoproliferative disease. *Annu Rev Immunol*. 1991;9:243–269.
8. Aprahamian T, Rifkin I, Bonegio R, Hugel B, Freyssinet JM, Sato K, Castellot JJ, Jr., Walsh K. Impaired clearance of apoptotic cells promotes synergy between atherogenesis and autoimmune disease. *J Exp Med*. 2004;199:1121–1131.
9. Grainger DJ, Reckless J, McKilligin E. Apolipoprotein E modulates clearance of apoptotic bodies in vitro and in vivo, resulting in a systemic proinflammatory state in apolipoprotein E-deficient mice. *J Immunol*. 2004;173:6366–6375.
10. Bro S, Bentzon JF, Falk E, Andersen CB, Olgaard K, Nielsen LB. Chronic renal failure accelerates atherogenesis in apolipoprotein E-deficient mice. *J Am Soc Nephrol*. 2003;14:2466–2474.
11. Ivanovski O, Szumilak D, Nguyen-Khoa T, Ruellan N, Phan O, Lacour B, Descamps-Latscha B, Drueke TB, Massy ZA. The antioxidant N-acetylcysteine prevents accelerated atherosclerosis in uremic apolipoprotein E knockout mice. *Kidney Int*. 2005;67:2288–2294.
12. Go AS, Chertow GM, Fan D, McCulloch CE, Hsu CY. Chronic kidney disease and the risks of death, cardiovascular events, and hospitalization. *N Engl J Med*. 2004;351:1296–1305.
13. Huby T, Doucet C, Dachet C, Ouzilleau B, Ueda Y, Afzal V, Rubin E, Chapman MJ, Lesnik P Knockdown expression and hepatic deficiency reveal an atheroprotective role for SR-BI in liver and peripheral tissues. *J Clin Invest*. 2006.
14. Lesnik P, Haskell CA, Charo IF. Decreased atherosclerosis in CX3CR1−/− mice reveals a role for fractalkine in atherogenesis. *J Clin Invest*. 2003;111:333–340.
15. Palinski W, Tangirala RK, Miller E, Young SG, Witztum JL. Increased autoantibody titers against epitopes of oxidized LDL in LDL receptor-deficient mice with increased atherosclerosis. *Arterioscler Thromb Vasc Biol*. 1995;15:1569–1576.
16. Munoz LE, Gaipl US, Franz S, Sheriff A, Voll RE, Kalden JR, Herrmann M. SLE–a disease of clearance deficiency? *Rheumatology (Oxford)*. 2005;44:1101–1107.
17. Stanic AK, Stein CM, Morgan AC, Fazio S, Linton MF, Wakeland EK, Olsen NJ, Major AS. Immune dysregulation accelerates atherosclerosis and modulates plaque composition in systemic lupus erythematosus. *Proc Natl Acad Sci U S A*. 2006;103:7018–7023.
18. Theofilopoulos AN, Lawson BR Tumour necrosis factor and other cytokines in murine lupus. *Ann Rheum Dis*. 1999;58 Suppl 1:I49–55.
19. Jones BM, Liu T, Wong RW. Reduced in vitro production of interferon-gamma, interleukin-4 and interleukin-12 and increased production of interleukin-6, interleukin-10 and tumour necrosis factor-alpha in systemic lupus erythematosus. Weak correlations of cytokine production with disease activity. *Autoimmunity* 1999;31:117–124.
20. Hagiwara E, Gourley MF, Lee S, Klinman DK. Disease severity in patients with systemic lupus erythematosus correlates with an increased ratio of interleukin-10:interferon-gamma-secreting cells in the peripheral blood. *Arthritis Rheum*. 1996;39:379–385.
21. Horwitz DA, Gray JD, Behrendsen SC, Kubin M, Rengaraju M, Ohtsuka K, Trinchieri G. Decreased production of interleukin-12 and other Th1-type cytokines in patients with recent-onset systemic lupus erythematosus. *Arthritis Rheum*. 1998;41:838–844.
22. Richaud-Patin Y, Alcocer-Varela J, Llorente L. High levels of TH2 cytokine gene expression in systemic lupus erythematosus. *Rev Invest Clin*. 1995;47:267–272.
23. Lin LC, Chen YC, Chou CC, Hsieh KH, Chiang BL. Dysregulation of T helper cell cytokines in autoimmune prone NZB x NZW F1 mice. *Scand J Immunol*. 1995;42:466–472.
24. Alleva DG, Kaser SB, Beller DI. Aberrant cytokine expression and autocrine regulation characterize macrophages from young MRL+/+ and NZB/W F1 lupus-prone mice. *J Immunol*. 1997;159:5610–5619.
25. Gupta S, Pablo AM, Jiang X, Wang N, Tall AR, Schindler C. IFN-gamma potentiates atherosclerosis in ApoE knock-out mice. *J Clin Invest*. 1997;99:2752–2761.
26. Buono C, Come CE, Stavrakis G, Maguire GF, Connelly PW, Lichtman AH. Influence of interferon-gamma on the extent and phenotype of diet-induced atherosclerosis in the LDLR-deficient mouse. *Arterioscler Thromb Vasc Biol*. 2003;23:454–460.
27. Davenport P, Tipping PG. The role of interleukin-4 and interleukin-12 in the progression of atherosclerosis in apolipoprotein E-deficient mice. *Am J Pathol*. 2003;163:1117–1125.
28. Hauer AD, Uyttenhove C, de Vos P, Stroobant V, Renauld JC, van Berkel TJ, van Snick J, Kuiper J. Blockade of interleukin-12 function by protein vaccination attenuates atherosclerosis. *Circulation*. 2005;112:1054–1062.
29. King VL, Szilvassy SJ, Daugherty A. Interleukin-4 deficiency decreases atherosclerotic lesion formation in a site-specific manner in female LDL receptor−/− mice. *Arterioscler Thromb Vasc Biol*. 2002;22:456–461.
30. Kirii H, Niwa T, Yamada Y, Wada H, Saito K, Iwakura Y, Asano M, Moriwaki H, Seishima M. Lack of interleukin-1beta decreases the severity of atherosclerosis in ApoE-deficient mice. *Arterioscler Thromb Vasc Biol*. 2003;23:656–660.
31. Mallat Z, Besnard S, Duriez M, Deleuze V, Emmanuel F, Bureau MF, Soubrier F, Esposito B, Duez H, Fievet C, Staels B, Duverger N, Scherman D, Tedgui A. Protective role of interleukin-10 in atherosclerosis. *Circ Res*. 1999;85:e17–24.
32. Manderson AP, Botto M, Walport MJ. The role of complement in the development of systemic lupus erythematosus. *Annu Rev Immunol*. 2004;22:431–456.
33. Laderach D, Bach JF, Koutouzov S. Nucleosomes inhibit phagocytosis of apoptotic thymocytes by peritoneal macrophages from MRL+/+ lupus-prone mice. *J Leukoc Biol*. 1998;64:774–780.
34. Tabas I. Consequences and therapeutic implications of macrophage apoptosis in atherosclerosis: the importance of lesion stage and phagocytic efficiency. *Arterioscler Thromb Vasc Biol*. 2005;25:2255–2264.
35. Albert ML. Death-defying immunity: do apoptotic cells influence antigen processing and presentation? *Nat Rev Immunol*. 2004;4:223–231.
36. Boisvert WA, Rose DM, Boullier A, Quehenberger O, Sydlaske A, Johnson KA, Curtiss LK, Terkeltaub R. Leukocyte transglutaminase 2 expression limits atherosclerotic lesion size. *Arterioscler Thromb Vasc Biol*. 2006;26:563–569.
37. Binstadt BA, Patel PR, Alencar H, Nigrovic PA, Lee DM, Mahmood U, Weissleder R, Mathis D, Benoist C. Particularities of the vasculature can promote the organ specificity of autoimmune attack. *Nat Immunol*. 2006;7:284–292.
38. Cho CS, Cho ML, Chen PP, Min SY, Hwang SY, Park KS, Kim WU, Min DJ, Min JK, Park SH, Kim HY. Antiphospholipid antibodies induce monocyte chemoattractant protein-1 in endothelial cells. *J Immunol*. 2002;168:4209–4215.
39. Papa ND, Raschi E, Moroni G, Panzeri P, Borghi MO, Ponticelli C, Tincani A, Balestrieri G, Meroni PL. Anti-endothelial cell IgG fractions from systemic lupus erythematosus patients bind to human endothelial cells and induce a pro-adhesive and a pro-inflammatory phenotype in vitro. *Lupus*. 1999;8:423–429.
40. Carvalho D, Savage CO, Isenberg D, Pearson JD. IgG anti-endothelial cell autoantibodies from patients with systemic lupus erythematosus or systemic vasculitis stimulate the release of two endothelial cell-derived mediators, which enhance adhesion molecule expression and leukocyte adhesion in an autocrine manner. *Arthritis Rheum*. 1999;42:631–640.
41. Libby P. Inflammation in atherosclerosis. *Nature*. 2002;420:868–874.
42. Hansson GK. Inflammation, atherosclerosis, and coronary artery disease. *N Engl J Med*. 2005;352:1685–1695.
43. Zhu J, Liu X, Xie C, Yan M, Yu Y, Sobel ES, Wakeland EK, Mohan C. T cell hyperactivity in lupus as a consequence of hyperstimulatory antigen-presenting cells. *J Clin Invest*. 2005;115:1869–1878.

Enhanced Dendritic Cell Survival Attenuates Lipopolysaccharide-Induced Immunosuppression and Increases Resistance to Lethal Endotoxic Shock[1]

Emmanuel L. Gautier,* Thierry Huby,*† Flora Saint-Charles,* Betty Ouzilleau,† M. John Chapman,*†‡ and Philippe Lesnik[2]*†‡

Impaired immune function and associated immunosuppression are hallmarks of septic syndromes. As part of an overall deactivation of the immune system, profound depletion of dendritic cells (DCs) occurs in both septic patients and septic mice. Such depletion of DCs is potentially associated with immunosuppression and with failure to induce a protective Th1 immune response; it may equally be predictive of fatal outcome in septic patients. To evaluate the impact of enhanced DC survival on LPS-induced immunosuppression and on survival after LPS-induced septic shock, we created a transgenic mouse model specifically overexpressing the human form of the antiapoptotic protein Bcl-2 in DCs (*DC-hBcl-2* mice). DCs derived from *DC-hBcl-2* mice exhibited higher resistance to maturation-induced apoptosis after LPS treatment both in vitro and in vivo. Moreover, prolongation of DC survival diminished sublethal LPS-induced DC loss and immunosuppression, with maintenance of the differentiation potential of Th1 cells and enhanced T cell activation. Such modulation of the immune response appears to constitute a key feature of the attenuated mortality observed after LPS-induced shock in *DC-hBcl-2* mice. Our study therefore identifies DC death as a key determinant of endotoxin-induced immunosuppression and mortality in mice. *The Journal of Immunology,* **2008, 180: 6941–6946.**

Impaired immune function and associated immunosuppression are hallmarks of septic syndromes, a major cause of mortality in intensive care units. As part of such an overall deactivation of the immune system, profound depletion of dendritic cells (DCs)[3] occurs in both septic patients (1, 2) and septic mice (3–5). In a similar manner, nonlethal LPS challenge reduced DC numbers in vivo (6). Under such conditions, depletion of DCs involves apoptotic cell death and may play a role in the pathogenesis of sepsis. As proposed recently, depletion of DCs is potentially associated with immunosuppression, failure to induce a protective Th1 immune response (5), and may be predictive of fatal outcome in septic patients (2).

As the antiapoptotic protein Bcl-2 is a key regulator of DC lifespan and immunogenicity (7, 8), we created a transgenic mouse model specifically overexpressing the human form of Bcl-2 in DCs. The impact of increased DC survival in response to LPS-induced immunosuppression and on survival after LPS-induced septic shock was then evaluated in this animal model.

Materials and Methods

Transgenic mice

hBcl-2 cDNA from pORF-hBcl-2 (Invivogen) was cloned downstream of the mouse DC-specific promoter CD11c (up to −821 bp from the ATG codon) amplified from a mouse BAC clone (BACPAC Resources). The linearized transgenic construct was injected into C57BL/6 fertilized female pronuclei, and progeny positive for the transgene were crossed to C57BL/6 mice. Of the three founders obtained, one animal gave germline transmission. Mice were used for experiments at 6–8 wk of age. All animal procedures were performed with accreditation from the French government and under strict compliance with Animal Welfare Regulations.

Mouse genotyping

Mice overexpressing hBcl-2 under the control of the CD11c promoter (*DC-hBcl-2* mice) were genotyped using the following primers: forward, 5′-GGCCACAAGTGAAGTCAACA-3′ and reverse, 5′-GGGGGAAAAC AACCCTATTC-3′. The amplicon size was 475 bp.

The PCR amplification cycle was as follows: 30 s at 94°C, 30 s at 54°C, and 30 s at 72°C for 30 cycles.

Generation of bone marrow-derived dendritic cells (BMDCs)

BMDCs were generated as described previously (9, 10). Briefly, at day 0, bone marrow cells were seeded at 2×10^6 per 100 mm dish in 10 ml complete R10 medium (RPMI 1640 supplemented with penicillin (100 U/ml), streptomycin (100 μg/ml), L-glutamine (2 mM), 2-ME (50 μM), 10% heat-inactivated FCS and 20 ng/ml mGM-CSF or 200 ng/ml fms-like tyrosine kinase 3 ligand (Flt3-L)). At day 3, another 10 ml R10 medium was added to the plates. At days 6 and 8, half of the culture supernatant volume was collected and centrifuged. Subsequently, the cell pellet was resuspended in 10 ml fresh R10 medium and transferred back to the original plate. Cells were used at day 10.

Survival assay

BMDCs were plated in 24-well plates at 2.10^5 cells/ml in complete medium containing 20 ng/ml mGM-CSF and then stimulated with LPS alone (100 ng/ml) or in combination with IFN-γ (20 ng/ml). After 72 h, numbers of dead BMDCs were determined by propidium iodide (PI) staining and

*Institut National de la Santé et de la Recherche Médicale, Unité Mixte de Recherche S551, Dyslipoproteinemia and Atherosclerosis Research Unit, Hôpital de la Pitié, Paris; †Université Pierre and Marie Curie-Université de Paris, Unité Mixte de Recherche S551, Paris; and ‡Assistance Publique-Hôpital de Paris, Groupe Hospitalier Pitié-Salpêtrière, Service d'Endocrinologie-Métabolisme, Paris, France

Received for publication May 10, 2007. Accepted for publication March 14, 2008.

The costs of publication of this article were defrayed in part by the payment of page charges. This article must therefore be hereby marked *advertisement* in accordance with 18 U.S.C. Section 1734 solely to indicate this fact.

[1] E.L.G. was supported by a Fellowship from the Ministère de la Recherche and the Fondation pour la Recherche Médicale. This work was supported by Institut National de la Santé et de la Recherche Médicale and by an Award from the Fondation de France to P.L. M.J.C. and P.L. are the recipients of a Contrat d'Interface from the Assistance Publique-Hôpitaux de Paris/ Institut National de la Santé et de la Recherche Médicale.

[2] Address correspondence and reprint requests to Dr. Philippe Lesnik, INSERM U551, Hôpital de la Pitié, 83 Bd de l'hôpital, 75651 Paris 13, France. E-mail address: lesnik@chups.jussieu.fr

[3] Abbreviations used in this paper: DC, dendritic cell; BMDC, bone marrow-derived dendritic cell; Flt3-L, fms-like tyrosine kinase 3 ligand; PI, propidium iodide; WT, wild type.

Table I. *Serum cytokine concentration following nonlethal LPS injection*[a]

	WT	*DC-hBcl-2*	*p*
IL-1α	1.6 ± 0.3	1.7 ± 0.2	NS
IL-1β	1.3 ± 0.2	1.3 ± 0.2	NS
IL-2	2.2 ± 0.3	2.0 ± 0.3	NS
IL-4	5.0 ± 0.9	4.8 ± 0.5	NS
IL-6	1.1 ± 0.2	1.3 ± 0.1	NS
IL-10	1.4 ± 0.2	1.2 ± 0.1	NS
IL-12	0.9 ± 0.1	0.9 ± 0.1	NS
IFN-γ	8.3 ± 1.3	8.3 ± 1.1	NS
TNF-α	0.7 ± 0.2	0.5 ± 0.2	NS
GM-CSF	0.6 ± 0.1	0.5 ± 0.1	NS

[a] Serum cytokine levels are expressed as ng/mL.

analyzed by flow cytometry. In a second experiment, BMDCs were both serum- and Flt3-L-deprived for 24 to 72 h and apoptosis was analyzed by PI staining and flow cytometry analysis.

Mice were injected i.v. with LPS (25 μg/mouse) and apoptosis of DCs was analyzed by flow cytometry 18 h later, as described earlier (11). Briefly, splenocytes were recovered and stained with an anti-CD11c Ab and Annexin V FITC to determine the percentage of apoptotic DCs.

In vivo LPS treatment

To induce nonlethal systemic inflammation, mice were injected i.v. with LPS (25 μg/mouse). Lethal endotoxic shock was induced in 8-wk-old mice of both genotypes by i.p. injection of LPS (40 mg/kg; *Escherichia coli* serotype 055.B5; Sigma-Aldrich) and the mice were monitored for 5 days.

Flow cytometry

Splenocytes were harvested, minced, and filtered through a 70-μm cell strainer. RBCs were lysed by ammonium chloride treatment (ACK) and cells were resuspended in PBS/1% BSA/0.01% sodium azide, preincubated for 5 min with Fc blocker (BD Pharmingen), and incubated for 30 min at 4°C with Abs directed against CD45 (clone 30F11, Miltenyi Biotec), CD3 (clone 145-2C11, BD Pharmingen), CD4 (clone GK1.5, Miltenyi Biotec), F4/80 (clone Cl:A3-1, Serotec), CD19 (clone 6D5, eBioscience), CD11c (clone N418, Miltenyi Biotec and BD Pharmingen), CD86 (clone GL1, eBioscience), CD69 (clone H1.2F3, eBioscience), and/or hBcl-2 (clone 6C8, BD Pharmingen) to analyze lymphocyte subpopulations and lymphocyte activation.

Cells were analyzed on a Coulter EPICS XL flow cytometer (Beckman Coulter) using EPICS XL32 software.

In vitro splenocyte restimulation

Mice were injected i.v. with LPS (25 μg/mouse) and splenocytes were harvested 48 h later. Splenocytes (5×10^5 cells/well) were then restimulated by LPS (100 ng/ml) for 48 h. Cell supernatants were recovered and analyzed for IL-12p40, IFN-γ, and IL-4 using specific ELISA kits (eBioscience).

Serum cytokine profile

The serum concentrations of IL-1α, IL-1β, IL-2, IL-4, IL-6, IL-10, IL-12p70, GM-CSF, IFN-γ, and TNF-α were determined using the ProteoPlex murine cytokine array kit (Novagen) according to the manufacturer's instructions.

Analysis of gene expression by quantitative PCR

RNAs were prepared using TRIzol reagent (Invitrogen) from frozen tissue specimens isolated from mice at sacrifice. Each RNA preparation was hybridized with random hexamer (Promega) and reverse-transcribed using Moloney murine leukemia virus reverse transcriptase (Invitrogen). Real-time quantitative PCR was performed using a LightCycler PCR system (Roche) as previously described (12). The specific primers are described in Table I. All reactions were performed in duplicate or triplicate and hypoxanthine phosphoribosyltransferase (HPRT) was used as a housekeeping gene to account for variability in the initial quantities of cDNA. In all PCR assays and for each primer set, expression of a control cDNA (pool of reverse-transcribed RNA prepared from different mouse tissues) was included and used as an interrun calibrator. Expression data were based on the crossing points calculated from the LightCycler analytical software and corrected for PCR efficiencies of both the target and the reference gene.

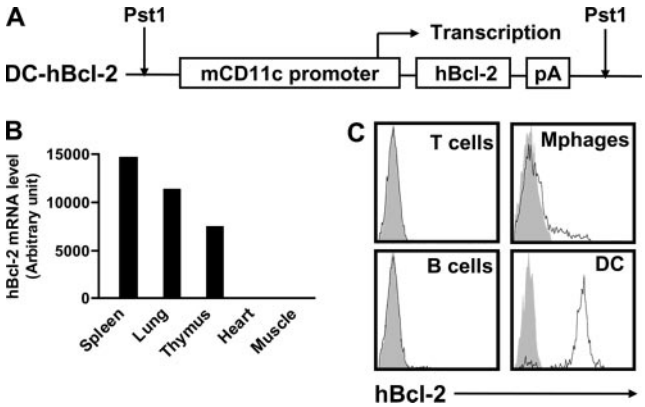

FIGURE 1. Transgene structure and specific expression of hBcl-2 in DCs of *DC-hBcl-2* mice. *A*, Structure of the DC-hBcl-2 transgene with the mouse CD11c promoter, hBcl2 cDNA, and a poly(A) tail (pA) from the EF1 cDNA. *B*, hBcl-2 mRNA expression was determined by quantitative PCR in tissues from WT (open bars, undetectable levels) and *DC-hBcl-2* mice (filled bars). *C*, Intracellular staining of hBcl-2 in spleen T cells, B cells, macrophages, and DCs from WT and *DC-hBcl-2* mice. The shaded profile represents WT mice and the open profile *DC-hBcl-2* mice.

Statistical analysis

Values are expressed as means ± SEM. The statistical significance of the differences between groups was evaluated using two-tailed Student's *t* tests for unpaired comparisons. Survival data were analyzed using the Kaplan-Meier test. $p < 0.05$ was considered significant.

Results

Generation and characterization of transgenic mice

Transgenic mice were generated by injection of a construct containing the human Bcl-2 cDNA under the DC-specific murine CD11c promoter into pronuclei of C57BL/6 ovocytes (Fig. 1*A*). Of the three founders obtained, one transmitted the transgene to its progeny, which were termed *DC-hBcl-2* mice.

To evaluate the expression of hBcl-2, we performed real-time quantitative PCR analysis on organs containing DCs (spleen, lung, and thymus) and on control tissues known to be devoid of DCs under normal conditions (heart and muscle) from both *DC-hBcl-2* and control mice. Significant expression of hBcl-2 was observed in spleen, lung, and thymus of *DC-hBcl-2* mice only, whereas hBcl-2 cDNA was undetectable in both heart and muscle of *DC-hBcl-2* and control mice (Fig. 1*B*). To demonstrate protein expression of hBcl-2, we prepared BMDCs from *DC-hBcl-2* and control mice and assessed the presence of hBcl-2 by intracellular staining and flow cytometry. Such staining revealed specific expression of hBcl-2 in BMDCs derived from *DC-hBcl-2* mice (data not shown). To demonstrate specificity of transgene expression in DCs, we performed double staining of splenocytes of *DC-hBcl-2* and control mice with an anti-hBcl-2 Ab and either a DC marker (CD11c), a B cell marker (CD19), a T cell marker (CD3), or a macrophage marker (F4/80). As shown in Fig. 1*C*, hBcl-2 expression was restricted to the DC population of *DC-hBcl-2* mice. Moreover, as expected, confocal microscopy revealed that *hBcl-2* protein colocalized with its characteristic subcellular compartments (i.e., mitochondria and endoplasmic reticulum; data not shown).

Increased survival of DCs from DC-hBcl-2 mice

As Bcl-2 is a key regulator of the mitochondrial death pathway, we hypothesized that *DC-hBcl-2*-derived BMDCs might exhibit higher survival capacity and resistance to apoptosis than those derived from their wild-type (WT) controls. First, to specifically challenge the mitochondrial apoptotic pathway, BMDCs derived from both *DC-hBcl-2* and WT mice were serum- and GM-CSF-deprived for 24, 48,

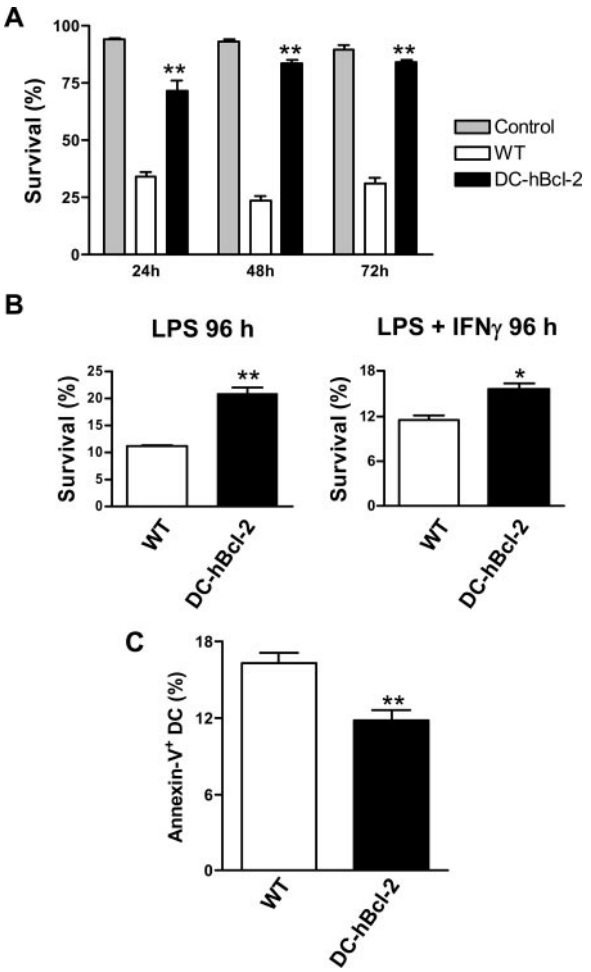

FIGURE 2. BMDCs derived from *DC-hBcl-2* mice exhibited higher resistance to apoptosis in vitro. *A*, BMDCs derived from WT and *DC-hBcl-2* mice were submitted to serum and growth factor deprivation for 24, 48, and 72 h, and survival was determined by Annexin V/PI staining. Controls are BMDCs derived from WT mice grown in complete medium containing serum and growth factors. *B*, BMDCs derived from WT and *DC-hBcl-2* mice were activated by LPS (100 ng/ml) or LPS (100 ng/ml) + IFN-γ (20 ng/ml), and survival was assessed 96 h after stimulation and evaluated by PI staining. *C*, Apoptosis of spleen DCs ($CD11c^{high}$) was determined by flow cytometry 18 h after nonlethal LPS injection. * and ** indicate statistically significant differences between the two groups: $p < 0.05$ and $p < 0.01$, respectively.

and 72 h. Annexin V/PI staining revealed ~2-fold, 4-fold, and 3-fold increase in the proportion of viable cells in transgenic BMDCs as compared with controls after 24, 48, and 72 h, respectively (Fig. 2*A*). As Bcl-2 has been proposed to confer resistance against apoptosis induced by DC activators such as LPS (8) or LPS + IFN-γ (13), BMDCs were incubated with LPS or LPS + IFN-γ and survival was analyzed 96 h after activation. After LPS and LPS + IFN-γ stimulation, BMDCs derived from *DC-hBcl-2* mice exhibited enhanced survival (90% and 40%, respectively) as compared with control BMDCs (Fig. 2*B*). To validate these results in vivo, we injected mice with LPS and measured apoptosis of DCs 18 h later as previously described (11). As shown in Fig. 2*C*, DCs from *DC-hBcl-2* mice were 40% more resistant to LPS-induced apoptosis than were DCs from control mice.

DCs accumulate in DC-hBcl-2 mice and enhance T cell activation

As we demonstrated that BMDCs derived from *DC-hBcl-2* mice display increased survival in vitro, we evaluated the potential impact of enhanced DC survival on DC homeostasis in vivo. Flow cytometry analysis of spleen DCs revealed their significant expansion (Fig. 3*A*, 1.6-fold increase, $p < 0.05$) in *DC-hBcl-2* mice as compared with WT controls. In light of the role of DCs as T cell response inducers, we analyzed T cell activation in both *DC-hBcl-2* and WT mice. A marked increase in the activation marker CD69 was found among CD3 T cells ($p < 0.01$) and CD4 T cells ($p < 0.001$) in *DC-hBcl-2* mice as compared with nontransgenic controls (Fig. 3, *B* and *C*, respectively).

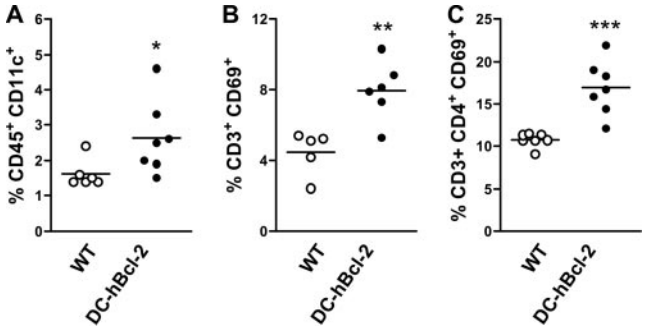

FIGURE 3. *DC-hBcl-2* mice exhibited greater DC abundance and enhanced T cell activation. *A*, DC ($CD45^+CD11c^{high}$) content in spleen from WT and *DC-hBcl-2* mice was determined by flow cytometry. *B*, Activated $CD69^+$ T cells in the spleens of WT and *DC-hBcl-2* mice. *C*, Activated $CD69^+$ CD4 T cells in the spleens of WT and *DC-hBcl-2* mice. *, **, and *** indicate statistically significant differences between the two groups: $p < 0.05$, $p < 0.01$, and $p < 0.001$, respectively.

Attenuated DC loss in DC-hBcl-2 mice after nonlethal LPS injection enhanced T and B cell activation

Injection of a nonlethal dose of LPS has been previously associated with induction of DC apoptosis (11, 14) and subsequent loss of DCs 48 h after injection (6, 14, 15). Such treatment mimics DC loss and immunosuppression observed in severe septic shock. In this setting, *DC-hBcl-2* mice and their WT controls were injected i.v. with 25 μg LPS (1.25 μg/g), and the impact on spleen DC content and T cell activation was evaluated 48 h later. Two days after nonlethal LPS injection, we observed a 2.8-fold increase in the DC population in *DC-hBcl-2* mice as compared with controls (Fig. 4*A*, $p < 0.01$). Such a marked increase in the DC population in *DC-hBcl-2* mice vs WT mice is greater than that observed in the basal state (Fig. 3*A*, 1.6-fold increase, $p < 0.05$). As compared with the basal state, DC loss after nonlethal LPS injection in WT and *DC-hBcl-2* mice was 65% and 35%, respectively (Fig. 4*A*). Under these conditions, such attenuated loss of DC in *DC-hBcl-2* mice was associated with a greater proportion of activated CD3 T cells (Fig. 4*B*, $p < 0.005$) and CD19 B cells (Fig. 4*C*, $p < 0.05$). Independently of mouse genotype, DC content was highly correlated with the proportion of activated T cells (Fig. 4*D*, $r = 0.85$, $p < 0.005$) and moderately associated with B cell activation (data not shown, $r = 0.37$, $p < 0.05$). Moreover, consistent with these results, we observed that splenocytes from *DC-hBcl-2* mice exhibited a higher proliferation rate as compared with controls 48 h after in vitro restimulation of splenoyte with LPS (data not shown).

Attenuated DC loss in DC-hBcl-2 mice is without effect on the systemic cytokine profile after nonlethal LPS injection

DCs possess the capacity to produce a wide range of immunomodulatory cytokines and to drive lymphocyte cytokine expression. The impact of the attenuated loss of DCs following LPS treatment on systemic cytokine profile was therefore assessed in *DC-hBcl-2* and WT mice 48 h after injection. As shown in Table

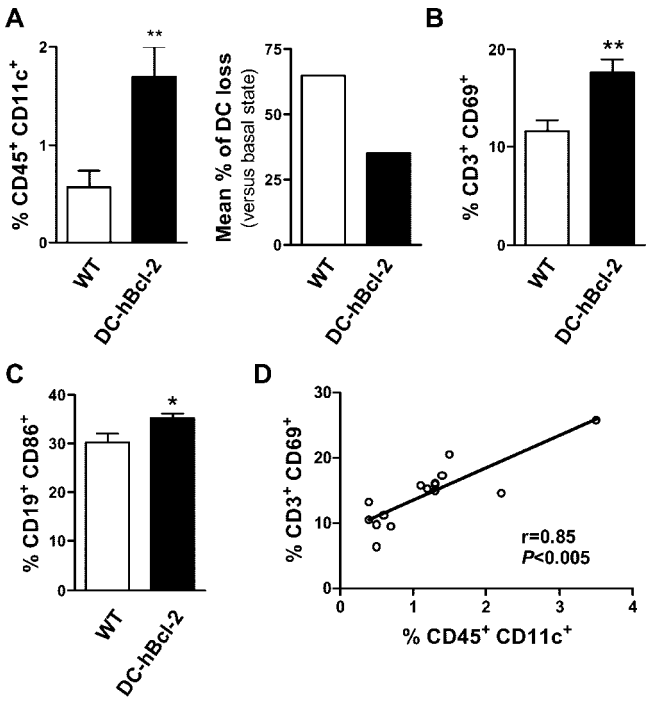

FIGURE 4. Attenuated DC loss and enhanced T and B cell activation in *DC-hBcl-2* mice after nonlethal LPS injection. *A*, DC ($CD45^+CD11c^{high}$) content in spleen from WT and *DC-hBcl-2* mice after nonlethal LPS injection was determined by flow cytometry. The percentage of DC loss after nonlethal LPS injection as compared with basal state was reported for WT and *DC-hBcl-2* mice. *B*, Activated $CD69^+$ T cells in the spleens of WT and *DC-hBcl-2* mice after nonlethal LPS injection. *C*, Activated $CD86^+$ B cells in the spleens of WT and *DC-hBcl-2* mice after nonlethal LPS injection. *D*, Correlation between DC content and activated T cells in spleens of WT and *DC-hBcl-2* mice. * and ** indicate statistically significant differences between the two groups: $p < 0.05$ and $p < 0.01$, respectively.

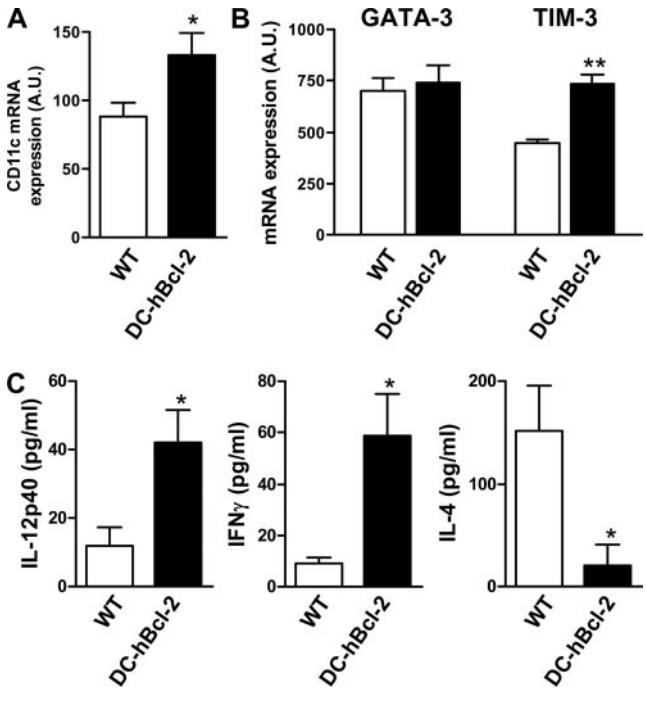

FIGURE 5. Attenuated DC loss and Th1 polarization in the spleens of *DC-hBcl-2* mice after nonlethal LPS injection. *A*, mRNA expression of the DC marker CD11c was evaluated by quantitative PCR in spleens from WT and *DC-hBcl-2* mice after nonlethal LPS injection. *B*, mRNA expression of the transcription factors GATA-3 and TIM-3, which are known to promote Th2 and Th1 development, respectively, by quantitative PCR in spleen from WT and *DC-hBcl-2* mice after nonlethal LPS injection. *C*, Cytokine secretion after splenocyte restimulation by LPS was measured in 48-h supernatants. * and ** indicate statistically significant differences between the two groups: $p < 0.05$ and $p < 0.001$, respectively.

I, no differences in the plasma concentrations of IL-1α, IL-1β, IL-2, IL-4, IL-6, IL-10, IL-12p70, GM-CSF, IFN-γ, and TNF-α were found between *DC-hBcl-2* mice and their WT controls 48 h after nonlethal LPS injection.

Attenuated DC loss is associated with increased immunostimulatory cytokine expression in spleens of DC-hBcl-2 mice after nonlethal LPS injection

We next determined the impact of the attenuated loss of DCs observed in *DC-hBcl-2* mice on immune polarization and cytokine mRNA expression. First, we confirmed that DC content was greater in the spleen of *DC-hBcl-2* mice, as the mRNA coding for the DC-specific marker CD11c was elevated in splenic tissue as compared with that in WT controls (Fig. 5*A*, $p < 0.05$). We next analyzed the expression of two transcription factors, GATA-3 and TIM-3, which are known to promote Th2 and Th1 development, respectively. mRNA quantification using quantitative PCR revealed no difference in GATA-3 expression (Fig. 5*B*), whereas TIM-3 mRNA levels were increased by 60% in spleens of *DC-hBcl-2* mice as compared with controls (Fig. 5*B*, $p < 0.001$). Such Th1 polarization in *DC-hBcl-2* mice is consistent with significant increase in mRNA levels coding for the costimulatory molecule CD86 and the immunostimulatory cytokines IL-12p40, IL-15, and IL-23 as compared with controls (Table II). Additionally, a trend toward increased IL-18 mRNA expression in transgenic mice was observed (Table II). Consistent with both enhanced T cell activation and elevated levels of mRNA coding for immunostimulatory cytokine in *DC-hBcl-2* mice, we observed enhanced IFN-γ mRNA expression in these mice as compared with WT controls (+75%, Table II). To corroborate these data, splenocytes were recovered from both *DC-hBcl-2* and control mice 48 h after nonlethal LPS injection, restimulated in vitro with LPS, and cell supernatants were analyzed for cytokine production. As compared with controls, production of the Th1 cytokines IL-12p40 and IFN-γ was increased, whereas the secretion of the Th2 cytokine IL-4 was decreased in *DC-hBcl-2* splenocyte supernatants (Fig. 5*C*). These data were consistent with the gene expression profile obtained in spleen, and they are in accordance with a Th1 bias and decreased immunosupression after nonlethal LPS injection.

DC-hBcl-2 mice display higher resistance to lethal endotoxic shock

LPS injection is an established surrogate for Gram-negative bacteria-induced septic shock. In this setting, we injected lethal doses of LPS (i.e., 40 mg/kg) to induce septic shock in both *DC-hBcl-2*

Table II. *mRNA expression levels of immunostimulatory cytokines in spleens of WT and* DC-hBcl-2 *mice after nonlethal LPS injection*

mRNA Expression (AU)[a]	WT	*DC-hBcl-2*	*p*
CD86	80 ± 6	97 ± 11	<0.05
IL-12p40	27 ± 12	61 ± 12	<0.01
IL-15	218 ± 42	386 ± 48	<0.001
IL-18	115 ± 14	132 ± 11	0.06
IL-23p19	108 ± 32	335 ± 150	<0.05
IFN-γ	79 ± 18	138 ± 18	<0.01

[a] AU indicates arbitrary units.

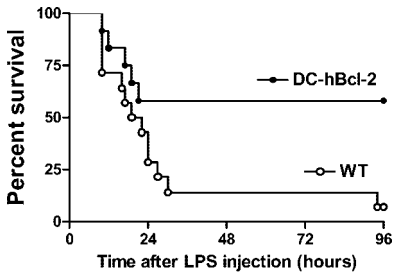

FIGURE 6. Overexpression of hBcl-2 in DCs improves survival after LPS-induced endotoxic shock. Transgenic mice overexpressing the anti-apoptotic protein hBcl-2, under the DC-specific promoter CD11c, underwent LPS-induced septic shock and their survival was monitored for 96 h. Mice overexpressing hBcl-2 displayed a statistically significant improvement in survival as compared with WT controls, $p = 0.02$.

and WT mice and subsequently monitored their survival for 96 h. Transgenic mice overexpressing hBcl-2 in DCs exhibited a marked improvement in survival after LPS-induced septic shock as compared with their WT controls. After 4 days, survival rate was 58% and 7% for *DC-hBcl-2* and WT mice, respectively (Fig. 6, $p = 0.02$).

Discussion

At present, the treatment of septic shock is not optimal, notably due to incomplete knowledge of the dysregulation of the immune system that leads to organ injury and subsequent mortality. The role of DCs in septic shock has recently been highlighted by the fact that these cells are profoundly depleted in both septic mice (3–5) and patients (1, 2). Herein, we provide evidence that enhanced DC survival diminished nonlethal LPS-induced DC loss and immunosuppression, with maintainance of Th1 differentiation potential and enhanced T cell activation, thereby accounting for the decreased mortality observed after LPS-induced septic shock.

It is now well documented that extensive apoptosis of leukocytes, including T lymphocytes and DCs, occurs upon sepsis and endotoxic shock, and thus it may contribute to the immune suppression characteristic of these disorders (16). Indeed, modulation of DC survival in mice has been shown to influence their immunogenicity (7, 8, 17, 18). Herein, we revealed that under basal conditions, mice overexpressing hBcl-2 in DCs (*DC-hBcl-2* mice) presented an accumulation of DCs in their spleens in association with increased T cell activation. Moreover, after nonlethal LPS shock, Bcl-2 regulated DC survival after maturation and led both to accumulation of DCs and to enhanced T and B cell activation. These observations are consistent with the established function of DCs in regulating both T and B cell responses. The elevated DC content in *DC-hBcl-2* mice after nonlethal LPS shock was associated with a Th1 polarization as assessed by increased TIM-3 expression in the spleen, with no change in levels of GATA-3 mRNA. Th1 responses are characterized by IFN-γ secretion, a cytokine primarily produced by activated T cells, and that is associated with enhanced resistance to lethal septic shock in mice (19–21). In this setting, septic shock-associated DC depletion may lead to decreased T cell activation and IFN-γ production, and subsequently to increased mortality. Consistent with this hypothesis, we observed that *DC-hBcl-2* mice exhibited higher IFN-γ expression and production than did their controls after nonlethal LPS challenge, thereby suggesting that these mice are more immunocompetent as compared with control mice. Moreover, induction of tolerance in mice by nonlethal LPS injection was associated with immunosuppression characterized by suppressed IFN-γ secretion (22). In this latter study, induction of tolerance by LPS may arise from DC loss and suppression of IL-12 production, as observed in a similar model by Wysocka and colleagues (23). The role of IL-12 expression in DCs is well established and is known to drive Th1 cell differentiation and activation. With respect to this central role for IL-12, immunosuppression after LPS challenge or other types of infection has been shown to be essentially due to decreased IL-12p40 production by DCs (20, 23, 24). In this context, increased IL-12p40 expression and production in the spleens of *DC-hBcl-2* mice provide a rationale for decreased immunosuppression after LPS challenge in our transgenic mouse model. This hypothesis is further corroborated by the finding that mRNA levels coding for the immunostimulatory cytokines IL-15 and IL-23p19 were elevated in the spleens of *DC-hBcl-2* mice as compared with controls. Moreover, we observed that the production of the prototypic Th2 cytokine IL-4 by *DC-hBcl-2* splenocytes was decreased following restimulation in vitro as compared with controls. Considered together, *DC-hBcl-2* mice exhibited decreased LPS-associated DC loss, which led to increased mRNA levels of the immunostimulatory cytokines IL-12p40, IL-15, IL-23p19, and IFN-γ; in turn, these cytokines enhanced T and B cell activation. Our results are concordant with recent findings highlighting the fact that IL-12p40-deficient mice show reduced survival rates after septic shock, primarily due to defective IFN-γ production (20). Moreover, IL-15 is necessary for mature DC survival in mice (13). Consequently, IL-15-deficient mice are characterized by decreased DC numbers in blood and spleen, and transgenic overexpression of IL-15 in IL-15-deficient mice restores DC numbers (13). Under these conditions, IL-15 overexpression in mice is associated with enhanced survival following *E. coli*-induced septic shock (25). In this context, Flt3-L treatment, which enhances differentiation and mobilization of DCs, has been shown to suppress endotoxin-induced immunosuppression (26).

Consistent with the decreased immunosuppression observed in our transgenic model following nonlethal LPS injection, we demonstrated that *DC-hBcl-2* mice exhibited marked improvement in survival after LPS-induced septic shock as compared with their WT controls. It is therefore relevant that depletion of DCs has recently been associated with increased mortality following septic shock (27); however, the mechanisms underlying the protective potential of DCs have not been addressed. Consistent with findings in the present study, Scumpia and colleagues found no differences in plasma cytokine concentrations (27). DCs may not dramatically impact the circulating cytokine pool; in contrast, however, maintenance of DC numbers together with their immunostimulatory properties maintains Th1 potential differentiation, IFN-γ production, and confers protection against septic shock. As maintenance of the potential of the immune system by enhancing T lymphocyte survival (19, 28, 29) appears to attenuate septic shock-associated immunosuppression and mortality in mice, we hypothesize therefore that such benefit may be partly mediated by DCs, as they may regulate T cell survival (30–33), and notably through enhanced MHC class II/TCR interactions (30, 34, 35).

Additionally, as shown by the study of Hotchkiss et al. (36), adoptive transfer of apoptotic cells, which exerts antiinflammatory/immunosuppressive effects, has been shown to decrease survival in sepsis. In this context, we can hypothesize that *hBcl-2* expression in DCs may protect mice from overt immunosuppression by reduction in the production of apoptotic DCs. Hotchkiss et al. equally demonstrated that the diminished survival of mice associated with adoptive transfer of apoptotic cells was associated with a decreased production of IFN-γ and a slight increase in IL-4 levels, thereby indicating a shift toward a Th2 response (36). Our *DC-hBcl-2* mice model mirrors this phenotype with maintenance of a Th1 propensity that is associated with increased survival; indeed, these findings are consitent with the studies of Bommhardt

et al. (19) in a transgenic model of Akt overexpression in T cells, and equally with the work of Moreno et al. (20) in which IL-12$^{-/-}$ and IFN-$\gamma^{-/-}$ mice showed higher susceptibility to sepsis. We cannot however exclude the possibility that DCs from *DC-hBcl2* mice may have exhibited tolerogenic properties, as splenic IL-10 expression and splenocyte production of IL-10 is increased in *DC-hBcl-2* mice as compared with controls (data not shown). In this way, *DC-hBcl2* mice may have afforded protection against endotoxin-induced cell death via IL-10, as demonstrated by the studies of Oberholzer at al. and of Fujita et al. (37, 38). Additionally, elevated numbers of DCs in all tissues can provide a source both of endotoxin-binding and of endotoxin-degrading proteins such as CD14, MD-2-TLR4-complex, and the LPS-detoxifying enzyme acyloxyacyl hydrolase, respectively (39).

In conclusion, we provide evidence that enhancement of DC survival is associated with decreased immunosuppression following nonlethal LPS injection as assessed by increased immunostimulatory cytokine expression and enhanced T and B cell activation. In a model of LPS-induced septic shock, these findings are associated with increased survival. Our present study therefore identifies the DC as a key player in endotoxin-induced immunosuppression and mortality in mice.

Disclosures

The authors have no financial conflicts of interest.

References

1. Hotchkiss, R. S., K. W. Tinsley, P. E. Swanson, M. H. Grayson, D. F. Osborne, T. H. Wagner, J. P. Cobb, C. Coopersmith, and I. E. Karl. 2002. Depletion of dendritic cells, but not macrophages, in patients with sepsis. *J. Immunol.* 168: 2493–2500.
2. Guisset, O., M. S. Dilhuydy, R. Thiebaut, J. Lefevre, F. Camou, A. Sarrat, C. Gabinski, J. F. Moreau, and P. Blanco. 2007. Decrease in circulating dendritic cells predicts fatal outcome in septic shock. *Intensive Care Med.* 33: 148–152.
3. Tinsley, K. W., M. H. Grayson, P. E. Swanson, A. M. Drewry, K. C. Chang, I. E. Karl, and R. S. Hotchkiss. 2003. Sepsis induces apoptosis and profound depletion of splenic interdigitating and follicular dendritic cells. *J. Immunol.* 171: 909–914.
4. Efron, P. A., A. Martins, D. Minnich, K. Tinsley, R. Ungaro, F. R. Bahjat, R. Hotchkiss, M. Clare-Salzler, and L. L. Moldawer. 2004. Characterization of the systemic loss of dendritic cells in murine lymph nodes during polymicrobial sepsis. *J. Immunol.* 173: 3035–3043.
5. Flohe, S. B., H. Agrawal, D. Schmitz, M. Gertz, S. Flohe, and F. U. Schade. 2006. Dendritic cells during polymicrobial sepsis rapidly mature but fail to initiate a protective Th1-type immune response. *J. Leukocyte Biol.* 79: 473–481.
6. De Smedt, T., B. Pajak, E. Muraille, L. Lespagnard, E. Heinen, P. De Baetselier, J. Urbain, O. Leo, and M. Moser. 1996. Regulation of dendritic cell numbers and maturation by lipopolysaccharide in vivo. *J. Exp. Med.* 184: 1413–1424.
7. Nopora, A., and T. Brocker. 2002. Bcl-2 controls dendritic cell longevity in vivo. *J. Immunol.* 169: 3006–3014.
8. Hou, W. S., and L. Van Parijs. 2004. A Bcl-2-dependent molecular timer regulates the lifespan and immunogenicity of dendritic cells. *Nat. Immunol.* 5: 583–589.
9. Lutz, M. B., N. Kukutsch, A. L. Ogilvie, S. Rossner, F. Koch, N. Romani, and G. Schuler. 1999. An advanced culture method for generating large quantities of highly pure dendritic cells from mouse bone marrow. *J. Immunol. Methods* 223: 77–92.
10. Brasel, K., T. De Smedt, J. L. Smith, and C. R. Maliszewski. 2000. Generation of murine dendritic cells from flt3-ligand-supplemented bone marrow cultures. *Blood* 96: 3029–3039.
11. Reis e Sousa, C., G. Yap, O. Schulz, N. Rogers, M. Schito, J. Aliberti, S. Hieny, and A. Sher. 1999. Paralysis of dendritic cell IL-12 production by microbial products prevents infection-induced immunopathology. *Immunity* 11: 637–647.
12. Huby, T., C. Doucet, C. Dachet, B. Ouzilleau, Y. Ueda, V. Afzal, E. Rubin, M. J. Chapman, and P. Lesnik. 2006. Knockdown expression and hepatic deficiency reveal an atheroprotective role for SR-BI in liver and peripheral tissues. *J. Clin. Invest.* 116: 2767–2776.
13. Dubois, S. P., T. A. Waldmann, and J. R. Muller. 2005. Survival adjustment of mature dendritic cells by IL-15. *Proc. Natl. Acad. Sci. USA* 102: 8662–8667.
14. De Smedt, T., B. Pajak, G. G. Klaus, R. J. Noelle, J. Urbain, O. Leo, and M. Moser. 1998. Antigen-specific T lymphocytes regulate lipopolysaccharide-induced apoptosis of dendritic cells in vivo. *J. Immunol.* 161: 4476–4479.
15. Roake, J. A., A. S. Rao, P. J. Morris, C. P. Larsen, D. F. Hankins, and J. M. Austyn. 1995. Dendritic cell loss from nonlymphoid tissues after systemic administration of lipopolysaccharide, tumor necrosis factor, and interleukin 1. *J. Exp. Med.* 181: 2237–2247.
16. Hotchkiss, R. S., and D. W. Nicholson. 2006. Apoptosis and caspases regulate death and inflammation in sepsis. *Nat. Rev. Immunol.* 6: 813–822.
17. Chen, M., Y. H. Wang, Y. Wang, L. Huang, H. Sandoval, Y. J. Liu, and J. Wang. 2006. Dendritic cell apoptosis in the maintenance of immune tolerance. *Science* 311: 1160–1164.
18. Park, D., N. Lapteva, M. Seethammagari, K. M. Slawin, and D. M. Spencer. 2006. An essential role for Akt1 in dendritic cell function and tumor immunotherapy. *Nat. Biotechnol.* 24: 1581–1590.
19. Bommhardt, U., K. C. Chang, P. E. Swanson, T. H. Wagner, K. W. Tinsley, I. E. Karl, and R. S. Hotchkiss. 2004. Akt decreases lymphocyte apoptosis and improves survival in sepsis. *J. Immunol.* 172: 7583–7591.
20. Moreno, S. E., J. C. Alves-Filho, T. M. Alfaya, J. S. da Silva, S. H. Ferreira, and F. Y. Liew. 2006. IL-12, but not IL-18, is critical to neutrophil activation and resistance to polymicrobial sepsis induced by cecal ligation and puncture. *J. Immunol.* 177: 3218–3224.
21. Saleh, M., J. C. Mathison, M. K. Wolinski, S. J. Bensinger, P. Fitzgerald, N. Droin, R. J. Ulevitch, D. R. Green, and D. W. Nicholson. 2006. Enhanced bacterial clearance and sepsis resistance in caspase-12-deficient mice. *Nature* 440: 1064–1068.
22. Varma, T. K., T. E. Toliver-Kinsky, C. Y. Lin, A. P. Koutrouvelis, J. E. Nichols, and E. R. Sherwood. 2001. Cellular mechanisms that cause suppressed gamma interferon secretion in endotoxin-tolerant mice. *Infect. Immun.* 69: 5249–5263.
23. Wysocka, M., S. Robertson, H. Riemann, J. Caamano, C. Hunter, A. Mackiewicz, L. J. Montaner, G. Trinchieri, and C. L. Karp. 2001. IL-12 suppression during experimental endotoxin tolerance: dendritic cell loss and macrophage hyporesponsiveness. *J. Immunol.* 166: 7504–7513.
24. Liu, C. H., Y. T. Fan, A. Dias, L. Esper, R. A. Corn, A. Bafica, F. S. Machado, and J. Aliberti. 2006. Cutting edge: Dendritic cells are essential for in vivo IL-12 production and development of resistance against *Toxoplasma gondii* infection in mice. *J. Immunol.* 177: 31–35.
25. Hiromatsu, T., T. Yajima, T. Matsuguchi, H. Nishimura, W. Wajjwalku, T. Arai, Y. Nimura, and Y. Yoshikai. 2003. Overexpression of interleukin-15 protects against *Escherichia coli*-induced shock accompanied by inhibition of tumor necrosis factor-alpha-induced apoptosis. *J. Infect. Dis.* 187: 1442–1451.
26. Wysocka, M., L. J. Montaner, and C. L. Karp. 2005. Flt3 ligand treatment reverses endotoxin tolerance-related immunoparalysis. *J. Immunol.* 174: 7398–7402.
27. Scumpia, P. O., P. F. McAuliffe, K. A. O'Malley, R. Ungaro, T. Uchida, T. Matsumoto, D. G. Remick, M. J. Clare-Salzler, L. L. Moldawer, and P. A. Efron. 2005. CD11c^{+} dendritic cells are required for survival in murine polymicrobial sepsis. *J. Immunol.* 175: 3282–3286.
28. Hotchkiss, R. S., P. E. Swanson, C. M. Knudson, K. C. Chang, J. P. Cobb, D. F. Osborne, K. M. Zollner, T. G. Buchman, S. J. Korsmeyer, and I. E. Karl. 1999. Overexpression of Bcl-2 in transgenic mice decreases apoptosis and improves survival in sepsis. *J. Immunol.* 162: 4148–4156.
29. Hotchkiss, R. S., K. C. Chang, P. E. Swanson, K. W. Tinsley, J. J. Hui, P. Klender, S. Xanthoudakis, S. Roy, C. Black, E. Grimm, et al. 2000. Caspase inhibitors improve survival in sepsis: a critical role of the lymphocyte. *Nat. Immunol.* 1: 496–501.
30. Brocker, T. 1997. Survival of mature CD4 T lymphocytes is dependent on major histocompatibility complex class II-expressing dendritic cells. *J. Exp. Med.* 186: 1223–1232.
31. Martin, B., C. Bourgeois, N. Dautigny, and B. Lucas. 2003. On the role of MHC class II molecules in the survival and lymphopenia-induced proliferation of peripheral CD4^{+} T cells. *Proc. Natl. Acad. Sci. USA* 100: 6021–6026.
32. Bauer, A., A. Villunger, V. Labi, S. F. Fischer, A. Strasser, H. Wagner, R. M. Schmid, and G. Hacker. 2006. The NF-κB regulator Bcl-3 and the BH3-only proteins Bim and Puma control the death of activated T cells. *Proc. Natl. Acad. Sci. USA* 103: 10979–10984.
33. Zaft, T., A. Sapoznikov, R. Krauthgamer, D. R. Littman, and S. Jung. 2005. CD11c^{high} dendritic cell ablation impairs lymphopenia-driven proliferation of naive and memory CD8^{+} T cells. *J. Immunol.* 175: 6428–6435.
34. Kirberg, J., H. von Boehmer, T. Brocker, H. R. Rodewald, and S. Takeda. 2001. Class II essential for CD4 survival. *Nat. Immunol.* 2: 136–137.
35. Zhu, J., X. Liu, C. Xie, M. Yan, Y. Yu, E. S. Sobel, E. K. Wakeland, and C. Mohan. 2005. T cell hyperactivity in lupus as a consequence of hyperstimulatory antigen-presenting cells. *J. Clin. Invest.* 115: 1869–1878.
36. Hotchkiss, R. S., K. C. Chang, M. H. Grayson, K. W. Tinsley, B. S. Dunne, C. G. Davis, D. F. Osborne, and I. E. Karl. 2003. Adoptive transfer of apoptotic splenocytes worsens survival, whereas adoptive transfer of necrotic splenocytes improves survival in sepsis. *Proc. Natl. Acad. Sci. USA* 100: 6724–6729.
37. Oberholzer, A., C. Oberholzer, K. S. Bahjat, R. Ungaro, C. L. Tannahill, M. Murday, F. R. Bahjat, Z. Abouhamze, V. Tsai, D. LaFace, et al. 2002. Increased survival in sepsis by in vivo adenovirus-induced expression of IL-10 in dendritic cells. *J. Immunol.* 168: 3412–3418.
38. Fujita, S., K. Seino, K. Sato, Y. Sato, K. Eizumi, N. Yamashita, M. Taniguchi, and K. Sato. 2006. Regulatory dendritic cells act as regulators of acute lethal systemic inflammatory response. *Blood* 107: 3656–3664.
39. Lu, M., M. Zhang, R. L. Kitchens, S. Fosmire, A. Takashima, and R. S. Munford. 2003. Stimulus-dependent deacylation of bacterial lipopolysaccharide by dendritic cells. *J. Exp. Med.* 197: 1745–1754.

Macrophage Apoptosis Exerts Divergent Effects on Atherogenesis as a Function of Lesion Stage

Emmanuel L. Gautier, PhD; Thierry Huby, PhD; Joseph L. Witztum, MD; Betty Ouzilleau, BS; Elizabeth R. Miller, BS; Flora Saint-Charles, MSc; Pierre Aucouturier, PhD; M. John Chapman, PhD; Philippe Lesnik, PhD

Background—Because apoptotic cell clearance appears to be defective in advanced compared with early atherosclerotic plaques, macrophage apoptosis may differentially affect plaque progression as a function of lesion stage.

Methods and Results—We first evaluated the impact of targeted protection of macrophages against apoptosis at both early and advanced stages of atherosclerosis. Increased resistance of macrophages to apoptosis in early atherosclerotic lesions was associated with increased plaque burden; in contrast, it afforded protection against progression to advanced lesions. Conversely, sustained induction of apoptosis in lesional macrophages of advanced lesions resulted in a significant increase in lesion size. Such enhanced lesion size occurred as a result not only of apoptotic cell accumulation but also of elevated chemokine expression and subsequent intimal recruitment of circulating monocytes.

Conclusions—Considered together, our data suggest that macrophage apoptosis is atheroprotective in fatty streak lesions, but in contrast, defective clearance of apoptotic debris in advanced lesions favors arterial wall inflammation and enhanced recruitment of monocytes, leading to enhanced atherogenesis. (***Circulation*. 2009;119:1795-1804.)**

Key Words: atherosclerosis ■ cholesterol ■ inflammation ■ leukocytes ■ macrophages ■ pathology ■ survival

Atherosclerosis is an inflammatory vascular disease characterized by the intimal accumulation of macrophage foam cells, cell death, and chronic arterial inflammation.[1] Macrophage apoptosis has been identified as a prominent feature of atherosclerotic plaques because macrophage cell death is believed to support necrotic core growth. The apoptotic process is controlled by intracellular levels of proapoptotic and antiapoptotic proteins such as those of the *Bcl-2* family. Indeed, the relative expression of proapoptotic (eg, *Bax* and *Bak*) and antiapoptotic proteins (eg, *Bcl-2* and *Bcl-xL*) of the *Bcl-2* family determines the overall sensitivity of the cell to apoptotic stimuli. In macrophages of atherosclerotic lesions, the proapoptotic *Bax* and *Bak* proteins predominate, whereas the antiapoptotic *Bcl-2* and *Bcl-xL* are deficient,[2,3] thereby arguing for their enhanced susceptibility to apoptosis. However, the impact of macrophage apoptosis on plaque progression remains to be specifically investigated.

Clinical Perspective p 1804

Recent studies have shed light on the potential impact of apoptosis on atherosclerotic lesion progression. Indeed, disruption of either the proapoptotic molecule *Bax* in bone marrow–derived cells[4] or the antiapoptotic factor *AIM*[5] has revealed that apoptosis attenuates early plaque formation. However, because apoptotic cells accumulate preferentially in advanced rather than in early lesions,[6,7] macrophage apoptosis may differentially affect plaque progression as a function of lesion stage.[8] In addition, apoptotic cell clearance appears to be defective in advanced lesions but efficient in early ones.[9] Moreover, apoptotic cells may possess proinflammatory properties, in part as a result of the presence of oxidized phospholipids (oxPLs) at their surface,[10,11] which are known triggers of inflammatory responses in arterial tissues.[12] In this setting, studies of mice in which components of the apoptotic cell clearance machinery have been deleted[13] or of lupus-prone mice characterized by ineffective apoptotic cell clearance[14] have revealed that defective apoptotic cell clearance is associated with enhanced atherosclerotic plaque progression.

To understand the impact of macrophage apoptosis on atherosclerosis at both early and advanced stages of lesion progression, we first used a transgenic approach allowing specific protection of macrophages against apoptosis (*CD68-hBcl-2* mice). With this approach, we demonstrated that macrophage apoptosis was antiatherogenic during the early stages of atherosclerosis, whereas macrophage cell death accelerated plaque progression in more advanced lesions. To mirror this effect, we applied a complementary approach based on sustained induction of lesional macrophage apopto-

Received July 11, 2008; accepted February 2, 2009.

From INSERM UMR-S939, Hôpital de la Pitié (E.L.G., T.H., B.O., F.S.-C., M.J.C., P.L.), UPMC University Paris (E.L.G., T.H., B.O., F.S.-C., P.A., M.J.C., P.L.), AP-HP, Groupe Hospitalier Pitié-Salpêtrière, Service d'Endocrinologie-Métabolisme (T.H., M.J.C., P.L.), and INSERM UMR S 938, Hôpital St-Antoine (P.A.), Paris, France, and Department of Medicine, University of California San Diego, La Jolla (J.L.W., E.R.M.).

The online-only Data Supplement is available with this article at http://circ.ahajournals.org/cgi/content/full/CIRCULATIONAHA.108.806158/DC1.

Correspondence to Dr Philippe Lesnik, INSERM U939, Hôpital de la Pitié, 83 Bd de l'hôpital, 75651 Paris 13, France. E-mail philippe.lesnik@upmc.fr

Circulation **is available at http://circ.ahajournals.org** **DOI: 10.1161/CIRCULATIONAHA.108.806158**

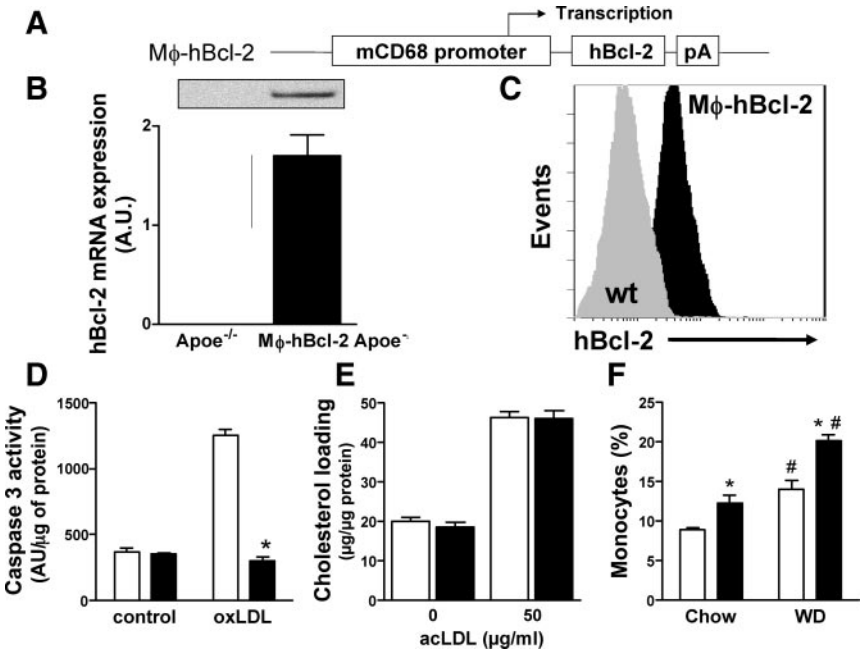

Figure 1. Transgene structure and characterization of *Mø-hBcl-2* mice. A, Structure of the *Mø-hBcl-2* transgene with the mouse CD68 promoter, *hBcl2* cDNA, and a polyA tail (pA) from the EF1 cDNA. B, *hBcl-2* mRNA expression was determined by quantitative polymerase chain reaction in resident peritoneal macrophages from wild-type and *Mø-hBcl-2* mice. C, Intracellular staining of hBcl-2 in peritoneal macrophages from wild-type and *Mø-hBcl-2* mice. The gray profile represents wild-type mice; black profile, *Mø-hBcl-2* mice. D, Bone marrow–derived macrophages from wild-type and *Mø-hBcl-2* mice incubated with acetylated LDL (acLDL) for 48 hours; cholesterol accumulation was measured to assess foam cell formation (E). F, The percentage of circulating monocytes in *Apoe*$^{-/-}$ and *Mø-hBcl-2 Apoe*$^{-/-}$ mice was determined by flow cytometry in mice fed a chow diet or a WD for 4 weeks. *Statistically significant difference between the 2 groups, $P<0.01$. #Statistically significant difference between chow- and WD-fed mice, $P<0.002$.

sis in *CD11c-DTR* transgenic mice and demonstrated that apoptotic cell accumulation in advanced lesions enhances plaque progression. Finally, short-term induction of macrophage apoptosis provided evidence that apoptotic cell accumulation in advanced atherosclerotic lesions promotes inflammatory gene expression, circulating monocyte recruitment, and accumulation of newly recruited macrophages.

Methods

Transgenic Animals and Atherosclerosis Studies Design

Transgenic mice overexpressing the antiapoptotic protein hBcl-2 in macrophages (*Mø-hBcl-2* mice) were generated using homologous recombination in embryonic stem cells to produce a single-copy transgene insertion at the hypoxanthine phosphoribosyl transferase (*Hprt*) locus located on the X chromosome. The transgene consists of the human *hBcl-2* cDNA from pORF-*hBcl-2* (InvivoGen, San Diego, Calif) cloned downstream of the mouse macrophage-specific promoter CD68 from pDRIVE-mCD68 (Invivogen). *Mø-hBcl-2* and *Apoe*$^{-/-}$ mice were crossed to obtain *Apoe*$^{-/-}$ and *Mø-hBcl-2 Apoe*$^{-/-}$ mice, and littermates were used for all experiments. Because the *Hprt* locus is located on the X chromosome, all experiments were performed with male littermates to avoid the potential variability of transgene expression related to random inactivation of the X chromosome in females. At 6 weeks of age, mice were fed a Western diet (WD; 0.15% cholesterol and 20% saturated fat) for 5 or 15 weeks.

Apoe$^{-/-}$ and *CD11c-DTR-GFP*[15] mice on the C57BL/6J background were obtained from Charles River Laboratories (Wilmington, Mass) and the European Mouse Mutant Archive (Centre National de la Recherche Scientifique, Centre de Distribution, de Typage et d'Archivage animal, Orléans, France), respectively, and crossed to obtain *CD11c-DTR Apoe*$^{-/-}$ mice. To evaluate the impact of sustained induction of macrophage apoptosis in atherosclerotic plaques, *Apoe*$^{-/-}$ mice (8 weeks old) were lethally irradiated, transplanted with 3×10^6 bone marrow cells from *CD11c-DTR Apoe*$^{-/-}$ mice, and fed a WD after a 4-week recovery period. After 5 weeks of WD feeding, mice were injected with either diphtheria toxin (DT; 4 ng/g; Sigma, St Louis, Mo) or PBS every 10 days for 50 days and killed 48 hours after the last injection. To study the impact of short-term induction of lesional macrophage apoptosis, 6-week-old *Apoe*$^{-/-}$ and *CD11c-DTR Apoe*$^{-/-}$ mice were fed a WD for 8 weeks to develop atherosclerotic lesions, injected intravenously with DT (4 ng/g) or vehicle, and killed 48 hours later. All animal procedures were performed with accreditation from the French government and under strict compliance with animal welfare regulations.

Plasma Lipid Analyses, Quantification of Atherosclerotic Plaques, Immunohistochemistry, Terminal Deoxynucleotidyl Transferase-Mediated dUTP-Biotin Nick-End Label Staining, Analysis of Gene Expression by Quantitative Polymerase Chain Reaction, and Flow Cytometry

All these procedures were performed as previously described[14,16] (see the Methods section in the online-only Data Supplement).

Quantification of Anti–Malondialdehyde-Modified Low-Density Lipoprotein, Anti–Oxidized Low-Density Lipoprotein, E06 Antibodies, and Serum-Oxidized Phospholipids

Antibody titers to oxidation-specific epitopes of malondialdehyde-modified (MDA) low-density lipoprotein (LDL) or copper-oxidized LDL (oxLDL) and T15 clonotypic (E06) natural antibodies were determined as described.[17]

Labeling of Blood Monocytes and Recruitment Assays

Monocyte labeling was performed as previously described.[18] To assess the recruitment of blood monocytes, 6-week-old *Apoe*$^{-/-}$ and *CD11c-DTR Apoe*$^{-/-}$ mice were fed a WD for 8 weeks, injected intravenously with 200 ng DT or vehicle and 250 μL of yellow green beads, and killed 48 hours later.

Statistical Analysis

Statistical calculations were performed with GraphPad Prism, version 4.03. Results were analyzed by Student unpaired *t* tests with the Welch correction if variances were unequal or Mann–Whitney *U* test as indicated in the figure legends. The statistical significance of the differences between >2 groups was compared by ANOVA followed by the Newman-Keuls multiple-comparison test. Values of $P<0.05$ were considered significant.

Table 1. Lipid Levels and Body Weights of *Apoe*$^{-/-}$ and *Mø-hBcl2 Apoe*$^{-/-}$ Mice After 5 and 15 Weeks of WE

	Apoe$^{-/-}$	*Mø-hBcl2 Apoe*$^{-/-}$	*P*
WD for 5 wk			
Total cholesterol, mg/dL	889.0±32.2	878.5±38.2	NS
Free cholesterol, mg/dL	271.1±15.5	260.6±11.4	NS
Triglycerides, mg/dL	156.8±25.6	149.4±15.3	NS
Free cholesterol/total cholesterol, %	30.5±1.4	29.8±1.0	NS
Body weight, g	23.7±1.1	24.3±0.4	NS
WD for 15 wk			
Total cholesterol, mg/dL	926.8±57.5	944.1±49.1	NS
Free cholesterol, mg/dL	302.7±32.0	289.0±21.7	NS
Triglyceride, mg/dL	132.7±26.2	131.0±14.7	NS
Free cholesterol/total cholesterol, %	32.1±1.9	30.4±0.9	NS
Body weight, g	28.6±0.7	27.6±1.0	NS

NS indicates not significant.

The authors had full access to and take full responsibility for the integrity of the data. All authors have read and agree to the manuscript as written.

Results

Generation and Characterization of *Mø-hBcl-2* Mice

To selectively overexpress *hBcl-2* cDNA in macrophages, we constructed a vector in which the expression of the human form of the antiapoptotic *Bcl-2* gene is driven by the macrophage-specific promoter *CD68* (Figure 1A). The *CD68-hBcl2* (*Mø-hBcl-2*) transgene transmitted with the expected frequency, and *Mø-hBcl-2* or *Mø-hBcl-2 Apoe*$^{-/-}$ mice exhibited no obvious developmental or morphological abnormalities on the C57BL/6J genetic background (data not shown). To confirm expression of the transgene, *hBcl-2* mRNA and protein were measured in thioglycollate-elicited peritoneal macrophages from *Mø-hBcl-2* and control mice by reverse-transcription polymerase chain reaction (Figure 1B) and flow cytometry (Figure 1C). To evaluate the impact of hBcl-2 expression on apoptosis of macrophages, ox-LDL–induced caspase-3 activity was measured. Macrophages derived from *Mø-hBcl-2* mice were markedly protected against oxLDL-induced apoptosis compared with nontransgenic controls ($P<0.01$; Figure 1D).

We next evaluated whether *hBcl2* overexpression in macrophages exerted an impact on foam cell formation. Macrophages from *Mø-hBcl-2* or control mice displayed similar cholesterol-loading capacity on incubation with acetylated LDL (Figure 1E). In addition, because CD68 also is expressed in circulating monocytes, we assessed the expression of the transgene in this cell type. Cytometric analysis revealed that splenic CD19^{+} B cells, CD4^{+} and CD8^{+} T cells, and CD11c^{high} dendritic cells from *Mø-hBcl-2* mice did not express hBcl2, whereas blood CD115^{+} monocytes did at a low level (Figure I of the online-only Data Supplement). Consistent with this finding, we found that monocyte count

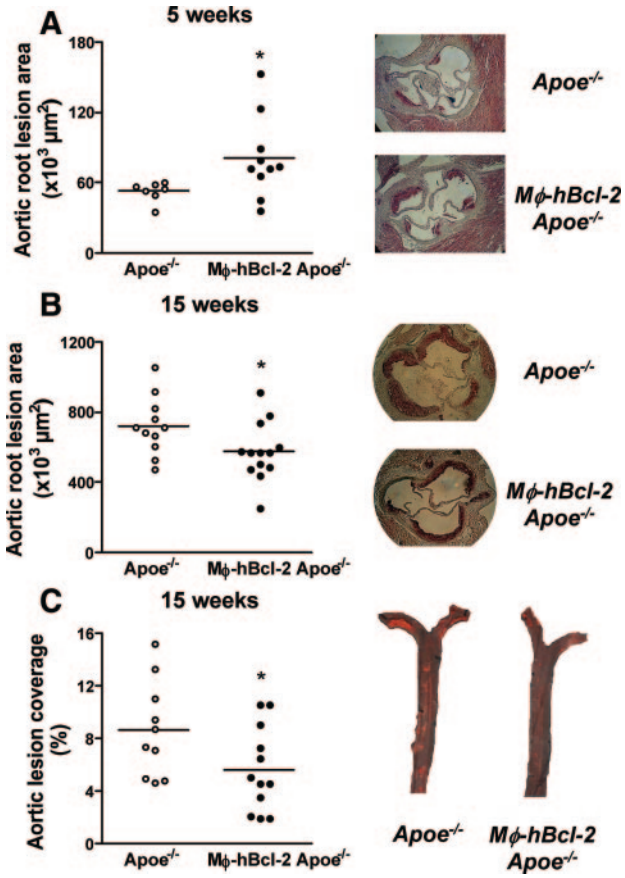

Figure 2. Quantification of atherosclerosis in *Apoe*$^{-/-}$ and *Mø-hBcl-2 Apoe*$^{-/-}$ mice. The degree of atherosclerosis in *Apoe*$^{-/-}$ and *Mø-hBcl-2 Apoe*$^{-/-}$ was determined by oil-red O (ORO) staining of aortic root sections after 5 weeks (A) or 15 weeks (B) of WD diet and ORO staining of the descending aorta after 15 weeks of diet (C). Photographs illustrate representative ORO staining of aortic root sections or of the descending aortas from *Apoe*$^{-/-}$ and *Mø-hBcl-2 Apoe*$^{-/-}$ mice. Results were analyzed by Student unpaired *t* tests with Welch correction in A (*$P<0.04$).

was 40% higher in the *Mø-hBcl-2 Apoe*$^{-/-}$ mice than in wild-type *Apoe*$^{-/-}$ mice on both chow and WD (Figure 1F).

Impact of Macrophage Resistance to Apoptosis on Atherogenesis

To assess the impact of macrophage resistance to apoptosis on the progression of early versus advanced atherosclerotic lesions, *Mø-hBcl-2 Apoe*$^{-/-}$ and *Apoe*$^{-/-}$ littermates were fed a WD for 5 or 15 weeks. No significant differences in plasma lipid levels or body weight were found between *Mø-hBcl-2 Apoe*$^{-/-}$ and *Apoe*$^{-/-}$ mice at either time point (Table 1). After 5 weeks of diet, aortic root lesion area was 50% larger in *Mø-hBcl-2 Apoe*$^{-/-}$ mice than in *Apoe*$^{-/-}$ mice ($P<0.03$; Figure 2A). As expected, 10 additional weeks on diet shifted the early cellular lesions to larger (>10-fold) and more complicated lesions with signs of necrotic core formation. In contrast to the 5-week time point, the mean area of the aortic root lesion in *Mø-hBcl-2 Apoe*$^{-/-}$ mice was 25% smaller than that in controls after 15 weeks of diet ($P<0.04$; Figure 2B). At this time point, en face analysis of the descending aorta confirmed this finding; the lesion area was 50% smaller in

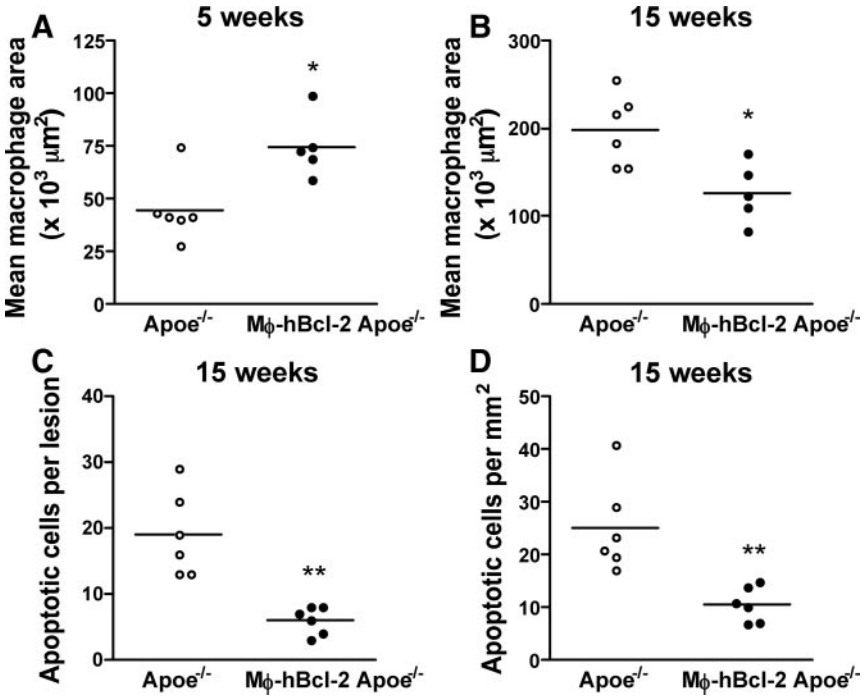

Figure 3. Macrophage and apoptotic cell accumulation in atherosclerotic lesions of *Apoe*$^{-/-}$ and *Mø-hBcl-2 Apoe*$^{-/-}$ mice. Atherosclerotic lesions were immunostained for the macrophage CD68 antigen to evaluate the degree of macrophage accumulation after 5 weeks (A) and 15 weeks (B) of diet. Atherosclerotic lesions were stained by the TUNEL method. The number of apoptotic cells per lesion was counted (C), and the ratio of TUNEL-positive cells to ORO^{+} area was calculated for both groups (D). Results were analyzed by Student unpaired *t* tests except for B, in which the Mann-Whitney *U* test was used. (*$P<0.01$; **$P<0.003$).

Mø-hBcl-2 Apoe$^{-/-}$ mice compared with controls ($P<0.04$; Figure 2C).

To determine whether lesional macrophage number was equally influenced in *Mø-hBcl-2 Apoe*$^{-/-}$ mice, CD68-positive area was quantified by immunohistochemistry on aortic sinus sections. After 5 weeks of diet, macrophage area was 50% greater in *Mø-hBcl-2 Apoe*$^{-/-}$ mice than in littermate controls ($P<0.01$; Figure 3A), whereas after 15 weeks of this diet, the macrophage area was 35% lower in *Mø-hBcl-2 Apoe*$^{-/-}$ mice ($P<0.01$; Figure 3B). We next quantified apoptotic cell accumulation in aortic sinus lesions. Terminal deoxynucleotidyl transferase-mediated dUTP-biotin nick-end label (TUNEL)–positive cells were detectable only in advanced lesions (15 weeks) but not in early ones (5 weeks), consistent with earlier reports.[6,7] At 15 weeks of diet, apoptotic cells in plaques from *Mø-hBcl-2 Apoe*$^{-/-}$ mice were 3-fold less abundant than in controls ($P<0.003$; Figure 3C), corresponding to a 3-fold reduction in apoptotic cell content per 1 mm^2 lesion ($P<0.003$; Figure 3D). Because macrophages undergoing apoptosis in advanced plaque express tissue factor,[19] we investigated its pattern of expression in early and advanced lesions of *Mø-hBcl-2 Apoe*$^{-/-}$ mice and controls. Tissue factor staining localized at the site of lipid accumulation mainly in acellular areas of advanced lesions (online-only Data Supplement Figures II and III). However, no difference in staining was revealed between *Mø-hBcl-2 Apoe*$^{-/-}$ mice lesions and controls at this advanced stage of plaque growth.

Impact of Macrophage Resistance to Apoptosis on Circulating Levels of Autoantibodies Against Oxidation-Specific Epitopes and Levels of Oxidized Phospholipids

Apoptotic cells contain bioactive oxPL and other oxidized lipids on their cell surface and are highly immunogenic, leading primarily to an enhanced IgM response to oxidation-specific epitopes in immunized mice.[11] In this context, we evaluated serum levels of autoantibodies directed against oxidation-specific epitopes and the quantity of circulating oxPL on apoB-100 lipoproteins. After 5 weeks of WD, levels of IgG1, IgG2c, IgG3, and IgM anti–MDA-LDL and anti-oxLDL antibodies were comparable in *Apoe*$^{-/-}$ and *Mø-hBcl-2 Apoe*$^{-/-}$ mice (Figure 4A and 4B). Plasma levels of these IgG subspecies were not different between the 2 groups at 15 weeks of diet (Figure 4C and 4D); however, a significant increase in the titer of IgM anti–MDA-LDL antibodies ($P<0.05$; Figure 4C) and a trend toward higher IgM anti-oxLDL titers (Figure 4D) were observed in *Mø-hBcl-2 Apoe*$^{-/-}$ mice compared with *Apoe*$^{-/-}$ mice. Moreover, titers of the T15/E06 natural antibody, which binds to oxPL, were more elevated in *Mø-hBcl-2 Apoe*$^{-/-}$ mice after 15 weeks (Figure 4E). Without reaching statistical significance, a similar trend could be observed at the 5-week time point (Figure 4E). Next, because atherosclerotic lesions, including the apoptotic cells within them, are a likely source of oxPLs with proinflammatory and immunogenic properties, we measured circulating levels of oxPLs bound to apoB-100 lipoproteins in both groups of mice. After 5 and 15 weeks of the diet, the relative amounts of oxPL/apoB-100 were significantly lower in *Mø-hBcl-2 Apoe*$^{-/-}$ mice compared with controls at each time point (Figure 4F).

Effect of Sustained Induction of Apoptosis of Lesional Macrophages on Atherosclerotic Plaque Progression

Because increased resistance to apoptosis of macrophages was associated with a reduced progression of advanced plaques, we designed an experimental strategy to evaluate whether sustained induction of apoptosis in established lesions would mirror this effect. To address this point, we used

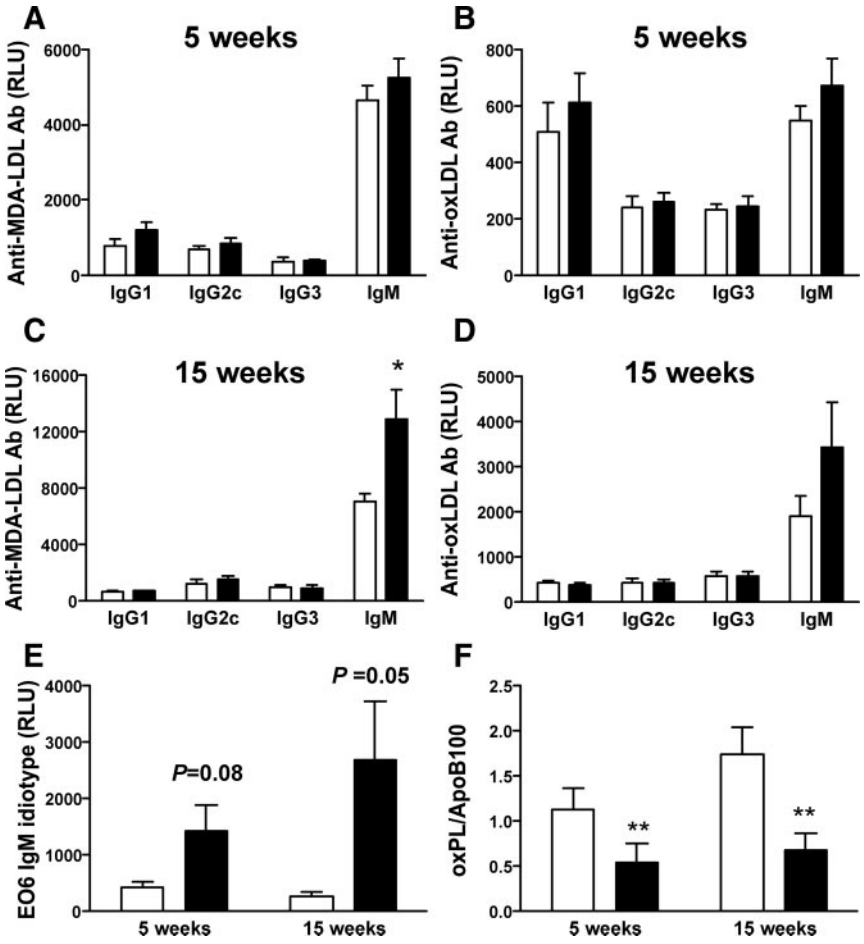

Figure 4. Determination of serum levels of antioxidatively modified LDL autoantibodies, EO6 antibody, and oxPLs in *Apoe*$^{-/-}$ and *Mø-hBcl-2 Apoe*$^{-/-}$ mice. Determination of either anti–MDA-LDL (A and C) or anti-oxLDL (B, D) IgG1, IgG2c, IgG3, and IgM levels was performed by ELISA on serum from *Apoe*$^{-/-}$ (white bars) and *Mø-hBcl-2 Apoe*$^{-/-}$ (black bars) mice fed a WD for 5 weeks (A and B) or 15 weeks (C and D). The EO6 antibody titers were determined by ELISA on *Apoe*$^{-/-}$ (white bars) and *Mø-hBcl-2 Apoe*$^{-/-}$ (black bars) mouse sera after either 5 or 15 weeks of WD (E). Serum oxPLs were quantified in *Apoe*$^{-/-}$ (white bars) and *Mø*-hBcl-2 *Apoe*$^{-/-}$ (black bars) mouse sera after either 5 or 15 weeks of WD by ELISA on apoB-100 lipoprotein particles captured per well and represented as a ratio of oxPL to apoB-100 (F). *$P<0.05$; **$P<0.01$.

CD11c-DTR-GFP transgenic mice that were developed to allow conditional depletion of CD11c-positive cells in vivo through administration of DT.[15] The expression of the DT receptor (DTR)–green fluorescent protein (GFP) fusion protein driven by the CD11c promoter was evaluated on aortic root lesions of *CD11c-DTR Apoe*$^{-/-}$ mice by immunostaining and revealed that GFP-expressing cells represent a subpopulation of CD68^{+} lesional cells (Figure 5A). In this context, administration of DT should lead to the induction of apoptosis in a subpopulation of lesional phagocytes, including macrophages in *CD11c-DTR Apoe*$^{-/-}$ mice lesions. Indeed, a marked accumulation of TUNEL^{+} cells was observed in lesions of *CD11c-DTR Apoe*$^{-/-}$ mice compared with controls 48 hours after DT injection (Figure 5B).

Because ongoing apoptosis of macrophages is thought to occur continuously during atherogenesis, we evaluated the impact of sustained induction of apoptosis of lesional cells on plaque progression. However, long-term repeated injection of DT in *CD11c-DTR Apoe*$^{-/-}$ mice was previously shown to be lethal.[15] To circumvent this problem, the hematopoietic system of mice was selectively reconstituted with *CD11c-DTR* cells by lethally irradiating *Apoe*$^{-/-}$ mice, followed by reconstitution with *CD11c-DTR Apoe*$^{-/-}$ bone marrow cells. Plasma total cholesterol and triglyceride levels were similar in DT- and PBS-treated animals fed a WD for 12 weeks. However, we observed a 25% increase in plasma free cholesterol concentration 48 hours after the final DT injection (Table 2). We further examined this phenomenon in another set of animals and found that this effect was transient, lasting 48 to 72 hours, and correlated with DT-induced depletion of CD11c-positive cells (data not shown). Importantly, although the proportion of splenic dendritic cells was markedly decreased in *Apoe*$^{-/-}$ mice reconstituted with bone marrow cells from *CD11c-DTR Apoe*$^{-/-}$ mice 48 hours after DT injection, the percentage of blood monocytes remained unchanged (online-only Data Supplement Figure IV). Apoptotic cell accumulation was markedly increased in lesions of chimeric mice treated with DT compared with PBS-injected controls ($P<0.0001$; Figure 5C). Moreover, aortic root lesion area was 20% larger in transplanted mice treated with DT compared with animals treated with PBS ($P=0.01$, Figure 5D), whereas a larger difference was observed in the descending thoracic and abdominal aorta (5-fold) in the DT group compared with controls ($P<0.0001$; Figure 5E). Surprisingly, the degree of CD68^{+} macrophage immunoreactivity was similar in both groups (data not shown) 48 hours after the final DT injection and may reflect an increased recruitment of circulating monocytes (see below), an effect that could mask the loss of lesional macrophages in the DT-treated group.

Effect of Short-Term Induction of Lesional Macrophage Apoptosis in Established Atherosclerotic Lesions

To further examine the molecular and cellular mechanisms that may underlie the enhanced plaque progression observed

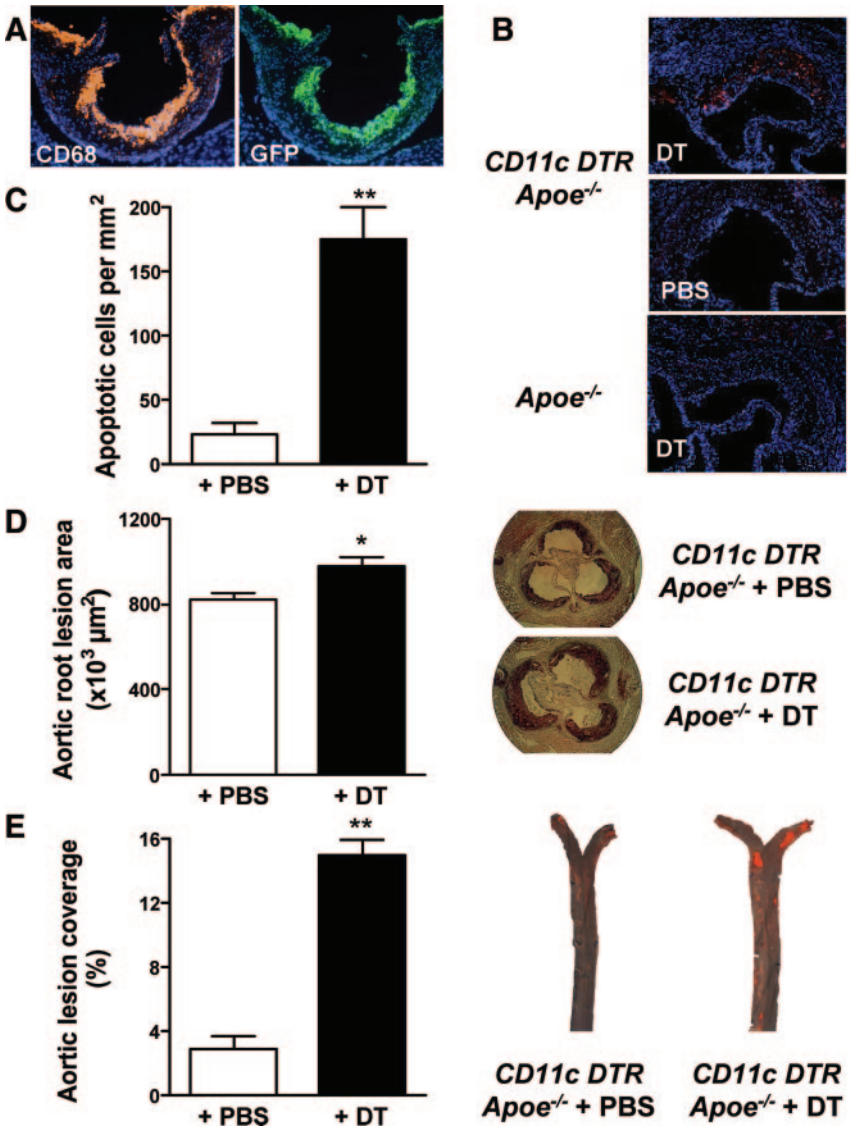

Figure 5. Sustained induction of lesional macrophage apoptosis increased atherosclerotic plaque progression. Expression of the *CD11c-DTR-GFP* transgene by macrophages in *CD11c-DTR Apoe*$^{-/-}$ mice lesions was determined by immunohistochemistry. The DTR-GFP fusion protein–expressing cells were localized with an anti-GFP antibody, and lesional macrophages were detected with CD68 staining on consecutive serial sections of *CD11c-DTR Apoe*$^{-/-}$ mice lesions (A). Apoptotic cells were detected by TUNEL staining on aortic root sections of either *CD11c-DTR Apoe*$^{-/-}$ mice treated with DT or PBS or *Apoe*$^{-/-}$ mice treated with DT 48 hours after injection. Photographs illustrate representative TUNEL staining from both groups of mice (B). Apoptotic cell accumulation was determined in *CD11c-DTR Apoe*$^{-/-}$→*Apoe*$^{-/-}$ chimeric mice injected with DT and PBS-injected controls (C). The degree of atherosclerosis in *Apoe*$^{-/-}$ mice reconstituted with bone marrow cells from *CD11c-DTR Apoe*$^{-/-}$ that received DT or vehicle was determined by ORO staining of both aortic root sections (D) and the descending aorta (E) after 12 weeks of diet. Photographs illustrate representative ORO staining of aortic root sections or of the descending aortas from both groups of mice. *$P<0.05$; **$P<0.0001$.

on sustained induction of lesional macrophage apoptosis, we evaluated the impact of short-term DT treatment on vascular inflammation in established lesions. For this purpose, *Apoe*$^{-/-}$ and *CD11c-DTR Apoe*$^{-/-}$ mice with established atherosclerotic lesions were injected with DT and either PBS or DT, respectively, and the cellular response to lesional induction of apoptosis was evaluated 48 hours after injection. We first determined the content of apoptotic cells in the aortic sinus of the 3 groups of mice 2 days after injection. TUNEL staining revealed marked accumulation of apoptotic cells in *CD11c-DTR Apoe*$^{-/-}$ mice treated with DT compared with the control groups, thereby confirming that DT injection had induced apoptosis in lesions ($P<0.05$; Figure 6A and 6B). The persistence of apoptotic cells 2 days after DT injection in *CD11c-DTR Apoe*$^{-/-}$ mice is consistent with defective clearance of dead cells in advanced plaques as previously suggested[20] ($P<0.05$; Figure 6A and 6B). By comparison, TUNEL staining was not observed in the spleens of *CD11c-DTR Apoe*$^{-/-}$ mice 48 hours after DT treatment, suggesting efficient removal in this tissue (data not shown).

Table 2. Lipid Levels and Body Weight of *CD11c-DTR Apoe*$^{-/-}$→*Apoe*$^{-/-}$ Chimeric Mice Injected With PBS or DT After 12 Weeks of WD

	+PBS	+DT	*P*
Total cholesterol, mg/dL	1035.2±45.0	1174.1±101.0	NS
Free cholesterol, mg/dL	302.5±9.5	377.8±27.0	<0.05
Triglycerides, mg/dL	125.4±15.1	124.3±11.1	NS
Free cholesterol/total cholesterol, %	29.3±0.4	33.0±3.2	NS
Body weight, g	27.1±0.9	27.2±1.2	NS

NS indicates not significant.

The accumulation of apoptotic cells in the lesions of the *CD11c-DTR Apoe*$^{-/-}$ mice was associated with dense DAPI staining indicative of accumulation of cells in TUNEL^{+} areas (Figure 6A). These cells stained positively for the newly recruited macrophage marker CD11b[16] (Figure 6A), and quantitative analysis revealed that these CD11b^{+} macrophages accumulated in the lesions of *CD11c-DTR Apoe*$^{-/-}$ mice treated with DT to a greater degree compared with controls ($P<0.05$; Figure 6C). Interestingly, we noted that

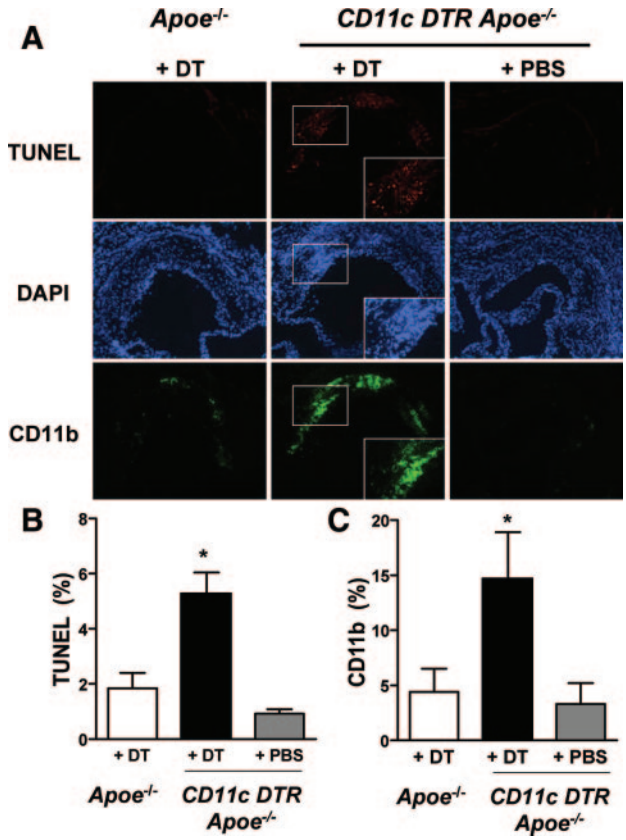

Figure 6. Apoptotic cell deposition in atherosclerotic lesions of *CD11c-DTR Apoe*$^{-/-}$ mice treated with DT promotes newly recruited macrophage accumulation. Atherosclerotic lesions were stained with the monocyte/macrophage marker CD11b for visualization of newly recruited macrophages (green), the TUNEL method for detection of apoptotic cells (red), and DAPI for staining of nuclei (blue) (A). Photomicrographs are representative of 5 to 6 mice analyzed per group (magnification ×200). The ratio of TUNEL-positive areas to ORO-positive staining areas was calculated for each mouse (B). The degree of newly recruited macrophage (CD11b$^+$) accumulation relative to lesion area was determined (C). Values represent the mean±SEM of 5 to 6 mice per group. *Statistically significant difference between *CD11c-DTR Apoe*$^{-/-}$ and control groups, $P<0.05$.

rare lesional TUNEL$^+$ areas were equally associated with the presence of adjacent CD11b$^+$ macrophages in *Apoe*$^{-/-}$ mice, thereby suggesting that apoptotic cell death, which occurred independently of DT-triggered apoptosis, equally induced newly recruited macrophage accumulation (data not shown).

To investigate the potential molecular mechanisms underlying the recruitment of new macrophages within lesions, we next evaluated the expression of monocyte markers and chemokines in the aorta. Levels of mRNA encoding the monocyte markers CD11b, CCR2, and CX3CR1 were significantly elevated ($P<0.05$ each) in the aortas of *CD11c-DTR Apoe*$^{-/-}$ mice treated with DT compared with controls (Figure 7A through 7C, respectively). The expression of the activation marker VCAM-1 also was significantly elevated in DT-treated *CD11c-DTR Apoe*$^{-/-}$ mice compared with controls ($P<0.05$; Figure 7D). Moreover, expression levels of the chemokines monocyte chemoattractant protein-1 (MCP-1) (Figure 7E), macrophage inflammatory protein (MIP)-1α (Figure 7F), MIP-1β (Figure 7G), and MIP-2 (Figure 7H) were significantly increased ($P<0.05$ each) in *CD11c-DTR Apoe*$^{-/-}$ mice treated with DT compared with control groups.

Effect of Short-Term Induction of Lesional Macrophage Apoptosis in Established Atherosclerotic Lesions on Recruitment of Circulating Monocytes

The observation that induction of apoptosis within the lesion was associated with higher levels of chemokines and the presence of CD11b$^+$ cells strongly suggests that apoptotic cell deposition triggered the recruitment of monocytes. Thus, we designed an experiment to dynamically measure the level of monocyte infiltration in response to accumulation of apoptotic cells in the atherosclerotic vascular bed. Systemic injection of fluorescein-labeled microspheres (FITC-M) was used to label monocytes in the circulation. Within 18 hours after intravenous injection of microspheres, ≈1% of leukocytes were FITC-M$^+$, of which two thirds were monocytes (data not shown). Overall, ≈10% of blood monocytes were phagocytically labeled with this approach (Figure 8A). Only a few beads were detected in atherosclerotic lesions of *Apoe*$^{-/-}$ mice 48 hours after injection of FITC-M, reflecting the "basal" recruitment of monocytes into the plaque (Figure 8B). The majority of the beads that had not been phagocytosed by peripheral blood leukocytes were found in the spleen (data not shown). In *CD11c-DTR Apoe*$^{-/-}$ mice, monocytes were labeled in vivo with FITC-M, whereas apoptosis was simultaneously induced in the lesions by DT injection. Forty-eight hours after injection, aortic root sections were prepared and stained both for TUNEL to detect apoptotic cells and with DAPI to visualize nuclei, whereas recruited monocytes were discriminated with green bead fluorescence. As shown in Figure 8C, DT injection induced apoptotic cell accumulation in lesions of *CD11c-DTR Apoe*$^{-/-}$ mice, which in turn promoted recruitment of circulating monocytes as evidenced by detection of FITC-M$^+$ cells in the lesions of these mice; in contrast, rare beads were detected in control groups.

Discussion

Our data suggest that macrophage survival exerts proatherogenic effects during the early stages of atherosclerotic plaque progression, whereas it reduced plaque burden when lesions were at a more advanced stage. Second, we report that accumulation of apoptotic macrophages in established lesions has a major incidence on the vascular inflammatory response by promoting inflammatory gene expression, circulating monocyte recruitment, subsequent accumulation of newly recruited macrophages, and ultimately plaque progression.

The present experiments demonstrated that protection of macrophage cell death in *Mø-hBcl-2 Apoe*$^{-/-}$ mice enhanced lesion size compared with *Apoe*$^{-/-}$ littermate controls at early stages of plaque development (5 weeks of WD). At this early stage, lesions in both *Apoe*$^{-/-}$ and *Mø-hBcl-2 Apoe*$^{-/-}$ mice did not contain TUNEL-positive cells, consistent with previous studies that revealed that apoptotic cells are detectable only in advanced lesions.[6,7] The absence of apoptotic cells in early lesions might reflect an efficient clearance mechanism at this stage rather than the absence of apoptosis[8,9] because notably the free cholesterol–induced apoptosis pathway has

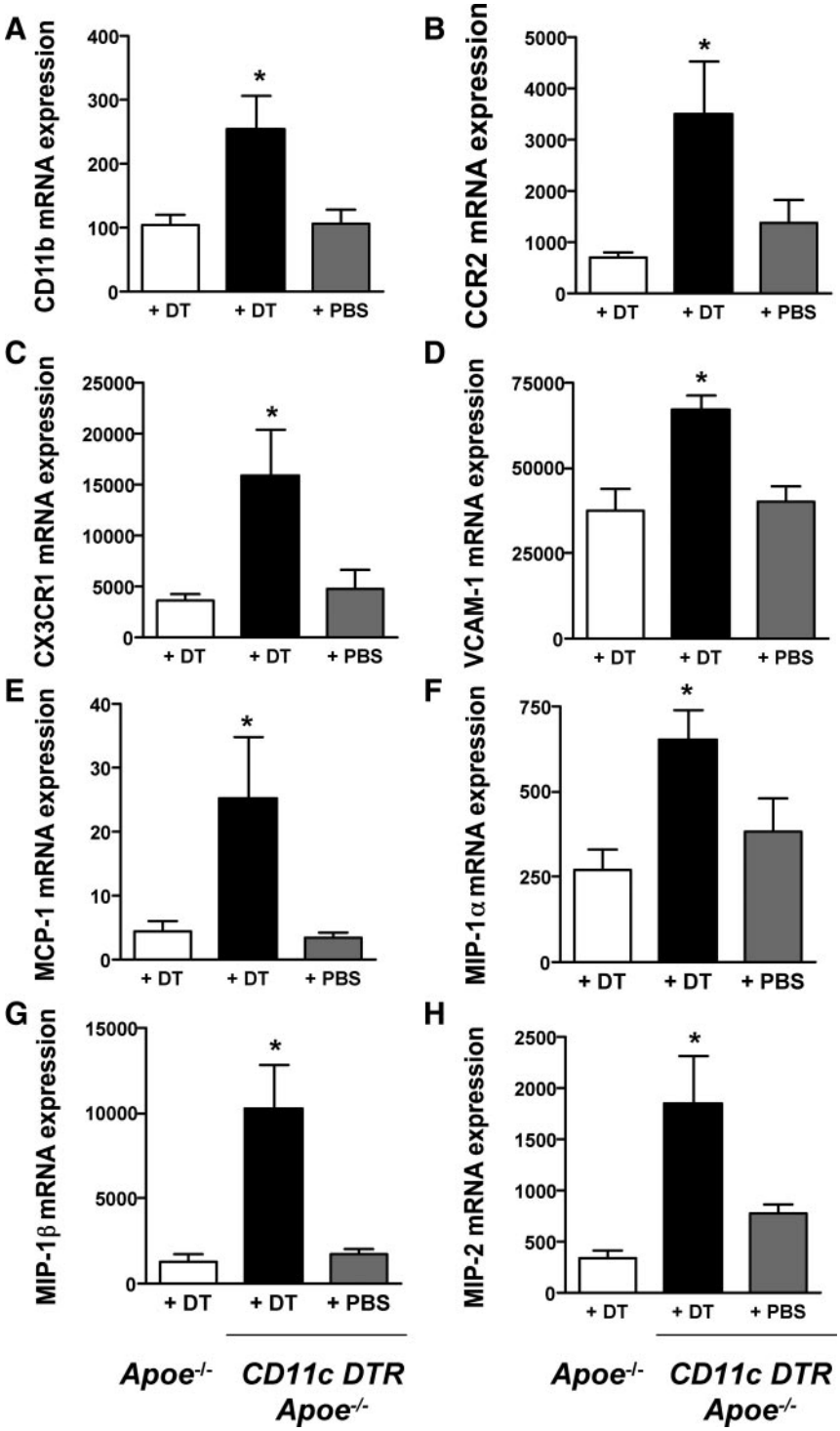

Figure 7. Monocyte marker and small inducible chemokine mRNA expression is increased in the lesions of *CD11c-DTR Apoe*$^{-/-}$ mice treated with DT. The levels of CD11b (A), CCR2 (B), CX3CR1 (C), VCAM-1 (D), and small inducible chemokines MCP-1 (E), MIP-1α (F), MIP-1β (G), and MIP-2 (H) mRNA were determined by quantitative polymerase chain reaction in the aortas of each group of mice. Values represent the mean±SEM of 5 to 6 mice per group. *Statistically significant difference between *CD11c-DTR Apoe*$^{-/-}$ and control groups, $P<0.05$.

been shown to be operative (unfolding protein response activation) in the early phases of plaque development.[7,21] Furthermore, if lesions are larger in *Mø-hBcl-2 Apoe*$^{-/-}$ mice compared with *Apoe*$^{-/-}$ mice, that might suggest that hBcl-2 overexpression could protect the lesion from an apoptotic activity masked by an efficient clearance machinery, thereby increasing the overall cellularity of the plaque and its subsequent growth.

In contrast, at a more advanced stage of atherosclerosis (15 weeks on WD), we observed smaller lesion size in *Mø-hBcl-2 Apoe*$^{-/-}$ mice compared with *Apoe*$^{-/-}$ controls. This finding was associated with a lower abundance of apoptotic cells present in the lesions of *Mø-hBcl-2 Apoe*$^{-/-}$ mice. Because the opposite situation was noted after 5 weeks on the WD, our data indicate that a marked shift occurred within the following 10-week period. Therefore, we speculate that this period of plaque growth was associated with a growing impairment of apoptotic cell clearance mechanisms. Thus, in this context, enhanced macrophage resistance to apoptosis would confer protection against plaque progression. This hypothesis is consistent with studies in mice in which components of the

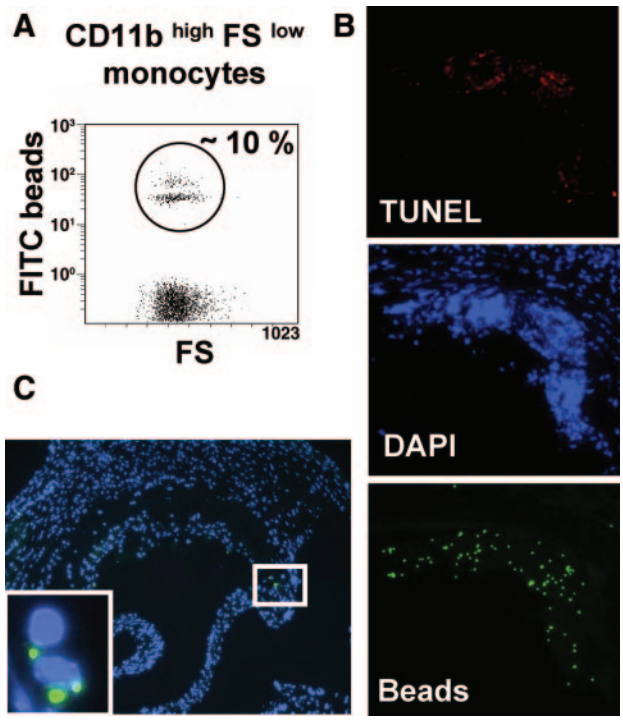

Figure 8. In vivo–labeled circulating monocytes are recruited in areas of apoptotic cell accumulation in lesions of *CD11c-DTR Apoe*$^{-/-}$ mice treated with DT. A, The percentage of CD11b^{high} FS^{low} monocytes that had phagocytosed fluorescent microspheres was determined by flow cytometry. B, Photomicrograph illustrating atherosclerotic lesions of *Apoe*$^{-/-}$ mice 48 hours after injection of fluorescent microspheres. C, Photomicrograph illustrating atherosclerotic lesions of *CD11c-DTR Apoe*$^{-/-}$ stained by the TUNEL method to detect apoptotic cells and DAPI to stain nuclei. Green bead fluorescence visualizes monocytes labeled with fluorescent microspheres recruited to the atherosclerotic lesion. Fluorescent microspheres were either absent or rare in control groups. Photomicrographs are representative of 5 mice (magnification ×200).

apoptotic cell clearance machinery have been deleted[13] as well as with other models of ineffective apoptotic cell clearance (lupus-prone mice)[14] that suggested that lesional apoptotic cell accumulation from early lesion stages was associated with increased atherosclerotic plaque progression. Another potential explanation for such a dual effect was that overexpression of *hBcl-2* preferentially protected macrophage foam cells from potential inducers of apoptosis present in advanced versus early lesions (such as high levels of oxLDL), thereby reflecting the various potential pathways that can trigger cell death in plaques.[8,22] Alternatively, the presence of macrophages protected from apoptosis in advanced lesions of *Mø-hBcl-2 Apoe*$^{-/-}$ mice might favor the phagocytosis of plaque debris and might therefore delay or limit the adverse impact of apoptotic cell accumulation, thereby contributing to the limitation of plaque growth. It is noteworthy that monocytes were constitutively increased in *Mø-hBcl-2 Apoe*$^{-/-}$ mice, an effect most likely due to leakage of the *CD68-hBcl2* transgene in this cell type. As a result, increased resistance to apoptosis of macrophages but equally, to a certain degree, monocytes may have contributed to plaque development in *Mø-hBcl-2 Apoe*$^{-/-}$ mice at an early stage. Alternatively, the increased monocyte count could also have participated in the observed early plaque progression in those mice. Nevertheless, such a scenario would not hold true in advanced lesions and/or would be markedly counterbalanced by the protected effect afforded by increased resistance of macrophage to apoptosis.

By using the CD11c-DTR system, we provide equal evidence that lesional accumulation of apoptotic cells could induce inflammatory signals and favor monocyte recruitment, thereby further demonstrating that advanced lesions progress when apoptotic cells accumulate. Indeed, we demonstrate that the accumulation of dead cells in plaques induces a proinflammatory milieu as assessed by elevated expression of small inducible chemokines (*MCP-1*, *MIP-1α*, *MIP-1β*, and *MIP-2*) and monocyte markers. Our results are consistent with recent studies showing that membranes of apoptotic cells contain significant amounts of active oxPLs,[11] which are known inducers of inflammation in murine arteries.[12] It is interesting to note that circulating oxPL levels were decreased in *Mø-hBcl-2 Apoe*$^{-/-}$ mice compared with controls after both 5 and 15 weeks on WD, potentially as a result of both decreased macrophage apoptosis and higher titers of IgM antibodies (particularly oxPL-specific E06 titers), which might facilitate oxPL clearance.

We provide dynamic evidence that the accumulation of CD11b^{+} newly recruited macrophages in areas of apoptotic cell deposition most probably arose from recruitment of circulating monocytes. Our data are consistent with in vitro experiments that revealed that apoptotic cells, through their oxPLs, can induce endothelial cell activation and subsequent monocyte adhesion[10,11] and provide the first evidence in vivo that apoptotic cells can stimulate the migration of phagocytes, as previously demonstrated in vitro.[11,23] Some discrepancies may exist between our results and those of Stoneman and colleagues,[24] who reported that short-term DT treatment of *CD11b-DTR-GFP* mice triggered macrophage apoptosis in lesions without inducing plaque inflammation, whereas long-term DT treatment of atherosclerotic *CD11b-DTR-GFP* mice had no impact on plaque progression. The fact that monocytes are CD11b^{high} cells that were massively depleted in DT-treated *CD11b-DTR-GFP* mice, thus significantly impairing recruitment to the lesion and consequently reducing the potential impact on vascular inflammation and plaque development, may partly explain the differences with our data. One limitation for the use of the *CD11c-DTR* model in the present study, however, was the elevation in plasma cholesterol observed after long-term DT treatment of these mice. We cannot exclude that such an effect may have accelerated plaque progression in DT-treated *CD11c-DTR Apoe*$^{-/-}$ mice. Nevertheless, it is doubtful that a periodic, temporary, and moderate elevation in plasma cholesterol levels might explain the 4-fold increase in lesion size we observed in the aortas of these mice.

Conclusions

The present study provides strong support for a divergent impact of apoptosis on plaque progression as a function of the stage of lesion development, thereby providing a rationale for the association between apoptotic cell accumulation and plaque progression. Considered together, our data suggest that reducing apoptotic cell accumulation in advanced atherosclerotic

plaques may be beneficial in attenuating either recruitment of monocytes, the resulting local inflammatory response, or both.

Sources of Funding

This work was funded by INSERM, Fondation de France, Leducq Foundation, PPG grant HL088093, and NIH HL086559 (Dr Witztum). Dr Gautier was supported by a fellowship from the Fondation pour la Recherche Médicale. Drs Lesnik, Huby, and Chapman are recipients of Contrat d'Interface from Assistance Publique-Hopitaux de Paris/INSERM.

Disclosures

None.

References

1. Geng YJ, Libby P. Progression of atheroma: a struggle between death and procreation. *Arterioscler Thromb Vasc Biol*. 2002;22:1370–1380.
2. Saxena A, McMeekin JD, Thomson DJ. Expression of Bcl-x, Bcl-2, Bax, and Bak in endarterectomy and atherectomy specimens. *J Pathol*. 2002; 196:335–342.
3. Kockx MM, De Meyer GR, Buyssens N, Knaapen MW, Bult H, Herman AG. Cell composition, replication, and apoptosis in atherosclerotic plaques after 6 months of cholesterol withdrawal. *Circ Res*. 1998;83:378–387.
4. Liu J, Thewke DP, Su YR, Linton MF, Fazio S, Sinensky MS. Reduced macrophage apoptosis is associated with accelerated atherosclerosis in low-density lipoprotein receptor-null mice. *Arterioscler Thromb Vasc Biol*. 2005;25:174–179.
5. Arai S, Shelton JM, Chen M, Bradley MN, Castrillo A, Bookout AL, Mak PA, Edwards PA, Mangelsdorf DJ, Tontonoz P, Miyazaki T. A role for the apoptosis inhibitory factor AIM/Spalpha/Api6 in atherosclerosis development. *Cell Metab*. 2005;1:201–213.
6. Kolodgie FD, Petrov A, Virmani R, Narula N, Verjans JW, Weber DK, Hartung D, Steinmetz N, Vanderheyden JL, Vannan MA, Gold HK, Reutelingsperger CP, Hofstra L, Narula J. Targeting of apoptotic macrophages and experimental atheroma with radiolabeled annexin V: a technique with potential for noninvasive imaging of vulnerable plaque. *Circulation*. 2003;108:3134–3139.
7. Zhou J, Lhotak S, Hilditch BA, Austin RC. Activation of the unfolded protein response occurs at all stages of atherosclerotic lesion development in apolipoprotein E-deficient mice. *Circulation*. 2005;111:1814–1821.
8. Tabas I. Apoptosis and efferocytosis in mouse models of atherosclerosis. *Curr Drug Targets*. 2007;8:1288–1296.
9. Schrijvers DM, De Meyer GR, Kockx MM, Herman AG, Martinet W. Phagocytosis of apoptotic cells by macrophages is impaired in atherosclerosis. *Arterioscler Thromb Vasc Biol*. 2005;25:1256–1261.
10. Berliner JA, Gharavi NM. Endothelial cell regulation by phospholipid oxidation products. *Free Radic Biol Med*. 2008;45:119–123.
11. Chang MK, Binder CJ, Miller YI, Subbanagounder G, Silverman GJ, Berliner JA, Witztum JL. Apoptotic cells with oxidation-specific epitopes are immunogenic and proinflammatory. *J Exp Med*. 2004;200:1359–1370.
12. Furnkranz A, Schober A, Bochkov VN, Bashtrykov P, Kronke G, Kadl A, Binder BR, Weber C, Leitinger N. Oxidized phospholipids trigger atherogenic inflammation in murine arteries. *Arterioscler Thromb Vasc Biol*. 2005;25:633–638.
13. Ait-Oufella H, Kinugawa K, Zoll J, Simon T, Boddaert J, Heeneman S, Blanc-Brude O, Barateau V, Potteaux S, Merval R, Esposito B, Teissier E, Daemen MJ, Leseche G, Boulanger C, Tedgui A, Mallat Z. Lactadherin deficiency leads to apoptotic cell accumulation and accelerated atherosclerosis in mice. *Circulation*. 2007;115:2168–2177.
14. Gautier EL, Huby T, Ouzilleau B, Doucet C, Saint-Charles F, Gremy G, Chapman MJ, Lesnik P. Enhanced immune system activation and arterial inflammation accelerates atherosclerosis in lupus-prone mice. *Arterioscler Thromb Vasc Biol*. 2007;27:1625–1631.
15. Jung S, Unutmaz D, Wong P, Sano G, De los Santos K, Sparwasser T, Wu S, Vuthoori S, Ko K, Zavala F, Pamer EG, Littman DR, Lang RA. In vivo depletion of CD11c(+) dendritic cells abrogates priming of CD8(+) T cells by exogenous cell-associated antigens. *Immunity*. 2002;17:211–220.
16. Lesnik P, Haskell CA, Charo IF. Decreased atherosclerosis in CX3CR1$^{-/-}$ mice reveals a role for fractalkine in atherogenesis. *J Clin Invest*. 2003;111:333–340.
17. Binder CJ, Hartvigsen K, Chang MK, Miller M, Broide D, Palinski W, Curtiss LK, Corr M, Witztum JL. IL-5 links adaptive and natural immunity specific for epitopes of oxidized LDL and protects from atherosclerosis. *J Clin Invest*. 2004;114:427–437.
18. Tacke F, Ginhoux F, Jakubzick C, van Rooijen N, Merad M, Randolph GJ. Immature monocytes acquire antigens from other cells in the bone marrow and present them to T cells after maturing in the periphery. *J Exp Med*. 2006;203:583–597.
19. Hutter R, Valdiviezo C, Sauter BV, Savontaus M, Chereshnev I, Carrick FE, Bauriedel G, Luderitz B, Fallon JT, Fuster V, Badimon JJ. Caspase-3 and tissue factor expression in lipid-rich plaque macrophages: evidence for apoptosis as link between inflammation and atherothrombosis. *Circulation*. 2004;109:2001–2008.
20. Schrijvers DM, De Meyer GR, Herman AG, Martinet W. Phagocytosis in atherosclerosis: molecular mechanisms and implications for plaque progression and stability. *Cardiovasc Res*. 2007;73:470–480.
21. Feng B, Yao PM, Li Y, Devlin CM, Zhang D, Harding HP, Sweeney M, Rong JX, Kuriakose G, Fisher EA, Marks AR, Ron D, Tabas I. The endoplasmic reticulum is the site of cholesterol-induced cytotoxicity in macrophages. *Nat Cell Biol*. 2003;5:781–792.
22. Stoneman VE, Bennett MR. Role of apoptosis in atherosclerosis and its therapeutic implications. *Clin Sci (Lond)*. 2004;107:343–354.
23. Lauber K, Bohn E, Krober SM, Xiao YJ, Blumenthal SG, Lindemann RK, Marini P, Wiedig C, Zobywalski A, Baksh S, Xu Y, Autenrieth IB, Schulze-Osthoff K, Belka C, Stuhler G, Wesselborg S. Apoptotic cells induce migration of phagocytes via caspase-3-mediated release of a lipid attraction signal. *Cell*. 2003;113:717–730.
24. Stoneman V, Braganza D, Figg N, Mercer J, Lang R, Goddard M, Bennett M. Monocyte/macrophage suppression in CD11b diphtheria toxin receptor transgenic mice differentially affects atherogenesis and established plaques. *Circ Res*. 2007;100:884–893.

CLINICAL PERSPECTIVE

Acute ischemic syndromes are related primarily to rupture of unstable plaques, leading to thrombus formation and occlusive complications. Unstable plaques are typically constituted of the most prominent cell types in atherosclerosis: macrophages and macrophage-derived foam cells. Most of these macrophages are postapoptotic and form a graveyard of dead collapsed cells that might contribute to constitution of the necrotic core. Genetic manipulations of apoptotic genes have been shown to differentially alter atherosclerotic lesion size in murine models of atherosclerosis; however, the potential beneficial or detrimental role of apoptotic macrophage death in plaque development remains controversial. To address this question, we created transgenic mice in which both the lifespan of macrophages was increased in response to elevated resistance to apoptosis (CD68-hBcl2) and targeted induction of lesional macrophage apoptosis (CD11c-DTR) could be achieved. These data provide the first in vivo evidence that macrophage apoptosis is atheroprotective in fatty streak lesions; in contrast, however, defective clearance of apoptotic debris in advanced lesions favors arterial wall inflammation and enhanced recruitment of monocytes, thereby leading to enhanced atherogenesis. Considered together, these findings suggest that attenuating macrophage apoptosis in advanced plaques represents a promising therapeutic strategy.

Conventional Dendritic Cells at the Crossroads Between Immunity and Cholesterol Homeostasis in Atherosclerosis

Emmanuel L. Gautier, PhD; Thierry Huby, PhD; Flora Saint-Charles, MSc; Betty Ouzilleau, BS; John Pirault, MSc; Virginie Deswaerte, MSc; Florent Ginhoux, PhD; Elizabeth R. Miller, BS; Joseph L. Witztum, MD; M. John Chapman, PhD, DSc; Philippe Lesnik, PhD

Background—Immunoinflammatory mechanisms are implicated in the atherogenic process. The polarization of the immune response and the nature of the immune cells involved, however, are major determinants of the net effect, which may be either proatherogenic or antiatherogenic. Dendritic cells (DCs) are central to the regulation of immunity, the polarization of the immune response, and the induction of tolerance to antigens. The potential role of DCs in atherosclerosis, however, remains to be defined.

Methods and Results—We created a mouse model in which the lifespan and immunogenicity of conventional DCs are enhanced by specific overexpression of the antiapoptotic gene *hBcl-2* under the control of the CD11c promoter. When studied in either low-density lipoprotein receptor–deficient or apolipoprotein E–deficient backgrounds, *DC-hBcl2* mice exhibited an expanded DC population associated with enhanced T-cell activation, a T-helper 1 and T-helper 17 cytokine expression profile, and elevated production of T-helper 1–driven IgG2c autoantibodies directed against oxidation-specific epitopes. This proatherogenic signature, however, was not associated with acceleration of atherosclerotic plaque progression, because expansion of the DC population was unexpectedly associated with an atheroprotective decrease in plasma cholesterol levels. Conversely, depletion of DCs in hyperlipidemic CD11c–diphtheria toxin receptor/apolipoprotein E–deficient transgenic mice resulted in enhanced cholesterolemia, thereby arguing for a close relationship between the DC population and plasma cholesterol levels.

Conclusions—Considered together, the present data reveal that conventional DCs are central to the atherosclerotic process, because they are directly implicated in both cholesterol homeostasis and the immune response. **(*Circulation*. 2009;119: 2367-2375.)**

Key Words: atherosclerosis ■ immune system ■ homeostasis ■ dendritic cells ■ lymphocytes

Dendritic cells (DCs) are the most potent antigen-presenting cells. Indeed, DCs possess a markedly elevated capacity to stimulate T cells, B cells, and natural killer T cells and to drive T-cell differentiation along both T-helper 1 (Th1) and T-helper 2 (Th2) pathways.[1] Moreover, DCs are known to favor tolerance to antigens, possibly via the generation of regulatory T cells.[2] As major regulators of immune responses and T-cell polarization, DCs are potentially key players in chronic inflammatory diseases such as atherosclerosis. Indeed, available evidence suggests that immune responses are directly implicated in the pathogenesis of atherosclerosis.[3,4] Although the presence of DCs has been reported in atherosclerotic plaques,[5–7] no mechanistic insight into the potential central immunoregulatory role of DCs in the immunoinflammatory dimension of atherosclerosis has been provided in atherosclerosis-prone mice. Modulation of the capacity of DCs to induce an immune response may facilitate evaluation of their impact on the pathogenesis of atherosclerosis. Indeed, enhancement of the lifespan of DCs has been reported to increase their immunogenicity in mice.[8–11] In this context, it is especially relevant that Bcl-2 has been shown to be a major regulator of DC lifespan and immunogenicity.[12] We therefore developed a mouse model in which DC lifespan and immunogenicity are enhanced by overexpression of human Bcl-2 (hBcl-2) under the control of the DC-specific CD11c promoter. This experimental approach allowed us to modulate the half-life and thus the immunogenicity of DCs in vivo with a view to evaluate their impact on the immune response during atherosclerosis.

Received July 15, 2008; accepted March 6, 2009.

From INSERM UMR-S 939, Hôpital de la Pitié (E.L.G., T.H., F.S.-C., B.O., J.P., V.D., M.J.C., P.L.), Paris, France; Université Pierre et Marie Curie, Université Paris 06, UMR-S 939 (E.L.G., T.H., F.S.-C., B.O., J.P., V.D., M.J.C., P.L.), Paris, France; Assistance Publique–Hôpitaux de Paris, Groupe Hospitalier Pitié-Salpêtrière, Service d'Endocrinologie-Métabolisme (T.H., M.J.C., P.L.), Paris, France; Department of Medicine, University of California San Diego (E.R.M., J.L.W.), La Jolla, Calif; and Department of Gene and Cell Medicine and Department of Medicine, Mount Sinai School of Medicine (F.G.), New York, NY.

The online-only Data Supplement is available with this article at http://circ.ahajournals.org/cgi/content/full/CIRCULATIONAHA.108.807537/DC1.

Correspondence to Dr Philippe Lesnik, INSERM U939, Hôpital de la Pitié, 83 Bd de l'hôpital, 75651 Paris 13, France. E-mail philippe.lesnik@upmc.fr

Circulation **is available at http://circ.ahajournals.org** **DOI: 10.1161/CIRCULATIONAHA.108.807537**

Clinical Perspective on p 2375

Methods

Transgenic mice expressing hBcl-2 under the murine CD11c promoter were described previously.[13] All procedures (bone marrow transplantation, plasma lipid analyses, chimerism, quantification of atherosclerotic plaques, immunohistochemistry, quantification of autoantibodies, analysis of gene expression by quantitative polymerase chain reaction, flow cytometry, cytokine assays, and generation of bone marrow–derived DCs) were performed as described previously[13–16] and are detailed in the online-only Data Supplement, along with details about the animal model.

Statistical Analysis

The statistical significance of the differences between groups was evaluated with the unpaired or paired 2-tailed Student *t* test. $P<0.05$ was considered significant. Values are expressed as mean±SEM.

Results

Characterization of *DC-hBcl2* Mice

Because CD11c is differentially expressed by DC subpopulations, and to gain insight into the specificity of transgene expression, we assessed the expression of hBcl-2 in DC subpopulations and in different types of leukocytes (online-only Data Supplement Figure I). Flow cytometric analysis revealed that splenic conventional DCs ($CD11c^{high}$, $MHCII^+$), comprising $CD11b^+$ DCs ($CD11c^{high}$, $CD11b^+$) and $CD8^+$ DCs ($CD11c^{high}$, $CD8^+$), expressed hBcl-2, whereas plasmacytoid DCs ($CD11c^{int}$, $PDCA\text{-}1^+$) did not. Equally, we demonstrated that splenic B cells, T cells, and macrophages did not express hBcl-2. Another population of leukocytes known to express CD11c, bronchoalveolar macrophages ($CD11c^+$, $F4/80^+$), did not express hBcl-2 in the *DC-hBcl-2* mice in the present study (online-only Data Supplement Figure I). This finding may be explained by the nature of the CD11c promoter used, which is a minimal promoter previously described to drive expression only in DCs with high endogenous expression of CD11c.[17] In our model, monocytes ($CD11b^+$, $F4/80^+$) did not express hBcl-2, and therefore, monocyte count was similar in control apolipoprotein E–deficient ($Apoe^{-/-}$) mice and *DC-hBcl-2* $Apoe^{-/-}$ mice (online-only Data Supplement Figure II).

hBcl-2 Overexpression in DCs Enhances Their Lifespan and Immunogenicity

DCs generated from bone marrow cells of *DC-hBcl-2* mice expressed hBcl-2 protein as expected (online-only Data Supplement Figure IIIA) and displayed enhanced resistance to apoptotic stress (online-only Data Supplement Figure IIIB). Such enhanced survival impacted the relative number of DCs in vivo. Indeed, the DC population was enriched in spleens from *DC-hBcl-2* mice (online-only Data Supplement Figure IIIC; $P<0.05$). Then, because DCs may control lymphocyte homeostasis, we assessed T-cell activation in splenocytes of *DC-hBcl-2* and control mice at the basal state. The data revealed that activated T cells, $CD3^+$ and $CD4^+$ cells expressing the activation marker CD69, were significantly increased in *DC-hBcl-2* mice compared with controls (online-only Data Supplement Figure IIID; $P<0.01$ and $P<0.001$, respectively), whereas expression of CD25 by $CD4^+$ T cells was similar in both groups in the basal state (online-only Data Supplement Figure IIID). These data are consistent with an enhanced immunogenicity of DCs in *DC-hBcl-2* mice fed a chow diet. In this regard, it is relevant that on a nonlethal lipopolysaccharide challenge, we reported that *DC-hBcl-2* mice equally exhibited significant elevation in the DC population, as well as in activation of T and B cells, compared with their littermate controls.[14] Collectively, *hBcl-2* overexpression in DCs prolonged their lifespan, led to a significant increase in the DC population, and enhanced T-cell activation in vivo.

Effect of Enhanced DC Lifespan and Immunogenicity on T-Cell Activation in *Ldl-r*$^{-/-}$ Mice

To evaluate whether DC lifespan and immunogenicity impact both immunity and atherogenesis, irradiated female low-density lipoprotein (LDL) receptor–deficient ($Ldl\text{-}r^{-/-}$) mice were reconstituted with bone marrow cells from *DC-hBcl-2* mice or wild-type (WT) littermates. After 4 weeks of recovery, mice were switched to a Western diet for 12 weeks. The efficiency of transplantation was established by the detection of <5% of *Ldl-r* knockout alleles in bone marrow cells from these mice (online-only Data Supplement Figure IV), thereby indicating a chimerism in the range of 95% to 100%.

We first evaluated the impact of enhancement of DC lifespan on the DC population itself and on T-cell activation and Th1 polarization. DCs were enriched in the spleens of *DC-hBcl-2*→$Ldl\text{-}r^{-/-}$ compared with *wt*→$Ldl\text{-}r^{-/-}$ mice (+56%, $P<0.01$; Figure 1A). Analysis of splenic T cells revealed an elevation in the proportion of both $CD3^+$ and $CD4^+$ T cells expressing the activation marker CD69 ($P<0.0001$ for each) and of $CD4^+$ T cells expressing CD25 (+25%, $P<0.01$) in *DC-hBcl-2*→$Ldl\text{-}r^{-/-}$ compared with controls (Figure 1B). Concomitantly, an increment of 20% in the percentage of CD44-expressing $CD4^+$ memory T cells was observed in *DC-hBcl-2*→$Ldl\text{-}r^{-/-}$ mice compared with *wt*→$Ldl\text{-}r^{-/-}$ mice ($P<0.0001$; Figure 1C). We next quantified the mRNA expression of key mediators of DC function, as well as T-cell responses and polarization in the spleen. Analysis of the expression of genes characteristic of DC function revealed a significant increase in the mRNA of interleukin (IL)-12p40, IL-23p19, and IL-15 in *DC-hBcl-2*→$Ldl\text{-}r^{-/-}$ mice, whereas expression of the IL-12p35 and IL-18 genes was unchanged (Figure 1D). This was associated with enhanced expression of interferon (IFN)-γ and TIM-3 (T-cell immunoglobulin- and mucin-containing molecule, a transcription factor promoting Th1 development), together with unchanged levels of GATA3 mRNA (a transcription factor promoting Th2 development) in *DC-hBcl-2*→$Ldl\text{-}r^{-/-}$ mice (Figure 1E). Expression levels of classic inflammatory genes revealed elevated levels of IL-1β mRNA but similar levels of CD40L and tumor necrosis factor-α mRNAs in the spleens of *DC-hBcl-2*→$Ldl\text{-}r^{-/-}$ mice compared with controls (Figure 1E). These findings support the contention that an enhanced DC lifespan leads to elevation in DC immunogenicity and increased T-cell activation with polarization toward a Th1 profile.

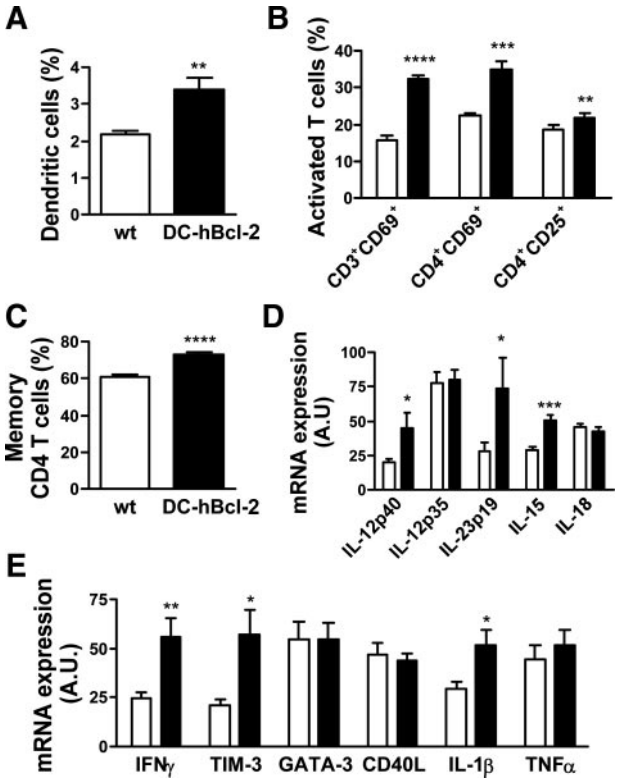

Figure 1. *DC-hBcl-2→Ldl-r*$^{-/-}$ mice exhibited greater DC abundance, enhanced T-cell activation, and elevated immunostimulatory cytokine expression. Percentages of CD11c^{high} DCs (A), activated CD3$^+$ CD69$^+$, CD4$^+$ CD69$^+$, and CD4$^+$ CD25$^+$ T cells (B), and memory CD4$^+$ CD44$^+$ T cells (C) were determined in spleens from *DC-hBcl-2→Ldl-r*$^{-/-}$ and *wt→Ldl-r*$^{-/-}$ mice by flow cytometry. D and E, Levels of mRNA expression of functional markers in DCs were evaluated by quantitative polymerase chain reaction in spleens from *DC-hBcl-2→Ldl-r*$^{-/-}$ and *wt→Ldl-r*$^{-/-}$ mice. A.U. indicates arbitrary units; TNFα, tumor necrosis factor-α. *P<0.05, **P<0.01, ***P<0.001, and ****P<0.0001.

Effect of Enhanced DC Lifespan and Immunogenicity on Regulatory T Cells in *Ldl-r*$^{-/-}$ Mice

Natural regulatory T cells (Treg) exhibit marked antiatherogenic properties[18] as a consequence of their ability to counteract both Th1- and Th2-mediated immune responses. Because DCs might influence the content and function of regulatory T cells, we evaluated whether the Treg population was modified in *DC-hBcl-2→Ldl-r*$^{-/-}$ compared with *wt→Ldl-r*$^{-/-}$ mice. As shown in Figure 2A, flow cytometric analysis revealed that spleen CD4$^+$ Foxp3$^+$ and CD4$^+$ CD25$^+$ Foxp3$^+$ T cells were similar in both groups, thereby arguing for the absence of an altered natural Treg population. We next quantified the expression of key markers of Treg cell population and function in the spleens of both groups of mice. Real-time quantitative polymerase chain reaction analysis confirmed the unaltered Foxp3 expression consistent with the absence of elevation in the natural Treg population. In this context, it was relevant that expression levels of transforming growth factor-β and CTLA-4 (cytotoxic T-lymphocyte–associated protein 4) were similar in splenic cells of both *DC-hBcl-2→Ldl-r*$^{-/-}$ and *wt→Ldl-r*$^{-/-}$ mice (Figure 2B). By contrast, a marked 7-fold increment in IL-10 mRNA expression was observed in *DC-hBcl-2→Ldl-r*$^{-/-}$ mice (Figure 2B; P=0.01). Overall, these data indicate that Treg cells are not markedly altered in *DC-hBcl-2→Ldl-r*$^{-/-}$ compared with *wt→Ldl-r*$^{-/-}$ mice.

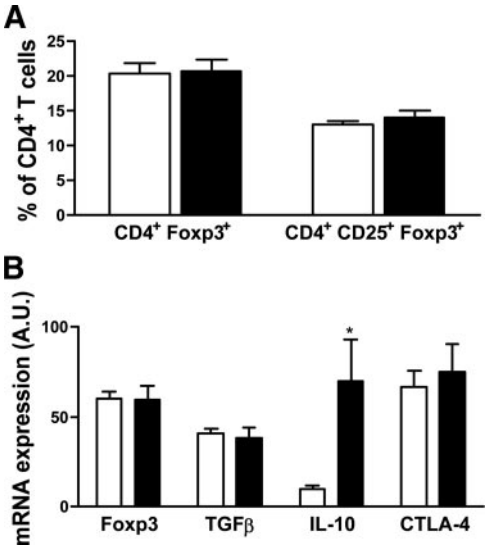

Figure 2. Regulatory T-cell content and expression of associated genes in *DC-hBcl-2→Ldl-r*$^{-/-}$ and *wt→Ldl-r*$^{-/-}$ mice. A, Flow cytometric analysis of gated CD4$^+$ mouse splenocytes expressing FoxP3 or FoxP3 and CD25. B, Levels of mRNA expression of functional markers of regulatory response in spleens from *DC-hBcl-2→Ldl-r*$^{-/-}$ and *wt→Ldl-r*$^{-/-}$ mice. A.U. indicates arbitrary units; TGFβ, transforming growth factor-β. *P=0.01.

Effect of Enhanced DC Lifespan and Immunogenicity on B-Cell Activation and Circulating Levels of Autoantibodies Against Oxidation-Specific Epitopes in *Ldl-r*$^{-/-}$ Mice

Several recent studies have emphasized the protective role of B lymphocytes in atherosclerosis.[15,19,20] These findings led us to question whether the increment in the DC population in our mouse model might affect levels of antibodies directed against oxidation-specific epitopes, the titer of the atheroprotective EO6 antibody idiotype, and the polarization of the humoral response (Th2-driven IgG1 versus Th1-driven IgG2c/IgG3 isotype production). We first evaluated B-cell activation by measuring the proportion of B cells bearing the activation marker CD86. A minor increment in B-cell activation was observed in *DC-hBcl-2→Ldl-r*$^{-/-}$ compared with *wt→Ldl-r*$^{-/-}$ mice (Figure 3A; P<0.05). Quantification of anti-malondialdehyde-LDL and anti-oxidized LDL IgG1, IgG2c, IgG3, and IgM antibody production revealed significant elevation in the IgG2c fraction of both anti-MDA-LDL and anti-oxidized LDL antibodies (2-fold; Figure 3B and 3C; P<0.0005 for each) in *DC-hBcl-2→Ldl-r*$^{-/-}$ compared with control mice, whereas levels of IgG1, IgG3, and IgM fractions were comparable between groups (Figure 3B and 3C). Moreover, titers of the EO6 antibody were markedly elevated in *DC-hBcl-2→Ldl-r*$^{-/-}$ compared with *wt→Ldl-r*$^{-/-}$ mice (Figure 3D; P<0.0005). In conclusion, the increment in IgG2c titer in *DC-hBcl-2→Ldl-r*$^{-/-}$ mice, which is characteristic of a Th1-driven immune response, is consistent

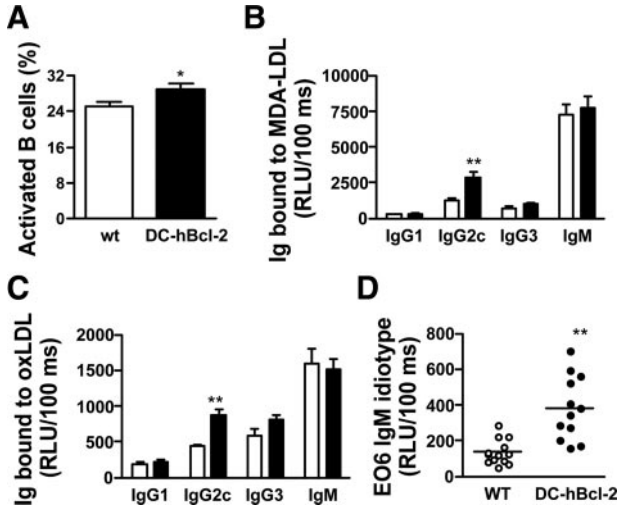

Figure 3. B-cell activation, production of antioxidatively modified LDL antibodies, and EO6 levels in *DC-hBcl-2→Ldl-r*$^{-/-}$ and *wt→Ldl-r*$^{-/-}$ mice. A, Percentage of activated B cells (CD19^{+} CD69^{+}) was determined in spleens from *DC-hBcl-2→Ldl-r*$^{-/-}$ and *wt→Ldl-r*$^{-/-}$ mice by flow cytometry. Serum titers of IgG1, IgG2c, IgG3, and IgM antibodies that bind malondialdehyde (MDA)-LDL (B), or copper-oxidized (Ox)-LDL (C), and phosphorylcholine-specific (EO6) antibodies were detected by isotype-specific ELISA (D). RLU indicates relative light units. **P*<0.05 and ***P*<0.0005.

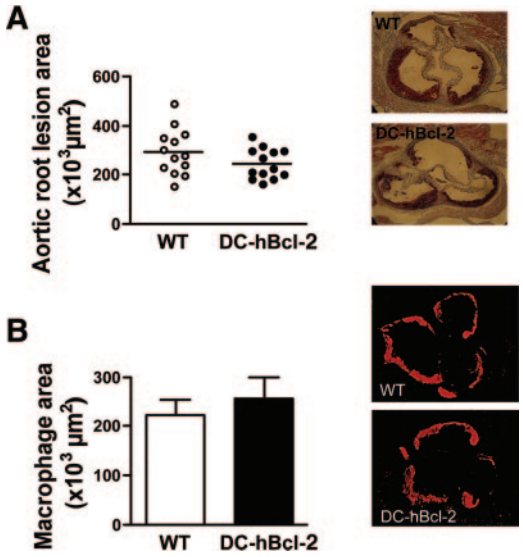

Figure 4. Quantification of atherosclerotic lesion surface and macrophage areas in *Ldl-r*–deficient mice. A, The degree of atherosclerosis was determined by oil red O staining of aortic root sections of *DC-hBcl-2→Ldl-r*$^{-/-}$ and *wt→Ldl-r*$^{-/-}$ mice after 12 weeks of Western diet. Each symbol represents mean area in a single mouse; horizontal bar indicates mean value for the respective group. B, Lesions were immunostained for the macrophage CD68 antigen, and the degree of macrophage accumulation was determined.

with the cytokine expression profile observed in the spleens of these animals and indicates that expansion of the DC population favors Th1 polarization in an atherogenic environment.

Effect of DC Lifespan on Atherosclerotic Lesion Progression, Plasma Lipids, and Lipoprotein Profile in *Ldl-r*$^{-/-}$ Mice

The impact of enhanced DC lifespan and immunogenicity on the progression of atherosclerosis was evaluated in *DC-hBcl-2* transgenic and control mice on an *Ldl-r*–deficient background. As shown in Figure 4A, the lesion area in the aortic root of *Ldl-r*$^{-/-}$ recipients reconstituted with *DC-hBcl-2* marrow cells was unchanged compared with their wild-type reconstituted controls after 12 weeks of Western diet (247.0±17.1×10^3 µm^2 versus 294.9±26.0×10^3 µm^2, respectively; P=0.2). Furthermore, macrophage areas were comparable in lesions of *DC-hBcl-2→Ldl-r*$^{-/-}$ and *wt→Ldl-r*$^{-/-}$ mice (Figure 4B; P=0.5). Because lesion formation and progression are predominantly dependent on plasma cholesterol levels and its distribution among the different lipoprotein subclasses, we then assessed whether elevated numbers of DCs might alter cholesterol homeostasis. Compared with controls, *Ldl-r*$^{-/-}$ mice transplanted with *DC-hBcl-2* bone marrow cells displayed a significant reduction in plasma total cholesterol (547±61 versus 426±64 mg/dL, respectively; P<0.005) and in free cholesterol levels (198±45 versus 149±33 mg/dL, respectively; P<0.05); by contrast, triglyceride levels were similar in both groups of mice (192±48 versus 170±42 mg/dL, respectively; Table). Analysis of cholesterol distribution among plasma lipoprotein subclasses revealed that the lower total cholesterol level in *DC-hBcl-2→Ldl-r*$^{-/-}$ compared with *wt→Ldl-r*$^{-/-}$ mice was due to a reduction in the abundance of VLDL and LDL subclasses (−59% and −57%, respectively), whereas the HDL fraction was decreased to a lesser degree (−33%; Figure 5A). Because a larger DC population in *DC-Bcl-2* animals was associated with lower circulating cholesterol levels, thereby revealing that the role of DC is important in the setting of hypercholesterolemia, we sought to determine whether the opposite mechanism (ie, acute depletion of DCs) was associated with an enhanced degree of cholesterolemia. We took advantage of the DT receptor (*DTR*)/diphtheria toxin (DT)

Table. Body Weight and Lipid Parameters

Study	Wild-Type	*DC-hBcl-2*	*P*
Bone marrow transplantation in *Ldl-r*$^{-/-}$ mice, n	13	14	
Weight, g	19.7±1.1	19.6±1.3	0.89
Total cholesterol, mg/dL	547±61	426±63	<0.001
Free cholesterol, mg/dL	198±45	149±33	<0.02
Triglycerides, mg/dL	192±48	170±42	0.34
Apoe$^{-/-}$ background, chow diet	n=12	n=10	
Weight, g	21.2±0.4	20.9±.3	0.23
Total cholesterol, mg/dL	370±7	317±18	<0.01
Free cholesterol, mg/dL	121±4	102±6	<0.01
Triglycerides, mg/dL	79±6	87±9	0.60
Apoe$^{-/-}$ background, Western diet, n	8	13	
Weight, g	19.8±0.5	20.7±0.3	0.12
Total cholesterol, mg/dL	686±65	509±19	<0.005
Free cholesterol, mg/dL	196±18	156±4	<0.05
Triglycerides, mg/dL	79±17	97±10	0.41

Values are expressed as mean±SEM unless otherwise indicated.

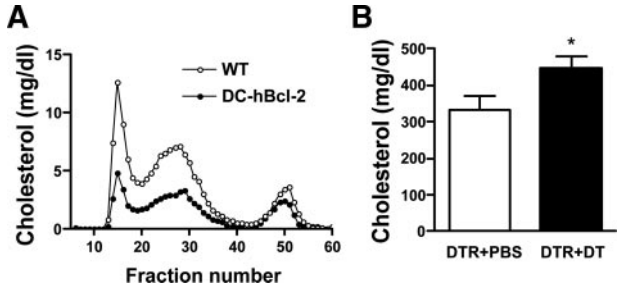

Figure 5. DCs modulate plasma cholesterol and lipoprotein profile in *Ldl-r*–deficient mice. A, Cholesterol distribution across the VLDL, LDL, and HDL lipoprotein classes was analyzed by gel filtration in *DC-hBcl-2→Ldl-r*$^{-/-}$ and *wt→Ldl-r*$^{-/-}$ mice after 12 weeks of Western diet. B, *DC-hBcl-2→Ldl-r*$^{-/-}$ mice were treated with PBS or diphtheria toxin (DT) to induce DC depletion. Plasma total cholesterol was determined in both groups. **P*<0.05.

system, which allows depletion of DCs after DT injection in transgenic mice expressing *DTR* under the *CD11c* promoter.[21] First, *Ldl-r*$^{-/-}$ mice were irradiated, transplanted with *CD11c-DTR* bone marrow cells, and submitted to a 4-week recovery period. These mice were fed a Western diet for 2 weeks, and then half of the mice were injected with DT whereas the other half were treated with vehicle. Plasma total cholesterol level was measured 24 hours after treatment (Figure 5B) and revealed an increment of 34% in *CD11c-DTR→Ldl-r*$^{-/-}$ mice treated with DT compared with vehicle-treated animals (333±36 versus 446±32 mg/dL, respectively; $P<0.05$).

Effect of DC Lifespan and Immunogenicity on Immune Response in *Apoe*$^{-/-}$ Mice

We next evaluated whether the impact of DC lifespan and immunogenicity on immunity that we documented in *Ldl-r*$^{-/-}$ mice, and more especially that which involved T-cell activation and B-cell responses, was equally manifest in an alternative atherosclerotic model (ie, *Apoe*$^{-/-}$ mice). We first showed that the DC population was significantly expanded in chow-fed 20-week-old *DC-hBcl-2 Apoe*$^{-/-}$ mice compared with *Apoe*$^{-/-}$ controls (Figure 6A; $P<0.05$). Flow cytometric analysis revealed that both the CD3$^+$- and CD4$^+$-activated T-cell populations were larger in *DC-hBcl-2 Apoe*$^{-/-}$ mice than in controls (Figure 6B; $P<0.001$ each), whereas the CD25-expressing CD4$^+$ T-cell population was unaltered (Figure 6B). With regard to the B-cell compartment, no change was observed in CD86 expression by B cells in *DC-hBcl-2 Apoe*$^{-/-}$ mice compared with controls (Figure 6C). The main alteration in the antibody response observed on the *Ldl-r*$^{-/-}$ background (ie, elevation in circulating levels of both anti-malondialdehyde-LDL and anti-oxidized LDL IgG2c antibodies in *DC-hBcl-2* mice) was equally observed on an *Apoe*$^{-/-}$ background (Figure 6D and 6E; $P<0.05$), whereas no statistically significant differences were observed for the other isotypes. Finally, levels of the E06 antibody were not affected in *DC-hBcl-2 Apoe*$^{-/-}$ mice compared with controls. To further evaluate whether changes in the polarization of the immune response observed in *DC-hBcl-2→Ldl-r*$^{-/-}$ were equally present in the *Apoe*$^{-/-}$ background, additional experiments were conducted in *DC-hBcl-2 Apoe*$^{-/-}$ and *Apoe*$^{-/-}$ mice fed a Western diet. We thus confirmed activation of key

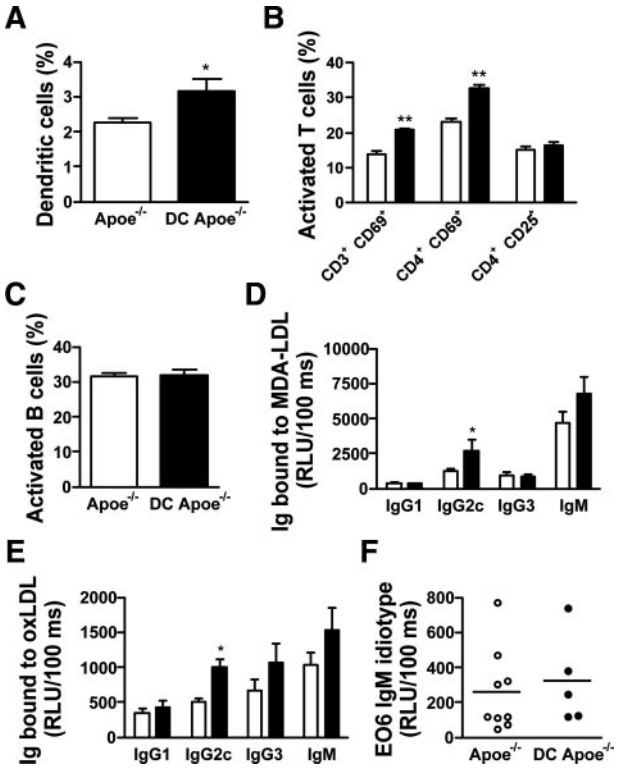

Figure 6. Immune system activation in *DC-hBcl-2 Apoe*$^{-/-}$ mice and in *Apoe*$^{-/-}$ mice. Percentages of DCs (A), activated T cells (B), and activated B cells (C) were determined in spleens from *Apoe*$^{-/-}$ and wild-type mice by flow cytometry. Serum titers of modified-LDL–specific IgG1, IgG2c, IgG3, and IgM antibodies that bind malondialdehyde (MDA)-LDL (D), copper-oxidized (Ox)-LDL (E), and phosphorylcholine-specific (EO6) antibodies (F) were detected by isotype-specific ELISA. RLU indicates relative light units. **P*<0.05 and ***P*<0.001.

mediators of DC function and T-cell responses in the spleen of *DC-hBcl-2* in this background (ie, IL-12p40 and IL-23p19 mRNAs; online-only Data Supplement Figure VA). In addition, we characterized the regulatory response in the *Apoe*$^{-/-}$ background and confirmed the absence of an effect on natural Treg (nTreg) as shown by the absence of major changes in the expression of key genes involved in nTreg function and development (CD25, GITR, ICOS, neuropilin-1, and Drosha; online-only Data Supplement Figure VB). Although a major increase in IL-10 mRNA levels was observed in spleens of *DC-hBcl-2→Ldl-r*$^{-/-}$ mice (Figure 2B), a trend for higher IL-10 mRNA levels in Western diet–fed-*DC-hBcl-2 Apoe*$^{-/-}$ mice was detectable (online-only Data Supplement Figure VA). However, in assays of restimulated splenocytes, CD4$^+$ T cells from *DC-hBcl-2* mice produced significantly more IL-10 than control CD4$^+$ T cells, whereas DCs from *DC-hBcl-2* mice produced less IL-10 than controls (Figure 7A and 7B). Such data suggest that changes in DC function and population are associated with increased production of IL-10 by CD4$^+$ T cells, most likely T regulatory type-1 (Tr-1) T cells. Finally, we observed a 4.2-fold increase in the percentage of CD4$^+$IL-17$^+$ cells compared with control *Apoe*$^{-/-}$ mice in restimulated splenocytes (Figure 7C). Moreover, intracellular staining for IL-12 and IFN-γ in CD4$^+$ T cells (Figure 7D and 7E) confirmed the Th1 signature, which indicates that

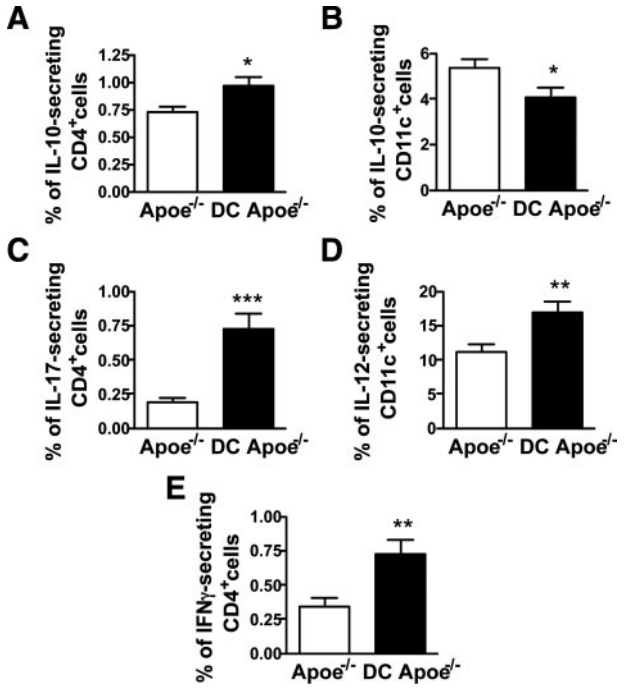

Figure 7. Intracellular staining for specific cytokines of $CD11c^+$ and $CD4^+$ splenocytes stimulated with lipopolysaccharide. Splenocytes from *DC-hBcl-2 Apoe*$^{-/-}$ (n=16) and *Apoe*$^{-/-}$ (n=15) mice fed a Western diet for 4 to 9 weeks were stimulated for 15 hours with lipopolysaccharide. A–E, Flow cytometric analysis of gated $CD4^+$ (A, C, E) and $CD11c^+$ (B, D) mouse splenocytes expressing IL-10 (A and B), IL-17 (C), IL-12p40 (D), and IFN-γ (E). *$P<0.05$, **$P<0.01$, ***$P<0.0001$.

both Th1 and Th17 phenotypes were upregulated in our model.

In conclusion, the main changes in immune system activation observed on the *Ldl-r*$^{-/-}$ background (ie, enhanced Th1 activation along with Th1-driven IgG2c anti-oxidized LDL and anti-malondialdehyde-LDL production) were equally present on an *Apoe*$^{-/-}$ background. Additionally, we observed an increase in the activity of the Th17 pathway and a potential increase in Tr-1 regulatory T cells.

Effect of DC Lifespan and Immunogenicity on Atherosclerotic Lesion Progression, Plasma Lipids, and Lipoprotein Profile in *Apoe*$^{-/-}$ Mice

We analyzed lesion area in chow-fed 20-week-old *DC-hBcl-2 Apoe*$^{-/-}$ and *Apoe*$^{-/-}$ mice and reported the absence of a significant difference between the 2 groups of animals (Figure 8A; 149.5±20.9 versus 181.4±17.5×10^3 μm^2, respectively; $P=0.3$). Moreover, comparison of plaque burden in *DC-hBcl-2 Apoe*$^{-/-}$ and *Apoe*$^{-/-}$ mice fed a Western diet for 8 weeks revealed no difference in lipid deposition between groups (Figure 8B; 184.1±21.7 versus 247.4±35.3×10^3 μm^2, respectively; $P=0.13$). Taken together, and despite marked elevation in T-cell activation and a Th1-polarized immune response in *DC-hBcl-2* mice compared with controls, no significant difference in lesion areas was found between groups. On the contrary, we observed a consistent trend toward attenuated lesion progression in *DC-hBcl-2* mice compared with controls in all mouse models studied. We next compared plasma lipid levels in *Apoe*$^{-/-}$ and *DC-hBcl-2*

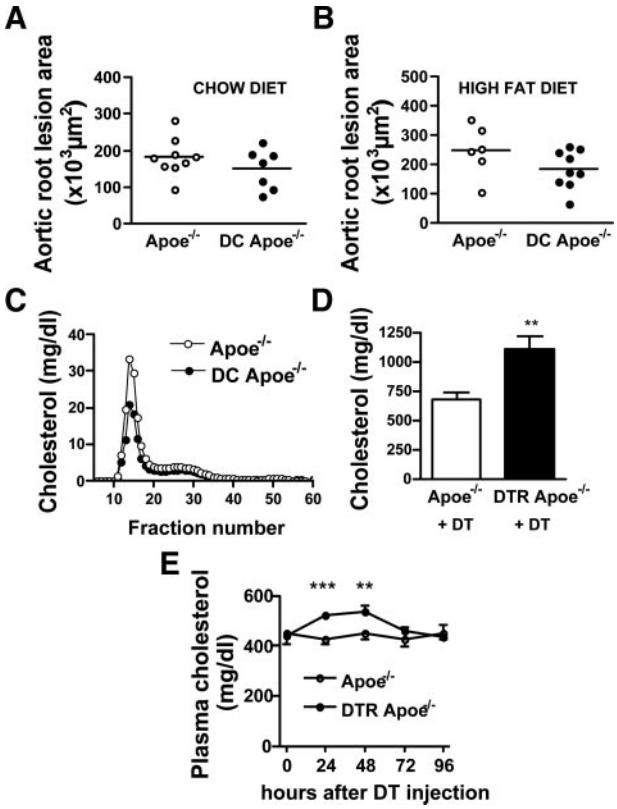

Figure 8. Quantification of atherosclerotic lesion surface, modulation of plasma cholesterol levels, and lipoprotein cholesterol profiles in *DC-hBcl-2 Apoe*$^{-/-}$ and *Apoe*$^{-/-}$ mice. The degree of atherosclerosis was determined by oil red O staining of aortic root sections from chow-fed 20-week-old *DC-hBcl-2 Apoe*$^{-/-}$ mice and *Apoe*$^{-/-}$ controls (A) and from *DC-hBcl-2 Apoe*$^{-/-}$ mice and *Apoe*$^{-/-}$ controls fed a Western diet for 8 weeks (B). Each symbol represents mean lesion area in a single mouse; horizontal bar indicates mean value for the respective group. C, Cholesterol distribution across VLDL, LDL, and HDL lipoprotein classes was analyzed by gel filtration in *DC-hBcl-2 Apoe*$^{-/-}$ and *Apoe*$^{-/-}$ mice fed a Western diet for 8 weeks. D, DC depletion was achieved by DT injection in *CD11c-DTR Apoe*$^{-/-}$ mice fed a Western diet, and plasma total cholesterol was determined and compared with *Apoe*$^{-/-}$ controls injected with DT. E, Time course of changes in plasma cholesterol levels in DT-treated *Apoe*$^{-/-}$ and *DC-hBcl2 Apoe*$^{-/-}$ mice maintained on a chow diet; values represent mean±SEM of 5 to 6 mice per group. Statistically significant differences between *CD11c-DTR Apoe*$^{-/-}$ and control groups: *$P=0.01$, **$P<0.01$, ***$P<0.0001$. Unpaired (A, B, and D) and paired (E) 2-tailed Student *t* tests were used.

Apoe$^{-/-}$ fed either a chow or a Western diet and observed that plasma total and free cholesterol levels were significantly decreased in *DC-hBcl-2 Apoe*$^{-/-}$ mice compared with controls in both conditions, whereas triglyceride levels were unchanged (Table). Analysis of cholesterol distribution among plasma lipoprotein classes in *DC-hBcl-2 Apoe*$^{-/-}$ animals fed the Western diet revealed a reduction in the cholesterol content of particles in the size range of both VLDL and LDL (−37% and −22%, respectively; Figure 8C). It is interesting to note that we did not observe such changes in plasma lipid levels in *DC-Bcl-2* mice on a wild-type background maintained on a chow diet (online-only Data Supplement Figure VI).

To confirm whether depletion of DCs in the *Apoe*$^{-/-}$ background would also result in an increase in cholesterol

levels as seen in the *LDL-r*–deficient background (Figure 5B), cholesterol-fed *CD11c-DTR Apoe*$^{-/-}$ mice and *Apoe*$^{-/-}$ controls were injected with DT. An increment of 63% in plasma cholesterol concentration was observed in DT-treated *CD11c-DTR Apoe*$^{-/-}$ mice compared with DT-treated *Apoe*$^{-/-}$ controls after 24 hours (1102±110 versus 676±64 mg/dL, respectively, $P=0.01$; Figure 8D). Next, we analyzed the time course of changes in plasma cholesterol levels in another set of *CD11c-DTR Apoe*$^{-/-}$ mice fed a normal chow and observed a transient increase (Figure 8E) that was statistically significant 24 and 48 hours after DT injection. This time course is consistent with published data on the duration of CD11c-positive cell depletion in DT treated-*CD11c-DTR* mice.[21] Such depletion was specific to conventional DCs and did not affect plasmacytoid DCs (online-only Data Supplement Figure VII). Considered together, these results reveal that modulation of conventional DC number impacts plasma cholesterol levels under conditions of hypercholesterolemia.

Discussion

A central question in the pathogenesis of atherosclerosis concerns the potential impact of DCs. Although DCs are present in human and murine atherosclerotic lesions,[5–7] a paucity of experimental data exists on the role of DCs in atherosclerotic plaque progression. Therefore, we designed genetically modified mouse models to address this question. For this purpose, we examined the relationship between DC lifespan and progression of atherosclerosis and made several novel findings: (1) The extended lifespan of DCs impacts on T-cell activation status and polarization of the immune response toward the Th1 pathway; (2) DCs markedly alter the degree of cholesterolemia in mice; and (3) the hypocholesterolemic action of DCs compensates for the proatherogenic Th1 response, thereby resulting in the absence of modification in atherosclerotic lesion size in *DC-hBcl-2* mice compared with controls.

DCs undergo accelerated clearance from lymphoid organs after interaction with antigen-specific T cells,[22] which indirectly indicates that their lifespan may influence the duration of their ability to stimulate lymphocytes. Indeed, in several mouse models in which apoptosis of DCs was inhibited (including overexpression of p35 or deletion of Bim), enhanced DC lifespan was associated with expansion of the DC population and enhanced immunogenicity, as revealed by a major impact on T-cell activation.[9,10] This is consistent with the increase in CD25$^+$, CD69$^+$, and CD44$^+$ CD4 T cells we observed in *DC-hBcl-2* mice. Moreover, in our model, we observed that DCs profoundly modulated both IL-12p40 and thereby IFN-γ expression. Such activated T cells and Th1 cytokines are proatherogenic, because they promote both lesion progression and plaque destabilization.[4,23] Moreover, we showed that IL-12p35 expression was not altered in *DC-hBcl-2* in either the *Ldl-r*$^{-/-}$ or the *Apoe*$^{-/-}$ background, whereas IL-23p19 mRNA levels were markedly elevated. Because the IL-12p40 subunit is common to both IL-12 (which is formed of the p40 and p35 subunits) and IL-23 (formed of the p40 and p19 subunits), such an expression profile is consistent with a marked increase in activity of the IL-23 pathway and suggests that the effect of DCs on immune system activation may also involve the IL-23 axis. This recently discovered pathway has been shown to drive the differentiation of Th17 cells, which are known to be triggers of autoimmune-driven inflammation.[24] Interestingly, we report activation of the Th17 pathway in our model. Nevertheless, to date, this pathway has not been implicated in plaque progression but might represent another proatherogenic arm of the immune system.

DCs had similarly been known to favor tolerance to antigens, and several studies suggest that this process may involve the generation of regulatory T cells.[2,25] In this context, we examined whether in atherosclerotic-prone mice, DCs may be critical for maintaining immune tolerance through their impact on the regulatory T-cell population. Treg cells are of particular importance in atherosclerosis, because recent evidence suggests that they are associated with protection against atherogenesis.[18,26] In an atherosclerotic context, we found no significant changes in the percentage of the splenic natural Treg population (CD4$^+$ Foxp3$^+$ CD25$^+$) in *DC-hBcl-2* mice, consistent with previous studies showing that DC lifespan and immunogenicity did not alter the natural Treg compartment.[9,10] Nevertheless, expression of IL-10 mRNA was upregulated in the spleen of *DC-hBcl-2→Ldl-r*$^{-/-}$ compared with control mice, and IL-10–producing CD4$^+$ T cells were increased in the spleen of *DC-hBcl-2 Apoe*$^{-/-}$ mice. Such enhancement would predict protection against lesion development, as suggested by studies in which the IL-10 axis was modulated.[23] Moreover, expansion of CD4$^+$ IL-10$^+$ T cells, also termed Tr-1 cells or adaptive Tregs, could exert an antiatherogenic effect in our model. Indeed, this specific T-cell compartment has been described as a potent antiatherogenic population that may help to combat Th1 proatherogenic bias.[27]

Th2 or Th1 responses are associated with an immunoglobulin class switching to IgG1 or IgG2c, respectively.[28,29] We therefore quantified titers of serum antibodies directed against oxidation-specific epitopes. Statistically significant increases occurred in titers of anti-malondialdehyde-LDL IgG2c and anti-oxidized LDL IgG2c in *DC-hBcl-2* mice on *Ldl-r*- or *Apoe*-deficient backgrounds, which corroborates the development of a Th1 bias immune response in these mice observed at the level of cytokine expression (IFN-γ, IL-12, IL-15, and TIM-3).

As a major result of the present study, we unexpectedly observed that elevation in the DC population led to markedly decreased plasma cholesterol levels in both the *Ldl-r*$^{-/-}$ and *Apoe*$^{-/-}$ backgrounds. Using a mouse model that allowed a reverse approach (ie, specific depletion of DCs), we observed that conventional DC elimination induced elevation in plasma cholesterol levels, thereby arguing that conventional DCs may contribute to correction of hyperlipidemia and that such cells may be implicated in cholesterol homeostasis. Interestingly, the impact of expansion of the DC population on plasma cholesterol levels is consistent with other observations in both mice and humans supporting a role for mononuclear phagocytes (macrophages, DCs, and Kupffer cells) in cholesterol homeostasis. For example, granulocyte-macrophage colony-stimulating factor, a key factor for DC growth

and differentiation,[30] has been reported to exhibit a cholesterol-lowering effect in patients with aplastic anemia,[31] a finding later confirmed in rabbits[32] and in patients with coronary artery disease.[33] Similarly, the hematopoietic growth factor macrophage colony-stimulating factor was also reported to lower cholesterol levels in rabbits and nonhuman primate models.[34,35] In mice, the opposite effect was observed in the *op/op* strain mutated for macrophage colony-stimulating factor, in which monocytes and tissue macrophage populations such as Kupffer cells are reduced.[36] Indeed, when bred on an *Apoe*$^{-/-}$ background, the *op/op Apoe*$^{-/-}$ mice present a 3-fold increase in cholesterol levels.[37] Considered together, these data indicate a strong relationship between the mononuclear phagocyte system and the potential control of cholesterol homeostasis. In the present study, we report for the first time the implication of conventional DCs as a cell type able to favor cholesterol lowering in a hyperlipidemic environment. The precise mechanisms that underlie the decrement in plasma cholesterol levels in our mouse model were not explored in the framework of the present study; however, because they are present in many tissues (spleen, liver, gut, and intestine), DCs might favor lipoprotein uptake and clearance from the circulation. Of note, Stoneman et al[38] reported no significant change in cholesterol levels in *CD11b-DTR Apoe*$^{-/-}$ mice treated with DT. In this latter model, DT-induced CD11b^{+} cell depletion was restricted to monocyte/macrophages, neutrophils, and CD11b^{+} conventional DCs, thereby indicating that depletion of these myeloid cells does not reproduce the effect observed on cholesterol levels in the *CD11c-DTR Apoe*$^{-/-}$ mice in the present study.

In addition to the role of DCs in facilitating a Th1-polarized immune response, the prevailing paradigm that underlies the proatherogenic effects of T cells, the present study revealed that the size of the conventional DC population was closely associated with regulation of cholesterol homeostasis. Overall, these antagonistic responses balanced each other out, with a null effect on atherosclerotic plaque progression. Clearly then, our findings identify the DC as a key player in atherosclerosis through its impact on both immune response regulation and cholesterol homeostasis.

Sources of Funding

This work was funded by INSERM, Fondation de France, Leducq Foundation, and National Institutes of Health HL086559 (Dr Witztum). Dr Gautier was supported by a Fellowship from the Fondation pour la Recherche Médicale. Drs Lesnik, Huby, and Chapman are recipients of "Contrat d'Interface" from Assistance Publique–Hôpitaux de Paris/INSERM.

Disclosures

None.

References

1. Guermonprez P, Valladeau J, Zitvogel L, Thery C, Amigorena S. Antigen presentation and T cell stimulation by dendritic cells. *Annu Rev Immunol*. 2002;20:621–667.
2. Groux H, Fournier N, Cottrez F. Role of dendritic cells in the generation of regulatory T cells. *Semin Immunol*. 2004;16:99–106.
3. Binder CJ, Chang MK, Shaw PX, Miller YI, Hartvigsen K, Dewan A, Witztum JL. Innate and acquired immunity in atherogenesis. *Nat Med*. 2002;8:1218–1226.
4. Hansson GK, Libby P. The immune response in atherosclerosis: a double-edged sword. *Nat Rev Immunol*. 2006;6:508–519.
5. Bobryshev YV, Taksir T, Lord RS, Freeman MW. Evidence that dendritic cells infiltrate atherosclerotic lesions in apolipoprotein E-deficient mice. *Histol Histopathol*. 2001;16:801–808.
6. Moos MP, John N, Grabner R, Nossmann S, Gunther B, Vollandt R, Funk CD, Kaiser B, Habenicht AJ. The lamina adventitia is the major site of immune cell accumulation in standard chow-fed apolipoprotein E-deficient mice. *Arterioscler Thromb Vasc Biol*. 2005;25:2386–2391.
7. Tacke F, Alvarez D, Kaplan TJ, Jakubzick C, Spanbroek R, Llodra J, Garin A, Liu J, Mack M, van Rooijen N, Lira SA, Habenicht AJ, Randolph GJ. Monocyte subsets differentially employ CCR2, CCR5, and CX3CR1 to accumulate within atherosclerotic plaques. *J Clin Invest*. 2007;117:185–194.
8. Nopora A, Brocker T. Bcl-2 controls dendritic cell longevity in vivo. *J Immunol*. 2002;169:3006–3014.
9. Chen M, Wang YH, Wang Y, Huang L, Sandoval H, Liu YJ, Wang J. Dendritic cell apoptosis in the maintenance of immune tolerance. *Science*. 2006;311:1160–1164.
10. Chen M, Huang L, Wang J. Deficiency of Bim in dendritic cells contributes to overactivation of lymphocytes and autoimmunity. *Blood*. 2007;109:4360–4367.
11. Park D, Lapteva N, Seethammagari M, Slawin KM, Spencer DM. An essential role for Akt1 in dendritic cell function and tumor immunotherapy. *Nat Biotechnol*. 2006;24:1581–1590.
12. Hou WS, Van Parijs L. A Bcl-2-dependent molecular timer regulates the lifespan and immunogenicity of dendritic cells. *Nat Immunol*. 2004;5:583–589.
13. Gautier EL, Huby T, Ouzilleau B, Doucet C, Saint-Charles F, Gremy G, Chapman MJ, Lesnik P. Enhanced immune system activation and arterial inflammation accelerates atherosclerosis in lupus-prone mice. *Arterioscler Thromb Vasc Biol*. 2007;27:1625–1631.
14. Gautier EL, Huby T, Saint-Charles F, Ouzilleau B, Chapman MJ, Lesnik P. Enhanced dendritic cell survival attenuates lipopolysaccharide-induced immunosuppression and increases resistance to lethal endotoxic shock. *J Immunol*. 2008;180:6941–6946.
15. Binder CJ, Hartvigsen K, Chang MK, Miller M, Broide D, Palinski W, Curtiss LK, Corr M, Witztum JL. IL-5 links adaptive and natural immunity specific for epitopes of oxidized LDL and protects from atherosclerosis. *J Clin Invest*. 2004;114:427–437.
16. Gautier EL, Huby T, Witztum JL, Ouzilleau B, Miller ER, Saint-Charles F, Aucouturier P, Chapman MJ, Lesnik P. Macrophage apoptosis exerts divergent effects on atherogenesis as a function of lesion stage. *Circulation*. 2009;119:1795–1804.
17. Sapoznikov A, Fischer JA, Zaft T, Krauthgamer R, Dzionek A, Jung S. Organ-dependent in vivo priming of naive CD4+, but not CD8+, T cells by plasmacytoid dendritic cells. *J Exp Med*. 2007;204:1923–1933.
18. Ait-Oufella H, Salomon BL, Potteaux S, Robertson AK, Gourdy P, Zoll J, Merval R, Esposito B, Cohen JL, Fisson S, Flavell RA, Hansson GK, Klatzmann D, Tedgui A, Mallat Z. Natural regulatory T cells control the development of atherosclerosis in mice. *Nat Med*. 2006;12:178–180.
19. Caligiuri G, Nicoletti A, Poirier B, Hansson GK. Protective immunity against atherosclerosis carried by B cells of hypercholesterolemic mice. *J Clin Invest*. 2002;109:745–753.
20. Major AS, Fazio S, Linton MF. B-lymphocyte deficiency increases atherosclerosis in LDL receptor-null mice. *Arterioscler Thromb Vasc Biol*. 2002;22:1892–1898.
21. Jung S, Unutmaz D, Wong P, Sano G, De los Santos K, Sparwasser T, Wu S, Vuthoori S, Ko K, Zavala F, Pamer EG, Littman DR, Lang RA. In vivo depletion of CD11c(+) dendritic cells abrogates priming of CD8(+) T cells by exogenous cell-associated antigens. *Immunity*. 2002;17:211–220.
22. Kamath AT, Henri S, Battye F, Tough DF, Shortman K. Developmental kinetics and lifespan of dendritic cells in mouse lymphoid organs. *Blood*. 2002;100:1734–1741.
23. Tedgui A, Mallat Z. Cytokines in atherosclerosis: pathogenic and regulatory pathways. *Physiol Rev*. 2006;86:515–581.
24. Kikly K, Liu L, Na S, Sedgwick JD. The IL-23/Th(17) axis: therapeutic targets for autoimmune inflammation. *Curr Opin Immunol*. 2006;18:670–675.
25. Steinman R. Ralph Steinman: pioneering new perspectives on the immune system and infectious diseases. Interviewed by Marilynn Larkin. *Lancet Infect Dis*. 2003;3:383–386.
26. van Puijvelde GH, van Es T, van Wanrooij EJ, Habets KL, de Vos P, van der Zee R, van Eden W, van Berkel TJ, Kuiper J. Induction of oral

tolerance to HSP60 or an HSP60-peptide activates T cell regulation and reduces atherosclerosis. *Arterioscler Thromb Vasc Biol*. 2007;27:2677–2683.
27. Mallat Z, Gojova A, Brun V, Esposito B, Fournier N, Cottrez F, Tedgui A, Groux H. Induction of a regulatory T cell type 1 response reduces the development of atherosclerosis in apolipoprotein E-knockout mice. *Circulation*. 2003;108:1232–1237.
28. Toellner KM, Luther SA, Sze DM, Choy RK, Taylor DR, MacLennan IC, Acha-Orbea H. T helper 1 (Th1) and Th2 characteristics start to develop during T cell priming and are associated with an immediate ability to induce immunoglobulin class switching. *J Exp Med*. 1998;187:1193–1204.
29. Martin RM, Brady JL, Lew AM. The need for IgG2c specific antiserum when isotyping antibodies from C57BL/6 and NOD mice. *J Immunol Methods*. 1998;212:187–192.
30. Hanada K, Tsunoda R, Hamada H. GM-CSF-induced in vivo expansion of splenic dendritic cells and their strong costimulation activity. *J Leukoc Biol*. 1996;60:181–190.
31. Nimer SD, Champlin RE, Golde DW. Serum cholesterol-lowering activity of granulocyte-macrophage colony-stimulating factor. *JAMA*. 1988;260:3297–3300.
32. Ishibashi T, Yokoyama K, Shindo J, Hamazaki Y, Endo Y, Sato T, Takahashi S, Kawarabayasi Y, Shiomi M, Yamamoto T. Potent cholesterol-lowering effect by human granulocyte-macrophage colony-stimulating factor in rabbits: possible implications of enhancement of macrophage functions and an increase in mRNA for VLDL receptor. *Arterioscler Thromb*. 1994;14:1534–1541.
33. Zbinden S, Zbinden R, Meier P, Windecker S, Seiler C. Safety and efficacy of subcutaneous-only granulocyte-macrophage colony-stimulating factor for collateral growth promotion in patients with coronary artery disease. *J Am Coll Cardiol*. 2005;46:1636–1642.
34. Shimano H, Yamada N, Motoyoshi K, Matsumoto A, Ishibashi S, Mori N, Takaku F. Plasma cholesterol-lowering activity of monocyte colony-stimulating factor (M-CSF). *Ann N Y Acad Sci*. 1990;587:362–370.
35. Stoudemire JB, Garnick MB. Effects of recombinant human macrophage colony-stimulating factor on plasma cholesterol levels. *Blood*. 1991;77:750–755.
36. Witmer-Pack MD, Hughes DA, Schuler G, Lawson L, McWilliam A, Inaba K, Steinman RM, Gordon S. Identification of macrophages and dendritic cells in the osteopetrotic (op/op) mouse. *J Cell Sci*. 1993;104(pt 4):1021–1029.
37. Qiao JH, Tripathi J, Mishra NK, Cai Y, Tripathi S, Wang XP, Imes S, Fishbein MC, Clinton SK, Libby P, Lusis AJ, Rajavashisth TB. Role of macrophage colony-stimulating factor in atherosclerosis: studies of osteopetrotic mice. *Am J Pathol*. 1997;150:1687–1699.
38. Stoneman V, Braganza D, Figg N, Mercer J, Lang R, Goddard M, Bennett M. Monocyte/macrophage suppression in CD11b diphtheria toxin receptor transgenic mice differentially affects atherogenesis and established plaques. *Circ Res*. 2007;100:884–893.

CLINICAL PERSPECTIVE

In healthy and pathological tissues, dendritic cells (DCs) are the most effective cells to present antigens and to initiate immune responses. DCs have an elevated capacity to stimulate T lymphocytes, natural killer lymphocytes, and B lymphocytes. Thus, they represent a potential tool for vaccination or immunotherapy in infectious disease, cancers, transplant rejection, autoimmune diseases, and immunoinflammatory diseases. During atherogenesis, immunoinflammatory mechanisms contribute to the progression of atherosclerotic lesions; however, the precise role of DCs in the progression of atherosclerosis and related cardiovascular disease is indeterminate. To address this question, we created transgenic mice in which the lifespan of DCs was increased in response to elevated resistance to apoptosis (CD11c-hBcl2) on the one hand, and on the other, we used mice in which targeted depletion of DCs (CD11c-DTR [diphtheria toxin receptor]) could be achieved. The present data provide the first in vivo evidence that DCs profoundly and broadly impact immune responses in atherosclerosis and, unexpectedly, circulating cholesterol levels, a major cardiovascular risk factor. The impact of DCs on cholesterolemia level is relevant to data published in preclinical and clinical studies using granulocyte-macrophage colony stimulating factor, a well-known DC growth factor. Indeed, granulocyte-macrophage colony stimulating factor induced a reduction in circulating cholesterol levels in treated patients. Considered together, the potential role of DCs as a central regulator of both immunity and cholesterol homeostasis opens new therapeutic horizons in the treatment of atherosclerosis.

Systemic Analysis of PPARγ in Mouse Macrophage Populations Reveals Marked Diversity in Expression with Critical Roles in Resolution of Inflammation and Airway Immunity

Emmanuel L. Gautier,[*,†,‡] Andrew Chow,[†,§] Rainer Spanbroek,[¶] Genevieve Marcelin,[‖] Melanie Greter,[†,§] Claudia Jakubzick,[*,†,1] Milena Bogunovic,[†,§] Marylene Leboeuf,[†,§] Nico van Rooijen,[#] Andreas J. Habenicht,[¶] Miriam Merad,[†,§] and Gwendalyn J. Randolph[*,†,‡]

Although peroxisome proliferator-activated receptor γ (PPARγ) has anti-inflammatory actions in macrophages, which macrophage populations express PPARγ in vivo and how it regulates tissue homeostasis in the steady state and during inflammation remains unclear. We now show that lung and spleen macrophages selectively expressed PPARγ among resting tissue macrophages. In addition, Ly-6C^{hi} monocytes recruited to an inflammatory site induced PPARγ as they differentiated to macrophages. When PPARγ was absent in Ly-6C^{hi}–derived inflammatory macrophages, initiation of the inflammatory response was unaffected, but full resolution of inflammation failed, leading to chronic leukocyte recruitment. Conversely, PPARγ activation favored resolution of inflammation in a macrophage PPARγ-dependent manner. In the steady state, PPARγ deficiency in red pulp macrophages did not induce overt inflammation in the spleen. By contrast, PPARγ deletion in lung macrophages induced mild pulmonary inflammation at the steady state and surprisingly precipitated mortality upon infection with *Streptococcus pneumoniae*. This accelerated mortality was associated with impaired bacterial clearance and inability to sustain macrophages locally. Overall, we uncovered critical roles for macrophage PPARγ in promoting resolution of inflammation and maintaining functionality in lung macrophages where it plays a pivotal role in supporting pulmonary host defense. In addition, this work identifies specific macrophage populations as potential targets for the anti-inflammatory actions of PPARγ agonists. *The Journal of Immunology*, **2012, 189: 2614–2624.**

Peroxisome proliferator-activated receptor γ (PPARγ) is a ligand-controlled transcription factor of the nuclear receptor family capable of regulating gene expression by transactivation or transrepression (1). First discovered as the master regulator of the genetic program supporting adipocyte differentiation, PPARγ is involved in the regulation of a number of physiological processes such as the response to insulin, cell proliferation, cellular lipid metabolism, and inflammation (2). Thus, PPARγ activation is an attractive therapeutic target in a variety of diseases such as type 2 diabetes, cancer, atherosclerosis, and immune disorders. Activation of PPARγ can be achieved by natural fatty acid derivatives as well as synthetic ligands from the thiazolidinedione family, the latter being used clinically to improve insulin sensitivity in type 2 diabetic patients (3).

The anti-inflammatory role of PPARγ came to the forefront in the late 1990s when 15-deoxy-δ-12,14-PG J2 (15d-PGJ$_2$) and thiazolidinediones were shown to dampen macrophage activation in vitro by activating PPARγ (4, 5). Since then, the anti-inflammatory role of PPARγ agonists has been extensively documented in vitro and in vivo (1, 6). Indeed, PPARγ agonists suppress dextran sodium sulfate-induced colitis (7), obesity-induced insulin resistance (8), and the progression of atherosclerosis (9). By contrast, deletion of PPARγ in macrophages exacerbates the development of atherosclerosis (10, 11), colitis (12), and obesity-induced insulin

*Department of Developmental and Regenerative Biology, Mount Sinai School of Medicine, New York, NY 10029; [†]Immunology Institute, Mount Sinai School of Medicine, New York, NY 10029; [‡]Department of Pathology and Immunology, Washington University, St. Louis, MO 63110; [§]Department of Oncological Sciences, Mount Sinai School of Medicine, New York, NY 10029; [¶]Institute for Vascular Medicine, Friedrich Schiller University of Jena, Jena University Hospital, 07743 Jena, Germany; [‖]Albert Einstein College of Medicine, Bronx, NY 10461; and [#]Department of Molecular Cell Biology, Free University Medical Center, 1007 Amsterdam, The Netherlands

[1]Current address: Integrated Department of Immunology, National Jewish Health, University of Colorado, Denver, CO.

Received for publication February 9, 2012. Accepted for publication July 4, 2012.

This work was supported by National Institutes of Health Grants AI061741 and AI049653 and American Heart Association Established Investigator Award 0740052 (to G.J.R.), National Institutes of Health Grant HL086899 (to M.M.), Deutsche Forschungsgemeinschaft Project Grant SP71314-1 (to R.S.), and Deutsche Forschungsgemeinschaft Project Grants Ha 1083/16-1 and Ha 1083/15-1 (to A.J.H.). E.L.G. is supported by a fellowship from the American Heart Association (10POST4160140), and A.C. is funded by a fellowship from the National Institutes of Health, National Heart, Lung, and Blood Institute 5F30HL099028-02.

The datasets presented in this article have been submitted to the National Center for Biotechnology Information/Gene Expression Omnibus (http://www.ncbi.nlm.nih.gov/geo/) under accession numbers GSE15907 and GSE32034.

Address correspondence and reprint requests to Dr. Emmanuel L. Gautier and Dr. Gwendalyn J. Randolph, Department of Pathology and Immunology, Washington University, 660 South Euclid Avenue, Campus Box 8118, St. Louis, MO 63110. E-mail addresses: egautier@path.wustl.edu (E.L.G.) and GRandolph@path.wustl.edu (G.J.R.)

The online version of this article contains supplemental material.

Abbreviations used in this article: DC, dendritic cell; 15d-PGJ$_2$, 15-deoxy-δ-12,14-PG J2; FABP4, fatty acid binding protein 4; PAP, pulmonary alveolar proteinosis; PPAR, peroxisome proliferator-activated receptor.

www.jimmunol.org/cgi/doi/10.4049/jimmunol.1200495

resistance (13). On the basis of these studies, a model emerges wherein macrophages are universally central targets of PPARγ modulation. However, it is not known whether all monocyte/macrophage populations express PPARγ or rely on its activation to maintain homeostasis or to carry out their functions in different organs during inflammation. Ultimately, the design and development of therapeutic strategies based on the use of PPARγ agonists to combat inflammatory diseases would benefit from the identification of the specific macrophage populations potentially responsive to these agonists.

In this context, we decided to profile the expression of PPARγ in a range of macrophage populations extracted from different organs, delineate its preferential site of expression, and examine the impact of its deficiency during the steady state and after inflammatory challenge in relevant tissues. We show in vivo that PPARγ is induced in monocytes recruited to sites of inflammation as they differentiate into macrophages, and its function is required to fully turn off inflammatory cell recruitment during resolution. In resting tissue macrophages, PPARγ expression was found to be restricted to specific populations, which are lung and splenic red pulp macrophages. In the lung but not the spleen, deficiency of PPARγ in macrophages was associated with low-level spontaneous inflammation in the steady state and profound alterations in macrophage gene expression. Challenge with *Streptococcus pneumoniae* revealed that deletion of PPARγ in lung macrophages impaired host defense, delaying bacterial clearance and thereby accelerating infection-induced mortality. Overall, these findings uncovered a key role of macrophage PPARγ in supporting resolution of inflammation while pointing specifically to the lung as a central organ where the function of PPARγ goes beyond an anti-inflammatory role and extends critically into maintenance of host defense.

Materials and Methods

Animals and treatments

LysM-cre mice (C57BL/6J) and PPARγ floxed mice (C57BL/6J) were obtained from The Jackson Laboratory and crossed in house to generate mice with PPARγ deficiency in myeloid cells (hereafter named LysM-Cre × PPARγ$^{flox/flox}$). LysM-cre × Rosa26-stop^{flox}EGFP reporter mice were bred in-house. *Csf2rb*$^{-/-}$*Csf2rb2*$^{-/-}$ and C57BL/6J control mice were obtained from The Jackson Laboratory. For acute inflammation and resolution experiments, peritonitis was induced by i.p. injection of 1 ml sterile thioglycollate (3% w/v; Sigma-Aldrich). Induction of inflammation in the spleen was achieved by i.v. LPS injection (*Escherichia coli* 026:B6; 20 μg/mouse). For infection experiments, mice were inoculated intranasally with 2×10^6 or 5×10^5 CFU *Streptococcus pneumoniae* serotype 3 (ATCC number 6303; American Type Culture Collection), and survival was assessed every other day over a period of 12 d. Mice were housed in a specific pathogen-free environment and used in accordance with protocols approved by the Institutional Animal Care and Utilization Committee at Mount Sinai School of Medicine.

Microarray analysis

Monocytes were identified as CD115$^+$ low side-scatter cells and sorted into two subsets based on Ly6-C expression as described previously (14, 15). All other microarrays on mononuclear phagocytes were carried out as part of the Immunological Genome Project (http://www.immgen.org) (16). The isolation procedures and corresponding flow plots for all cells can be found on the ImmGen Web site. Steady-state macrophages from the peritoneum were sorted into two populations (17), including CD115$^+$F4/80^{hi}MHC II$^-$ Ly6-C$^-$B220$^-$ and CD115$^+$ F4/80^{lo}MHC II$^+$Ly6-C$^-$B220$^-$ populations; inflamed peritoneal macrophages were CD115$^+$F4/80^{int}Ly6-C$^-$B220$^-$, whereas neutrophils were sorted as Ly6-G$^+$Ly6-C^{int}CD115$^-$B220$^-$ cells. In the lung, macrophages were sorted as CD11c$^+$MHC II^{lo}SiglecF$^+$ CD11b$^-$ cells (18), and lung dendritic cells (DCs) as CD11c$^+$MHC II$^+$ cells that were either CD11b$^+$ (CD11b$^+$ DCs) or CD103$^+$ (CD103$^+$ DCs) (18). Brain microglia were sorted as CD45^{lo}CD11b$^+$F4/80$^+$ cells (19). Gut macrophages were CD45$^+$CD11c^{lo}MHC II$^+$CD103$^-$CD11b$^+$ cells (20). In the spleen, red pulp macrophages were F4/80^{hi}MHC^{int} cells, and DC subsets were CD11c$^+$MHC II$^+$ cells that differentially expressed CD4 (CD11b$^+$CD4$^+$CD8$^-$) or CD8 (CD11b$^-$CD4$^-$CD8$^+$) (21). RNA was prepared from sorted populations from C57BL/6J mice after sorting directly into TRIzol reagent, amplified, and hybridized on the Affymetrix Mouse Gene 1.0 ST. For data analysis using ImmGen datasets, raw data for all populations were normalized using the robust multiarray averaging algorithm. Extensive quality control documents are available on the Immgen Web site. All datasets have been deposited at the National Center for Biotechnology Information/Gene Expression Omnibus under accession number GSE15907 (http://www.ncbi.nlm.nih.gov/geo/query/acc.cgi?acc=GSE15907). Microarrays on blood monocytes treated with a PPARγ agonist were performed as previously described (15) using Affymetrix GeneChip 430 2.0 arrays. Corresponding datasets have been deposited at National Center for Biotechnology Information/Gene Expression Omnibus under accession number GSE32034 (http://www.ncbi.nlm.nih.gov/geo/query/acc.cgi?acc=GSE32034).

Blood and tissue sample preparation for flow cytometry

Mouse blood was collected by nonterminal submandibular or terminal cardiac puncture, and RBCs were lysed in hypotonic buffer (PharmLyse; BD Biosciences). Total leukocytes were quantitated by fresh blood dilution in Turk's solution (Ricca Chemical). Lungs were harvested, minced, incubated in HBSS containing 3% FBS and collagenase D for 1 h, passed through an 18-gauge needle to obtain homogeneous cell suspensions, and filtered using a 100-μm cell strainer. Bronchoalveolar lavage was obtained by flushing the airways four times with HBSS. Spleens were minced, placed into the cup portion of a cell strainer, and then gently mashed and pushed through the cell strainer. RBCs were then lysed in hypotonic buffer. Peritoneal exudates were collected using cold HBSS. Cell suspensions were then stained with appropriate Abs for 30 min on ice, and data were acquired on a BD FACSCanto II Flow Cytometer (BD Biosciences) and analyzed with FlowJo software (Tree Star).

Fluorescent conjugates of anti-mouse CD115 (AFS98), F4/80 (BM8), CD45 (30-F11), CD11c (N418), IA-IE (M5/114.15.2), CD4 (GK1.5), CD8 (53-6.7), CD45.2 (104), and CD45.1 (A20) were purchased from eBioscience. Anti-mouse Gr-1 (Ly-6C/G and RB6-8C5) and CD36 (HM36) were purchased from BioLegend. Anti-mouse F4/80 (CI:A3-1) was purchased from Serotec. Anti-mouse CD36 (CRF D-2712), Ly6G (1A8), and siglec F (E50-2440) were purchased from BD Biosciences. Anti-mouse fatty acid binding protein 4 (FABP4) (BAF1443) was from R&D Systems.

Immunoblot analysis

FACS sorted cells were homogenized in lysis buffer containing protease inhibitors. Protein extracts were run on Criterion gels (Bio-Rad) and blotted onto nitrocellulose membranes. After blocking, immunoblots were incubated with primary Abs against PPARγ and β-actin (Cell signaling). Blots were then incubated with fluorescent secondary Abs and proteins were detected using the fluorescence-based Odyssey Infrared Imaging System (LI-COR Biosciences).

Macrophage transfer

Peritoneal macrophages were retrieved by lavage from CD45.2 Lys-Cre × PPARγ$^{flox/flox}$ and wild-type controls 5 d after thioglycollate instillation. Then, 5×10^6 macrophages were injected into the peritoneum of naive CD45.1 wild-type mice, and the number of recruited CD45.1$^+$ neutrophils was assessed 24 h later.

Monocyte labeling in vivo

Ly-6C^{lo} monocytes were labeled in vivo by i.v. injection of 1 μm Fluoresbrite green fluorescent (YG) plain microspheres (Polysciences) diluted 1:4 in sterile PBS (22, 23). Ly-6C^{hi} monocytes were labeled with beads using the same protocol, except that beads were administered 3 d after i.v. injection of clodronate-loaded liposomes (250 μl/mouse) (22). Labeling efficiency was verified by flow cytometry 1 and/or 2 d after labeling by analysis of blood collected i.v. through the submandibular vein. Clodronate was a gift from Roche and was incorporated into liposomes as described previously (24).

Analysis of gene expression by quantitative real-time PCR

RNA samples were prepared using TRIzol reagent (Invitrogen) from thioglycollate-elicited macrophages isolated from mice at sacrifice. Each RNA preparation was hybridized with oligo dT (Invitrogen) and reverse transcribed using Superscript III reverse transcriptase (Invitrogen). Quantitative real-time PCR was performed using a LightCycler PCR System (Roche) as described previously (25). Expression data were analyzed by

crossing points calculated from the LightCycler data analysis software and corrected for PCR efficiencies of both the target and the reference gene.

Analysis of bacterial burden

Bacterial burden was quantified by plating 10 μl of lung homogenates serially diluted in trypticase soy broth (BD) on blood agar plates (trypticase soy broth plus 1.875% agar plus 5% sheep blood). After incubating plates at 37°C for 18–24 h, colonies were counted.

Statistical analysis

Data are expressed as mean ± SEM. Statistical differences were assessed using a two-tailed *t* test or ANOVA (with Tukey's posttest analysis) with GraphPad Prism software. A p value <0.05 was considered statistically significant.

Results

Differential expression of PPARγ and regulation of canonical PPARγ target genes among different tissue macrophage populations

To better understand the role of PPARγ in mononuclear phagocytes, we first assessed PPARγ mRNA expression in blood monocytes, resident macrophages from different tissues, including the lung, splenic red pulp, brain (microglia), gut, and peritoneum, as well as in inflammatory peritoneal macrophages. For monocytes, we independently assessed the two major circulating subsets that in mice differentially express Ly6-C and which have counterparts in other species, including humans (14, 26). We compared these populations to spleen and lung conventional DC subsets as well as neutrophils. The populations were sorted (see http://www.immgen.org for detailed sorting strategies) and further analyzed by gene array. PPARγ mRNA was differentially expressed over several orders of magnitude in different mononuclear phagocytes (Fig. 1A). Macrophages from the steady-state peritoneum, brain, and gut expressed only low levels of PPARγ, equivalent to the signal intensity in Ly-6C^{hi} blood monocytes and neutrophils. By contrast, high levels of PPARγ mRNA were observed in Ly-6C^{lo} monocytes, splenic red pulp macrophages, and pulmonary macrophages (Fig. 1A). Consistent with this, treatment of wild-type mice with the PPARγ agonist rosiglitazone induced further expression of the PPARγ-inducible CD36 protein at the cell surface of Ly-6C^{lo} but not Ly-6C^{hi} monocytes in wild-type animals, suggesting that only the Ly-6C^{lo} but not Ly6-C^{hi} monocytes were responsive to PPARγ activation (Fig. 1B). Indeed, PPARγ activation profoundly impacted the transcriptome of Ly-6C^{lo} monocytes (602 genes downregulated and 1222 genes upregulated, 2-fold cutoff) (Fig. 1C, Supplemental Table I) and especially affected gene signatures such as "DC maturation," "p53 signaling," and "NFAT and immune response" (E.L. Gautier and G.J. Randolph, unpublished observations). By contrast, Ly-6C^{hi} monocytes were largely unresponsive to the agonist (66 genes downregulated and 77 genes upregulated) (Fig. 1C, Supplemental Table II), suggesting that the levels of PPARγ in Ly-6C^{hi} monocytes, and by extension in neutrophils, DCs, steady-state peritoneum, brain, and gut macrophages, are too low to confer significant responsiveness to PPARγ ligands under homeostatic conditions. This was further confirmed as neutrophils, DCs, and peritoneal macrophages did not upregulate the expression of the two prototypic PPARγ target genes CD36 and FABP4 following PPARγ agonist treatment (pioglitazone), whereas other populations that express PPARγ upregulated CD36 and/or FAPB4 (Fig. 1D). Populations that upregulated CD36 and FABP4 in response to PPARγ agonists typically did so in a PPARγ-dependent manner (Fig. 1E), but diversity in expression of these canonical PPARγ targets was substantial. Lung macrophages did not express surface levels of CD36, even after PPARγ agonist treatment (Fig. 1E), but blood Ly6-C^{lo} monocytes increased CD36 expression in response to pioglitazone in a PPARγ-dependent manner (Fig. 1E). FABP4 was differentially expressed among lung macrophages, raising the possibility of heterogeneity in this population, and its expression was completely dependent on PPARγ, whether at baseline or after pioglitazone treatment. By contrast, basal FABP4 was not dependent on PPARγ in spleen macrophages, although it was responsive to induction by pioglitazone in a PPARγ-dependent manner (Fig. 1E). Overall, these data point to a great diversity in PPARγ expression among resting differentiated macrophages, indicating that PPARγ upregulation is not necessarily an inevitable consequence of macrophage development (27) and revealing that the expression of putative PPARγ target genes are regulated somewhat differently in different tissue macrophage populations.

Acquisition of PPARγ expression by Ly-6C^{hi} monocyte-derived inflammatory macrophages is necessary for full resolution of acute inflammation

PPARγ activity has been associated with anti-inflammatory responses. In the inflammatory milieu of the thioglycollate-treated peritoneum, elicited macrophages from the peritoneal cavity expressed 3-fold higher PPARγ mRNA than blood Ly-6C^{hi} monocytes (Fig. 2A) from which they derive (14, 28). PPARγ was functional in these cells because PPARγ activation using a synthetic ligand increased cell surface expression of the PPARγ-inducible protein CD36 (data not shown), and PPARγ was efficiently deleted in these cells in LysM-Cre × PPARγ$^{flox/flox}$ mice (Fig. 2B). In wild-type mice, leukocytes accumulate for several days after thioglycollate injection, with a marked resolution phase between days 5 and 8 when inflammatory macrophage numbers decline to baseline levels (29). To examine whether PPARγ deficiency in Ly-6C^{hi} monocyte-derived inflammatory peritoneal macrophages would alter the initiation and/or the resolution of thioglycollate-induced inflammation, we used LysM-Cre × PPARγ$^{flox/flox}$ mice that in this study lack PPARγ expression specifically in macrophages, because neutrophils do not express PPARγ. First, using LysM-Cre × Rosa26-stop^{flox}EGFP reporter mice to identify cells with use of the LysM promoter using GFP expression, we confirmed that >90% of inflammatory macrophages in the inflamed peritoneum would be targeted in LysM-Cre × PPARγ$^{flox/flox}$ mice in addition to macrophages in resting peritoneum and neutrophils (data not shown). In the steady state, the total numbers of the two peritoneal resident macrophage populations (17) (CD115^{+}F480^{hi}MHC-II^{-} or CD115^{+} F480^{lo}MHC-II^{+}) were unchanged in LysM-Cre × PPARγ$^{flox/flox}$ mice as compared with controls, and the numbers of infiltrated neutrophils and Ly-6C^{hi} monocytes were similarly very low in the presence or absence of PPARγ (data not shown).

During the course of peritonitis, early accumulation of CD115^{hi} inflammatory macrophages (Fig. 2C) in the peritoneum was unaltered by PPARγ deficiency 1 d after instillation of thioglycollate but was slightly decreased after 5 and 8 d in LysM-Cre × PPARγ$^{flox/flox}$ mice (Fig. 2D). However, we noted a 3-5-fold increase in the number of infiltrated Ly-6C^{hi} monocytes at both days 5 and 8 compared with control mice (Fig. 2C, 2E), whereas circulating monocyte subset numbers remained similar over time in both LysM-Cre × PPARγ$^{flox/flox}$ mice and controls (data not shown). Because Ly-6C is retained only transiently after monocyte recruitment into tissues (26, 30, 31), these data revealed that monocyte recruitment to the peritoneal cavity did not fully shut down in LysM-Cre × PPARγ$^{flox/flox}$ mice. Furthermore, although early accumulation of neutrophils (6 and 24 h) was comparable between LysM-Cre × PPARγ$^{flox/flox}$ mice and control animals, peritoneal neutrophil numbers were likewise elevated 3- to 4-fold

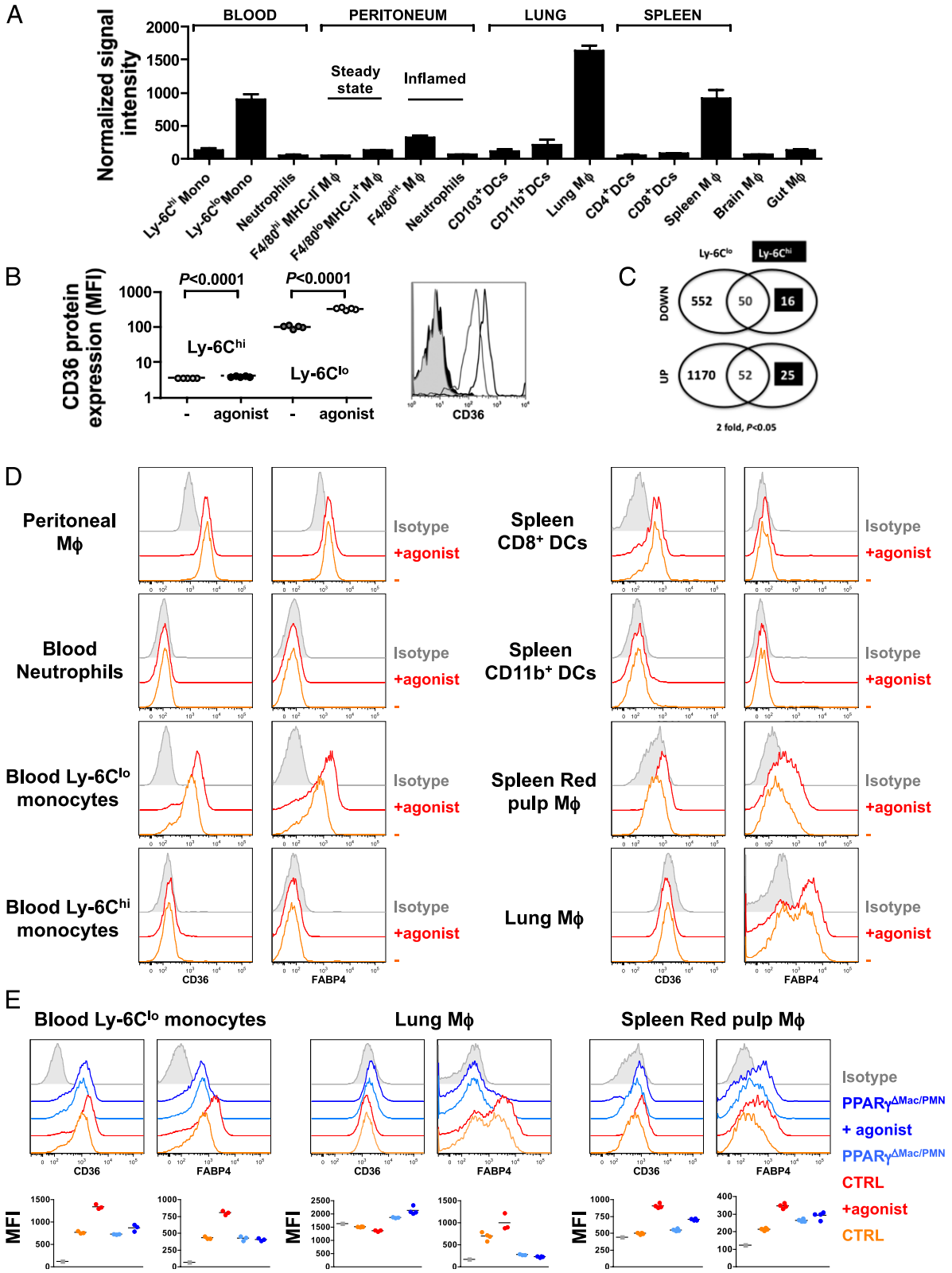

FIGURE 1. PPARγ gene expression profiling and regulation of canonical PPARγ target genes in mononuclear phagocytes. (**A**) PPARγ mRNA expression was analyzed by gene array and depicted to show signal intensity in sorted myeloid cell populations. Data are derived from three separate analyses that are each derived from $n = 5$ mice. (**B**) Cell surface expression of CD36 analyzed by flow cytometry on monocyte subsets from mice fed a regular chow diet (−) or a diet supplemented with the PPARγ agonist rosiglitazone (agonist) for a week ($n = 5$ mice/group). (**C**) The number of genes regulated in monocyte subsets following PPARγ activation by rosiglitazone assessed through whole-genome array analysis. (**D**) Protein levels of CD36 and FABP4 in myeloid populations at the steady state and following PPARγ agonist treatment (agonist, pioglitazone) were monitored by flow cytometry. (**E**) Expression of CD36 and FABP4 in myeloid populations of LysM-Cre × PPARγ$^{flox/flox}$ mice (PPARγ$^{\Delta Mac/PMN}$) and controls (CTRL) at the steady state and following PPARγ agonist treatment (agonist, pioglitazone). Mean fluorescence intensity (MFI) is plotted ($n = 3$–4 mice/group). Mϕ, Macrophage.

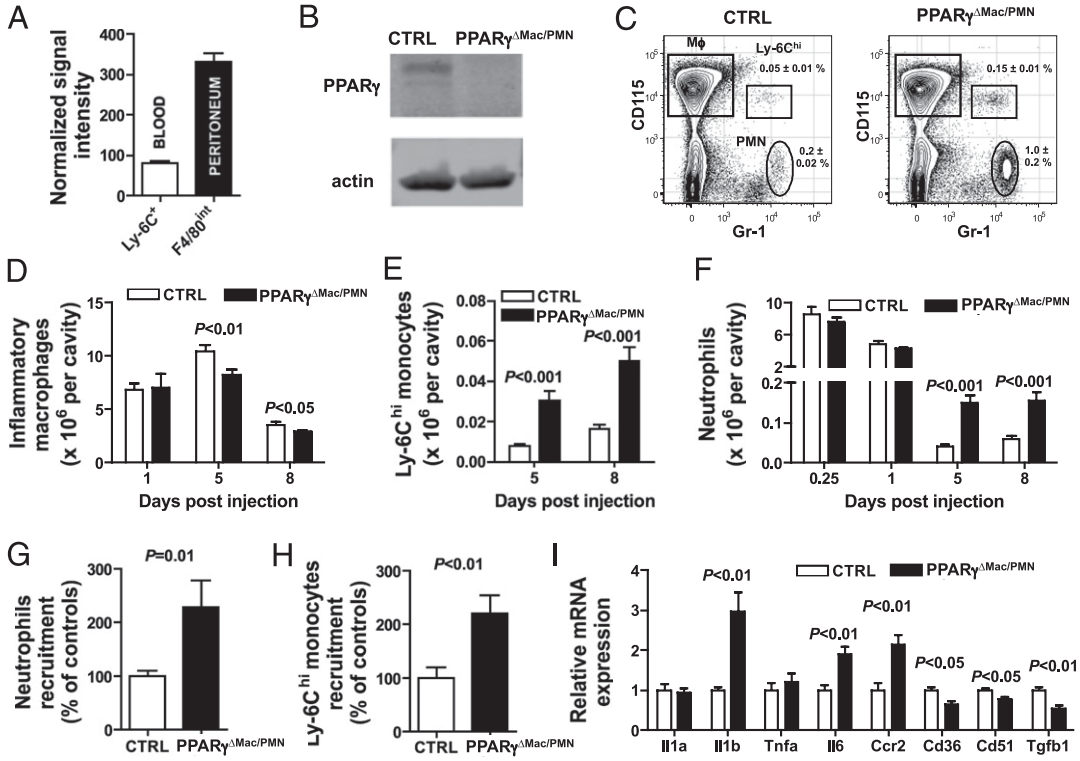

FIGURE 2. PPARγ expression in peritoneal inflammatory macrophages favors the resolution of acute inflammation. (**A**) Relative PPARγ mRNA expression in inflammatory macrophages from the peritoneum and their peripheral blood Ly-6C^{hi} monocyte precursors. (**B**) Western blot analysis of PPARγ protein in cell-sorted thioglycollate-elicited peritoneal macrophages. (**C**) FACS plot illustrating the gating strategy used for inflammatory peritoneal macrophages (Mϕ; CD115^{+} Gr-1/Ly-6C^{-}), Ly-6C^{hi} monocytes (CD115^{+}Gr-1/Ly-6C^{+}), and polymorphonuclear neutrophils (PMN; Gr-1/Ly-6G^{+}CD115$^{lo/-}$) in the peritoneal cavity 5 d after initiation of peritonitis. (**D**) Inflammatory peritoneal macrophage number in LysM-Cre × PPARγ$^{flox/flox}$ mice (PPARγ$^{\Delta Mac/PMN}$) and controls (CTRL) during the course of thioglycollate-induced peritonitis (n = 5–9 mice/group). (**E**) Ly-6C^{hi} monocyte numbers in the peritoneal cavity at 5 and 8 d postinduction of peritonitis (n = 8–14/group). (**F**) Neutrophil counts in the peritoneum at 0.25, 1, 5, and 8 d after peritonitis induction (n = 4–12 mice/group). (**G**) Inflammatory peritoneal macrophages from LysM-Cre × PPARγ$^{flox/flox}$ mice (PPARγ$^{\Delta Mac/PMN}$) and controls (CTRL) (both CD45.2) were transferred into naive CD45.1 recipients, and recipient neutrophils recruitment was evaluated 24 h later (n = 6–8 mice/group). (**H**) Circulating Ly-6C^{hi} monocytes were labeled i.v. with latex fluorescent beads 3 d after induction of inflammation, and the number of recruited bead-positive Ly-6C^{hi} monocytes in the peritoneal cavity was assessed 48 h later in LysM-Cre × PPARγ$^{flox/flox}$ mice (PPARγ$^{\Delta Mac/PMN}$) and controls (CTRL) (n = 6–7 mice/group). (**I**) Quantification of mRNA expression by peritoneal inflammatory macrophages recovered 5 d after induction of inflammation assessed by quantitative real-time PCR for select genes (n = 5 mice/group).

in LysM-Cre × PPARγ$^{flox/flox}$ mice during the usual resolution phase occurring between days 5 and 8 (Fig. 2F). Concomitantly, blood neutrophil counts were elevated at these later time points in LysM-Cre × PPARγ$^{flox/flox}$ mice compared with controls (data not shown), marking systemic inflammation. Interestingly, the increase in peritoneal neutrophils and Ly-6C^{hi} monocytes, as well as the decrease in inflammatory macrophages, were still evident at day 14 postthioglycollate treatment, the latest time point examined (data not shown). Transfer of 5 × 10^6 thioglycollate-elicited macrophages, retrieved from donors during the early resolution period at day 5, to the peritoneum of resting mice led to recruitment of neutrophils (Fig. 2G) and monocytes (Fig. 2H), and these numbers were doubled when transferred macrophages lacked PPARγ. PPARγ-deficient thioglycollate-elicited macrophages, retrieved at day 5, had increased mRNA expression of *Il1b*, *Il6*, and *Ccr2* and decreased levels of *Cd36*, *Cd51*, and *Tgfb1* compared with controls (Fig. 2I). Collectively, these data show that PPARγ deficiency in myeloid cells has little impact on the early phases of an inflammatory response. However, macrophage PPARγ expression in thioglycollate-elicited inflammatory macrophages is necessary to bring about resolution. Indeed, its deficiency leads to a state of chronic low-grade inflammation, at least in part because macrophages retain a more proinflammatory phenotype.

PPARγ activation promotes macrophage-dependent cessation of neutrophil recruitment and favors resolution of acute inflammation

Given the data above indicating that the cessation of leukocyte recruitment that characterizes resolution of inflammation is impaired in LysM-Cre × PPARγ$^{flox/flox}$ mice, we sought to determine whether treatment with PPARγ agonists would conversely favor the shutdown of leukocyte recruitment in wild-type animals. Indeed, PPARγ agonist treatment reduced neutrophil counts in the peritoneum following thioglycollate administration at each time point studied, especially in the later phases of inflammation (Fig. 3A). This effect required PPARγ expression in macrophages because treatment with the PPARγ agonist failed to reduce neutrophil counts in the cavity of LysM-Cre × PPARγ$^{flox/flox}$ mice (Fig. 3B). These data support the concept that PPARγ activation suppresses the recruitment of leukocytes in later phases of tissue injury in a macrophage PPARγ-dependent manner, promoting resolution of inflammation.

PPARγ deletion in macrophages leads to low-grade constitutive inflammation in the lung but not in the spleen

Considering our findings that PPARγ expression in inflammatory macrophages as well as its activation by pharmacological agonists

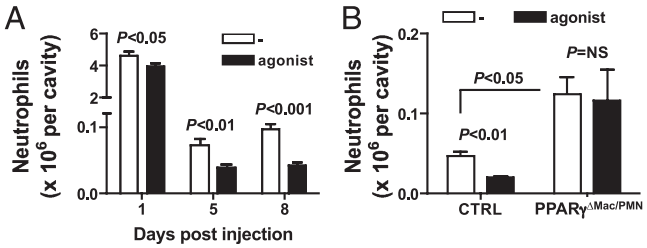

FIGURE 3. PPARγ activation favors the resolution of acute inflammation. (**A**) Neutrophil counts in the peritoneum at 1, 5, and 8 d after peritonitis induction in wild-type mice fed a regular diet (−) or a diet containing the PPARγ agonist pioglitazone (agonist) (n = 8–10 mice/group). (**B**) Peritoneal neutrophil counts 5 d after peritonitis induction in LysM-Cre × PPARγ$^{flox/flox}$ mice (PPARγ$^{\Delta Mac/PMN}$) fed a regular diet (−) or a diet containing the PPARγ agonist pioglitazone (agonist) (n = 4–5 mice/group).

favors resolution of acute inflammation, we wondered whether deletion of PPARγ in resting macrophage populations that normally express high levels of PPARγ (lung and splenic red pulp macrophages) would promote inflammation. LysM-Cre × Rosa26-stop^{flox}EGFP reporter mice confirmed that resident lung and splenic red pulp macrophages would be targeted in LysM-Cre × PPARγ$^{flox/flox}$ mice (data not shown). Total splenocyte numbers were similar in LysM-Cre × PPARγ$^{flox/flox}$ mice and controls (data not shown), but red pulp macrophages (F4/80^{hi} CD11b^{lo}) were approximately one-third less numerous in LysM-Cre × PPARγ$^{flox/flox}$ spleens (Fig. 4A), possibly arguing for a role of PPARγ in the maintenance of this population. There were no signs of inflammation in the resting spleen of LysM-Cre × PPARγ$^{flox/flox}$ mice because splenic Ly-6C^{hi} monocyte and neutrophil numbers were comparable to controls (Fig. 4B). Consistent with peritoneal inflammation, macrophage PPARγ deficiency did not have an impact on the induction of inflammation in the spleen at an early time point after i.v. administration of LPS (day 1; Fig. 4C), whereas it led to increased neutrophils and Ly-6C^{hi} monocytes recruitment to the spleen at a later time point (day 5; Fig. 4D), again arguing for a key role of PPARγ in resolution of inflammation.

When we examined the lung, we observed that PPARγ deletion in macrophages led to a low-grade inflammatory response without supplying an overt exogenous stimulus. Indeed, we observed increased leukocyte infiltration with elevated numbers of neutrophils (Fig. 4E) and CD4$^+$ and CD8$^+$ T lymphocytes (Fig. 4F), whereas macrophage numbers were comparable to controls (Fig. 4E).

Overall, whereas PPARγ is expressed by both splenic red pulp and pulmonary macrophages, its deficiency only obviously had an impact on lung tissue homeostasis in the steady state, arguing for an interaction between tissue environment and the outcome of altered macrophage PPARγ signaling.

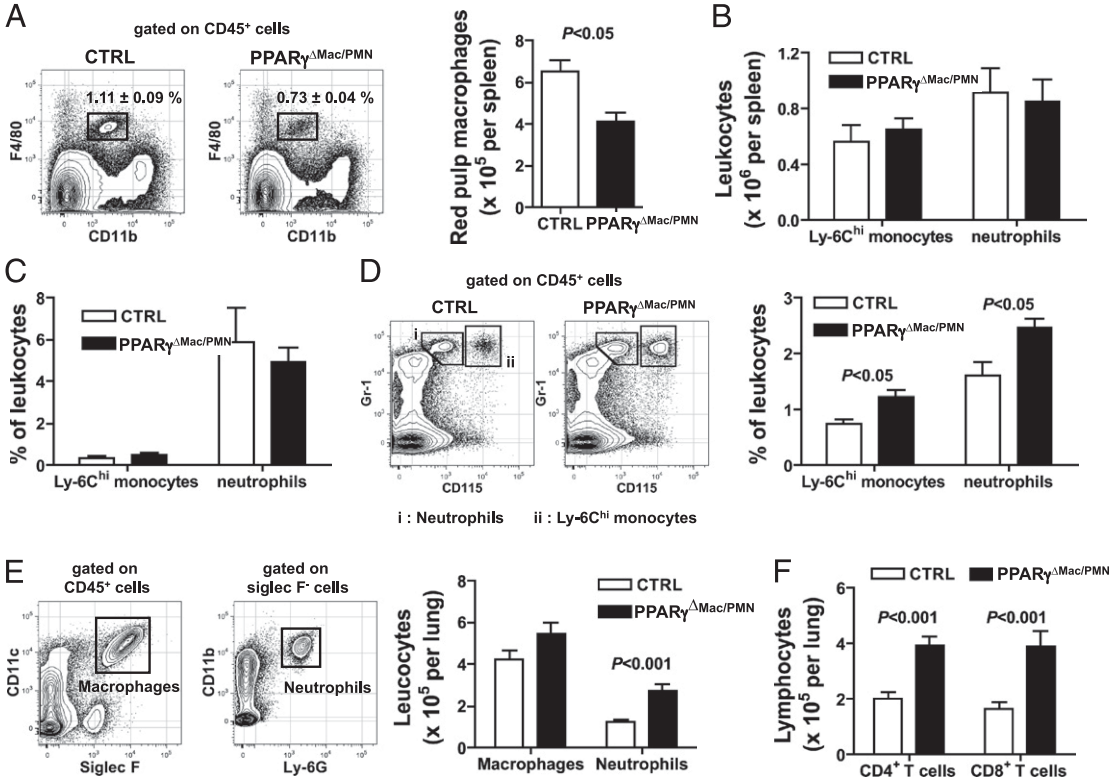

FIGURE 4. Impact of PPARγ deletion in splenic red pulp and lung macrophage. (**A**) Red pulp macrophage percentages and counts in the spleen of LysM-Cre × PPARγ$^{flox/flox}$ mice (PPARγ$^{\Delta Mac/PMN}$) and controls (CTRL) in the steady state (n = 4 mice/group). (**B**) Neutrophil and Ly-6C^{hi} monocyte counts in the spleen of LysM-Cre × PPARγ$^{flox/flox}$ mice (PPARγ$^{\Delta Mac/PMN}$) and controls (CTRL) in the steady state (n = 4 mice/group). (**C**) Neutrophil and Ly-6C^{hi} monocyte counts in the spleen of LysM-Cre × PPARγ$^{flox/flox}$ mice (PPARγ$^{\Delta Mac/PMN}$) and controls (CTRL) 24 h after LPS was injected i.v. (n = 3 mice/group). (**D**) FACS plot illustrating the gating strategy used for Ly-6C^{hi} monocytes (CD115^{hi}Gr-1/Ly-6C$^+$) and neutrophils (Gr-1/Ly-6G$^+$CD115^{lo}), and neutrophil and Ly-6C^{hi} monocyte counts in the spleen of LysM-Cre × PPARγ$^{flox/flox}$ mice (PPARγ$^{\Delta Mac/PMN}$) and controls (CTRL) 5 d after i.v. administration of LPS (n = 3 mice/group). (**E**) FACS plot illustrating the gating strategy used for lung macrophages (CD11c$^+$Siglec-F$^+$) and neutrophils (CD11b$^+$ Ly-6G$^+$) and respective cell counts in the lung of LysM-Cre × PPARγ$^{flox/flox}$ mice (PPARγ$^{\Delta Mac/PMN}$) and controls (CTRL) in the steady state (n = 6–8 mice/group). (**F**) CD4$^+$ and CD8$^+$ T lymphocyte counts in the lung of LysM-Cre × PPARγ$^{flox/flox}$ mice (PPARγ$^{\Delta Mac/PMN}$) and controls (CTRL) in the steady state (n = 6–8 mice/group).

Altered gene expression and lipid homeostasis in lung macrophages deficient in PPARγ

The low-grade inflammation observed only in the lung but not in the spleen suggested that the impact of PPARγ might be environment dependent. The alveolar space is permanently filled with a surfactant made of lipids (90%) and proteins (10%) (32), and we noted increased cellular lipid content in lung macrophages lacking PPARγ, as indicated by increased sterol staining using Bodipy FL (Fig. 5A), in line with previous work reporting the development of pulmonary alveolar proteinosis in these mice (33, 34). Then, to better understand the role of PPARγ in lung macrophages, microarray analysis was performed on sorted lung macrophages from LysM-Cre × PPARγ$^{flox/flox}$ mice and controls. This whole-genome array analysis uncovered 721 genes that were downregulated, and 2088 genes whose expression was increased in lung macrophages lacking PPARγ, highlighting a profound alteration of their transcriptome (Supplemental Tables III, IV). In line with their increased intracellular sterol content, we found that PPARγ-deficient lung macrophages induced a number of mRNA transcripts associated with cellular lipid metabolism and in particular those associated with an increase in activity of the LXR transcription factor. Expression levels of *Nr1h2* (also known as LXRβ), a sensor of intracellular sterol levels, and its partner *Rxra* were increased in lung macrophages obtained from LysM-Cre × PPARγ$^{flox/flox}$ mice as compared with controls (Fig. 5B). Consequently, the expression levels of several target genes of the LXR/RXR heterodimer (*Abca1*, *Srebf1*, *Apoe*, *Mylip, Abcg1*, *Scd2*, and *Scd1*) were equally increased (Fig. 5B). Finally, the mRNA level of the scavenger receptor *Msr1* and of the triacylglycerol synthesis enzyme Dgat1 were also enhanced (Fig. 5B). This expression profile was mirrored by decreased expression of genes involved in the cholesterol biosynthetic pathway (*Hmgcs1*, *Srebf2*, *Hmgcr*, *Fdft1*, *Dhcr24*, *Sqle*, and *Idi1*) and in the uptake of extracellular cholesterol (*Ldlr*) (Fig. 5B). Because the vast majority of these genes are not known to be under the direct control of PPARγ, these data suggest that many of the genes regulated in this study are regulated indirectly. Because we observed an increase in the percentage of MHC-II^{+} lung macrophages in LysM-Cre × PPARγ$^{flox/flox}$ mice (Fig. 5C), we sought to determine whether this was correlated with an increased expression of genes associated with macrophage activation. We found increased mRNA levels of genes encoding costimulatory molecules (*Cd86*, *H2-DMb2*, *H2-Ab1*, and *H2-Aa*), members of the IFN regulatory factor family of transcription factors (*Irf3*, *Irf5*, and *Irf8*), innate immune receptors (*Tlr7*, *Tlr8*, and *Trem2*), and the proinflammatory mediator *Mif* (Fig. 5D). Moreover, mRNA expression levels of members of the S100 protein family (*S100a13*, *S100a4*, and *S100a6*), known to mediate inflammatory signals, were upregulated in lung macrophages from LysM-Cre × PPARγ$^{flox/flox}$ mice (Fig. 5D). However, other genes involved in inflammation such as transcription factors (*Fos*, *Nr4a1*, *Jun*, *Jund*, and *Junb*), the TLR *Tlr2*, the scavenger receptor *Marco*, and the surfactant opsonin *Sftpc* were downregulated (Fig. 5D). Consistent with the increased intracellular lipid content observed in lung macrophages from LysM-Cre × PPARγ$^{flox/flox}$ mice, we noted that the mRNA expression of several phospholipases (*Pla2g6*, *Plcb1*, *Pnpla6*, *Pld3*, and *Pld4*) was increased in these cells as well as the expression of genes involved in PG and thromboxane synthesis (*Pgs1*, *Ptgr2*, *Ptgs1*, and *Tbxas1*) (Fig. 5E). We also noted that numerous genes regulated by the transcription factor Nrf2, a master regulator of the anti-

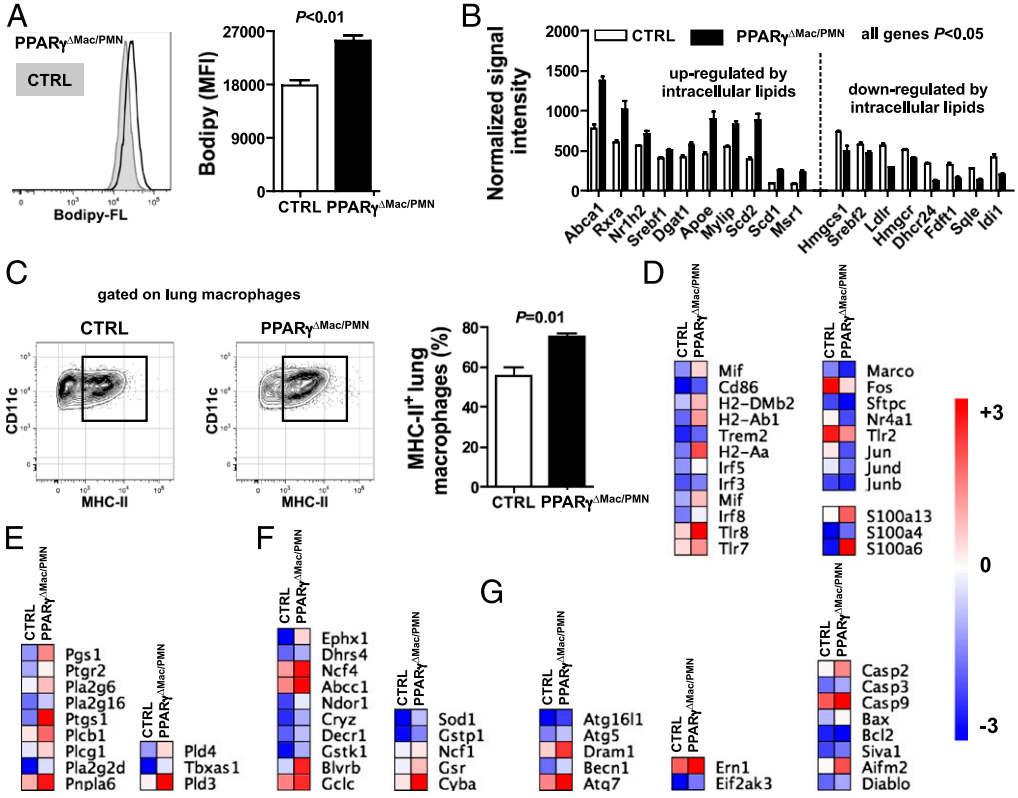

FIGURE 5. PPARγ is critical to preserve lung macrophage cellular homeostasis. (**A**) Cellular lipid levels were assessed in resting lung macrophages from LysM-Cre × PPARγ$^{flox/flox}$ mice (PPARγ$^{\Delta Mac/PMN}$) and controls (CTRL) using Bodipy-FL staining (n = 3 mice/group). (**B**) mRNA expression of genes modulated by intracellular lipid levels was determined by microarray. (**C**) Flow cytometry plot and quantification of cell surface MHC-II protein levels in lung macrophages from LysM-Cre × PPARγ$^{flox/flox}$ mice (PPARγ$^{\Delta Mac/PMN}$) and controls (CTRL) (n = 3–4 mice/group). Heat maps representing mRNA levels of genes involved in macrophage activation (**D**), lipid signaling (**E**), oxidative stress signaling (**F**), and cell death/autophagy (**G**).

oxidant response, were upregulated in PPARγ-deficient pulmonary macrophages compared with controls, indicating increased oxidative stress in LysM-Cre × PPARγ$^{flox/flox}$ mice (Fig. 5F). Finally, mRNA levels of mediators of autophagy (*Atg5*, *Dram1*, *Becn1*, and *Atg7*) and apoptosis (*Casp2*, *Casp9*, *Bax*, and *Aifm2*) were increased in lung macrophages lacking PPARγ compared with controls (Fig. 5G). Taken together, these findings reveal that PPARγ-deficient pulmonary macrophages present a markedly altered transcriptome, most likely secondary to the lipid loading, affecting several key pathways related to classical macrophage functions.

Impaired bacterial clearance in the lungs and accelerated mortality in mice lacking PPARγ in macrophages following S. pneumoniae *infection*

Given that the gene expression profile of lung macrophages deficient in PPARγ is profoundly altered, we next investigated whether infectious challenge of LysM-Cre × PPARγ$^{flox/flox}$ mice would lead to a perturbed innate immune response to pathogens. In this study, we found that LysM-Cre × PPARγ$^{flox/flox}$ mice were more susceptible to infection with *S. pneumoniae*. Weight loss associated with infection was more pronounced in LysM-Cre × PPARγ$^{flox/flox}$ compared with controls over a period of 4 d before death occurred (Fig. 6A). This increased susceptibility to *S. pneumoniae* infection was due to impaired bacterial clearance because bacterial burden was increased by ∼1 log in the lung of LysM-Cre × PPARγ$^{flox/flox}$ mice compared with controls 48 h postinfection (Fig. 6B). This correlated with faster dissemination of the bacteria into the bloodstream (data not shown) as well as accelerated death in these mice (Fig. 6C). LysM-Cre × PPARγ$^{flox/flox}$ mice challenged with a lower dose of the pathogen similarly succumbed faster than controls. Indeed, whereas 100% of control mice were still alive 6 d postinfection, only 40% of LysM-Cre × PPARγ$^{flox/flox}$ mice survived to this time point (Fig. 6D). Surprisingly, we observed similar neutrophil and Ly-6C^{hi} monocyte recruitment to the bronchoalveolar space and the lung 24 h postinfection in LysM-Cre × PPARγ$^{flox/flox}$ mice and controls (Fig. 6E). Increased bacterial burden in LysM-Cre × PPARγ$^{flox/flox}$ mice was not due to impaired phagocytosis because labeled *S. pneumoniae* were taken up by PPARγ-deficient alveolar macrophages as efficiently as controls in vivo (Fig. 6F). However, resident alveolar and interstitial pulmonary macrophage counts were significantly decreased by ∼50 and 35%, respectively, 24 h after instillation of *S. pneumoniae* (Fig. 6G). Finally, the disease pulmonary alveolar proteinosis (PAP) is due to alterations in GM-CSF signaling, and it was recently shown that PPARγ expression in GM-CSF–deficient lung macrophages was low (35). Furthermore, viral vectors to restore PPARγ in GM-CSF knockout mice led to reduced lipid accumulation and increased cholesterol efflux in lung macrophages (36). Because PAP is associated with increased susceptibility to infection, we sought to determine whether PPARγ activation could improve bacterial clearance in *Csf2rb*$^{-/-}$*Csf2rb2*$^{-/-}$ mice (37). Indeed, *Csf2rb*$^{-/-}$*Csf2rb2*$^{-/-}$ mice, which also display alveolar proteinosis, have significantly higher bacterial burden (∼2 logs) than wild-type control mice and PPARγ activation by

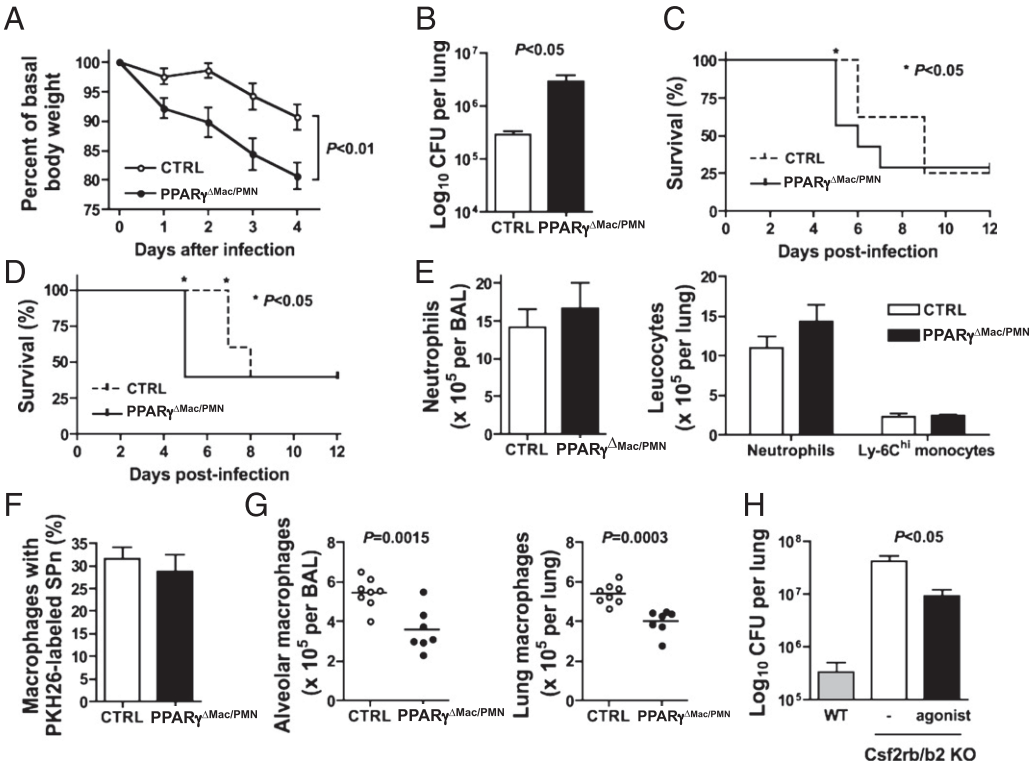

FIGURE 6. PPARγ expression in lung macrophage is necessary to combat infection. (**A**) Body weight loss was determined following infection in LysM-Cre × PPARγ$^{flox/flox}$ mice (PPARγ$^{\Delta Mac/PMN}$) and controls (CTRL) (n = 9 mice/group). (**B**) Lung bacterial load was measured 48 h postinfection in LysM-Cre × PPARγ$^{flox/flox}$ mice (PPARγ$^{\Delta Mac/PMN}$) and controls (CTRL) (n = 9 mice/group). Survival from infection was assessed over a period of 12 d following high-dose (2×10^6 CFU) (**C**) and low-dose (5×10^5 CFU) (**D**) *S. pneumoniae* inoculation in the lung of LysM-Cre × PPARγ$^{flox/flox}$ mice (PPARγ$^{\Delta Mac/PMN}$) and controls (CTRL) (n = 5–8 mice/group). (**E**) Neutrophil and Ly-6C^{hi} monocyte counts in the bronchoalveolar lavage (BAL) and the lung of LysM-Cre × PPARγ$^{flox/flox}$ mice (PPARγ$^{\Delta Mac/PMN}$) and controls (CTRL) were determined 24 h postinfection (n = 7–8 mice/group). (**F**) PKH26-labeled *S. pneumoniae* phagocytosis by resident alveolar macrophages was assessed by flow cytometry 30 min after inoculation (n = 6 mice/group). (**G**) Alveolar and pulmonary-resident macrophages counts in LysM-Cre × PPARγ$^{flox/flox}$ mice (PPARγ$^{\Delta Mac/PMN}$) and controls (CTRL) 24 h postinfection (n = 7–8 mice/group). (**H**) Lung bacterial burden was determined 48 h after *S. pneumoniae* inoculation in the lungs of wild-type mice, *Csf2rb*$^{-/-}$*Csf2rb2*$^{-/-}$ mice, and *Csf2rb*$^{-/-}$*Csf2rb2*$^{-/-}$ mice with prior treatment with the PPARγ agonist pioglitazone for 2 wk (n = 3–4 mice/group).

pioglitazone partially decreased this enhanced burden (Fig. 6H). Therefore, these data now connect PPARγ to host defense and control of bacterial burden in the lung through maintenance of local macrophage functions.

Discussion

The anti-inflammatory role of PPARγ in macrophages is well established. However, little is known regarding its impact on specific resting macrophage populations as well as on the dynamic of inflammation in vivo. It was recently recognized that establishing the expression profile of PPARγ in tissue macrophages in vivo would be helpful in clarifying its role in the regulation of inflammatory processes (38). In this study, we unexpectedly revealed that many resident macrophages do not express substantial levels of PPARγ, including those in the brain, peritoneum, and gut. The level of PPARγ in these cells was as low as in Ly-6C^{hi} monocytes, which show no PPARγ activity after synthetic PPARγ agonist administration in vivo. By contrast to these tissues and cells, Ly-6C^{lo} blood monocytes and resting red pulp splenic and pulmonary macrophages expressed high levels of mRNA for PPARγ. In addition, PPARγ was induced in inflammatory macrophages differentiating from circulating Ly-6C^{hi} monocytes entering an inflammatory site, albeit to a lower level than observed in the resting macrophages that were positive. In different tissues, the expression of canonical PPARγ target genes such as CD36 and FABP4 was distinct even among those macrophages that were PPARγ^{+}, highlighting the importance of context in regulation of PPARγ-related pathways and underscoring the diversity observed among macrophages from different organs.

Because the ability of PPARγ to transrepress inflammatory genes has been thoroughly documented (1), we expected that macrophage loss of PPARγ during thioglycollate-mediated peritonitis would lead to a more proinflammatory phenotype. However, the absence of PPARγ in LysM-Cre × PPARγ$^{flox/flox}$ mice did not impact the accumulation of leukocytes during the initial phase of the inflammatory response. This could be explained by the fact that immature and differentiating Ly-6C^{hi} monocytes, which express negligible or low levels of PPARγ, were dominant at this time point. By contrast, persistent neutrophil and Ly-6C^{hi} monocyte influx occurs in LysM-Cre × PPARγ$^{flox/flox}$ mice during the later period when more differentiated inflammatory macrophages, which now express PPARγ, begin to dominate and when resolution is observed in control mice. These data suggest, therefore, that PPARγ plays especially important roles in the late stages and resolution of inflammation. These roles very likely include repression of proinflammatory genes, and indeed, we observed that proinflammatory genes were elevated in PPARγ-deficient thioglycollate-elicited macrophages but may also include impaired induction of genes associated with repair and healing. Previous studies have linked PPARγ with the development of alternatively activated macrophages (39) and with tissue repair in injured muscle (30), and IL-4 is known to promote the production of PPARγ ligands (40). An elegant in-depth study recently revealed that although PPARγ is not required for development of alternatively activated macrophages in C57BL/6J mice, there is synergy with IL-4 such that the transcription factor Stat6 that is critical for IL-4 signaling binds to the enhancer elements in PPARγ target genes and markedly augments the PPARγ response (41). Our findings that PPARγ appears to play a bigger role in determining the rate/magnitude of contraction of the inflammatory response rather than the magnitude of earlier phases fits well with concepts of PPARγ playing a key role in tissue repair, healing, and overall resolution.

Future studies on the possible interface between PPARγ and lipids previously associated with resolution (42) seem in order. At present, resolvins are known not to serve as PPARγ ligands (42), but an intersection between PPARγ and the pathways that regulate such proresolution mediators may exist. Ligands for PPARγ during resolution may be limiting, because we observed that provision of synthetic ligands to mice hastened the shutdown of neutrophil recruitment in a macrophage PPARγ-dependent manner during the terminal phases of thioglycollate-induced inflammation. This finding is in line with recent published data in a model of granulomatous disease (43) and supports the logic of therapeutically enhancing PPARγ activity to promote resolution of ongoing inflammation.

Highest expression of PPARγ mRNA among macrophages in the mouse, resting or inflamed, was observed in the lung. Analysis of FABP4 expression in lung macrophages suggests that there may be heterogeneity among lung macrophages with regard to expression or activity of PPARγ. We show that the absence of PPARγ in LysM-Cre × PPARγ$^{flox/flox}$ mice induced mild lung inflammation in the absence of experimental challenge. This underlying inflammation may stem from a key role for PPARγ expression by macrophages to maintain cellular as well as tissue lipid homeostasis in the presence of pulmonary surfactant lipids. Indeed, previous work indicates that lipid surfactant accumulates in the alveoli of LysM-Cre × PPARγ$^{flox/flox}$ mice (33, 34). Consistent with this observation, we found that expressions of genes that regulate intracellular lipid homeostasis are markedly altered in pulmonary macrophages lacking PPARγ. Genes involved in sterol uptake and synthesis were downregulated, whereas genes linked to cholesterol sensing and efflux were upregulated, and in particular, mRNA transcripts controlled by LXR were induced. Likely, the enhanced sterol loading drives induction of the LXR pathway as a mechanism to deal with the high lipid loading. In addition, we found that numerous pathways associated with a range of macrophage functions were altered in the absence of PPARγ in lung macrophages, and genes associated with cell death were upregulated, leading to the conclusion that disruption of PPARγ signaling profoundly altered their transcriptome. However, the changes in gene expression are complex and most likely do not reflect changes associated only with direct PPARγ targets. Indirect changes likely reflect a sequence of events that occur in response to the loss of PPARγ in macrophages, which usually express PPARγ in the lung.

With the expectation that the absence of PPARγ in lung macrophages would exacerbate inflammation in the context of infection and subsequently favor bacterial clearance, we infected control and LysM-Cre × PPARγ$^{flox/flox}$ mice with *S. pneumoniae*. Bolstering our expectations that the inflammatory infiltrate may be increased in response to this infection were data in the literature indicating that mice lacking the cholesterol efflux gene *Abcg1*, and thus a gene expected to intersect functionally with PPARγ, manifest enhanced inflammation and increased bacterial clearance in response to infection in the lung (44). Following infection, weight loss and mortality were surprisingly accelerated in LysM-Cre × PPARγ$^{flox/flox}$ mice. As in the acute model of sterile inflammation induced by thioglycollate, the number of infiltrating neutrophils and monocytes was not changed in the first days following infection. Further similar to the thioglycollate model, but far more pronounced, the number of mature macrophages was significantly reduced in LysM-Cre × PPARγ$^{flox/flox}$ mice following infection with *S. pneumoniae*, although macrophage counts were similar to control mice in the steady state. These reduced macrophage numbers may account for the associated observation that clearance of *S. pneumoniae* was impaired under these conditions. Although we were unable to find more nonviable macrophages (using annexin V as a readout), the upregulation of cell death genes even in the steady state is consistent with this idea, and other explana-

tions such as impaired phagocytosis of bacteria were eliminated. Although future work will be required to be sure that macrophage death accounts for why LysM-Cre × PPARγ$^{flox/flox}$ mice succumb to *S. pneumoniae* infection more than control mice, we believe that the observation that macrophage PPARγ deficiency impacts the outcome of infection is quite significant on its own. Patients with PAP, a disease linked to impaired GM-CSF signaling, have an increased risk of superinfection (32), and it is known that suppressed GM-CSF signaling leads to lower PPARγ levels in the lung (35). Moreover, *Csf2rb*$^{-/-}$*Csf2rb2*$^{-/-}$ mice, a mouse model of PAP, are more susceptible to *S. pneumoniae* infection (37). Although it was already recognized that increasing PPARγ in models of PAP might reverse aspects of the disease such as lipid accumulation in macrophages, our data substantiate a link between the loss of PPARγ per se and increased susceptibility to infection in PAP. Importantly, downregulation of PPARγ and/or impairment in PPARγ signaling is also observed in cystic fibrosis (45–47), and PPARγ agonist treatment has been recently shown to ameliorate the severity of the cystic fibrosis phenotype in mice (47). Because cystic fibrosis is also tightly associated with an increased susceptibility to lung infection (48), PPARγ may participate centrally in impacting susceptibility to infection there as well. Future studies to investigate this possibility will be very important.

In summary, through taking the approach that started with characterization of the diversity of macrophages with respect to expression of PPARγ, the present work illustrates that PPARγ acts at the cellular level to favor contraction of inflammation and in the steady state is expressed in specific macrophage populations, especially in lung macrophages where it is critically involved in the maintenance of host defense.

Acknowledgments

We thank Christophe Benoist, Jeffrey Ericson, and Scott Davies for technical assistance with microarray analysis through the Immunological Genome Project (R24 AI072073). We also thank the Flow Cytometry Core at the Mount Sinai School of Medicine for assistance in use of the facility for flow cytometric cell sorting. We thank Andy Platt and Julie Helft for helpful discussion and reading of the manuscript.

Disclosures

The authors have no financial conflicts of interest.

References

1. Glass, C. K., and S. Ogawa. 2006. Combinatorial roles of nuclear receptors in inflammation and immunity. *Nat. Rev. Immunol.* 6: 44–55.
2. Tontonoz, P., and B. M. Spiegelman. 2008. Fat and beyond: the diverse biology of PPARγ. *Annu. Rev. Biochem.* 77: 289–312.
3. Yki-Järvinen, H. 2004. Thiazolidinediones. *N. Engl. J. Med.* 351: 1106–1118.
4. Ricote, M., A. C. Li, T. M. Willson, C. J. Kelly, and C. K. Glass. 1998. The peroxisome proliferator-activated receptor-γ is a negative regulator of macrophage activation. *Nature* 391: 79–82.
5. Jiang, C., A. T. Ting, and B. Seed. 1998. PPAR-γ agonists inhibit production of monocyte inflammatory cytokines. *Nature* 391: 82–86.
6. Daynes, R. A., and D. C. Jones. 2002. Emerging roles of PPARs in inflammation and immunity. *Nat. Rev. Immunol.* 2: 748–759.
7. Su, C. G., X. Wen, S. T. Bailey, W. Jiang, S. M. Rangwala, S. A. Keilbaugh, A. Flanigan, S. Murthy, M. A. Lazar, and G. D. Wu. 1999. A novel therapy for colitis utilizing PPAR-γ ligands to inhibit the epithelial inflammatory response. *J. Clin. Invest.* 104: 383–389.
8. Mukherjee, R., P. J. Davies, D. L. Crombie, E. D. Bischoff, R. M. Cesario, L. Jow, L. G. Hamann, M. F. Boehm, C. E. Mondon, A. M. Nadzan, et al. 1997. Sensitization of diabetic and obese mice to insulin by retinoid X receptor agonists. *Nature* 386: 407–410.
9. Li, A. C., K. K. Brown, M. J. Silvestre, T. M. Willson, W. Palinski, and C. K. Glass. 2000. Peroxisome proliferator-activated receptor γ ligands inhibit development of atherosclerosis in LDL receptor-deficient mice. *J. Clin. Invest.* 106: 523–531.
10. Babaev, V. R., P. G. Yancey, S. V. Ryzhov, V. Kon, M. D. Breyer, M. A. Magnuson, S. Fazio, and M. F. Linton. 2005. Conditional knockout of macrophage PPARγ increases atherosclerosis in C57BL/6 and low-density lipoprotein receptor-deficient mice. *Arterioscler. Thromb. Vasc. Biol.* 25: 1647–1653.
11. Chawla, A., W. A. Boisvert, C. H. Lee, B. A. Laffitte, Y. Barak, S. B. Joseph, D. Liao, L. Nagy, P. A. Edwards, L. K. Curtiss, et al. 2001. A PPARγ-LXR-ABCA1 pathway in macrophages is involved in cholesterol efflux and atherogenesis. *Mol. Cell* 7: 161–171.
12. Shah, Y. M., K. Morimura, and F. J. Gonzalez. 2007. Expression of peroxisome proliferator-activated receptor-γ in macrophage suppresses experimentally induced colitis. *Am. J. Physiol. Gastrointest. Liver Physiol.* 292: G657–G666.
13. Hevener, A. L., J. M. Olefsky, D. Reichart, M. T. Nguyen, G. Bandyopadyhay, H. Y. Leung, M. J. Watt, C. Benner, M. A. Febbraio, A. K. Nguyen, et al. 2007. Macrophage PPARγ is required for normal skeletal muscle and hepatic insulin sensitivity and full antidiabetic effects of thiazolidinediones. *J. Clin. Invest.* 117: 1658–1669.
14. Geissmann, F., S. Jung, and D. R. Littman. 2003. Blood monocytes consist of two principal subsets with distinct migratory properties. *Immunity* 19: 71–82.
15. Ingersoll, M. A., R. Spanbroek, C. Lottaz, E. L. Gautier, M. Frankenberger, R. Hoffmann, R. Lang, M. Haniffa, M. Collin, F. Tacke, et al. 2010. Comparison of gene expression profiles between human and mouse monocyte subsets. *Blood* 115: e10–e19.
16. Heng, T. S., and M. W. Painter. 2008. The Immunological Genome Project: networks of gene expression in immune cells. *Nat. Immunol.* 9: 1091–1094.
17. Ghosn, E. E., A. A. Cassado, G. R. Govoni, T. Fukuhara, Y. Yang, D. M. Monack, K. R. Bortoluci, S. R. Almeida, L. A. Herzenberg, and L. A. Herzenberg. 2010. Two physically, functionally, and developmentally distinct peritoneal macrophage subsets. *Proc. Natl. Acad. Sci. USA* 107: 2568–2573.
18. Sung, S. S., S. M. Fu, C. E. Rose, Jr., F. Gaskin, S. T. Ju, and S. R. Beaty. 2006. A major lung CD103 (α_E)-β_7 integrin-positive epithelial dendritic cell population expressing Langerin and tight junction proteins. *J. Immunol.* 176: 2161–2172.
19. Ginhoux, F., M. Greter, M. Leboeuf, S. Nandi, P. See, S. Gokhan, M. F. Mehler, S. J. Conway, L. G. Ng, E. R. Stanley, et al. 2010. Fate mapping analysis reveals that adult microglia derive from primitive macrophages. *Science* 330: 841–845.
20. Bogunovic, M., F. Ginhoux, J. Helft, L. Shang, D. Hashimoto, M. Greter, K. Liu, C. Jakubzick, M. A. Ingersoll, M. Leboeuf, et al. 2009. Origin of the lamina propria dendritic cell network. *Immunity* 31: 513–525.
21. Waskow, C., K. Liu, G. Darrasse-Jèze, P. Guermonprez, F. Ginhoux, M. Merad, T. Shengelia, K. Yao, and M. Nussenzweig. 2008. The receptor tyrosine kinase Flt3 is required for dendritic cell development in peripheral lymphoid tissues. *Nat. Immunol.* 9: 676–683.
22. Tacke, F., F. Ginhoux, C. Jakubzick, N. van Rooijen, M. Merad, and G. J. Randolph. 2006. Immature monocytes acquire antigens from other cells in the bone marrow and present them to T cells after maturing in the periphery. *J. Exp. Med.* 203: 583–597.
23. Potteaux, S., E. L. Gautier, S. B. Hutchison, N. van Rooijen, D. J. Rader, M. J. Thomas, M. G. Sorci-Thomas, and G. J. Randolph. 2011. Suppressed monocyte recruitment drives macrophage removal from atherosclerotic plaques of Apoe$^{-/-}$ mice during disease regression. *J. Clin. Invest.* 121: 2025–2036.
24. Van Rooijen, N., and A. Sanders. 1994. Liposome mediated depletion of macrophages: mechanism of action, preparation of liposomes and applications. *J. Immunol. Methods* 174: 83–93.
25. Gautier, E. L., T. Huby, B. Ouzilleau, C. Doucet, F. Saint-Charles, G. Gremy, M. J. Chapman, and P. Lesnik. 2007. Enhanced immune system activation and arterial inflammation accelerates atherosclerosis in lupus-prone mice. *Arterioscler. Thromb. Vasc. Biol.* 27: 1625–1631.
26. Qu, C., E. W. Edwards, F. Tacke, V. Angeli, J. Llodrá, G. Sanchez-Schmitz, A. Garin, N. S. Haque, W. Peters, N. van Rooijen, et al. 2004. Role of CCR8 and other chemokine pathways in the migration of monocyte-derived dendritic cells to lymph nodes. *J. Exp. Med.* 200: 1231–1241.
27. Moore, K. J., E. D. Rosen, M. L. Fitzgerald, F. Randow, L. P. Andersson, D. Altshuler, D. S. Milstone, R. M. Mortensen, B. M. Spiegelman, and M. W. Freeman. 2001. The role of PPAR-γ in macrophage differentiation and cholesterol uptake. *Nat. Med.* 7: 41–47.
28. Tacke, F., D. Alvarez, T. J. Kaplan, C. Jakubzick, R. Spanbroek, J. Llodra, A. Garin, J. Liu, M. Mack, N. van Rooijen, et al. 2007. Monocyte subsets differentially employ CCR2, CCR5, and CX3CR1 to accumulate within atherosclerotic plaques. *J. Clin. Invest.* 117: 185–194.
29. Bellingan, G. J., H. Caldwell, S. E. Howie, I. Dransfield, and C. Haslett. 1996. In vivo fate of the inflammatory macrophage during the resolution of inflammation: inflammatory macrophages do not die locally, but emigrate to the draining lymph nodes. *J. Immunol.* 157: 2577–2585.
30. Arnold, L., A. Henry, F. Poron, Y. Baba-Amer, N. van Rooijen, A. Plonquet, R. K. Gherardi, and B. Chazaud. 2007. Inflammatory monocytes recruited after skeletal muscle injury switch into antiinflammatory macrophages to support myogenesis. *J. Exp. Med.* 204: 1057–1069.
31. Cheong, C., I. Matos, J. H. Choi, D. B. Dandamudi, E. Shrestha, M. P. Longhi, K. L. Jeffrey, R. M. Anthony, C. Kluger, G. Nchinda, et al. 2010. Microbial stimulation fully differentiates monocytes to DC-SIGN/CD209$^+$ dendritic cells for immune T cell areas. *Cell* 143: 416–429.
32. Trapnell, B. C., J. A. Whitsett, and K. Nakata. 2003. Pulmonary alveolar proteinosis. *N. Engl. J. Med.* 349: 2527–2539.
33. Bonfield, T. L., M. J. Thomassen, C. F. Farver, S. Abraham, M. T. Koloze, X. Zhang, D. M. Mosser, and D. A. Culver. 2008. Peroxisome proliferator-activated receptor-gamma regulates the expression of alveolar macrophage macrophage colony-stimulating factor. *J. Immunol.* 181: 235–242.
34. Baker, A. D., A. Malur, B. P. Barna, S. Ghosh, M. S. Kavuru, A. G. Malur, and M. J. Thomassen. 2010. Targeted PPARγ deficiency in alveolar macrophages disrupts surfactant catabolism. *J. Lipid Res.* 51: 1325–1331.
35. Thomassen, M. J., B. P. Barna, A. G. Malur, T. L. Bonfield, C. F. Farver, A. Malur, H. Dalrymple, M. S. Kavuru, and M. Febbraio. 2007. ABCG1 is

deficient in alveolar macrophages of GM-CSF knockout mice and patients with pulmonary alveolar proteinosis. *J. Lipid Res.* 48: 2762–2768.
36. Malur, A., A. D. Baker, A. J. McCoy, G. Wells, B. P. Barna, M. S. Kavuru, A. G. Malur, and M. J. Thomassen. 2011. Restoration of PPARγ reverses lipid accumulation in alveolar macrophages of GM-CSF knockout mice. *Am. J. Physiol. Lung Cell. Mol. Physiol.* 300: L73–L80.
37. LeVine, A. M., J. A. Reed, K. E. Kurak, E. Cianciolo, and J. A. Whitsett. 1999. GM-CSF-deficient mice are susceptible to pulmonary group B streptococcal infection. *J. Clin. Invest.* 103: 563–569.
38. Szanto, A., and L. Nagy. 2008. The many faces of PPARγ: anti-inflammatory by any means? *Immunobiology* 213: 789–803.
39. Odegaard, J. I., R. R. Ricardo-Gonzalez, M. H. Goforth, C. R. Morel, V. Subramanian, L. Mukundan, A. Red Eagle, D. Vats, F. Brombacher, A. W. Ferrante, and A. Chawla. 2007. Macrophage-specific PPARγ controls alternative activation and improves insulin resistance. *Nature* 447: 1116–1120.
40. Huang, J. T., J. S. Welch, M. Ricote, C. J. Binder, T. M. Willson, C. Kelly, J. L. Witztum, C. D. Funk, D. Conrad, and C. K. Glass. 1999. Interleukin-4-dependent production of PPAR-γ ligands in macrophages by 12/15-lipoxygenase. *Nature* 400: 378–382.
41. Szanto, A., B. L. Balint, Z. S. Nagy, E. Barta, B. Dezso, A. Pap, L. Szeles, S. Poliska, M. Oros, R. M. Evans, et al. 2010. STAT6 transcription factor is a facilitator of the nuclear receptor PPARγ-regulated gene expression in macrophages and dendritic cells. *Immunity* 33: 699–712.
42. Serhan, C. N. 2010. Novel lipid mediators and resolution mechanisms in acute inflammation: to resolve or not? *Am. J. Pathol.* 177: 1576–1591.
43. Fernandez-Boyanapalli, R., S. C. Frasch, D. W. Riches, R. W. Vandivier, P. M. Henson, and D. L. Bratton. 2010. PPARγ activation normalizes resolution of acute sterile inflammation in murine chronic granulomatous disease. *Blood* 116: 4512–4522.
44. Draper, D. W., J. H. Madenspacher, D. Dixon, D. H. King, A. T. Remaley, and M. B. Fessler. 2010. ATP-binding cassette transporter G1 deficiency dysregulates host defense in the lung. *Am. J. Respir. Crit. Care Med.* 182: 404–412.
45. Ollero, M., O. Junaidi, M. M. Zaman, I. Tzameli, A. A. Ferrando, C. Andersson, P. G. Blanco, E. Bialecki, and S. D. Freedman. 2004. Decreased expression of peroxisome proliferator activated receptor gamma in $cftr^{-/-}$ mice. *J. Cell. Physiol.* 200: 235–244.
46. Maiuri, L., A. Luciani, I. Giardino, V. Raia, V. R. Villella, M. D'Apolito, M. Pettoello-Mantovani, S. Guido, C. Ciacci, M. Cimmino, et al. 2008. Tissue transglutaminase activation modulates inflammation in cystic fibrosis via PPARγ down-regulation. *J. Immunol.* 180: 7697–7705.
47. Harmon, G. S., D. S. Dumlao, D. T. Ng, K. E. Barrett, E. A. Dennis, H. Dong, and C. K. Glass. 2010. Pharmacological correction of a defect in PPAR-γ signaling ameliorates disease severity in Cftr-deficient mice. *Nat. Med.* 16: 313–318.
48. Grassmé, H., K. A. Becker, Y. Zhang, and E. Gulbins. 2010. CFTR-dependent susceptibility of the cystic fibrosis-host to *Pseudomonas aeruginosa. Int. J. Med. Microbiol.* 300: 578–583.

Gene-expression profiles and transcriptional regulatory pathways that underlie the identity and diversity of mouse tissue macrophages

Emmanuel L Gautier[1–3], Tal Shay[4], Jennifer Miller[2,5], Melanie Greter[2,5], Claudia Jakubzick[1,2], Stoyan Ivanov[3], Julie Helft[2,5], Andrew Chow[2,5], Kutlu G Elpek[6,7], Simon Gordonov[8], Amin R Mazloom[8], Avi Ma'ayan[8], Wei-Jen Chua[3], Ted H Hansen[3], Shannon J Turley[6,7], Miriam Merad[2,5], Gwendalyn J Randolph[1–3] & the Immunological Genome Consortium[9]

We assessed gene expression in tissue macrophages from various mouse organs. The diversity in gene expression among different populations of macrophages was considerable. Only a few hundred mRNA transcripts were selectively expressed by macrophages rather than dendritic cells, and many of these were not present in all macrophages. Nonetheless, well-characterized surface markers, including MerTK and FcγR1 (CD64), along with a cluster of previously unidentified transcripts, were distinctly and universally associated with mature tissue macrophages. TCEF3, C/EBP-α, Bach1 and CREG-1 were among the transcriptional regulators predicted to regulate these core macrophage-associated genes. The mRNA encoding other transcription factors, such as *Gata6*, was associated with single macrophage populations. We further identified how these transcripts and the proteins they encode facilitated distinguishing macrophages from dendritic cells.

The team of immunologists and computational biologists of the Immunological Genome (ImmGen) Project share the goal of generating an exhaustive definition of gene-expression and regulatory networks of the mouse immune system through shared resources and rigorously controlled data-generation pipelines[1]. Here we turned our attention to gene-expression and regulatory networks in tissue-resident macrophages. Macrophages are professional phagocytic cells, often long lived, that reside in all organs to maintain tissue integrity, clear debris and respond rapidly to initiate repair after injury or innate immunity after infection[2,3]. Accordingly, macrophages are specialized for the degradation and detoxification of engulfed cargo, and they are potent secretagogues able to develop an array of phenotypes[4]. Macrophages can also present antigens but lack the potency for stimulating T cells observed in dendritic cells (DCs), and they usually fail to mobilize to lymphoid tissues in which naive T cells are abundant. Partially overlapping functions for macrophages and DCs, reflected by overlapping molecular profiles, have for decades fueled some debate over the origins and overall distinction between macrophages and DCs[5].

In the past several years, considerable progress has been made in the identification of precursor cells specific to DCs[6–8]. Moreover, transcription factors have been identified, such as Batf3, that are essential for the development of some DCs but are not required for macrophage specification[9]. Advances have also been made in delineating the development of tissue macrophages. Contrary to the prevalent idea that monocytes are precursors of tissue macrophages, some earlier work contended that tissue macrophages arise from primitive hematopoietic progenitors present in the yolk sac during embryonic development independently of the monocyte lineage[10], and support for that contention has emerged from fate-mapping and genetic models[11,12]. Thus, in the adult, the maintenance of tissue macrophages involves local proliferation, again independently of monocytes and definitive hematopoiesis[10,12]. In this context, the transcription factor MAFB (c-Maf) has been shown to regulate macrophage self-renewal[13]. Some transcription factors that drive the development of specific macrophage types such as osteoclasts[14] or red-pulp macrophages[15] have also been reported. However, much remains to be determined about the transcriptional regulatory pathways that control other types of macrophages or global regulatory pathways that govern macrophages as a group of related cells[3]. The database generated by the ImmGen Project has created a unique resource for the comparison of gene-expression profiles and the identification of regulatory pathways that specify or

[1]Department of Developmental and Regenerative Biology, Mount Sinai School of Medicine, New York, New York, USA. [2]The Immunology Institute, Mount Sinai School of Medicine, New York, New York, USA. [3]Department of Pathology & Immunology, Washington University School of Medicine, St. Louis, Missouri, USA. [4]Broad Institute, Cambridge, Massachusetts, USA. [5]Department of Oncological Sciences and Department of Medicine, Mount Sinai School of Medicine, New York, New York, USA. [6]Department of Microbiology and Immunobiology, Harvard Medical School, Boston, Massachusetts, USA. [7]Department of Cancer Immunology and AIDS, Dana Farber Cancer Institute, Boston, Massachusetts, USA. [8]Department of Pharmacology and Systems Therapeutics & Systems Biology Center New York, Mount Sinai School of Medicine, New York, New York, USA. [9]Full list of members and affiliations appears at the end of the paper. Correspondence should be addressed to G.J.R. (grandolph@path.wustl.edu).

Received 11 April; accepted 9 August; published online 30 September 2012; doi:10.1038/ni.2419

unify macrophage populations from different organs. Our analysis here of the macrophage transcriptome in this context will enable the analysis of networks of genes and their regulators that can be used to better distinguish different types of macrophages and pinpoint the differences between macrophages and DCs.

RESULTS

Tissue macrophage diversity

As part of the ImmGen Project, we sorted several tissue macrophage populations from C57BL/6J mice according to strict, standardized procedures and analyzed these populations by whole-mouse genome miroarray. Strategies for sorting these populations are available at the ImmGen Project website. We began our analysis by examining the gene-expression profiles of resting macrophage populations that have historically been characterized and accepted as true resident tissue macrophages[12]. Although some classic macrophages, such as Kupffer cells of the liver and metallophilic or marginal-zone macrophages of the spleen, proved elusive for definitive identification and/or isolation through sorting by flow cytometry, the following four resting macrophage populations submitted to the ImmGen Project met the criteria of true macrophage populations: peritoneal macrophages; red-pulp splenic macrophages; lung macrophages; and microglia (brain macrophages). Principal-component analysis (PCA) of all genes expressed by the four sorted macrophage populations and several DC populations showed a greater distance between the macrophages than between the DCs (**Fig. 1a**). Pearson correlation values were high for replicates in a given DC or macrophage population according to the quality-control standards of the ImmGen Project; variability within replicates for a single population varied from 0.908 ± 0.048 for microglia to 0.995 ± 0.001 for peritoneal macrophages. Pearson correlations for the gene-expression profiles of various populations of DCs yielded coefficients that ranged from 0.877 (liver CD11b$^+$ DCs versus spleen CD8$^+$ DCs) to 0.966 (spleen CD4$^+$CD11b$^+$ DCs versus spleen CD8$^+$ DCs; mean of all DC populations, 0.931), whereas the correlation coefficients for the tissue macrophages ranged from 0.784 (peritoneal versus splenic red pulp) to 0.863 (peritoneal versus lung) with a mean of 0.812 (**Fig. 1b**). Several thousand mRNA transcripts had a difference in expression of at least twofold in, for example, lung macrophages versus red-pulp splenic macrophages (**Fig. 1c**). This degree of diversity was greater than that observed for DCs of different subsets (CD103$^+$ versus CD11b$^+$) from various organs (**Fig. 1c**). Finally, a dendrogram applied to the various populations showed that DCs clustered more closely than macrophages did (**Fig. 1d**), and this was true whether we considered all gene transcripts in the array (data not shown) or only the top 15% ranked by the cross-population maximum/minimum ratio or coefficient of variation (**Fig. 1d**). Overall, these comparisons indicated considerable diversity among tissue macrophage populations.

Distinct molecular signatures among tissue macrophages

The diversity among the four classical macrophage populations noted above extended to gene families previously associated with macrophage function: those encoding chemokine receptors, Toll-like receptors (TLRs), C-type lectins and efferocytic receptors. For example, in each population, at least one distinct chemokine receptor had much higher expression than the others (**Supplementary Fig. 1a**). The diversity in the expression of TLRs, C-type lectins and efferocytic receptors was also considerable (**Supplementary Fig. 1b–d**). Indeed, only a few of the mRNA transcripts profiled in these categories, including mRNA encoding the Mer tyrosine kinase receptor (MerTK), which is involved in the phagocytosis of apoptotic cells[16], as well as mRNA encoding TLR4, TLR7, TLR8 and TLR13, showed relatively uniform expression across all macrophages compared. Hundreds of mRNA transcripts had a selective difference in expression of at least twofold (higher or lower expression) in only one of the macrophage populations (**Fig. 2a**), and microglia in particular had low expression of hundreds of transcripts that were expressed in other macrophage populations (**Fig. 2a**). Using Ingenuity pathway-analysis software tools, we found enrichment for each specific signature in groups of transcripts encoding molecules with predicted specific functions, including oxidative metabolism in brain macrophages, lipid metabolism in lung macrophages, eicosanoid signaling in peritoneal macrophages and readiness for interferon responsiveness in red-pulp macrophages (**Supplementary Table 1**). Given that

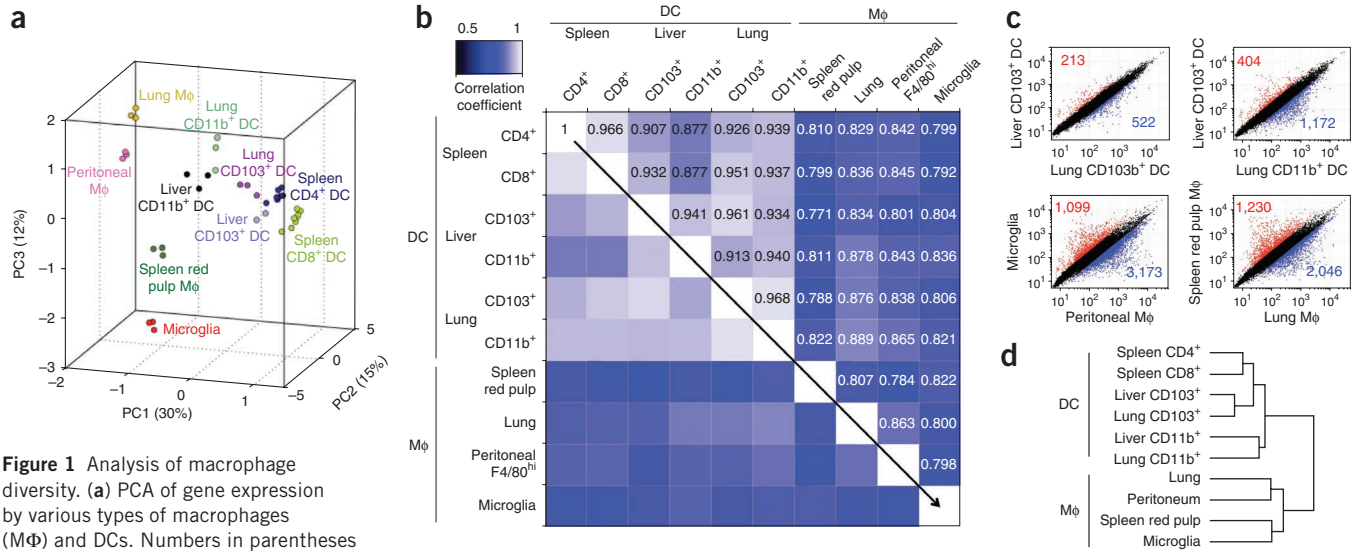

Figure 1 Analysis of macrophage diversity. (**a**) PCA of gene expression by various types of macrophages (MΦ) and DCs. Numbers in parentheses indicate relative scaling of the principal variables. (**b**) Correlation matrix of macrophages and DCs based on all available gene probes. Numbers in plot indicate correlation coefficient value. (**c**) Diversity of gene expression in macrophage populations and DCs. Numbers in plots indicate probes with a minimum change in expression of twofold (red, upregulated; blue, downregulated). (**d**) Hierarchical clustering of macrophages and DCs based on the 15% of genes with the greatest variability. Data are combined from three to seven independent experiments for each population, with cells pooled from three to five mice in each.

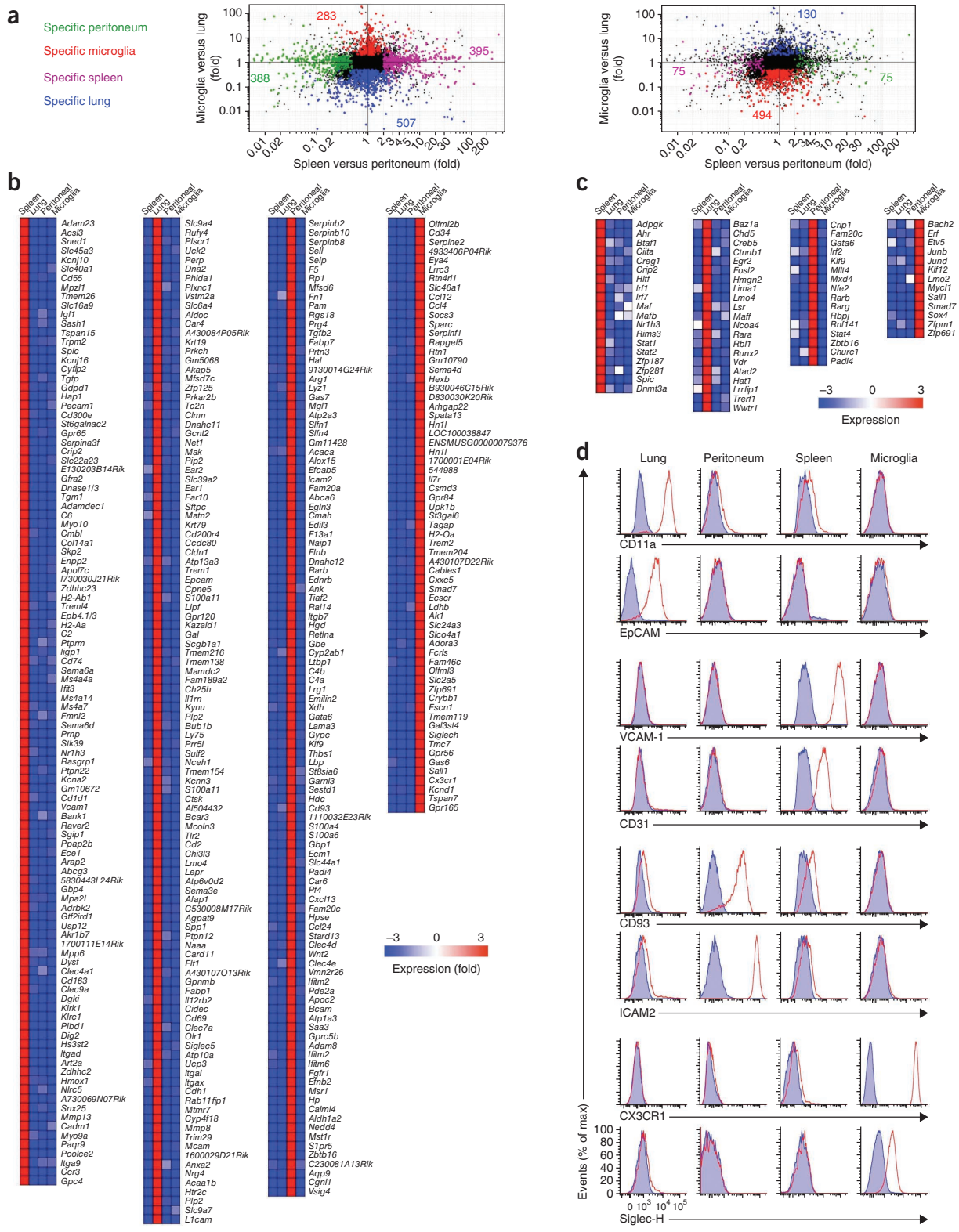

Figure 2 Unique gene-expression profiles of macrophages from various organs. (**a**) Quantification of mRNA transcripts upregulated twofold or more (left) or downregulated twofold or more (right) in one macrophage population relative to their expression in the remaining three populations. Numbers in plots indicate genes with a minimum change in expression of twofold (colors match key at left). (**b**) Heat map of mRNA transcripts upregulated in each single macrophage population (top) by fivefold or more relative to their expression in the remaining three populations. (**c**) Heat map of mRNA transcripts encoding transcription factors upregulated in only one of the four macrophage populations by twofold or more. (**d**) Flow cytometry analysis of specific cell-surface markers (identified by the gene-expression profiling data) for each macrophage population. Red line, specific antibody; blue shading, isotype-matched control antibody. Data combine results from three or more experiments.

we simultaneously compared the gene-expression profiles of the four macrophage populations, the number of transcripts with expression that was fivefold or more higher or lower in only one macrophage population relative to their expression in all three of the other populations was notable (**Fig. 2b**). We also found that many transcripts had much lower expression in only one population than in the others (**Supplementary Fig. 2**). Several transcription factors had much higher expression in just one of the four macrophage populations (**Fig. 2c**). For example, expression of the gene encoding the transcription factor Spi-C was restricted to splenic red-pulp macrophages, which fit with published work showing that Spi-C has a critical role in controlling the development of these cells[15]. Diversity at the gene-expression level corresponded to that at the protein level. For example, we detected the integrin CD11a (LFA-1) and the adhesion molecule EpCAM on lung macrophages but not on microglia, spleen or peritoneal macrophages; the adhesion molecules VCAM-1 and CD31 (PECAM-1) were selectively displayed by spleen macrophages; the C-type lectin transmembrane receptor CD93 and the adhesion molecule ICAM-2 were expressed by peritoneal macrophages but not the other macrophages; and the chemokine receptor CX3CR1 and the lectin Siglec-H were selectively present in microglia (**Fig. 2d**). Together these data indicated that macrophage populations in different organs expressed many unique mRNA transcripts that would equip them for specialized local functions.

Identification of a core macrophage signature

In the midst of the vast diversity among macrophages from different organs, we next sought to identify a core gene-expression profile that generally unified macrophages and distinguished them from other types of cells of the immune system. Among all hematopoietic cells, the cells anticipated to be most similar to macrophages are DCs[5]. To search for mRNA transcripts that distinguished macrophages from DCs, we compared the four selected prototypical macrophage populations with the most well-defined classic DC populations, including resting $CD8^+$ or $CD4^+$ $CD11b^+$ splenic DCs, $CD103^+$ tissue DCs and various populations of lymph node $CD11c^+$ migratory DCs with high expression of major histocompatibility complex (MHC) class II ($MHCII^{hi}$)[17,18]. Because tissue $CD11b^+$ DCs may be contaminated with macrophages[19], we initially excluded tissue $CD11b^+$ DCs from the comparison. This comparison identified only 14 transcripts that were expressed in all four macrophage populations but were not expressed in DCs (**Table 1**). These included mRNA anticipated to have high expression in macrophages, such as *Fcgr1* (which encodes the immunoglobulin Fc receptor CD64) and *Tlr4*. Two of these molecules, the receptor for the cytokine G-CSF (encoded by *Csf3r*) and the MHC class I–related molecule MR1 (encoded by *Mr1*), which is involved in the activation of mucosa-associated invariant T cells[20], function at least partly at the cell surface. In agreement with the pattern of mRNA expression, we found MR1 protein on spleen and lung macrophages but not on classical DCs (**Supplementary Fig. 3**), which suggested that MR1 on macrophages rather than on DCs may drive the activation of mucosa-associated invariant T cells. Other transcripts identified encode proteins involved in signal transduction, such as the kinase Fert2 (encoded by *Fer* (called '*Fert2*' here)), or in metabolism and lipid homeostasis, such as peroxisomal trans-2-enoyl-CoA reductase (encoded by *Pecr*) and alkyl glycerol monooxygenase (encoded by *Tmem195*), which is the only enzyme that cleaves the O-alkyl bond of ether lipids such as platelet-activating factor, shown to be actively catabolized in association with macrophage differentiation *in vitro*[21]. To that small number of mRNA transcripts, we added probe sets that did not lack expression by DCs but had signal intensity least twofold lower in all single DC populations than the lowest intensity of that same probe set in each macrophage population. Thus, we were able to add 25 more transcripts to that 'macrophage core' list (**Table 1**; mean transcript expression, **Supplementary Table 2**), including those known to be associated with macrophages, such as *Cd14*, *Mertk*, *Fcrg3* (which encodes the immunoglobulin Fc receptor CD16) and *Ctsd* (which encodes cathepsin D).

F4/80 (encoded by *Emr1*) has served as the most definitive marker of macrophages so far[5,12]. However, to identify additional mRNA transcripts widely associated with macrophages with the core list of macrophage-associated genes, including *Emr1*, *Mafb* and *Cebpb*, we found it necessary to adjust the criteria of the approach described above to include transcripts expressed in only three of four macrophage populations because, for example, *Emr1* mRNA had low expression in microglia. Making this adjustment expanded the list of mRNA transcripts associated with macrophages and added another 93 genes (**Table 1**). Additional macrophage-associated genes such as *Mrc1* (which encodes the mannose receptor CD206), *Marco* and *Pparg* were not identified until we 'loosened' the criteria so that only two of four prototypical macrophage populations needed to express a given transcript whose expression was otherwise absent or low on DCs (**Table 2**; transcript expression, **Supplementary Table 3**). *Cd68* mRNA, widely used to identify tissue macrophages, had similar expression in DCs and macrophages and we therefore excluded it from the list. However, as a protein, its expression was still several orders of magnitude higher in macrophages than in DCs of the spleen (**Supplementary Fig. 4**). In summary, the expression of 366 transcripts (**Tables 1** and **2**) was absent from classical DCs or was much lower in classical DCs than in macrophages. However, because of the great diversity among macrophages, expression of only 39 of these transcripts was shared by all tissue macrophages we compared.

Coexpressed genes and predicted transcriptional regulators

The computational biology groups of the ImmGen Project have analyzed the transcriptional program of the entire large database generated by the ImmGen Project (V. Jojic *et al.*, data not shown, and **Supplementary Note 1**). First, mRNA transcripts were clustered into 334 fine modules on the basis of patterns of coexpression. Then the Ontogenet algorithm (developed for the ImmGen Project data set) was applied to identify a regulatory program for each fine module on the basis of its expression pattern, the expression pattern of regulators and the position of the cells on the hematopoietic lineage tree. ImmGen Project modules, including the gene lists in each module, and regulatory program metadata are available online (http://www.immgen.org/ModsRegs/modules.html), and the numbering of the modules there is used here.

When we mapped the list of the 366 mRNA transcripts associated with macrophages according to their placement in various fine modules, 14 modules showed significant enrichment for the macrophage-associated gene signature we identified (**Fig. 3a**). In particular, the 11 genes of module 161 (*A930039a15Rik*, *Akr1b10*, *Blvrb*, *Camk1*, *Glul*, *Myo7a*, *Nln*, *Pcyox1*, *Pla2g15*, *Pon3* and *Slc48a*) were significantly induced in all four macrophage populations used to generate the list of macrophage-associated genes (**Fig. 3a**). Other modules, such as module 165, contained genes significantly induced in several specific groups of macrophages but not in all groups of macrophages (**Fig. 3a**). The 11 genes of module 161 encode molecules involved in redox regulation, heme biology, lipid metabolism and vesicular trafficking (**Supplementary Table 4**). Beyond the comparison to DCs, the genes in module 161, expressed in all macrophages, were not expressed by any other hematopoietic cell types, including granulocytes or any of

Table 1 Genes upregulated in tissue macrophages relative to their expression in DCs

All MΦ populations	– Peritoneal MΦ	– Lung MΦ	– Microglia	– Splenic red-pulp MΦ
Pecr	***Xrcc5***	***Mafb***	***Hgf***	***Cd151***
Tmem195	***Gm4878***	***Itga9***	***Pilrb2***	***Lonrf3***
Ptplad2	***Slco2b1***	***Cmklr1***	***Mgst1***	***Acy1***
1810011H11Rik	***Gpr77***	***Fez2***	***Klra2***	
Fert2	***Gpr160***	***Tspan4***	***Rnasel***	*C5ar1*
Tlr4	***P2ry13***	***Abcc3***	***Fcgr4***	*Pld1*
Pon3	***Tanc2***	***Nr1d1***	***Rhoq***	*Gpr177*
Mr1	***Sepn1***	***Ptprm***	***Fpr1***	*Arsk*
Arsg		***Ctsf***	***Cd302***	*Plod3*
Fcgr1	*Il1a*	***Tfpi***	***Slc7a2***	*Cd33*
Camk1	*Asph*		***Slc16a7***	*Cebpb*
Fgd4	*Dnase2a*	*Ptgs1*	***Slc16a10***	*Atp6ap1*
Sqrdl	*Slc38a7*	*C1qa*	***Slpi***	*Pros1*
Csf3r	*Siglece*	*Engase*	***Mitf***	*Dhrs3*
	Itgb5	*C1qb*	***Snx24***	*Rnf13*
Plod1	*Rhob*	*C1qc*	***Lyplal1***	*Man2b2*
Tom1	*Mavs*	*Timp2*	***St7***	*Ltc4s*
Myo7a	*Atp13a2*	*Slc11a1*		
A930039A15Rik	*Slc29a1*	*4632428N05Rik*	*Tlr8*	
Pld3	*Slc15a3*	*Sesn1*	*Gbp6*	
Tpp1	*Tmem86a*	*Plxnb2*	*6430548M08Rik*	
Ctsd	*Tgfbr2*	*Apoe*	*C130050O18Rik*	
Pla2g15	*Tnfrsf21*		*Pilra*	
Lamp2			*Pilrb1*	
Pla2g4a			*Lpl*	
MerTK			*Pstpip2*	
Tlr7			*Serpinb6a*	
Cd14			*Slc38a6*	
Tbxas1			*Abcc5*	
Fcgr3			*Lrp1*	
Sepp1			*Pcyox1*	
Glul			*Hmox1*	
Cd164			*Slc17a5*	
Tcn2			*Emr1*	
Dok3			*Hgsnat*	
Ctsl				
Tspan14				
Comt1				
Tmem77				
Abca1				

Genes with higher expression by all four prototypical macrophage populations (far left) or by three of the four populations (lacking (–) one of the four) than in classical or migratory DCs; bolding indicates signal intensity showing lack of expression by DCs; no bolding indicates expression in DCs, but higher expression in macrophages. Data are pooled from three or more experiments.

the blood monocyte subsets (**Fig. 3b**), which indicated that this list of genes was selectively associated with mature macrophage differentiation in the hematopoietic system.

As a framework for future studies of the transcriptional control of the development, maintenance and function of macrophages, we examined the predicted activators assigned by the Ontogenet algorithm to the modules associated with the macrophage core genes. One example is the activators predicted by Ontogenet algorithm to control the expression of the 11 gene transcripts of module 161 (**Fig. 3b**). Overall, a highly overlapping set of 22 regulators emerged from the 14 macrophage-associated modules (**Fig. 3c**). In particular, TCFE3, C/EBP-α and Bach1 were predicted activators in a majority of these modules (>75%). Other predicted regulators, such as CREG-1 (the cellular repressor of genes stimulated by the transcription factor E1A), were unexpectedly but prominently identified. Among the 22 regulators associated with the 14 modules, 18 were predicted by Ingenuity pathway tools to interact in a regulatory network on the basis of known protein-protein interactions or mutual transcriptional regulation (**Fig. 3d**). These regulators represented five main families of transcriptional factors (**Fig. 3d**). The evaluation score generated for this network had a *P* value of $\leq 10^{-35}$. Beyond modules of genes that unified the four tissue macrophage populations we studied, several modules were selectively associated with a single macrophage population (**Supplementary Table 5**). In these specific modules, predicted regulators included Spi-C for red-pulp macrophages, which confirmed a regulation already known[15] and thus provided support for the predictive power of the algorithm, and GATA-6 as a regulator of peritoneal macrophages (**Supplementary Table 6**).

Core signatures to identify macrophages

Finally, we used the core signature of resting macrophages defined above to assess mononuclear phagocyte populations that we excluded from our earlier core analysis because of the paucity of information on a given population or controversy in the literature about their origins or functional properties, including whether they should be classified as DCs or macrophages. In the ImmGen Project database, each population has been assigned a classification *a priori* as DC or macrophage. For clarity and for consistency with the database, the names of these populations will be used here (and in **Fig. 4**; glossary, **Supplementary Note 2**). These populations included resting and thioglycollate-elicited mononuclear phagocytes that expressed CD11c and MHC class II (**Supplementary Fig. 5**), skin Langerhans cells, bone marrow macrophages[22], and putative CD11b$^+$ tissue DCs, including those in the liver and gut. All thioglycollate-elicited cells from the peritoneal cavity, even those that coexpressed CD11c and MHC class II, had high expression of genes in the 39-gene macrophage core and in module 161 itself, similar to the prototypic macrophage populations used to generate the core (**Fig. 4a**,**b**); this indicated that these cells were indeed macrophages despite their coexpression of CD11c and MHC class II. However, Langerhans cells and CD11c$^+$MHCII$^+$CD11b$^+$ cells from the liver (CD11b$^+$ liver DCs in the ImmGen Project database) did not have robust expression of the 39-gene macrophage core signature or module 161 alone, nor did bone marrow macrophages (**Fig. 4a**,**b**). CD11c$^+$MHCII$^+$CD11b$^+$CD103$^-$ cells from the intestinal lamina propria and CD11c^{lo}MHCII$^+$CD11b$^+$ cells from the serosa that have been called DCs in many studies expressed genes of the macrophage core signature, including those from module 161 (**Fig. 4a**,**b**), which suggested a strong relationship to macrophages. Accordingly, we call these cells 'CD11b$^+$ gut macrophages' and 'CD11c^{lo} serosal macrophages' here (and on the ImmGen Project website). We clustered those mononuclear phagocytes on the basis of their expression of the 39-gene macrophage core to model their relatedness to each other (**Fig. 4c**). Langerhans cells of the skin and bone marrow macrophages were positioned at the interface between DCs and macrophages, with a distant relationship to classical DCs, but failed to cluster with macrophages (**Fig. 4c**).

As mentioned earlier, nonlymphoid tissue CD11b$^+$ DCs have been suggested to be heterogeneous[19]. Thus, we reasoned that the use of

antibodies to cell-surface proteins identified as macrophage specific by our gene-expression analysis might be used to identify macrophage 'contaminants' in a heterogeneous population. Furthermore, we aimed to determine if the same cell-surface markers might also prove valuable in identifying macrophages universally, including identification in organs beyond those we initially analyzed and/or those in which F4/80 has not proven sufficiently definitive. We selected the lipopolysaccharide receptor CD14, the FcγRI CD64 and the kinase MerTK as

Table 2 Genes upregulated in two of four tissue macrophage populations

Peritoneal + splenic red pulp	Peritoneal + lung	Lung + splenic red pulp	Peritoneal + microglia	Lung + microglia	Microglia + splenic red pulp
Ccl24	***Marco***	***Dmxl2***	***Hnmt***	***Scamp5***	***Lhfpl2***
Gstk1	***P2ry2***	***Dip2c***	***Mtus1***	***Ppp1r9a***	***Osm***
Aspa	***Aifm2***	***Galnt3***	***C3ar1***	***Tppp***	***Mgll***
2810405K02Rik	***Clec4e***	***Niacr1***	***Dagla***	***Abcb4***	***Bhlhe41***
B430306N03Rik	***Plcb1***	***Bckdhb***	***Wrb***	***Kcnj2***	***Ang***
Fcna	***Kcnn3***	***Angptl4***	***Gab1***	***P2ry12***	***D8ertd82e***
Gm5970	***Arhgap24***	***Lrp4***	***Fkbp9***		
Aoah	***Cd93***	***Sh3bgrl2***		*Slc37a2*	*X99384*
Cd5l	***Fundc2***	***Gm5150***	*Rab11fip5*	*Adrb1*	*Serpine1*
Gm4951	***Tspan32***	***Tcfec***	*6230427j02rik*	*Slc16a6*	*Abhd12*
Nr1d1	***Lmbr1***	***Sh2d1b1***	*Scn1b*	*Rab3il1*	*Ms4a6d*
Mlkl	***Adarb1***	***Galnt6***	*Scamp1*	*Mfsd11*	*Cebpa*
Vnn3	***Fzd4***	***Pdgfc***	*Msrb2*	*Flcn*	*Lpcat3*
Igf1	***F7***		*Abca9*	*Tmem63a*	*Manea*
	Ccr1	*6720489N17Rik*	*Plxdc2*	*P2rx7*	*Ctss*
Ptgis	***Hspa12a***	*Pparg*	*Adam15*	*Hpgds*	*Ccl3*
Pitpnc1	***Cav1***	*Megf9*	*Itgam*	*Hpgd*	*Cryl1*
Fam43a	***Nt5e***	*Adcy3*	*Itga6*	*Lpcat2*	*Man1c1*
Itsn1	***1190002a17rik***	*Enpp1*	*Vkorc1*	*Slc7a8*	*Ctns*
Ifi27l1		*Il18*	*1700017b05rik*	*Maf*	*Sgk1*
Rasgrp2	*Cav2*	*Siglec1*	*Smad3*	*Tmem86a*	*Pag1*
Aldh6a1	*Gda*	*Clec4n*	*Smpd1*	*Slc36a1*	*Tgfbr1*
Epb4.1l1	*Frrs1*	*Lgals8*	*Naglu*	*Gna12*	*Clec5a*
Cryzl1	*Tspan5*	*Nceh1*	*Pmp22*	*Adap2*	
Lrp12	*Pdk4*	*Lipa*	*Man2b2*	*Lgmn*	
Cd300ld	*Slc36a4*	*4931406c07rik*	*Tnfrsf1a*	*Hist1h1c*	
Pla2g7	*Fam3c*	*Sirpa*	*Lifr*	*Lair1*	
Cfp	*Ms4a8a*	*Rasgef1b*	*Tlr13*	*Slc40a1*	
Sdc3	*Atoh1*	*Wdfy3*	*Slc25a37*	*Csf1r*	
Dusp7	*Alox5*	*Ermp1*	*Grn*	*P4ha1*	
Tbc1d2b	*Thbd*	*Asah1*		*Iffo1*	
Igsf6	*Gstm1*	*Ear1*		*Dusp6*	
Man2a1	*Cxcl2*	*Ear10*			
Zswim6	*Nhlrc3*	*Ano6*			
Ifnar2	*Fry*	*Mrc1*			
Trf	*F10*	*Camk2d*			
Blvrb	*Sord*	*Gab3*			
Cd38	*Ncf2*	*Syne2*			
Ctsb	*Hexa*	*Axl*			
Tmem87b	*Dram1*	*Tcf7l2*			
Itfg3	*Plaur*	*Ctsc*			
Ninj1	*G6pdx*	*D730040f13rik*			
	Fn1	*Slc15a3*			
	Cybb	*Plk3*			
	Dennd4c	*Hebp1*			
	Mpp1	*Dst*			
	S100a1	*Blvra*			
	Gsr	*Sort1*			
	Abcd2	*Slc12a7*			
	Dab2	*Clec4a3*			
	Ccl6				
	Sepx1				
	Prdx5				
	Dusp3				
	Pgd				
	Gp49a				
	Capg				
	Cndp2				
	Vps13c				
	Adipor2				
	App				
	Atg7				
	Cebpb				

Genes with higher expression by two of four prototypical macrophage populations than in classical or migratory DCs (bolding and debolding as in **Table 1**). Data are pooled from three or more experiments.

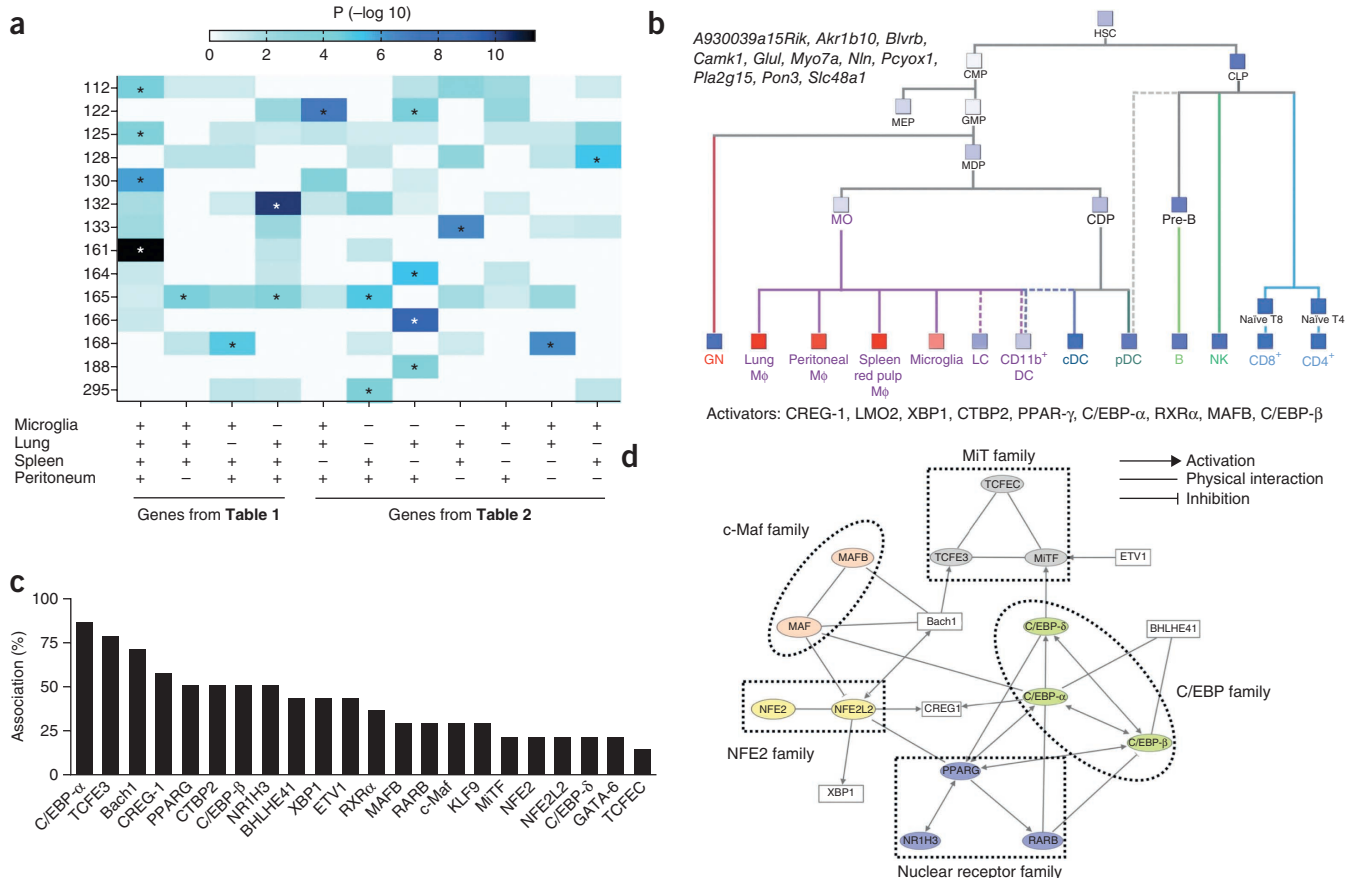

Figure 3 Identification of gene modules enriched for macrophage-related gene signatures and their predicted regulators. (**a**) Heat map of the overlap of ImmGen modules (left margin) and all macrophage-associated gene signatures (**Tables 1** and **2**), including only modules with significant enrichment for at least one signature. Stars indicate significant overlap (hypergeometric test). (**b**) Simplified hematopoietic tree showing expression (red, high; blue, low; purple, intermediate) of genes in module 161 (top left); bottom, predicted positive regulators of the module. HSC, hematopoietic stem cell; CMP, common myeloid progenitor; CLP, common lympoid progenitor; MEP, megakaryocyte-erythrocyte progenitor; GMP, granulocyte-macrophage precursor; MDP, macrophage and DC precursor; MO, monocyte; CDP, common DC precursor; Pre-B, pre-B cell; GN, granulocyte; LC, Langerhans cell; cDC, classical DC; pDC, plasmacytoid DC; B, B cell; NK, natural killer cell; T8 or CD8$^+$, CD8$^+$ T cell; T4 or CD4$^+$, CD4$^+$ T cell. (**c**) Frequency of the association between the 14 modules in **a** and positive regulators (activators; horizontal axis) predicted by the Ontogenet algorithm to regulate two or more of those modules. (**d**) Physical and regulatory interactions between the 18 regulators most frequently represented in the 14 macrophage-associated modules, assessed with Ingenuity pathway-analysis software; straight lines indicate links for established physical interactions; arrows and sideways 'T' symbols indicate known pathways of coactivation and inhibition, respectively. Data are pooled from three or more experiments.

cell-surface proteins among the group of proteins encoded by the 39 mRNA transcripts with expression deemed to be low or absent in DCs but present in all macrophages and to which high-quality monoclonal antibodies have been generated. Indeed, all of these proteins were expressed on all of the four resident macrophage populations used in our primary analysis (**Fig. 5a**), with lower expression of CD14 than of CD64 or MerTK (**Fig. 5a**). Two of these tissues, spleen and lung, have substantial DC populations. In the spleen, antibodies to MerTK, CD64 or CD14 did not stain CD8$^+$ or CD11b$^+$ DCs (**Fig. 5a**). However, in the lung, in which interstitial pulmonary macrophages are CD11b$^-$, there may still be an underlying heterogeneity of lung CD11b$^+$ DCs that includes a subset of CD11b$^+$ macrophages[19,23,24]. Indeed, CD14, CD64 and MerTK were expressed by a portion of lung CD11b$^+$ DCs but not by CD103$^+$ DCs (**Fig. 5a**). Gating on MerTK$^+$CD64$^+$ cells showed most of these cells were Siglec-F$^+$ lung macrophages, but a small proportion of MerTK$^+$CD64$^+$ cells in the lung were Siglec-F$^-$ cells with high expression of MHC class II (**Fig. 5b**). By our usual gating strategy for lung DCs (**Fig. 5c**), DCs were defined as Siglec F$^-$CD11c$^+$MHCII$^+$ cells. However, the small population of Siglec-F$^-$MerTK$^+$CD64$^+$ cells that may instead have been macrophages (**Fig. 5b**) were partially in the standard DC gate (**Fig. 5c**). Indeed, we were able to separate CD11b$^+$ DCs into CD11b$^+$CD24$^+$CD64^{lo}MerTK$^-$CD14^{int} cells and CD11b$^+$CD24^{lo}CD64$^+$MerTK$^+$CD14^{hi} cells (**Fig. 5d**). Thus, the latter was probably a population of macrophages that segregated together with DCs, through the use of many markers, but were not DCs. Indeed, the CD11b$^+$ DCs were segregated by CD24 expression in the ImmGen Project on the basis of the likelihood that those expressing CD24 were true DCs but those without CD24 were not. Our findings suggested that this possibility was likely and indicated the utility of using markers such as MerTK and CD64 as a panel to facilitate the identification of macrophages versus DCs.

We next turned to two tissues, liver and adipose, not analyzed by the ImmGen Project in terms of gene-expression profiling of macrophages to determine if the use of staining for MerTK and CD64 would facilitate the identification of macrophages in those tissues and distinguish them from DCs. In the liver, we started with a classic approach of plotting F4/80 expression versus CD11c expression. Eosinophils are now recognized as F4/80$^+$ cells with high side

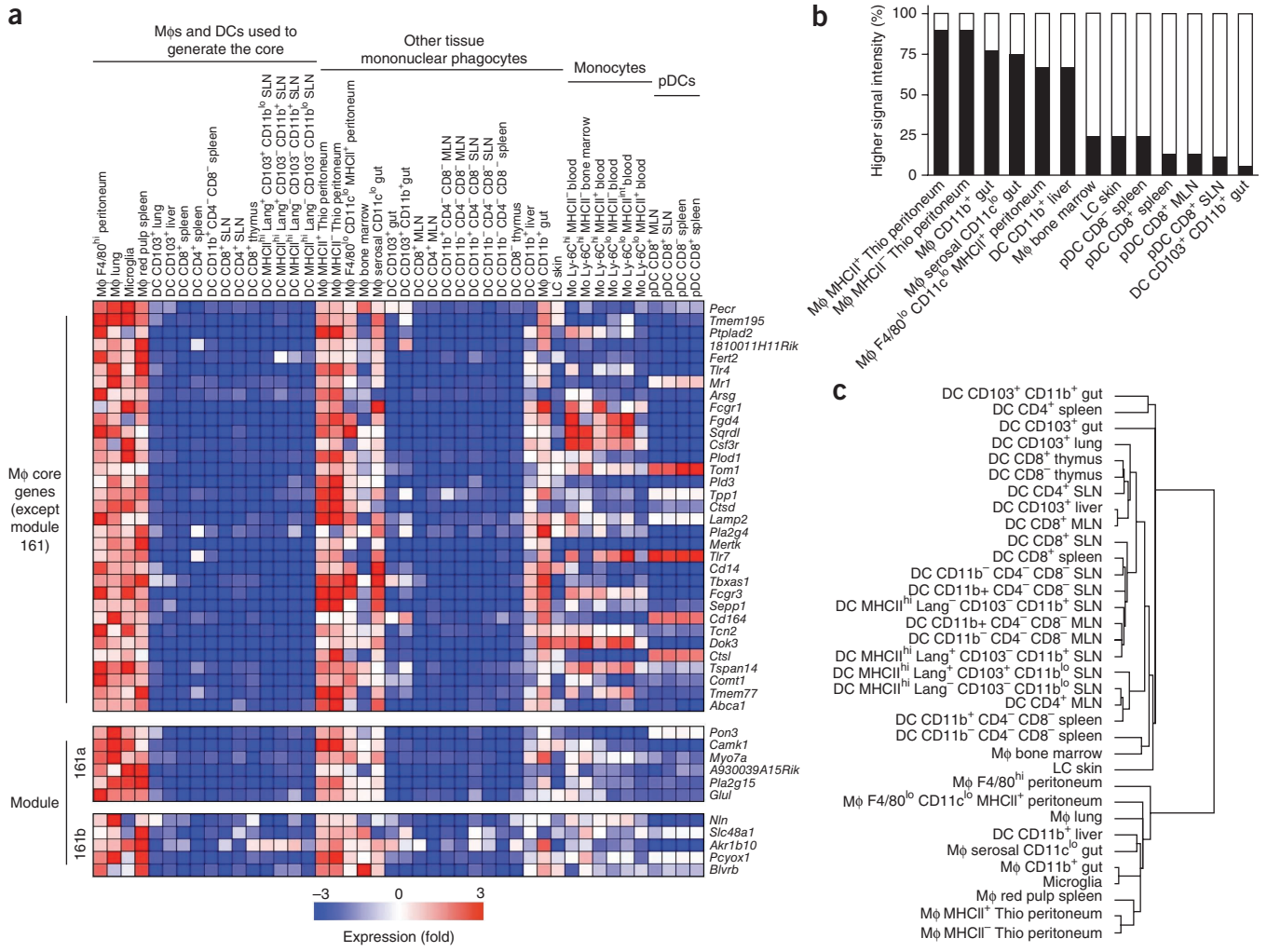

Figure 4 Expression of genes of the macrophage core signature by other populations of mononuclear phagocytes. (**a**) Heat map of 39 genes (right margin) with higher expression in spleen, brain, peritoneal and lung macrophages than in classical or migratory DCs (left); middle, tissue-derived mononuclear phagocytes not included in the generation of this list of genes; right, blood monocytes and plasmacytoid DCs; 161a, genes from module 161 included here; 161b, genes from module 161 that did not meet the criteria for inclusion (**Table 1**). SLN, skin lymph node; MLN, mesenteric lymph node; Thio, thioglycollate-elicited. (**b**) Frequency of signal intensity for the 39 genes in **a** at least twofold higher in various populations (horizontal axis) than in the DC population with the highest expression (filled bars; open bars indicate extension up to 100%). (**c**) Relationships among various mononuclear phagocytes based on their expression of the 39 genes in **a**. Lang, langerin; LC, Langerhans cell. Data are pooled from three or more experiments.

scatter that express Siglec-F universally[25]. Indeed, among macrophages, Siglec-F is observed only on macrophages in the lung[26,27] (as used to identify lung macrophages here; eosinophils did not contaminate lung macrophages, which we separated from eosinophils by their high CD11c expression and relative lack of CD11b expression in the macrophages (**Supplementary Fig. 6**)). In the liver, the abundance of F4/80 on eosinophils overlapped that of another population of F4/80$^+$ cells (those with low side scatter) that were CD11c^{lo} in liver (**Fig. 5e**). Even after excluding eosinophils, we found four gates of cells with various expression of F4/80 and CD11c (**Fig. 5e**). There was high expression of MerTK and CD64 in two of these gates, one composed of cells with the highest expression of F4/80 (gate 2) and another with lower expression of F4/80 (in gate 3). These findings suggested two populations of F4/80^{hi} and F4/80^{lo} liver macrophages that may correspond to the two types of macrophages believed to be present in many organs[12]. The liver CD45$^+$ cells with highest expression of CD11c were MerTK$^-$CD64$^-$ (**Fig. 5e**), which suggested they were liver DCs. Reverse gating showed that all MerTK$^+$CD64$^+$ cells were in one of the two putative macrophage gates (**Fig. 5e**). Gate 1 without eosinophils probably contained blood monocytes, which were not MerTK$^+$. We noted relatively similar results for adipose tissue (**Fig. 5f**), in which the cells with the highest F4/80 expression were MerTK$^+$CD64$^+$ and those with higher CD11c expression and lower F4/80 expression were MerTK$^-$CD64$^-$. In both liver and adipose tissue, expression of MHC class II was high on macrophages and DCs (**Fig. 5e,f**). Because F4/80 and CD11c are both expressed by many tissue macrophages and DCs, albeit in amounts that are somewhat different, distinguishing macrophages and DCs on the basis of these traditional markers can be difficult. Staining for MerTK and CD64 offers the advantage of distinct differences in the magnitude of expression in macrophages versus DCs. Thus, we propose that costaining for MerTK and CD64 provides a powerful approach for identifying macrophages universally and selectively in mouse tissues.

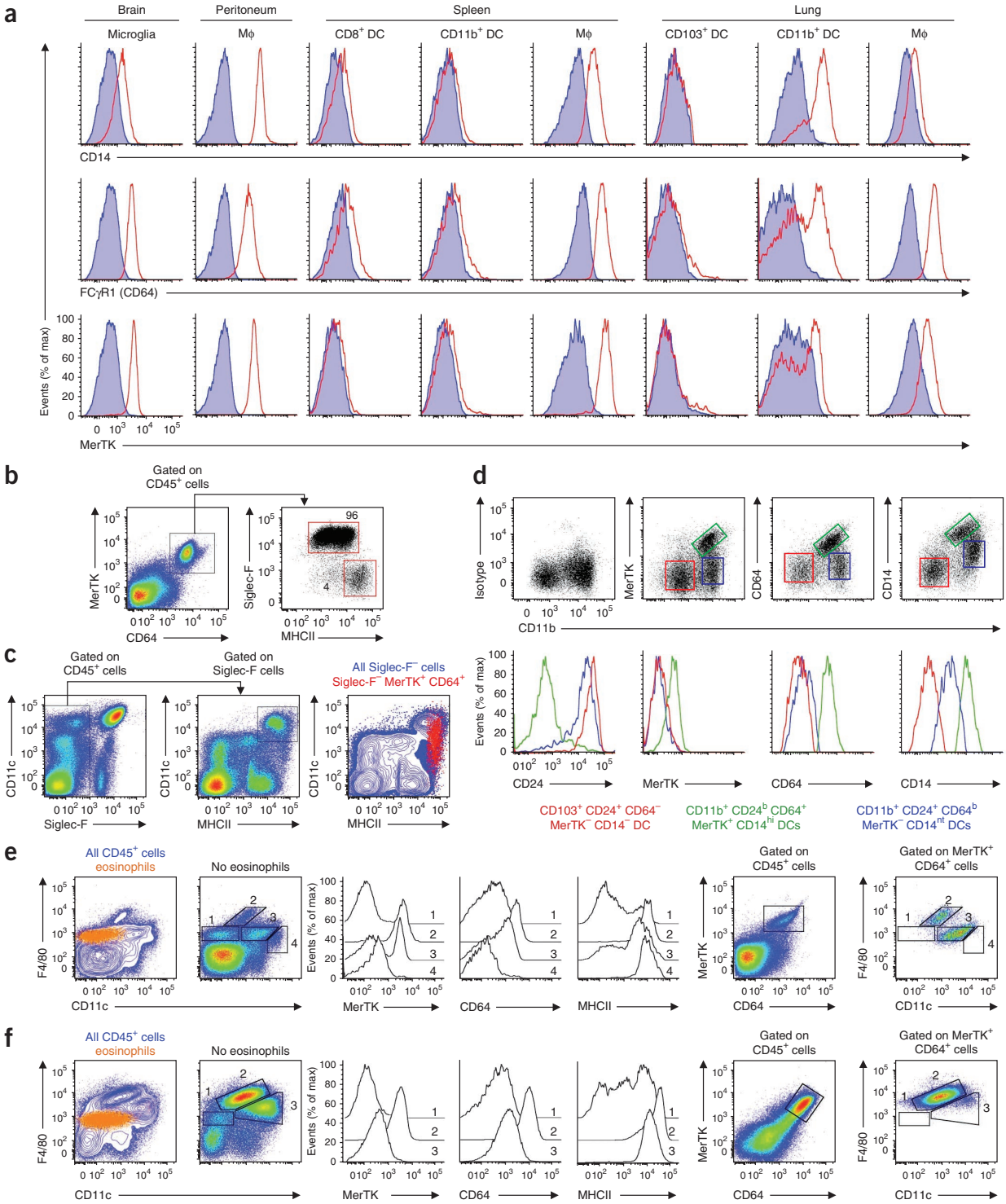

Figure 5 Transcripts of the macrophage core signature, assessed as protein in various tissues. (**a**) Expression of CD14, CD64 and MerTK in macrophages and DCs of brain, peritoneum, spleen and lung. Red line, specific antibody; blue shading, isotype-matched control antibody. (**b**) Flow cytometry of MerTK$^+$CD64$^+$ cells (gated at left), assessing expression of Siglec-F and MHC class II (right). Numbers adjacent to outlined areas indicate percent Siglec-F$^+$MHCII$^+$ cells (top) and Siglec-F$^+$MHCII$^+$ cells (bottom). (**c**) Gating strategy for lung DCs; DCs are CD45$^+$ cells that express CD11c and MHC class II but not Siglec-F. (**d**) Flow cytometry of DCs, gated on lung DCs, assessing expression of CD11b with MerTK, CD64 and CD14 (top), and of CD24, MerTK, CD64 and CD14 (bottom). (**e**,**f**) Flow cytometry of liver (**e**) or adipose (**f**) CD45$^+$ cells stained for F4/80 and CD11c (left), with eosinophils gated (Siglec-F$^+$ and high side scatter; far left) and without eosinophils (second from left), to identify four (**e**) or three (**f**) subsets of cells with differences in their expression of F4/80 and CD11c, followed by analysis of the expression of MerTK, CD64 and MHC class II by those subsets (middle), then reverse gating on MerTK$^+$CD64$^+$ cells (second from right) and analysis of the expression of F4/80 and CD11c by those gated cells (far right). Data are from at least two independent experiments with three mice per group.

DISCUSSION

The large and unique database and accompanying bioinformatics analysis of the ImmGen Project provide insight into macrophage populations isolated from various organs of mice. A notable initial revelation was that macrophage populations from different organs were considerably diverse, and it is likely that further profiling in macrophages will expand on this diversity. Only a very small group of mRNA transcripts were associated with all macrophages but not DCs. Proteins previously predicted to distinguish macrophages from other cell types, such as F4/80, CD68 and CD115 (c-Fms or CSF1R), did not emerge as the most powerful markers of macrophages. However, many canonical genes did, including those encoding CD14, CD64 (the high-affinity Fcγ receptor I), MerTK (the kinase involved in efferocytosis), cathespin D and the kinase Fert2 (which may have a substantial effect on CD115 signaling but which has not yet been studied in macrophages). The identification of these as being selectively associated with macrophages reinforced the idea of a key role for macrophages in innate immunity, efferocytosis and the clearance of debris, whereas genes encoding molecules associated with antigen presentation and migration to lymphoid tissues were more associated with DCs[28]. However, our data did suggest that macrophages may have a greater role than DCs in the activation of mucosa-associated invariant T cells. On the basis of follow-up protein-expression analysis of MerTK and CD64 in macrophages from six different tissues, we propose that analysis of MerTK and CD64 should serve as a starting point for the identification of macrophages in tissues, as staining for these markers seemed to identify F4/80^{hi} macrophages and other macrophages with somewhat lower F4/80 expression[12] in all tissues. We believe that staining for MerTK and CD64 provides an advantage over traditional staining for F4/80, CD11c and MHC class I but can also be used powerfully in addition to such staining. The expression of F4/80 and CD11c often overlaps in macrophages and DCs in nonlymphoid tissues, but it seems that DCs do not coexpress MerTK and CD64.

Beyond those cell-surface markers closely associated with macrophage identity, we identified other transcripts associated only with macrophages among hematopoietic cells. In particular, module 161 of the ImmGen Project identified a group of genes (*A930039a15Rik*, *Akr1b10*, *Blvrb*, *Camk1*, *Glul*, *Myo7a*, *Nln*, *Pcyox1*, *Pla2g15*, *Pon3* and *Slc48a*) coexpressed across the entire data set of the ImmGen Project and that encode molecules with functions compatible with the function of macrophages, but none of them have previously been considered macrophage markers. Both the genes from this module and their predicted regulators deserve attention in the future.

The Ontogenet algorithm makes it possible to extend the macrophage-associated genes we identified to regulatory programs that may control them. The finding of induction of expression of a single module (330) in red-pulp macrophages relative to its expression all other macrophages and the predictions generated by the algorithm indicating that this module is regulated by Spi-C supported the reliability of the prediction of the regulatory programs by the algorithm, as Spi-C is already known to be required selectively for the development or maintenance of red-pulp macrophages[15]. Additional information has also emerged, such as the association of modules unique to peritoneal macrophages that are predicted to be regulated by GATA-6.

Gene transcripts with high expression in multiple macrophage populations but without high expression in DCs were associated with predicted transcriptional regulatory programs that differed considerably from those identified in DCs[28]. The predicted regulatory programs of modules enriched for macrophage-associated genes included several members of the MiT family of transcription factors recognized as being expressed specifically in macrophages[3], as well as transcription factors not previously associated with macrophages, such as Bach1 and CREG-1. Bach1 has been studied very little in macrophages but has been linked to osteoclastogenesis[29] and is a regulator of heme oxygenase 1 (ref. 30). CREG-1 is a secreted regulator[31,32] associated broadly with differentiation[33] and cellular senescence[34] that has been associated with macrophage-enriched gene modules, although it has never been studied before in the context of macrophage biology, to our knowledge. The Ontogenet algorithm predicted that RXRα is the most prominent key activator of the highly specific and universal macrophage module 161. Future analysis of these predictions should be useful in showing how macrophage identity and function is controlled.

So far, the ImmGen Project has focused mainly on cells recovered from resting, uninfected mice, in which macrophages derive mainly from the yolk sac[12]. Macrophage polarization in the context of infection and inflammation is a topic of great interest that this study has scarcely been able to address beyond finding that monocytes recruited to the peritoneum in response to thioglycollate upregulated the expression of mRNA transcripts observed in resting tissue macrophages, even though it now seems that monocytes are not precursors of resting tissue macrophages as they are of inflammatory macrophages. The foundations laid here suggest that future additions to the ImmGen Project database of macrophages recovered in disease states should add to the understanding of how to manipulate these crucial cells to favor desired outcomes in disease. Given the great diversity of macrophages in different organs, which we anticipate is present even in inflamed organs, such studies may be expected to ultimately generate therapeutic approaches to selectively target macrophages in diseased organs without affecting other cell types.

METHODS

Methods and any associated references are available in the online version of the paper.

Accession codes. GEO: microarray data, GSE15907.

Note: Supplementary information is available in the online version of the paper.

ACKNOWLEDGMENTS

We thank our colleagues of the ImmGen Project consortium; V. Jojic, J. Ericson, S. Davis and C. Benoist for contributions; eBioscience and Affymetrix for material support of the ImmGen Project; and M. Colonna (Washington University School of Medicine) for monoclonal antibodies (including anti-Siglec-H) and other reagents. Supported by the National Institute of Allergy and Infectious Diseases of the US National Institutes of Health (R24 AI072073 to fund the ImmGen Project, spearheaded by C. Benoist), the US National Institutes of Health (R01AI049653 and R01AI061741 to G.J.R.; P50GM071558-03 and R01DK08854 to A.M.; and5T32DA007135-27 to A.R.M.) and the American Heart Association (10POST4160140 to E.L.G.).

AUTHOR CONTRIBUTIONS

E.L.G. purified macrophage populations, designed and did experiments, analyzed data and wrote the manuscript; G.J.R. designed and supervised experiments, analyzed data and wrote the manuscript; T.S. analyzed data and wrote the manuscript; J.M. designed analytical strategies and analyzed data; M.G., C.J., J.H., A.C. and K.G.E. purified macrophage and DC populations; S.I. did experiments; S.G., A.R.M. and A.M. analyzed data; W.-J.C. and T.H.H. provided reagents and supervised experiments; and S.J.T. and M.M. designed and supervised experiments.

COMPETING FINANCIAL INTERESTS

The authors declare no competing financial interests.

Published online at http://www.nature.com/doifinder/10.1038/ni.2419.
Reprints and permissions information is available online at http://www.nature.com/reprints/index.html.

1. Heng, T.S. & Painter, M.W. The Immunological Genome Project: networks of gene expression in immune cells. *Nat. Immunol.* **9**, 1091–1094 (2008).
2. Gordon, S. & Taylor, P.R. Monocyte and macrophage heterogeneity. *Nat. Rev. Immunol.* **5**, 953–964 (2005).
3. Hume, D.A. Differentiation and heterogeneity in the mononuclear phagocyte system. *Mucosal Immunol.* **1**, 432–441 (2008).
4. Mosser, D.M. & Edwards, J.P. Exploring the full spectrum of macrophage activation. *Nat. Rev. Immunol.* **8**, 958–969 (2008).
5. Geissmann, F., Gordon, S., Hume, D.A., Mowat, A.M. & Randolph, G.J. Unraveling mononuclear phagocyte heterogeneity. *Nat. Rev. Immunol.* **10**, 453–460 (2010).
6. Fogg, D.K. *et al.* A clonogenic bone marrow progenitor specific for macrophages and dendritic cells. *Science* **311**, 83–87 (2006).
7. Onai, N. *et al.* Identification of clonogenic common Flt3$^+$M-CSFR$^+$ plasmacytoid and conventional dendritic cell progenitors in mouse bone marrow. *Nat. Immunol.* **8**, 1207–1216 (2007).
8. Liu, K. *et al. In vivo* analysis of dendritic cell development and homeostasis. *Science* **324**, 392–397 (2009).
9. Hildner, K. *et al.* Batf3 deficiency reveals a critical role for CD8α^+ dendritic cells in cytotoxic T cell immunity. *Science* **322**, 1097–1100 (2008).
10. Takahashi, K. Development and differentiation of macrophages and related cells: Historical review and current concepts. *J. Clin. Exp. Hematop.* **41**, 1–33 (2001).
11. Ginhoux, F. *et al.* Fate mapping analysis reveals that adult microglia derive from primitive macrophages. *Science* **330**, 841–845 (2010).
12. Schulz, C. *et al.* A lineage of myeloid cells independent of Myb and hematopoietic stem cells. *Science* **336**, 86–90 (2012).
13. Aziz, A., Soucie, E., Sarrazin, S. & Sieweke, M.H. MafB/c-Maf deficiency enables self-renewal of differentiated functional macrophages. *Science* **326**, 867–871 (2009).
14. Teitelbaum, S.L. & Ross, F.P. Genetic regulation of osteoclast development and function. *Nat. Rev. Genet.* **4**, 638–649 (2003).
15. Kohyama, M. *et al.* Role for Spi-C in the development of red pulp macrophages and splenic iron homeostasis. *Nature* **457**, 318–321 (2009).
16. Lemke, G. & Rothlin, C.V. Immunobiology of the TAM receptors. *Nat. Rev. Immunol.* **8**, 327–336 (2008).
17. Ohl, L. *et al.* CCR7 governs skin dendritic cell migration under inflammatory and steady-state conditions. *Immunity* **21**, 279–288 (2004).
18. Ginhoux, F. *et al.* Blood-derived dermal langerin$^+$ dendritic cells survey the skin in the steady state. *J. Exp. Med.* **204**, 3133–3146 (2007).
19. Hashimoto, D., Miller, J. & Merad, M. Dendritic cell and macrophage heterogeneity in vivo. *Immunity* **35**, 323–335 (2011).
20. Chua, W.J. *et al.* Endogenous MHC-related protein 1 is transiently expressed on the plasma membrane in a conformation that activates mucosal-associated invariant T cells. *J. Immunol.* **186**, 4744–4750 (2011).
21. Elstad, M.R., Stafforini, D.M., McIntyre, T.M., Prescott, S.M. & Zimmerman, G.A. Platelet-activating factor acetylhydrolase increases during macrophage differentiation. A novel mechanism that regulates accumulation of platelet-activating factor. *J. Biol. Chem.* **264**, 8467–8470 (1989).
22. Chow, A. *et al.* Bone marrow CD169$^+$ macrophages promote the retention of hematopoietic stem and progenitor cells in the mesenchymal stem cell niche. *J. Exp. Med.* **208**, 261–271 (2011).
23. Hashimoto, D. *et al.* Pretransplant CSF-1 therapy expands recipient macrophages and ameliorates GVHD after allogeneic hematopoietic cell transplantation. *J. Exp. Med.* **208**, 1069–1082 (2011).
24. Satpathy, A.T. *et al.* Zbtb46 expression distinguishes classical dendritic cells and their committed progenitors from other immune lineages. *J. Exp. Med.* **209**, 1135–1152 (2012).
25. Kim, H.J., Alonzo, E.S., Dorothee, G., Pollard, J.W. & Sant'Angelo, D.B. Selective depletion of eosinophils or neutrophils in mice impacts the efficiency of apoptotic cell clearance in the thymus. *PLoS ONE* **5**, e11439 (2010).
26. Sung, S.S. *et al.* A major lung CD103 (α_E)-β_7 integrin-positive epithelial dendritic cell population expressing langerin and tight junction proteins. *J. Immunol.* **176**, 2161–2172 (2006).
27. Desch, A.N. *et al.* CD103$^+$ pulmonary dendritic cells preferentially acquire and present apoptotic cell-associated antigen. *J. Exp. Med.* **208**, 1789–1797 (2011).
28. Miller, J.C. *et al.* Deciphering the transcriptional network of the dendritic cell lineage. *Nat. Immunol.* **13**, 888–899 (2012).
29. Hama, M. *et al.* Bach1 regulates osteoclastogenesis via both heme oxygenase-1 dependent and independent pathways. *Arthritis Rheum.* **64**, 1518–1528 (2012).
30. Sun, J. *et al.* Hemoprotein Bach1 regulates enhancer availability of heme oxygenase-1 gene. *EMBO J.* **21**, 5216–5224 (2002).
31. Veal, E., Eisenstein, M., Tseng, Z.H. & Gill, G. A cellular repressor of E1A-stimulated genes that inhibits activation by E2F. *Mol. Cell. Biol.* **18**, 5032–5041 (1998).
32. Sacher, M. *et al.* The crystal structure of CREG, a secreted glycoprotein involved in cellular growth and differentiation. *Proc. Natl. Acad. Sci. USA* **102**, 18326–18331 (2005).
33. Veal, E., Groisman, R., Eisenstein, M. & Gill, G. The secreted glycoprotein CREG enhances differentiation of NTERA-2 human embryonal carcinoma cells. *Oncogene* **19**, 2120–2128 (2000).
34. Moolmuang, B. & Tainsky, M.A. CREG1 enhances p16^{INK4a}-induced cellular senescence. *Cell Cycle* **10**, 518–530 (2011).

ImmGen Consortium:

Emmanuel L Gautier[10,11], Claudia Jakubzick[10], Gwendalyn J Randolph[10,11], Adam J Best[12], Jamie Knell[12], Ananda Goldrath[12], Jennifer Miller[10], Brian Brown[10], Miriam Merad[10], Vladimir Jojic[13], Daphne Koller[13], Nadia Cohen[14], Patrick Brennan[14], Michael Brenner[14], Tal Shay[15], Aviv Regev[15], Anne Fletcher[16], Kutlu Elpek[16], Angelique Bellemare-Pelletier[16], Deepali Malhotra[16], Shannon Turley[16], Radu Jianu[17], David Laidlaw[17], Jim Collins[18], Kavitha Narayan[19], Katelyn Sylvia[19], Joonsoo Kang[19], Roi Gazit[20], Brian S Garrison[20], Derrick J Rossi[20], Francis Kim[21], Tata Nageswara Rao[21], Amy Wagers[21], Susan A Shinton[22], Richard R Hardy[22], Paul Monach[23], Natalie A Bezman[24], Joseph C Sun[24], Charlie C Kim[24], Lewis L Lanier[24], Tracy Heng[25], Taras Kreslavsky[13], Michio Painter[25], Jeffrey Ericson[25], Scott Davis[25], Diane Mathis[25] & Christophe Benoist[25]

[10]Icahn Medical Institute, Mount Sinai Hospital, New York, New York, USA. [11]Department of Pathology & Immunology, Washington University, St. Louis, Missouri, USA. [12]Division of Biological Sciences, University of California San Diego, La Jolla, California, USA. [13]Computer Science Department, Stanford University, Stanford, California, USA. [14]Division of Rheumatology, Immunology and Allergy, Brigham and Women's Hospital, Boston, Massachusetts, USA. [15]Broad Institute, Cambridge, Massachusetts, USA. [16]Dana-Farber Cancer Institute and Harvard Medical School, Boston, Massachusetts, USA. [17]Computer Science Department, Brown University, Providence, Rhode Island, USA. [18]Department of Biomedical Engineering, Howard Hughes Medical Institute, Boston University, Boston, Massachusetts, USA. [19]Department of Pathology, University of Massachusetts Medical School, Worcester, Massachusetts, USA. [20]Immune Diseases Institute, Children's Hospital, Boston, Massachusetts, USA. [21]Joslin Diabetes Center, Boston, Massachusetts, USA. [22]Fox Chase Cancer Center, Philadelphia, Pennsylvania, USA. [23]Department of Medicine, Boston University, Boston, Massachusetts, USA. [24]Department of Microbiology & Immunology, University of California San Francisco, San Francisco, California, USA. [25]Division of Immunology, Department of Microbiology & Immunobiology, Harvard Medical School, Boston, Massachusetts, USA.

ONLINE METHODS

Mice. Six-week-old male C57BL/6J mice (Jackson Laboratory) were used for sorting and confirmation of results. Mice with sequence encoding green fluorescent protein knocked in to the gene encoding CX3CR1 were from Jackson Laboratories, and *Mr1*-deficient mice[20] were generated, bred and maintained at the Washington University School of Medicine. Mice were housed in specific pathogen–free facilities at the Mount Sinai School of Medicine or Washington University School of Medicine, and experimental procedures were done in accordance with the animal-use oversight committees at these institutions. Most cell populations were sorted from resting mice. However, for thioglycollate-elicited peritoneal macrophages, macrophages were collected from the peritoneal cavity 5 d after the instillation of 1 ml of 3% thioglycollate.

Cell identification and isolation. All cells were purified according to the sorting protocol and antibodies on the ImmGen website (http://www.immgen.org/Protocols/ImmGen Cell prep and sorting SOP.pdf). Cells were sorted directly from mouse tissues and were processed from tissue procurement to a second round of sorting into TRIzol within 4 h with a Beckton-Dickinson FACSAria II. Resting red-pulp macrophages from the spleen were sorted after nonenzymatic disaggregation of the spleen and were identified as F4/80^{hi} cells that lacked B220 but had high expression of CD11c and MHC class II[35,36]; macrophages from the resting peritoneum were collected in a peritoneal lavage and were stained to identify CD115^{hi} cells that were F4/80^{hi}MHCII^{-}; resting pulmonary macrophages were isolated from lungs digested for 15 min with Liberase III and macrophages were identified as Siglec-F^{+}CD11c^{+} cells with low expression of MHC class II[26,27]; and resting brain microglial macrophages were sorted from cells separated by Percoll-gradient centrifugation and digested with Liberase III and were CD11b^{+}CD45^{lo}F4/80^{lo} (ref. 11). Liver and epididymal adipose tissues were digested for 45 min in collagenase D and Liberase III, respectively. Liver cells were further separated on a Percoll gradient, whereas adipocytes were floated for separation from the stromal vascular fraction containing CD45^{+} cells in adipose tissue. The data browser of the ImmGen Project website includes files of flow cytometry plots showing the purification strategies and purity after isolation of these and all other populations. A list of abbreviations used in the ImmGen Project database relevant to macrophages and DCs is in **Supplementary Note 2**.

Microarray analysis, normalization, and data-set analysis. RNA was amplified and hybridized on the Affymetrix Mouse Gene 1.0 ST array by the ImmGen Project consortium with double-sorted cell populations sorted directly into TRIzol (http://www.immgen.org/Protocols/Total RNA Extraction with Trizol.pdf). These procedures followed a highly standardized protocol for data generation and documentation of quality control[37] (http://www.immgen.org/Protocols/ImmGen QC Documentation_ALL-DataGeneration_0612.pdf). A table listing QC data, replicate information, and batch information for each sample is also available on the ImmGen Project website. Data were analyzed with the GenePattern genomic analysis platform (http://www.broadinstitute.org/cancer/software/genepattern/). Raw data were normalized with the robust multi-array algorithm, returning linear values between 10 and 20,000. A common threshold for positive expression at 95% confidence across the data set was determined to be 120 (http://www.immgen.org/Protocols/ImmGen QC Documentation_ALL-DataGeneration_0612.pdf). Differences in gene expression signatures were identified and visualized with the Multiplot module of GenePattern. Probe sets were considered to have a difference in expression with a coefficient of variation of <0.5 and a *P* value of ≥0.05 (Student's *t*-test). Signature transcripts were clustered (centered on the mean) with the Hierarchical Clustering module of GenePattern, employing Pearson's correlation as a metric, and data were visualized with the Hierarchical Clustering Viewer heat-map module. Clustering analyses across the database of the ImmGen Project centered on the most variable gene sets (objectively defined as the top 15% genes, ranked by cross-population maximum/minimum ratio) to avoid 'noise' from genes at background variation. Pearson correlation plots of gene-expression profiles for various cell populations were generated with Express Matrix software. Pathway analysis as well as construction of the transcription factor network were done with Ingenuity Systems Pathway Analysis software. This software calculates a significance score for each network. The score is generated with a *P* value indicative of the likelihood that the assembly of a set of focus genes in a network could be explained by random chance alone.

PCA. Only the 4,417 genes whose variance of expression across all samples from the ten cell types was at least within the 80th percentile of variance were considered for PCA (by MATLAB sofware). Expression normalized by the robust multi-array average method and $\log_2$-transformed was used.

Generation of the core macrophage signature. A macrophage core signature was generated by comparison of gene expression in brain, lung, peritoneal and red-pulp macrophages to that in populations deemed not to be macrophages but authentic DCs. These DCs included CD103^{+} DCs from lung and liver, CD8^{+} DCs from spleen and thymus, CD4^{+}CD11b^{+} DCs from spleen, CD4^{-}CD8^{-}CD11b^{+} DCs from spleen, and all DC populations (resident and migratory) isolated from skin-draining lymph nodes. A first list of possible genes that define macrophages was generated with the median value in the group of macrophages or DCs for each probe set to generate a list of probe sets with median expression that was twofold or more higher in the group of macrophages with a statistical significance of $P < 0.05$ (Student's *t*-test) and a coefficient of variation of <0.5. Then that list of probe sets was filtered for the removal of any probe sets that did not have a normalized intensity value of ≥120 (the threshold for positive expression) in at least two macrophage populations. From the remaining probe sets, we compared the mean expression values of each macrophage and DC population, filtering to identify the lowest mean value in any single macrophage population relative to the highest mean value in any of the DCs. The probe sets with expression at least twofold higher in macrophage with the lowest expression compared with the DC with the highest expression composed the core genes retained (**Table 1**, far left). To account for genes observed in only some macrophage populations but still not expressed in DCs, we also generated lists in which one or two macrophage populations were allowed to be excluded from consideration, but the criteria for comparing the remaining macrophages to the DCs was otherwise as described.

Generation of gene modules and prediction of module regulators. The gene modules, Ontogenet algorithm and regulatory programs have been described (V. Jojic *et al.*, unpublished data; methods described in **Supplementary Note 1**). The normalization of expression data was done as part of the ImmGen Project pipeline, March 2011 release. Data were $\log_2$-transformed. For genes presented on the array with more than one probe set, only the probe set with the highest mean expression was retained. Of those, only the 7,996 probe sets with an s.d. value above 0.5 across the entire data set were used for the clustering. Clustering was done by Super Paramagnetic Clustering[38] with default parameters, which resulted in 80 stable coarse modules of coexpressed genes. Each coarse module was further clustered by hierarchical clustering into more fine modules, which resulted in 334 fine modules.

The Ontogenet algorithm was developed for the ImmGen data set (V. Jojic *et al.*, data not shown, and **Supplementary Note 1**). Ontogenet finds a regulatory program for each coarse and fine module on the basis of regulator expression and the structure of the lineage tree. The regulatory program uses a form of regularized linear regression in which each cell type can have its own regulatory program, but regulatory programs of related cells are 'encouraged' to be similar. This allows switching in the regulatory program but still allows robust fitting given the available data. Fopr visualization of the expression of a module on the lineage tree, the expression of each gene was standardized by subtraction of the mean and division by its s.d. across all data set. Results for replicates were averaged. The mean expression of each module was projected on the tree. Expression values are color coded from minimal (blue) to maximal (red).

Association between the macrophage core signature and gene modules. A hypergeometric test for two groups was used to estimate the enrichment of all ImmGen fine modules for the 11 gene signatures in **Tables 1** and **2**. A Benjamini-Hochberg false-discovery rate of 0.05 or less was applied to the *P* value table of all 11 signatures across all 334 fine modules.

Antibodies used for confirmation studies. Antibody to (anti-) mouse CD11c (N418), anti-CD11b (M1/70), anti-CD24a (30-F1), anti-CD45

(30-F11), anti-CD14 (Sa2-8), anti-MHCII (M5/114.15.2), anti-F4/80 (BM8), anti-CD8a (53-6.7), anti-CD103 (2E7), anti-CD11a (M17/4), anti-EpCAM (G8.8), anti-VCAM-1 (429), anti-CD31 (390), anti-CD93 (AA4.1), anti-ICAM-2 (3C4 mIC2/4) anti-CD68 (FA-11), and isotype-matched control monoclonal antibodies were from eBioscience. Antibody to mouse MerTK (BAF591) was from R&D Systems. Antibody to mouse FcγRI (X54-5/7.1) and anti-Siglec-F (E50-2440) were from BD Biosciences. Antibody to mouse MR1 has been described[21]. Anti-Siglec-H was a gift from M. Colonna.

35. Nahrendorf, M. *et al.* The healing myocardium sequentially mobilizes two monocyte subsets with divergent and complementary functions. *J. Exp. Med.* **204**, 3037–3047 (2007).
36. Idoyaga, J., Suda, N., Suda, K., Park, C.G. & Steinman, R.M. Antibody to Langerin/CD207 localizes large numbers of CD8α+ dendritic cells to the marginal zone of mouse spleen. *Proc. Natl. Acad. Sci. USA* **106**, 1524–1529 (2009).
37. Narayan, K. *et al.* Intrathymic programming of effector fates in three molecularly distinct gammadelta T cell subtypes. *Nat. Immunol.* **13**, 511–518 (2012).
38. Blatt, M., Wiseman, S. & Domany, E. Superparamagnetic clustering of data. *Phys. Rev. Lett.* **76**, 3251–3254 (1996).

doi:10.1038/ni.2419

HDL and Glut1 inhibition reverse a hypermetabolic state in mouse models of myeloproliferative disorders

Emmanuel L. Gautier,[1] Marit Westerterp,[2,3] Neha Bhagwat,[4,5] Serge Cremers,[2] Alan Shih,[4,5] Omar Abdel-Wahab,[4,5] Dieter Lütjohann,[6] Gwendalyn J. Randolph,[1] Ross L. Levine,[4,5] Alan R. Tall,[2] and Laurent Yvan-Charvet[2,7]

[1]Department of Pathology and Immunology, Washington University in St. Louis School of Medicine, St. Louis, MO 63110
[2]Department of Medicine, Division of Molecular Medicine, Columbia University, New York, NY 10032
[3]Department of Medical Biochemistry, Academic Medical Center of Amsterdam, University of Amsterdam, 1105 Amsterdam, Netherlands
[4]Human Oncology and Pathogenesis Program; and [5]Leukemia Service, Department of Medicine; Memorial Sloan-Kettering Cancer Center, New York, NY 10065
[6]Institute of Clinical Chemistry and Clinical Pharmacology, University Clinic Bonn, 53127 Bonn, Germany
[7]Institut National de la Santé et de la Recherche Médicale U1065, Centre Mediterraneen de Medecine Moleculaire (C3M), Avenir, 06204 Nice, France

A high metabolic rate in myeloproliferative disorders is a common complication of neoplasms, but the underlying mechanisms are incompletely understood. Using three different mouse models of myeloproliferative disorders, including mice with defective cholesterol efflux pathways and two models based on expression of human leukemia disease alleles, we uncovered a mechanism by which proliferating and inflammatory myeloid cells take up and oxidize glucose during the feeding period, contributing to energy dissipation and subsequent loss of adipose mass. In vivo, lentiviral inhibition of Glut1 by shRNA prevented myeloproliferation and adipose tissue loss in mice with defective cholesterol efflux pathway in leukocytes. Thus, Glut1 was necessary to sustain proliferation and potentially divert glucose from fat storage. We also showed that overexpression of the human ApoA-I transgene to raise high-density lipoprotein (HDL) levels decreased Glut1 expression, dampened myeloproliferation, and prevented fat loss. These experiments suggest that inhibition of Glut-1 and HDL cholesterol–raising therapies could provide novel therapeutic approaches to treat the energy imbalance observed in myeloproliferative disorders.

CORRESPONDENCE
Laurent Yvan-Charvet:
ly2159@columbia.edu

Abbreviations used: 2-[^{14}C]-DG, 2-[^{14}C]-deoxyglucose; 2-NBDG, 2-[*N*-(7-nitrobenz-2-oxa-1, 3-diazol-4-yl)amino]-2-deoxy-D-glucose; ACL, ATP-citrate lyase; HDL, high-density lipoprotein; HSC, hematopoietic stem cell; PDP, pyruvate dehydrogenase phosphoserine phosphatase; PFK, phosphofructokinase; RQ, respiratory quotient; SDH, succinate dehydrogenase; TCA, tricarboxylic acid; TMRE, tetramethylrhodamine ethyl ester.

Chronic inflammatory diseases such as chronic infection, cancer, and heart failure are often associated with adipose tissue loss (Delano and Moldawer, 2006). Adipose tissue loss in the setting of chronic inflammatory diseases could ultimately represent a major health problem because of associated comorbidities such as weakness, fatigue, and impaired immunity. Loss of adipose tissue is ultimately caused by an imbalance between food intake and energy expenditure. Although food intake is often reduced in patients with chronic inflammatory diseases, these patients exhibit a persistent state of inappropriately high metabolic rate, and this substantially contributes to their adipose loss (Delano and Moldawer, 2006). However, the link between chronic inflammation, tissue metabolism, and enhanced energy expenditure in this state of chronic hypermetabolism is not fully understood.

Among chronic inflammatory diseases, hematological malignancies such as leukemias and myeloproliferative disorders are also associated with adipose tissue loss (Dingli et al., 2004). In humans, among the most common activating mutations in myeloid malignancies are mutations in the *FMS-like tyrosine kinase 3* (*Flt3*) gene, which occur in ∼30% of cases of acute myeloid leukemia as well as mutations in the

The Rockefeller University Press $30.00
J. Exp. Med. 2013 Vol. 210 No. 2 339-353
www.jem.org/cgi/doi/10.1084/jem.20121357

thrombopoietin receptor (proto-oncogene c-Mpl) observed in 5–10% of patients with myelofibrosis. These mutations confer a fully penetrant myeloproliferative disorder in mice (Kelly et al., 2002; Pikman et al., 2006), providing a useful tool for studying the mechanism of adipose tissue loss associated with myeloproliferative disorders.

We have recently shown that mice lacking the cholesterol efflux transporters ABCA1 and ABCG1 develop massive expansion and proliferation of hematopoietic stem and progenitor cells, marked monocytosis, neutrophilia, and infiltration of various organs with myeloid cells, resembling a classical myeloproliferative disorder (Hansson and Björkholm, 2010; Yvan-Charvet et al., 2010). As we noticed a dramatic loss of adipose tissue in *Abca1*$^{-/-}$*Abcg1*$^{-/-}$ BM chimeras, we hypothesized that the myeloproliferative disorder of these mice might be responsible for their wasting syndrome and proceeded to investigate the underlying mechanisms.

RESULTS

Lack of ABCA1 and ABCG1 in hematopoietic cells promotes adipose tissue atrophy

Determination of the fat and muscle mass of irradiated WT recipients transplanted with *Abca1*$^{-/-}$*Abcg1*$^{-/-}$ BM cells fed a chow diet revealed not only absence of adipose tissue growth but also reduced epididymal fat mass at 24 wk after reconstitution compared with controls (Fig. 1 A). Gastrocnemius muscle loss was also observed 30 wk after reconstitution in these mice (Fig. 1 B). Subcutaneous and retroperitoneal adipose depots were also decreased by more than threefold at 24 wk after reconstitution in *Abca1*$^{-/-}$*Abcg1*$^{-/-}$ BM chimeras, consistent with their reduced plasma leptin levels (Table 1). To test whether the adipose tissue atrophy of these mice was a direct consequence of their defective hematopoietic compartment and myeloproliferative syndrome (Yvan-Charvet et al., 2010), we generated hematopoietic stem cell (HSC)–specific chimeric animals by transplanting lethally irradiated WT recipients with purified WT or *Abca1*$^{-/-}$*Abcg1*$^{-/-}$ HSCs (Lin^{-}Sca^{+}cKit^{+}, LSK fraction). Mice transplanted with *Abca1*$^{-/-}$*Abcg1*$^{-/-}$ LSK cells reproduced the threefold increase in the Gr-1^{hi}/CD11b^{hi} blood myeloid population observed in *Abca1*$^{-/-}$*Abcg1*$^{-/-}$ BM transplanted mice (Yvan-Charvet et al., 2010) and exhibited a twofold reduction in fat mass 12 wk after reconstitution (Fig. 1 A). Similar findings were observed in mice with specific knockout of these transporters in the hematopoietic lineage (Mx1-Cre Abca1$^{fl/fl}$Abcg1$^{fl/fl}$) 10 wk after injections of PolyI:C to excise the STOP codon that prevents the expression of the cre recombinase (Fig. 1 C). Together, these observations revealed that the expansion of adipose tissue is severely compromised in mice lacking ABCA1 and ABCG1 in their hematopoietic system.

ABCA1 and ABCG1 deficiency in leukocytes impacts glucose homeostasis

We next compared the metabolic characteristics of chow-fed *Abca1*$^{-/-}$*Abcg1*$^{-/-}$ BM transplanted mice and their respective controls by indirect calorimetry. No significant changes in daily food intake, energy expenditure, or locomotor activity were observed in these mice (Table 1). Similar fat and cholesterol absorption and bile acid excretion were also observed in *Abca1*$^{-/-}$*Abcg1*$^{-/-}$ mice (not depicted). However, *Abca1*$^{-/-}$*Abcg1*$^{-/-}$ BM transplanted mice exhibited a higher respiratory quotient (RQ) during the feeding period (dark phase; Fig. 1 D), reflecting an ∼20% increase in glucose oxidation (Fig. 1 E) and exhibited hypoglycemia (Table 1). Injection i.p. of a glucose bolus also revealed faster glucose utilization in *Abca1*$^{-/-}$*Abcg1*$^{-/-}$ BM transplanted mice compared with WT transplanted controls (Fig. 1 F). We next examined the uptake of the radiolabeled D-glucose analogue 2-[^{14}C]-deoxyglucose (2-[^{14}C]-DG) in *Abca1*$^{-/-}$*Abcg1*$^{-/-}$ BM transplanted mice in the fed state. No significant changes were observed in the total uptake of 2-[^{14}C]-DG in the skeletal muscle and brain (Fig. 1 G), whereas, in line with their reduced fat mass, total 2-[^{14}C]-DG incorporation was reduced in their adipose tissue (Fig. 1 G). In contrast, the total uptake of 2-[^{14}C]-DG was increased by two- to threefold in the heart, lung, spleen, and BM of these mice (Fig. 1 G) and by ∼1.5-fold when expressed as the rate constant for net tissue uptake of 2-[^{14}C]-DG uptake (Fig. 1 H). Thus, we showed that *Abca1*$^{-/-}$*Abcg1*$^{-/-}$ BM transplanted mice have increased propensity to clear and use glucose.

Inflammation diverts glucose from fat storage by promoting adipose tissue insulin resistance in *Abca1*$^{-/-}$*Abcg1*$^{-/-}$ BM transplanted mice

Consistent with their myeloproliferative disorder, *Abca1*$^{-/-}$*Abcg1*$^{-/-}$ BM chimeras exhibited a chronic inflammatory state as reflected by a threefold increase in plasma TNF levels (Table 1). Microscopic examination of the adipose tissue of *Abca1*$^{-/-}$*Abcg1*$^{-/-}$ BM transplanted mice revealed an increased inflammatory infiltrate reflected by crown-like structures (Fig. 2 A). Because infiltrated leukocytes are a hallmark of insulin resistance in adipose tissue (Lumeng and Saltiel, 2011; Odegaard and Chawla, 2011), we wondered whether the adipose tissue infiltration observed in *Abca1*$^{-/-}$*Abcg1*$^{-/-}$ BM chimeras would promote local insulin resistance and contribute to their reduced adipose tissue glucose uptake. To address this question, a bolus of insulin was injected into WT and *Abca1*$^{-/-}$*Abcg1*$^{-/-}$ BM transplanted mice, and hallmarks of insulin signaling (AKT phosphorylation and GLUT4 addressing to the cell membrane) were assessed. Western blot analysis revealed reduced GLUT4 translocation from the low-density microsome fraction to the plasma membrane in response to insulin in the adipose tissue of *Abca1*$^{-/-}$*Abcg1*$^{-/-}$ BM transplanted mice (Fig. 2 B). This was associated with reduced AKT phosphorylation, suggesting insulin resistance in adipocytes is secondary to local inflammatory cell infiltration (Fig. 2 B). Accordingly, microscopic analysis of isolated adipocytes revealed smaller adipocytes in WT recipients transplanted with *Abca1*$^{-/-}$*Abcg1*$^{-/-}$ BM cells (Fig. 2 A and Table 1), whereas adipocyte cell numbers were comparable with controls (Table 1). Finally, depletion of Ly6C/G^{+}

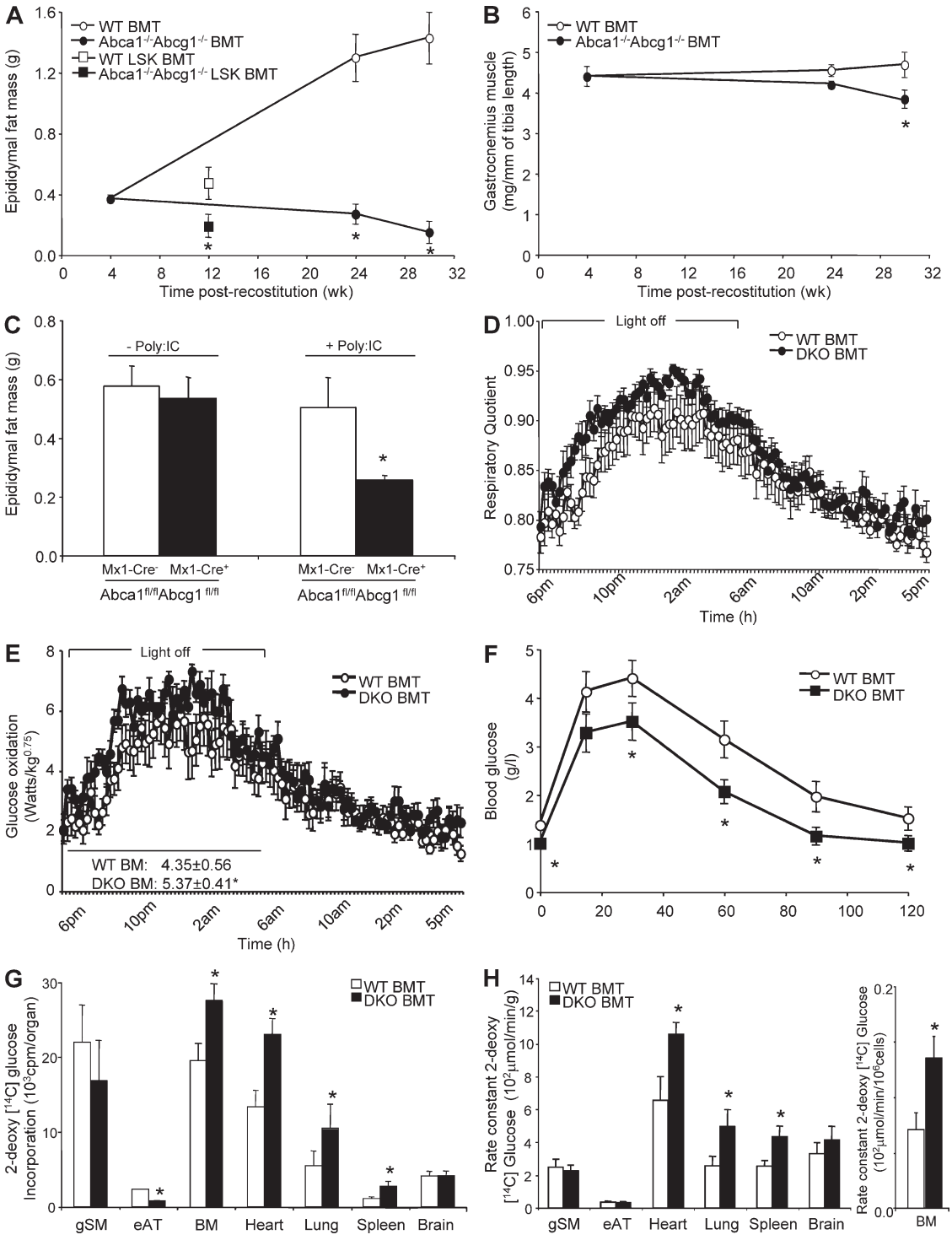

Figure 1. Adipose tissue atrophy and enhanced glucose utilization in *Abca1*$^{-/-}$*Abcg1*$^{-/-}$ BM chimeras. (A) Epididymal adipose tissue of WT recipient mice transplanted with WT or *Abca1*$^{-/-}$*Abcg1*$^{-/-}$ BM cells or WT and *Abca1*$^{-/-}$*Abcg1*$^{-/-}$ HSC (Lin^{-}Sca^{+}cKit^{+}, LSK fraction) transplanted mice. (B) Gastrocnemius skeletal muscle mass of these mice. (C) Epididymal fat mass in mice with specific knockout of these transporters in the hematopoietic lineage (Mx1-Cre Abca1$^{fl/fl}$Abcg1$^{fl/fl}$) 10 wk after three injections of 15 mg/kg PolyI:C to excise the STOP codon. (D and E) RQ (D) and glucose oxidation efficiency (E) measured by indirect calorimetry in chow-fed WT and *Abca1*$^{-/-}$*Abcg1*$^{-/-}$ BM transplanted (BMT) mice 10 wk after reconstitution. (F) Glucose tolerance test was performed i.p. on chow-fed WT and *Abca1*$^{-/-}$*Abcg1*$^{-/-}$ BM transplanted mice 12 wk after reconstitution. Blood glucose concentrations were measured at the indicate time points. (G and H) Tissue uptake (G) and rate constant of 2-[^{14}C]-DG (H) in 24-wk-old chow-fed WT and *Abca1*$^{-/-}$*Abcg1*$^{-/-}$ BM transplanted mice at the end of the study period (40 min after i.v. injection of the radiolabeled tracer). All results are means ± SEM and are representative of an experiment of five to seven animals per group. *, $P < 0.05$ versus WT.

Table 1. Effect of leukocyte ABCA1 and ABCG1 deficiencies on body weight, plasma leptin levels, subcutaneous and retroperitoneal adipose depots, plasma glucose, insulin and TNF levels, epididymal adipose tissue cellularity, and energy metabolism

Metabolic parameters	BM transplantation	
	WT	*Abca1*$^{-/-}$*Abcg1*$^{-/-}$
Body weight (g)	27.9 ± 0.9	27.4 ± 0.6
Plasma Leptin (ng/ml)	1.95 ± 0.4	0.7 ± 0.2*
Subcutaneous fat mass (g)	0.52 ± 0.12	0.15 ± 0.03*
Retroperitoneal fat mass (g)	0.28 ± 0.04*	0.09 ± 0.08*
Plasma glucose (g/liter)	2.1 ± 0.1	1.7 ± 0.1*
Plasma Insulin (ng/ml)	7.9 ± 0.8	6.1 ± 1.1
Plasma TNF (pg/ml)	3.1 ± 0.5	7.4 ± 0.6*
Fat cell number (×10^6)	4.8 ± 0.9	4.6 ± 0.8
Fat cell weight (ng)	119 ± 14*	36 ± 5*
Food intake (g/day)	3.28 ± 0.14	3.33 ± 0.13
Food intake (g/day/$g^{0.75}$)	0.29 ± 0.01	0.29 ± 0.01
Energy expenditure, EE (W/$kg^{0.75}$)	6.68 ± 0.25	7.11 ± 0.18
Locomotor activity (counts/14 min)	2,589 ± 544	2,560 ± 499

Values are mean ± SEM (n = 5 per group). *, $P < 0.05$ versus controls.

myeloid cells with the anti–granulocyte receptor-1 (Gr-1) antibody RB6-8C5 partially reversed the reduced glucose uptake in the adipose tissue of *Abca1*$^{-/-}$*Abcg1*$^{-/-}$ mice (not depicted). Together, these results indicate that myeloproliferation and associated adipose tissue infiltration compromise adipose tissue function and likely contribute to the loss of fat in *Abca1*$^{-/-}$*Abcg1*$^{-/-}$ BM transplanted mice. Moreover, these findings revealed that *Abca1*$^{-/-}$*Abcg1*$^{-/-}$ BM chimeras can efficiently clear glucose despite being insulin resistant.

Glucose consumption by proliferating myeloid cells contributes to whole body glucose dissipation in *Abca1*$^{-/-}$*Abcg1*$^{-/-}$ BM transplanted mice

Although local inflammation promoted adipose tissue insulin resistance, this could not explain the enhanced glucose uptake by noninsulin-sensitive tissues (Fig. 1 G) contributing to enhanced whole body glucose oxidation during the feeding period (Fig. 1 E). Because these tissues exhibit massive myeloid infiltration in *Abca1*$^{-/-}$*Abcg1*$^{-/-}$ BM transplanted mice (Yvan-Charvet et al., 2007; Out et al., 2008), we next investigated the uptake of glucose by *Abca1*$^{-/-}$*Abcg1*$^{-/-}$ leukocytes. To estimate glucose utilization by flow cytometry, we used the fluorescent D-glucose analogue 2-[*N*-(7-nitrobenz-2-oxa-1,3-diazol-4-yl)amino]-2-deoxy-D-glucose (2-NBDG) as a tool that reflects the glucose bound to the cells and its uptake. Leukocytes isolated from *Abca1*$^{-/-}$*Abcg1*$^{-/-}$ BM revealed a significant 30% increase in 2-NBDG staining (Fig. 3 A). This increase was massive in monocytes and neutrophils when the increased cell number was taken into account (Fig. 3 B; Yvan-Charvet et al., 2010), accounting for the total uptake of 2-[^{14}C]-DG in the BM (Fig. 1 G). As glucose uptake depends on the glucose transporter (Glut) family (Herman and Kahn, 2006), we next assessed the mRNA expression levels of several members of this family, namely Glut1, Glut2, Glut3, Glut4, and Glut6. *Abca1*$^{-/-}$*Abcg1*$^{-/-}$ BM cells exhibited a twofold up-regulation of the glucose transporter Glut1 mRNA expression, which was also the most highly expressed Glut member in leukocytes (Fig. 3 C). Flow cytometry analysis showed a 30% increase in the cell surface expression of Glut1 in vivo in *Abca1*$^{-/-}$*Abcg1*$^{-/-}$ CD45$^+$ leukocytes (not depicted), including monocytes, neutrophils, and lymphocytes (Fig. 3 D), and this correlated with increased mitochondrial membrane potential (Fig. 3 E). Together, these findings show that leukocytes have a major role in glucose uptake in *Abca1*$^{-/-}$*Abcg1*$^{-/-}$ BM transplanted mice exhibiting a myeloproliferative syndrome. This resulted in enhanced whole body glucose oxidation that could explain the increased energy dissipation in these mice.

Signaling via the IL-3/GM-CSF receptor common β-subunit enhances the expression of Glut1 and glycolytic enzymes in proliferating *Abca1*$^{-/-}$*Abcg1*$^{-/-}$ leukocytes

We next set out to better understand the mechanism leading to increased glucose uptake in *Abca1*$^{-/-}$*Abcg1*$^{-/-}$ leukocytes. Up-regulation of Glut-1 by oncogenes such as Ras or Src has been reported (Flier et al., 1987), and we recently showed enhanced Ras-Erk signaling in *Abca1*$^{-/-}$*Abcg1*$^{-/-}$ BM cells at basal state and in response to the hematopoietic growth factors IL-3 and GM-CSF (Yvan-Charvet et al., 2010). Therefore, we investigated the expression of Glut1 in response to IL-3 in BM leukocytes. As shown in Fig. 3 F, Glut1 mRNA levels were increased upon stimulation with IL-3 in WT BM cells and were further increased in *Abca1*$^{-/-}$*Abcg1*$^{-/-}$ cells. Inhibition of the Ras signaling pathway using a farnesyl transferase inhibitor, known to prevent the anchorage of Ras

in the plasma membrane and to inhibit the proliferation of *Abca1*$^{-/-}$*Abcg1*$^{-/-}$ BM cells (Yvan-Charvet et al., 2010), normalized Glut1 mRNA expression to WT levels (Fig. 3 F). Further characterization of signaling pathways downstream of the IL-3/GM-CSF receptor common β-chain (Chang et al., 2003) showed that the phosphoinositide 3-kinase inhibitor LY294002 prevented IL-3–induced Glut1 mRNA expression in *Abca1*$^{-/-}$*Abcg1*$^{-/-}$ leukocytes (Fig. 3 F), similar to the effect of this inhibitor on the proliferation of these cells (Yvan-Charvet et al., 2010). Analysis of the rates of [^{14}C]glucose oxidation revealed that in basal and IL-3–stimulated conditions, *Abca1*$^{-/-}$*Abcg1*$^{-/-}$ leukocytes exhibited a higher glycolytic rate (Fig. 3 G). This effect was inhibited by removal of membrane cholesterol by cyclodextrin (Fig. 3 G), consistent with the cholesterol-dependent regulation of IL-3Rβ signaling (Yvan-Charvet et al., 2010). Analysis of genes of the glycolytic and lipid synthetic pathways also revealed up-regulation of hexokinase 2 (Hk2), phosphofructokinase (PFK), and ATP-citrate lyase (ACL) mRNAs in *Abca1*$^{-/-}$*Abcg1*$^{-/-}$ leukocytes that was dependent on the IL-3/GM-CSF receptor common β-chain signaling pathway (Fig. 3 H). Fumarase and succinate dehydrogenase (SDH) mRNA expression was also increased in response to IL-3 in *Abca1*$^{-/-}$*Abcg1*$^{-/-}$ leukocytes (Fig. 3 H). Together, our results point to the IL-3/GM-CSF receptor common β-chain/GLUT1 axis as a major determinant of the increased glucose uptake observed in *Abca1*$^{-/-}$*Abcg1*$^{-/-}$ leukocytes.

Metabolic profiling reveals increased glycolysis and oxidative phosphorylation in proliferating *Abca1*$^{-/-}$*Abcg1*$^{-/-}$ leukocytes

Further quantification of glycolytic metabolites by LC-MS showed higher glucose 6-phosphate/fructose 6-phosphate (G6P+F6P) and fructose 1,6-diphosphate (F1,6BP) levels in basal and IL-3–stimulated *Abca1*$^{-/-}$*Abcg1*$^{-/-}$ leukocytes (Fig. 4 A). Increased citric acid cycle metabolites (citrate, isocitrate, succinate, fumarate, and malate) and related mitochondrial products (GTP and FAD) were also observed in *Abca1*$^{-/-}$*Abcg1*$^{-/-}$ leukocytes under basal and/or IL-3–stimulated conditions (Fig. 4, B and C). Consistent with these findings, a higher ATP to ADP ratio was observed in proliferating *Abca1*$^{-/-}$*Abcg1*$^{-/-}$ leukocytes (Fig. 4 D). This was associated with increased mitochondrial membrane potential measured using a fluorescent tetramethylrhodamine ethyl ester (TMRE) dye (not depicted) and increased SDH activity in *Abca1*$^{-/-}$*Abcg1*$^{-/-}$ leukocytes (Fig. 4 E).

The increased glycolysis in *Abca1*$^{-/-}$*Abcg1*$^{-/-}$ leukocytes is required for proliferation

To test whether high levels of glycolysis are required for *Abca1*$^{-/-}$*Abcg1*$^{-/-}$ leukocyte proliferation, we next cultured cells with media containing galactose or glucose. Galactose enters glycolysis through the Leloir pathway, which occurs at a significantly lower rate than glucose entry into glycolysis (Bustamante and Pedersen, 1977). Fig. 4 F shows that under glucose-free DMEM (DMEM poor), addition of glucose but not galactose enhanced the proliferation of *Abca1*$^{-/-}$*Abcg1*$^{-/-}$ leukocytes to the level of high-glucose DMEM (DMEM rich), pointing to a prominent role of the glycolysis pathway in cell growth. However, a potential contribution of the pentose phosphate pathway to *Abca1*$^{-/-}$*Abcg1*$^{-/-}$ leukocyte proliferation could not be completely excluded from this experiment. We next challenged the mitochondria with either

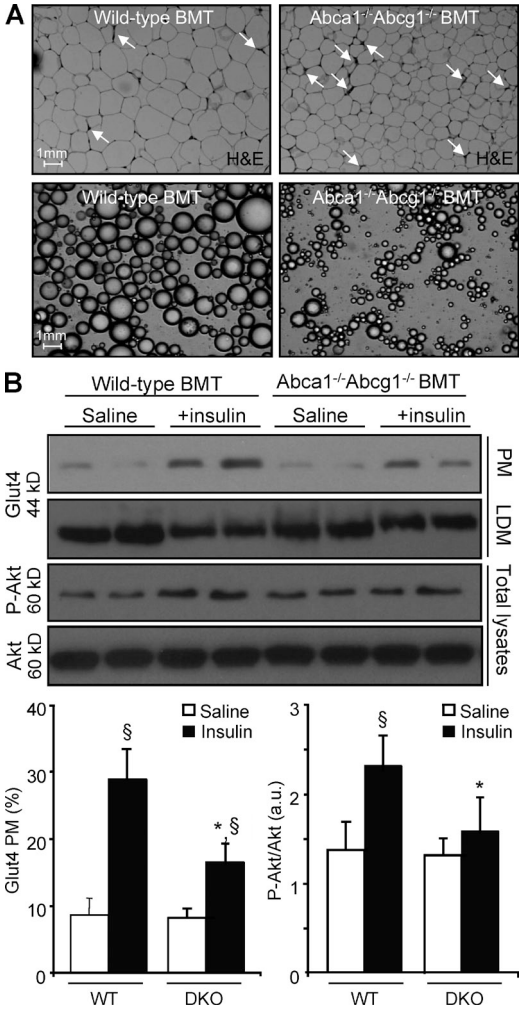

Figure 2. Infiltrated leukocytes modulate adipose tissue insulin sensitivity in *Abca1*$^{-/-}$*Abcg1*$^{-/-}$ BM chimeras. (A) Paraffin-embedded serial sections obtained from the adipose tissue of WT and *Abca1*$^{-/-}$*Abcg1*$^{-/-}$ BM transplanted (BMT) mice fed a chow diet. Representative H&E staining revealed an extensive myeloid cell infiltrate in *Abca1*$^{-/-}$*Abcg1*$^{-/-}$ BM transplanted mice compared with controls. Micrographs of isolated epididymal adipose cells confirmed reduced adipose cell size in *Abca1*$^{-/-}$*Abcg1*$^{-/-}$ BM transplanted mice. Data representative of four to six animals per group are shown. Bars, 1 mm. (B) Western blot analysis of plasma membrane (PM) and low-density microsome (LDM) Glut4, phospho-Akt, and total Akt in the adipose tissue of WT and *Abca1*$^{-/-}$*Abcg1*$^{-/-}$ BM transplanted mice after acute i.p. injection of an insulin bolus. Quantitative results were obtained from two independent experiments. Values are mean ± SEM and expressed as percent expression of PM Glut4 over HDM fraction or as arbitrary units (a.u.). *, $P < 0.05$ versus insulin-injected WT controls; §, $P < 0.05$ versus saline-injected mice.

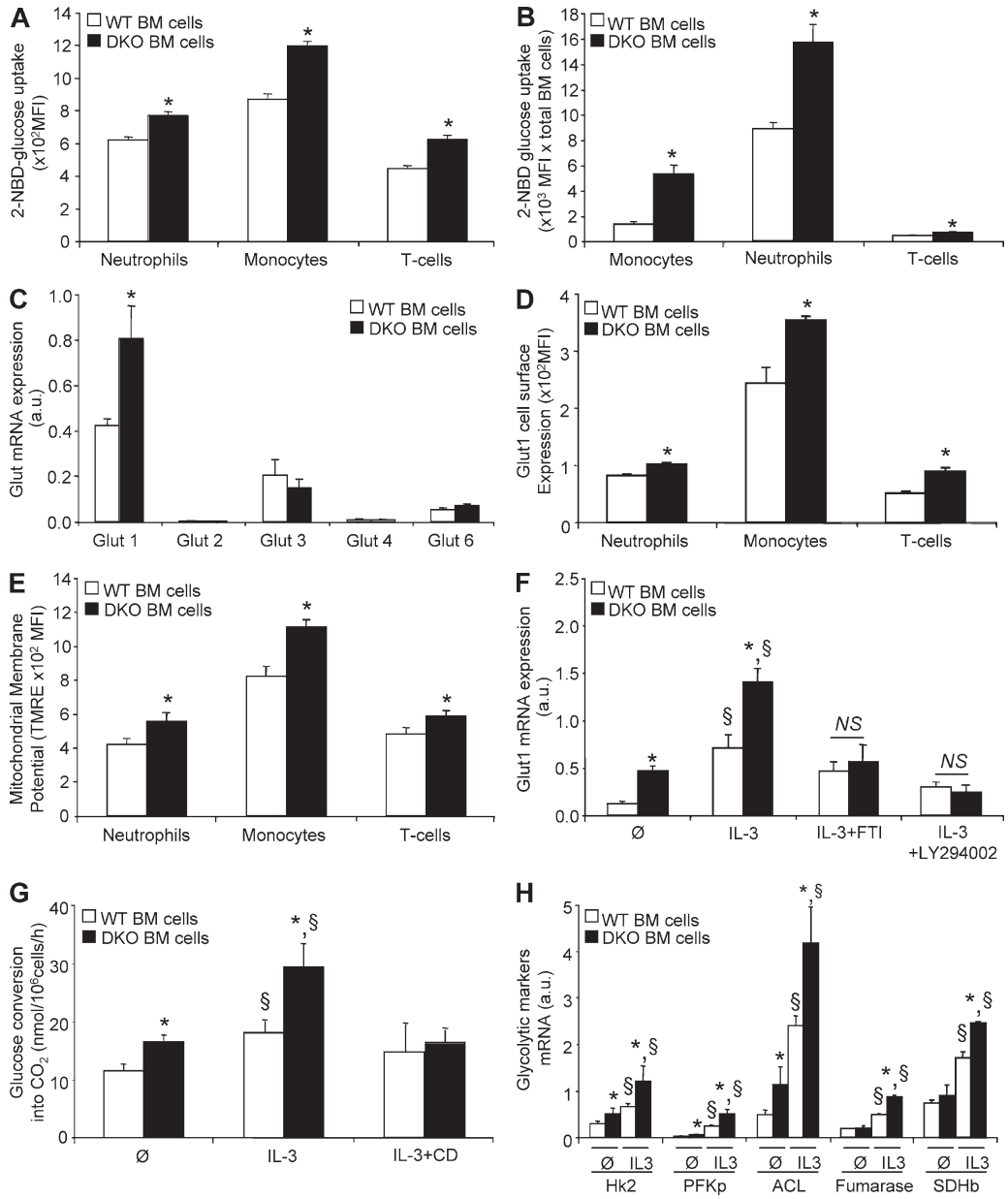

Figure 3. Enhanced glycolytic activity in *Abca1*$^{-/-}$*Abcg1*$^{-/-}$ leukocytes. (A) Ex vivo characterization of the glucose binding and/or uptake in WT and *Abca1*$^{-/-}$*Abcg1*$^{-/-}$ BM leukocyte subpopulations (i.e., CD115^{+} monocytes, CD115^{-}Grl^{+} neutrophils, and TCRb^{+} lymphocytes) using a fluorescent D-glucose analogue (2-NBDG). (B) Glucose uptake normalized by the amount of BM leukocytes. (C) mRNA expression of glucose transporters (Gluts) in freshly isolated WT and *Abca1*$^{-/-}$*Abcg1*$^{-/-}$ BM cells. (D) Cell surface expression of Glut1 was also quantified in WT and *Abca1*$^{-/-}$*Abcg1*$^{-/-}$ BM neutrophils, monocytes, and lymphocytes. (E) Mitochondrial membrane potential measured by fluorescent TMRE dye. All results are means ± SEM and are representative of two independent experiments (n = 5–6 animals per groups). *, P < 0.05 versus controls. MFI, mean fluorescence intensity. (F) Glut1 expression after BM cells were treated for 72 h with the indicated growth factors and in the presence or absence of 1 µM farnesyl transferase inhibitor (FTI) or 10 µM PI3K inhibitor (LY294002). Values were normalized to ribosomal 18S. (G) Effect of IL-3 treatment and cholesterol depletion by cyclodextrin (CD) on [^{14}C]glucose conversion into CO_2 in WT and *Abca1*$^{-/-}$*Abcg1*$^{-/-}$ BM cells. (H) mRNA expression of Hk2, PFK isoform p (PFKp), ACL, fumarase, and SDH subunit b (SDHb) in WT and *Abca1*$^{-/-}$*Abcg1*$^{-/-}$ BM-derived cells untreated or treated for 72 h with IL-3. Values were normalized to ribosomal 18S. Results are means ± SEM of cultures from three independent mice. *, P < 0.05 versus WT controls; §, P < 0.05 versus untreated condition.

branched-chain amino acids (i.e., valine, leucine, and isoleucine) or with cysteamine to fuel the tricarboxylic acid (TCA) cycle with acetyl-coA or coA, respectively, but these treatments did not increase the proliferation of *Abca1*$^{-/-}$*Abcg1*$^{-/-}$ leukocytes, suggesting the requirement of the pyruvate entry into the TCA cycle for proliferation (Fig. 4 G). We next used the phosphoserine phosphatase inhibitor DL-AP3 (Hawkinson et al., 1996), which blocks the rate-limiting step of the serine

biosynthetic pathway (Lunt and Vander Heiden, 2011) but also the pyruvate dehydrogenase phosphoserine phosphatases (PDPs) known to switch metabolic flux from glycolysis toward oxidative phosphorylation. This treatment prevented the enhanced proliferation of *Abca1*$^{-/-}$*Abcg1*$^{-/-}$ leukocytes (Fig. 4 G). Because inhibition of serine palmitoyltransferase by myriocin, downstream of the serine biosynthetic pathway, proportionately inhibited both WT and *Abca1*$^{-/-}$*Abcg1*$^{-/-}$ leukocytes (Fig. 4 G), this suggested that the effect of DL-AP3 was most likely related to inhibition of PDPs. Inhibition of diglyceride acyltransferase also proportionately inhibited both WT and *Abca1*$^{-/-}$*Abcg1*$^{-/-}$ leukocyte proliferation (Fig. 4 G), suggesting that despite enhanced lipid synthesis (Fig. 5 A), neither ceramide or triglyceride biosynthesis was the limiting step for the proliferation of these cells.

Proliferating *Abca1*$^{-/-}$*Abcg1*$^{-/-}$ leukocytes exhibit enhanced mitochondrial metabolism

To better understand the contribution of the mitochondrial metabolism, we next assessed the ability of *Abca1*$^{-/-}$*Abcg1*$^{-/-}$ leukocytes to proliferate after treatment with membrane-permeable antioxidants. Although glutathione monoethyl ester partially reduced the proliferation of all cells, tempol abrogated the enhanced proliferation of *Abca1*$^{-/-}$*Abcg1*$^{-/-}$ leukocytes (Fig. 4 H). Recently, Samudio et al. (2010) proposed that leukemia cells uncouple fatty acid oxidation from ATP synthesis and rely on de novo fatty acid synthesis to support fatty acid oxidation. Consistent with this observation, pharmacological inhibition of carnitine palmitoyltransferase I (CPT-1) with etomoxir prevented the hyperproliferative response of *Abca1*$^{-/-}$*Abcg1*$^{-/-}$ leukocytes (Fig. 4 H). Finally, carnitine supplementation of the cells to promote mitochondrial efflux of excess acetyl moieties from both glucose and fat oxidation (Muoio et al., 2012) prevented the higher proliferation rate of *Abca1*$^{-/-}$*Abcg1*$^{-/-}$ leukocytes (Fig. 4 H), providing additional evidence that the mitochondrial metabolism was responsible for the enhanced proliferation in *Abca1*$^{-/-}$*Abcg1*$^{-/-}$ leukocytes. Together, these findings showed that *Abca1*$^{-/-}$*Abcg1*$^{-/-}$ BM cells directed the available glucose toward oxidative phosphorylation (Fig. 4 I), which could explain the enhanced glucose oxidation observed in *Abca1*$^{-/-}$*Abcg1*$^{-/-}$ BM transplanted mice (Fig. 1 E).

Glut1 inhibition prevents both IL-3–mediated myeloid proliferation and TLR4-mediated macrophage inflammatory response

The increased glucose conversion into lipids at basal or after IL-3 activation in *Abca1*$^{-/-}$*Abcg1*$^{-/-}$ leukocytes was abolished by Fasentin, a Glut1 inhibitor (Fig. 5 A; Wood et al., 2008), as was the proliferation of these cells (Fig. 5 B). Together, these findings suggest that IL-3Rβ subunit signaling enhances the Glut1-dependent glucose uptake of *Abca1*$^{-/-}$*Abcg1*$^{-/-}$ leukocytes to promote their proliferation. Enhanced glucose consumption and Glut1 expression were previously observed in macrophages during inflammatory responses (Fukuzumi et al., 1996; Gamelli et al., 1996). Consistent with the previously observed enhancement in Toll-like receptor signaling in *Abca1*$^{-/-}$*Abcg1*$^{-/-}$ macrophages (Yvan-Charvet et al., 2008), analysis of the rates of [^{14}C]glucose oxidation in vitro in BM-derived macrophages revealed that in basal and LPS-stimulated conditions, *Abca1*$^{-/-}$*Abcg1*$^{-/-}$ macrophages exhibited a higher glucose consumption that was associated with increased Glut1 mRNA levels (not depicted). Interestingly, Glut1 inhibition by Fasentin reduced the inflammatory response induced by LPS in *Abca1*$^{-/-}$*Abcg1*$^{-/-}$ macrophages (Fig. 5 C). Although the mRNA levels of Hk2 and glucose-6-phosphate dehydrogenase followed the inflammatory pattern (Fig. 5 D), glycolytic genes such as PFK and ACL were barely affected by LPS in either WT or *Abca1*$^{-/-}$*Abcg1*$^{-/-}$ macrophages (Fig. 5 D). This contrasted with proliferating *Abca1*$^{-/-}$*Abcg1*$^{-/-}$ leukocytes (Fig. 4 I). Thus, *Abca1*$^{-/-}$*Abcg1*$^{-/-}$ macrophages could contribute not only to the enhanced glucose oxidation observed in *Abca1*$^{-/-}$*Abcg1*$^{-/-}$ BM transplanted mice (Fig. 1 E), but also to the local adipose tissue insulin resistance mediated by enhanced inflammatory response (Fig. 2 B). Together, these findings revealed that Glut1 controls both the proliferative and inflammatory status of *Abca1*$^{-/-}$*Abcg1*$^{-/-}$ leukocytes.

Both Glut1 inhibition and ApoA-I overexpression prevent fat loss in *Abca1*$^{-/-}$*Abcg1*$^{-/-}$ BM transplanted mice

We next explored the in vivo relevance of reducing the proliferation and inflammatory status of myeloid cells through Glut1 inhibition on the adipose tissue loss of *Abca1*$^{-/-}$*Abcg1*$^{-/-}$ BM chimeras. Mice that received WT or *Abca1*$^{-/-}$*Abcg1*$^{-/-}$ BM transduced with lentiviruses encoding Glut1 shRNA exhibited a 1.6-fold reduction in Glut1 mRNA expression (not depicted) and a 20–30% reduction in the cell surface expression of Glut1 in their BM cells 7 wk after reconstitution, and this was sufficient to normalize the Glut1 cell surface expression to WT levels in *Abca1*$^{-/-}$*Abcg1*$^{-/-}$ BM transplanted mice (Fig. 5 E). This was associated with normalization of the 2-NBDG uptake in *Abca1*$^{-/-}$*Abcg1*$^{-/-}$ BM leukocytes (Fig. 5 F) and with normalization of the leukocyte counts in these mice (Fig. 5 G). Remarkably, the adipose tissue loss of mice transplanted with *Abca1*$^{-/-}$*Abcg1*$^{-/-}$ BM was rescued by transduction with Glut1 shRNA lentiviral particles (Fig. 5 H). We previously reported that the myeloproliferative syndrome and inflammatory phenotype of *Abca1*$^{-/-}$*Abcg1*$^{-/-}$ BM chimeras was reversed by overexpression of the human apoA-I transgene (ApoA-I^{Tg}; Yvan-Charvet et al., 2008, 2010). We now show that overexpression of the human apoA-I transgene also reversed fat loss in *Abca1*$^{-/-}$*Abcg1*$^{-/-}$ BM transplanted mice (Fig. 5 I). Additionally, the apoA-I transgene normalized Glut1 cell surface expression in *Abca1*$^{-/-}$*Abcg1*$^{-/-}$ BM cells (Fig. 5 J). Together, our results suggest that suppression of Glut1 in myeloproliferative disorders may represent a novel approach not only to treat leukocytosis but also associated adipose tissue loss. Additionally, we now show that the rescue of the myeloproliferative disease of *Abca1*$^{-/-}$*Abcg1*$^{-/-}$ BM chimeras by overexpression of the human apoA-I transgene

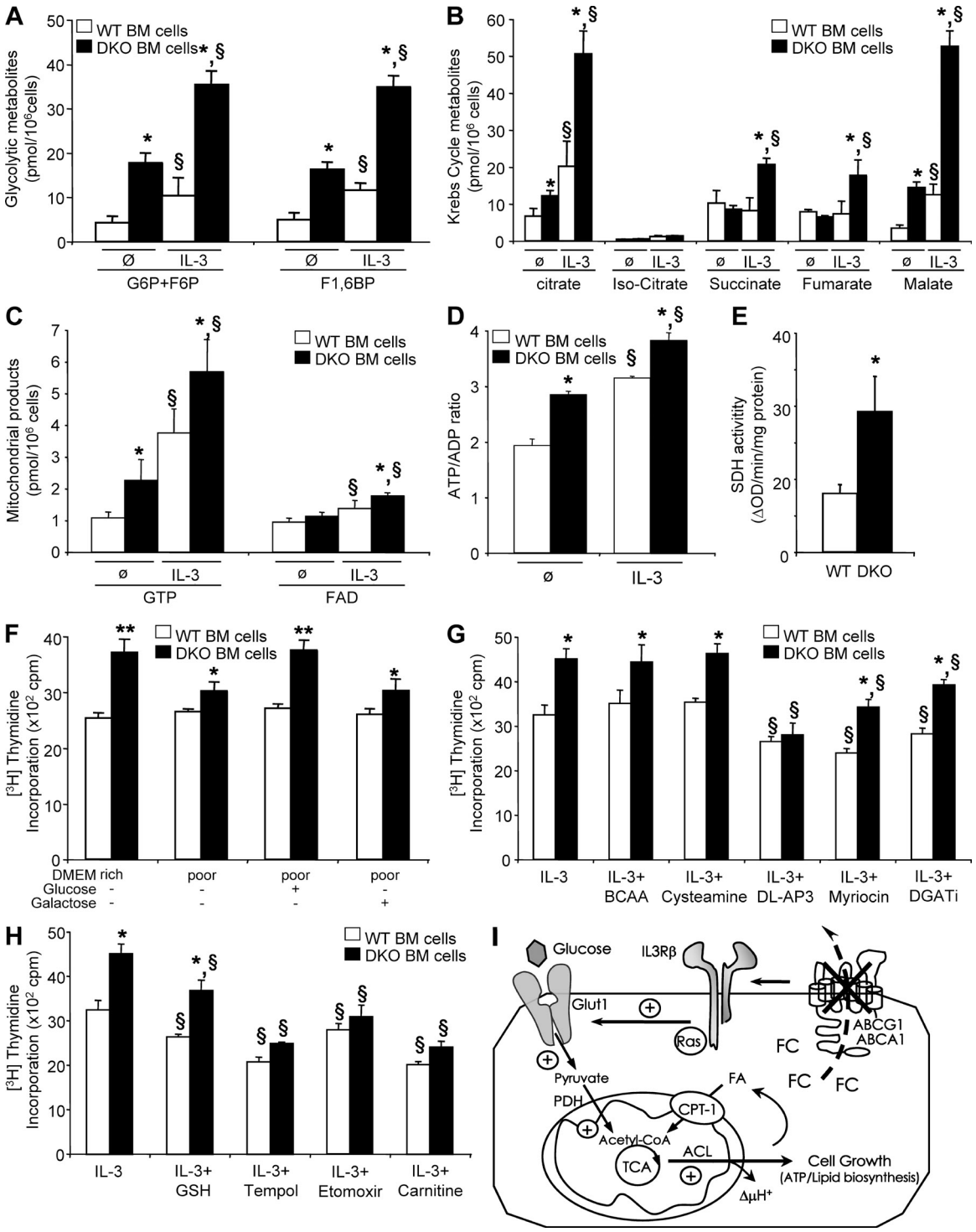

Figure 4. The IL-3Rβ–dependent proliferation of *Abca1*$^{-/-}$*Abcg1*$^{-/-}$ leukocytes is driven by increased mitochondrial metabolism. (A–D) Effect of IL-3 treatment on glycolytic metabolites (glucose 6-phosphate/fructose 6-phosphate and fructose 1,6-diphosphate; A), citric acid metabolites (B), related mitochondrial products (GTP and FAD; C), and ATP/ADP ratio (D) in WT and *Abca1*$^{-/-}$*Abcg1*$^{-/-}$ BM cells determined by LC-MS. (E) SDH activity in these cells. Results are means ± SEM of cultures from three independent mice. *, $P < 0.05$ versus WT controls; §, $P < 0.05$ versus treatment. (F) WT and *Abca1*$^{-/-}$*Abcg1*$^{-/-}$ BM cells were grown for 48 h in 20 mM glucose DMEM (DMEM rich) or low-glucose DMEM (DMEM poor) supplemented with 20 mM glucose or 20 mM galactose in the presence of IL-3. Proliferation rates were determined after 2-h [³H]thymidine pulse labeling. (G and H) BM cells were grown for 48 h in liquid culture containing 10% FBS IMDM in the presence of the indicated chemical compounds and IL-3. Proliferation rates were determined after 2-h [³H]thymidine pulse labeling. Results are means ± SEM of an experiment performed in triplicate. *, $P < 0.05$ versus WT controls; §, $P < 0.05$ versus untreated condition. BCAA, branched-chain amino acids; DGATi, diglyceride acyltransferase inhibitor.

(Yvan-Charvet et al., 2010) was in part associated with reduced Glut1 levels on leukocytes and prevented their adipose loss.

ApoA-I overexpression prevents the increased glucose oxidation and adipose tissue atrophy in Flt3-ITD and Mpl-W515L mutant–mediated myeloproliferative disorders

As altered high-density lipoprotein (HDL) cholesterol homeostasis has been previously observed in myeloproliferative disorders (Fiorenza et al., 2000; Westerterp et al., 2012), we further tested whether the increased glucose oxidation and associated adipose tissue atrophy observed in *Abca1*$^{-/-}$*Abcg1*$^{-/-}$ BM transplanted mice could be observed as a more general phenotype in other mouse models of myeloproliferative disorders and whether overexpression of the human apoA-I transgene would still be an efficient therapeutic in these models. The Flt3-ITD and Mpl-W515L alleles have been identified in patients with acute myeloid leukemia and myelofibrosis, respectively, and confer a fully penetrant myeloproliferative disorder in mice (Kelly et al., 2002; Pikman et al., 2006). Accordingly, mice that received BM transduced with retroviruses encoding Flt3-ITD or Mpl-W515L exhibited massive myeloid expansion compared with control retrovirus (Fig. 6, A and B), an effect which was partially reversed by overexpression of the human ApoA-I transgene (Fig. 6, A and B). We also observed epididymal fat mass atrophy and reduced plasma leptin levels in both models (Fig. 6 C and not depicted, respectively). Massive leukocyte infiltration was also observed in their adipose tissue (not depicted). Similar to *Abca1*$^{-/-}$*Abcg1*$^{-/-}$ BM transplanted mice, these features were associated with an increased RQ during the dark phase (Fig. 6, D and E), reflecting an ∼20% increase in glucose oxidation during this period (Fig. 6 F). Interestingly, Mpl-W515L and Flt3-ITD mutant leukocytes exhibited a significant increase in Glut1 cell surface expression (Fig. 6 G). Remarkably, overexpression of the human ApoA-I transgene not only prevented the fat mass loss (Fig. 6 C) of mice bearing the Mpl-W515L and Flt3-ITD mutations, but also significantly reversed the increased Glut1 cell surface expression in Mpl-W515L and Flt3-ITD leukocytes (Fig. 6 G) that was associated with increased RQ (Fig. 6, H and I) and glucose oxidation during the feeding period (Fig. 6 F).

DISCUSSION

Although there is growing evidence that weight loss, and especially the loss of muscle and adipose tissue mass, is a hallmark of chronic inflammatory diseases such as chronic infection, cancer, and heart failure (Delano and Moldawer, 2006), the underlying mechanisms remain poorly understood, leading to a lack of effective therapy. Most of the emerging therapeutic approaches to prevent adipose tissue loss focus on reducing the elevated circulating cytokine levels (Argilés et al., 2011) in part because of their action on insulin resistance and fat mobilization (Delano and Moldawer, 2006; Das et al., 2011). However, traditional antiinflammatory approaches such as COX-2 inhibitors showed for instance limited effectiveness in reversing the metabolic abnormalities seen in cancer patients (Kumar et al., 2010). Thus, there is a crucial need to better understand the mechanisms of adipose loss in this state of chronic hypermetabolism. Using three different mouse models of myeloproliferative disorders, including two models based on expression of human leukemia disease alleles (Flt3-ITD and Mpl-W515L), we uncovered a glucose steal mechanism by which proliferating and inflammatory myeloid cells take up and oxidize glucose during the feeding period, contributing to energy dissipation and subsequent loss of adipose mass. This reflected in part increased numbers of proliferating myeloid cells and tissues infiltrated with inflammatory myeloid cells.

Although only partially understood, there is a relationship between leukemia-causing genes and cellular energy metabolism as the survival and proliferation of leukemic cells may require glucose for de novo lipid biosynthesis (DeBerardinis et al., 2008; Lunt and Vander Heiden, 2011). The increased glucose utilization in hyperproliferating *Abca1*$^{-/-}$*Abcg1*$^{-/-}$ BM myeloid cells resulted in part from a Ras-dependent upregulation of Glut1 expression in response to enhanced IL-3 signaling (Flier et al., 1987; Yvan-Charvet et al., 2010). Similarly, Mpl and Flt3 are receptor tyrosine kinases coupled to Ras signaling, and activating mutations in these receptors (Kelly et al., 2002; Pikman et al., 2006) were shown to cause higher Glut1 expression. In this context, it is tempting to parallel our myeloproliferative mouse models with other cancer models in which malignant cells rely on high levels of aerobic glycolysis as the major source of ATP to fuel cellular proliferation, known as the Warburg effect (Vander Heiden et al., 2009). However, the classical view of the Warburg effect, which involves defect in mitochondrial oxidative phosphorylation, has been recently challenged, and mitochondrial metabolism may indeed be functional in different types of tumor cells (Jose et al., 2011). We now provide both in vitro and in vivo evidence for increased mitochondrial potential in leukocytes of our mouse

(I) Scheme illustrating the induction of glycolysis through modulation of plasma membrane cholesterol by ABCA1 and ABCG1 deficiency and increased mitochondrial metabolism that produces ATP and synthesizes lipids for cell growth. Lack of these transporters promotes growth factors dependent on IL-3Rβ signaling–mediated glycolysis as reflected by (a) enhanced Hk2 and PFKp mRNA expression, (b) enhanced glycolytic metabolites content, (c) enhanced glucose oxidation (i.e., conversion into CO_2), and (d) reversal of enhanced glucose oxidation by removal of cellular cholesterol by cyclodextrin. The pyruvate generated through glycolysis is directed into the TCA cycle and increases mitochondrial metabolism as reflected by (a) enhanced mRNA expression of fumarase and SDHb, (b) enhanced SDH activity, (c) enhanced mitochondrial metabolites and mitochondrial membrane potential ($\Delta\mu H^+$), and (d) enhanced ATP/ADP ratio. Increased lipid synthesis was also observed in *Abca1*$^{-/-}$*Abcg1*$^{-/-}$ BM cells as reflected by (a) enhanced mRNA expression of ACL and (b) enhanced glucose conversion into lipids.

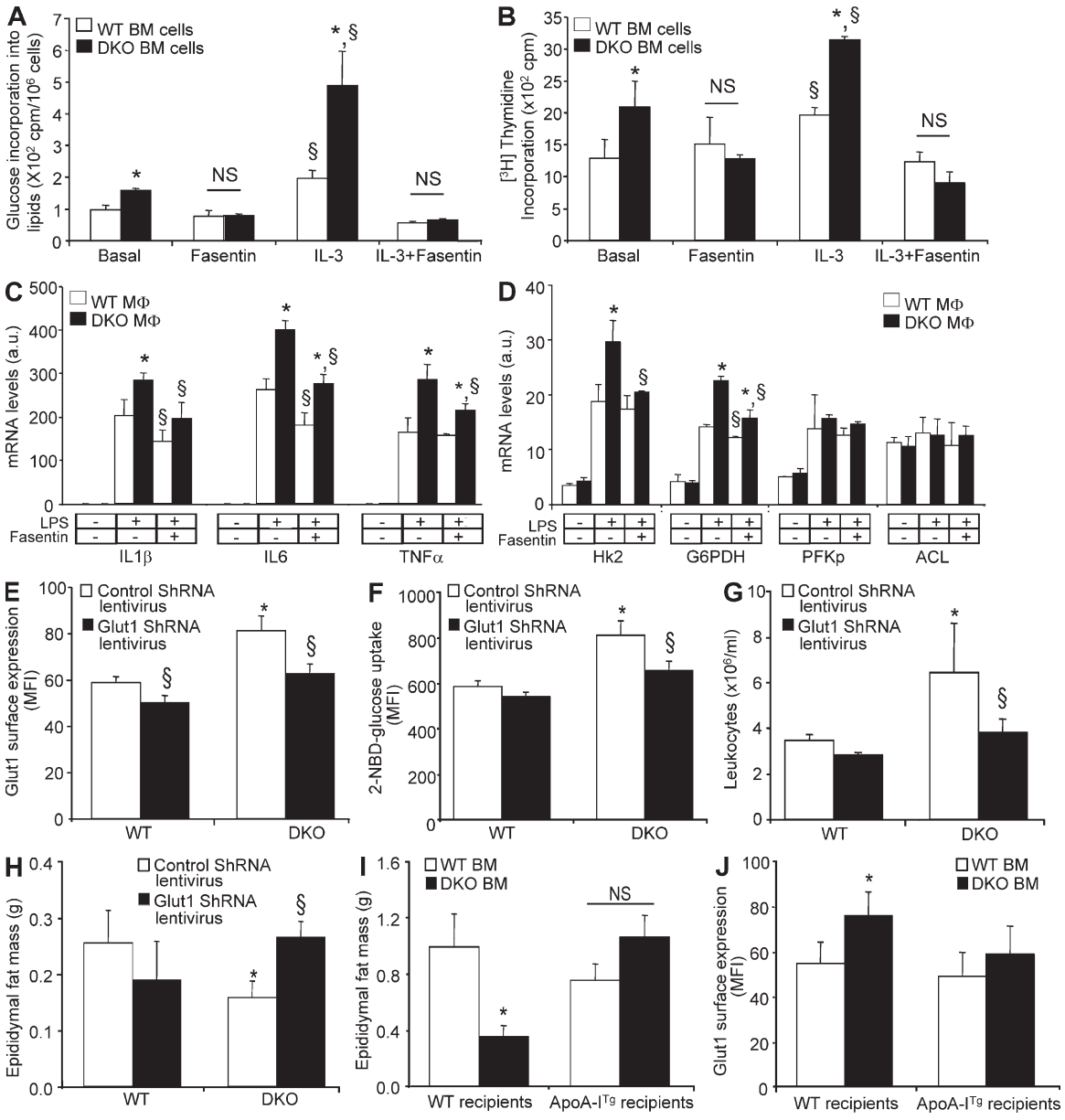

Figure 5. Inhibition of Glut1 or overexpression of the human apoA-I transgene rescues adipose atrophy in *Abca1*$^{-/-}$*Abcg1*$^{-/-}$ BM chimeras. (A) Effect of IL-3 treatment on [^{14}C]glucose conversion into lipids in WT and *Abca1*$^{-/-}$*Abcg1*$^{-/-}$ BM cells in the presence or absence of 50 µM fasentin, a Glut1 inhibitor. (B) Effect of Fasentin on IL-3–mediated proliferation in WT and *Abca1*$^{-/-}$*Abcg1*$^{-/-}$ BM cells. (C and D) Effect of Fasentin on LPS-mediated inflammatory (C) and glycolytic (D) responses in WT and *Abca1*$^{-/-}$*Abcg1*$^{-/-}$ BM-derived macrophages. Values were normalized to ribosomal 18S. Results are means ± SEM of three independent experiments performed in triplicate. *, $P < 0.05$ versus WT mice; §, $P < 0.05$ versus LPS treatment. (E and F) Quantification of Glut1 cell surface expression (E) and 2-NBDG uptake by flow cytometry (F) in CD45$^+$ leukocytes isolated from the BM of WT recipients mice transplanted with WT or *Abca1*$^{-/-}$*Abcg1*$^{-/-}$ BM transduced with a lentivirus encoding Glut1 shRNA 7 wk after reconstitution. (G and H) Peripheral leukocyte counts (G) and epididymal fat mass (H) of these mice at the end of the experiment. (I and J) Histograms showing epididymal fat mass loss (I) and Glut1 cell surface expression (J) in CD45$^+$ peripheral leukocytes in chow-fed transgenic recipient mice overexpressing the human apoA-I transgene transplanted with *Abca1*$^{-/-}$*Abcg1*$^{-/-}$ BM. Results are ± SEM of an experiment of four to six animals per group. *, $P < 0.05$ versus WT recipients transplanted with WT BM; §, $P < 0.05$ versus control retrovirus. MFI, mean fluorescence intensity.

model of myeloproliferative disorder. Surprisingly, not only inhibition of PDPs but also inhibition of CPT-1 prevented the proliferation of *Abca1*$^{-/-}$*Abcg1*$^{-/-}$ leukocytes. This emphasizes a scenario in which high rates of aerobic glycolysis in leukemia cells are necessary to support the mitochondrial metabolism of fatty acids (i.e., fats burn in the fire of carbohydrates; Samudio et al., 2010). Although the mechanisms orchestrating this phenomenon remain to be investigated, it appears unlikely to be mediated by triglyceride or ceramide biosynthesis. Interestingly, the antiproliferative effect

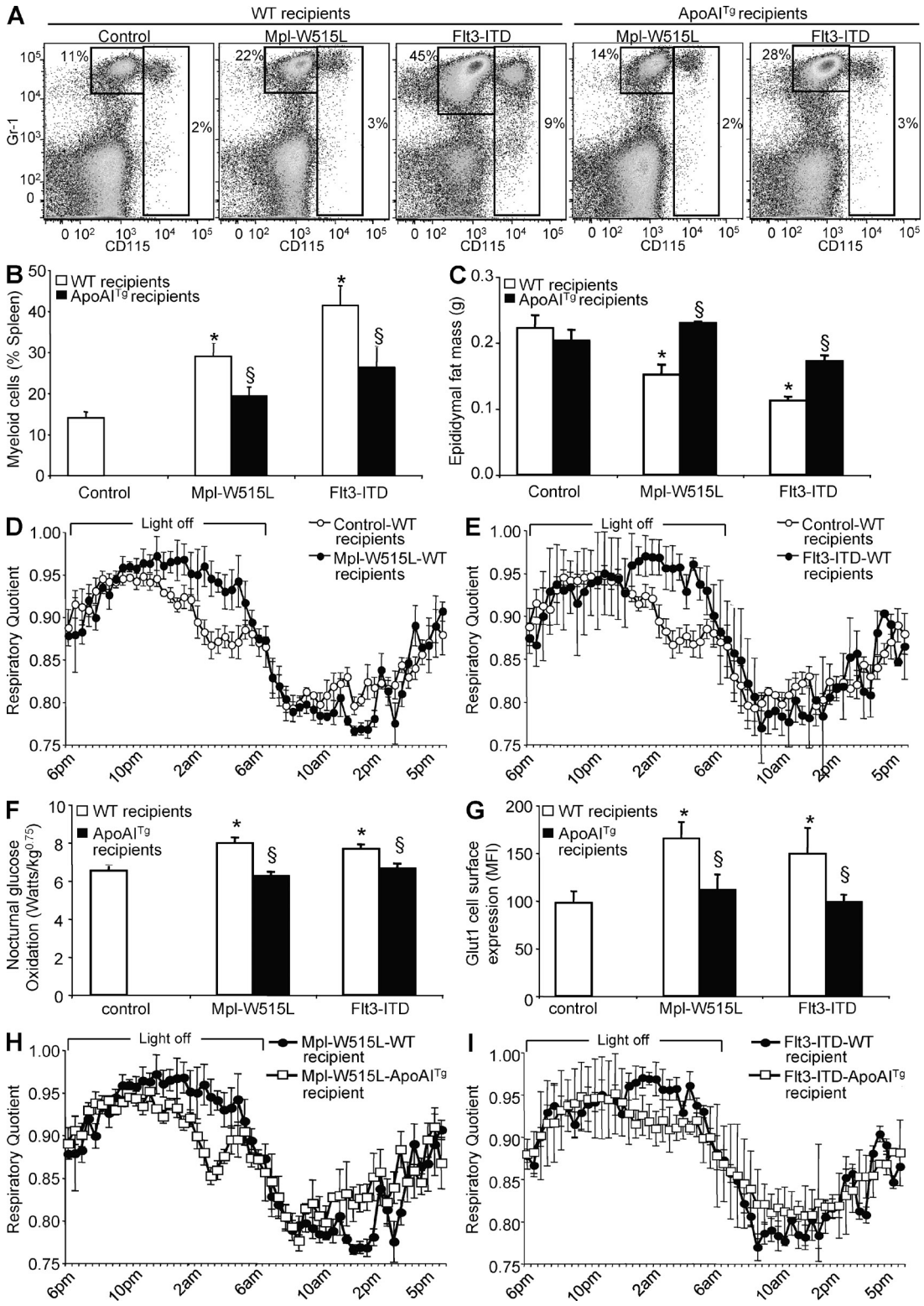

Figure 6. HDL prevents the adipose tissue atrophy and enhanced glucose oxidation caused by Mpl-W515L and Flt3-ITD activating mutations. (A) Representative dot plots and quantification of the splenic myeloid cells ($CD115^+$ monocytes and $CD115^-Gr1^+$ neutrophils) of WT and ApoA-I transgenic recipient mice transplanted with Mpl-W515L– and Flt3-ITD–transduced BM cells. (B and C) Quantification of the myeloid cells (B) and epididymal fat mass (C) of these mice. (D, E, F, H, and I) RQ measured by indirect calorimetry (D, E, H, and I) and quantification of the nocturnal glucose oxidation of these mice (F). (G) Quantification of the cell surface expression of Glut1 in $CD45^+$ leukocytes of these mice. Results are mean ± SEM of an experiment of four to five animals per group. *, $P < 0.05$ versus control mice; §, $P < 0.05$ versus respective WT recipients. MFI, mean fluorescence intensity.

of carnitine suggested that prevention of oxidative phosphorylation by efflux of excess mitochondrial acetyl moieties (Muoio et al., 2012) might represent a novel strategy for the treatment of hematological malignancies. In conclusion, increased glucose oxidation and mitochondrial metabolism–dependent proliferation of myeloid cells likely contributed to energy dissipation and subsequent loss of adipose mass.

Leukocytes and adipocytes can communicate through interaction between secreted inflammatory cytokines and their cognate receptors (Lumeng and Saltiel, 2011; Odegaard and Chawla, 2011). The finding that highly infiltrated adipose depots were associated with impaired Glut4 translocation to the plasma membrane in response to insulin in *Abca1*$^{-/-}$*Abcg1*$^{-/-}$ BM chimeras was strongly implied by prior studies indicating insulin resistance in peripheral tissues secondary to increased tumor-derived cytokines (Delano and Moldawer, 2006). Nevertheless, these findings provide strong evidences that local inflammation driving adipose tissue insulin resistance is not restricted to a role on fat mobilization in cancer-associated adipose tissue loss (Das et al., 2011). This suggests that myeloproliferative cells develop efficient strategies to divert glucose from its expected destination, i.e., fat storage as a mean to meet their energetic needs. In part, this could be related to a shunt of glucose to the pentose phosphate pathway that has been recently shown to modulate the inflammatory response of activated immune cells (Ham, M., et al. 2008. *The FASEB Journal* Meeting. Abstr. 615.1; Blagih and Jones, 2012). This could ultimately contribute not only to the enhanced glucose oxidation observed in our mouse models of myeloproliferative disorders but also to the local adipose tissue insulin resistance mediated by enhanced inflammatory response.

Finally, we showed that Glut1 blockade prevented both basal and IL-3–induced proliferation of *Abca1*$^{-/-}$*Abcg1*$^{-/-}$ leukocytes in vitro and prevented LPS-induced inflammatory cytokine response in *Abca1*$^{-/-}$*Abcg1*$^{-/-}$ macrophages. This translated in vivo into the rescue of leukocytosis and adipose tissue infiltration of *Abca1*$^{-/-}$*Abcg1*$^{-/-}$ BM transplanted mice in response to Glut1 inhibition. Remarkably, this prevented the adipose tissue loss of these mice, confirming the key role of myeloid Glut1 in the diversion of energy stores from adipose to myeloid cells. Similarly, overexpression of the human ApoA-I transgene, previously shown to raise plasma HDL levels and prevent the myeloproliferative syndrome of *Abca1*$^{-/-}$*Abcg1*$^{-/-}$ BM transplanted mice (Yvan-Charvet et al., 2010), reduced Glut1 cell surface expression in leukocytes and prevented their fat loss. This reflected in part the removal of excess cholesterol from plasma membrane in *Abca1*$^{-/-}$*Abcg1*$^{-/-}$ myeloid cells that prevented the IL-3Rβ signaling (Yvan-Charvet et al., 2010) and subsequent increase in Glut1-dependent glucose uptake (Fig. 3 G). These findings were further extended in two mouse models of myeloproliferative disorders based on expression of human leukemia disease alleles (Flt3-ITD and Mpl-W515L) in which overexpression of the human ApoA-I transgene reduced myeloid expansion, decreased cell surface expression of Glut1 in leukocytes, reduced glucose oxidation during the feeding period, and prevented adipose tissue loss.

In conclusion, our study elucidates a glucose steal mechanism by proliferating and inflammatory myeloid cells that contributes to depletion of adipose tissue in myeloproliferative disorders. This mechanism involved enhanced glucose oxidation by myeloid cells that led to energy dissipation with consequences on fat storage. Inhibition of glucose uptake by leukocytes with a Glut1 inhibitor or by treatments that increase HDL levels could ultimately provide new therapeutic approaches not only to limit cell proliferation but also to prevent the energy imbalance and fat atrophy observed in myeloproliferative disorders and in other human malignancies.

MATERIALS AND METHODS

Mice and treatments. WT, *Abca1*$^{-/-}$, *Abcg1*$^{-/-}$, and *Abca1*$^{-/-}$*Abcg1*$^{-/-}$ littermates in a mixed C57BL/6 × DBA background (Yvan-Charvet et al., 2007) were used for this study. Human apoA-1 transgenic (hapoA-1^{Tg}) mice were obtained from the Jackson Laboratory. BM transplantation into the genetically uniform F1 generation obtained by crossing C57BL/6 WT, hapoA-1^{Tg} mice with WT DBA mice (The Jackson Laboratory) was performed as previously described (Yvan-Charvet et al., 2007). Animal protocols were approved by the Institutional Animal Care and Use Committee of Columbia University. Animals had ad libitum access to both food and water.

HSC transplantation. HSC transplantation was adapted from a previously described protocol (Wagers et al., 2002). In brief, congenic CD45.1$^+$ B6.SJL-Ptprca—Pep3b-/BoyJ were purchased from the Jackson Laboratory and used to isolate Sca-1–depleted BM cells by FACS sorting. HSCs were isolated by FACS sorting of lineage-depleted BM from WT and *Abca1*$^{-/-}$*Abcg1*$^{-/-}$ backcrossed for 10 generations on a C57/BL6 background, based on the following cell surface markers: c-kit and Sca-1 (LSK, Lin$^-$Sca$^+$c-kit$^+$). Lethally irradiated WT recipients were i.v. injected with 10^6 cells containing a mixture of CD45.1$^+$ Sca-1–depleted BM cells and CD45.2$^+$ LSK cells from either WT or *Abca1*$^{-/-}$*Abcg1*$^{-/-}$ mice in the ratio 1:2,000. Transplanted recipients were screened by flow cytometry for reconstitution of CD45.2$^+$ leukocytes in peripheral blood at 6 wk after transplant. More than 90% of leukocytes stained for the congenic marker CD45.2, thereby confirming the engraftment of LSK cells (Wagers et al., 2002).

Retroviral BM transplantation. The retroviral BM transplant assay was performed as previously described (Pikman et al., 2006). In brief, control, Mpl-W515L and Flt3-ITD retroviral supernatants were titered and used to transduce WT BM cells. In independent experiments, premade control and Glut1 shRNA lentiviral particles (Santa Cruz Biotechnology, Inc.) were used to transduce WT and *Abca1*$^{-/-}$*Abcg1*$^{-/-}$ BM cells. BM cells were cultured for 24 h in transplantation media (RPMI + 10% FBS + 6 ng/ml IL-3, 10 ng/ml IL-6, and 10 ng/ml stem cell factor) and treated by spin infection with retroviral supernatants (1 ml supernatant per 4 × 10^6 cells in the presence of polybrene) and centrifuged at 1,800 *g* for 90 min. The spin infection was repeated 24 h later. After washing, the cells were used for BM transplantation into lethally irradiated WT recipient mice.

Energy expenditure. Metabolic activity was performed by in vivo indirect open circuit calorimetry at the Mouse Phenotyping Core of Columbia University using a CaloSys calorimetry system (TSE Systems, Inc). Animals were placed into experimental chambers with free access to food and water for a 4-d consecutive period. Food intake was recorded with an automated feeding monitor system through the study period. Constant airflow (0.5 liter/min) was drawn through the chamber and monitored by a mass-sensitive flow meter. To calculate oxygen consumption (VO_2), carbon dioxide production (VCO_2), and RQ (ratio of VCO_2 to VO_2), gas concentrations were monitored at the inlet and outlet of the scaled chambers.

Total metabolic rate (energy expenditure) was calculated from oxygen consumption and carbon dioxide production using Lusk's equation and expressed as watts per kilogram to the 0.75 power of body weight (Yvan-Charvet et al., 2005). Glucose and lipid oxidation were calculated as previously described (Yvan-Charvet et al., 2005).

In vivo 2-[^{14}C]-DG uptake. Uptake of 2-[^{14}C]-DG in peripheral tissues was measured as previously described (Rofe et al., 1988). In brief, 2 μCi 2-[^{14}C]-DG was i.v. injected, and blood samples were collected at 5, 10, 20, 30, and 40 min. Blood glucose was monitored through the study period with a glucometer (Roche). After 40 min, adipose tissue, skeletal muscle, heart, lung, spleen, and brain were rapidly dissected, weighed, and homogenized with 5% $HClO_4$ solution. BM cells were collected from leg bones, and peripheral leukocytes were obtained after RBC lysis. The radioactivity incorporated in both 2-[^{14}C]-DG and its 6-phosphate derivative was measured in the $HClO_4$ extract and expressed as total radioactivity per tissue weight. The rate constant of net tissue uptake of 2-[^{14}C]-DG was calculated as described previously (Rofe et al., 1988). In brief, the relative glucose uptake was calculated by dividing the area under the blood 2-[^{14}C]-DG disappearance curve (cpm/min/ml) to the steady-state glucose concentration (mM) multiplied by the tissue 2-[^{14}C]-DG (cpm/g tissue or cpm/10^6 cells for the BM) at 40 min.

Blood parameters. Plasma leptin and insulin were determined by ELISA (Mouse Leptin Quantikine ELISA kit [R&D Systems]; Mouse insulin ELISA kit [Crystal Chem, Inc.]). Plasma TNF was measured by Luminex assay (Cytokine Core Laboratory). Blood glucose was assayed with a glucometer (Roche).

Histopathology. Mice were euthanized in accordance with the American Veterinary Association Panel of Euthanasia. Adipose tissue was serially paraffin sectioned and stained with hematoxylin and eosin (H&E) for morphological analysis as previously described (Yvan-Charvet et al., 2007).

Adipose tissue cellularity. Cellularity of epididymal adipose tissue was determined as previously described (Yvan-Charvet et al., 2005). In brief, images of isolated adipocytes were acquired from a light microscope (IX-70; Olympus) fitted with a charge-coupled device camera (RS Photometrics), and the measurement of ~400 cell diameters was performed allowing calculation of a mean fat cell weight. Tissue triglyceride content was measured from a sample of adipose tissue using a commercial kit (Sigma-Aldrich). Fat cell number was estimated by dividing the tissue lipid content by the fat cell weight.

Glucose tolerance tests. After 6 h of fasting, mice were injected i.p. with D-glucose (2 g/kg of body weight), and blood samples were obtained by tail bleeding at 0, 15, 30, 60, 90, and 120 min after injection (Yvan-Charvet et al., 2005). Blood glucose was assayed with a glucometer (Roche).

Flow cytometry analysis. BM cells were collected from leg bones or spleen, lysed to remove RBCs, and filtered before use. Freshly isolated cells were stained with the appropriate antibodies for 30 min on ice. For peripheral blood leukocytes analysis, 100 μl blood was collected into EDTA tubes before RBC lysis, filtration, and staining for 30 min on ice. To assess the uptake of 2-NBDG, prestained peripheral blood leukocytes (Yvan-Charvet et al., 2010) were incubated with 10 μM 2-NBDG (Invitrogen) for 30 min, followed by flow cytometric detection of fluorescence produced by the cells (Zou et al., 2005). The mitochondrial membrane potential was analyzed with 25 nM fluorescent TMRE (AnaSpec) staining for 30 min on prestained leukocytes. Viable cells, gated by light scatter or exclusion of CD45$^-$ cells, were analyzed on a four-laser LSRII cell analyzer (BD) or sorted on a FACSAria Cell Sorter (BD), both running with DiVa software (BD). Data were analyzed using FlowJo software (Tree Star).

Antibodies. Anti–mouse CD45 (clone 30F11), CD115 (AFS98), TCR-β (H57-597), F4/80 (BM8), CD2 (RM2-5), CD3e (145-2C11), CD4 (GK1.5), CD8b (53-6.7), CD19 (eBio1D3), CD45R (B220, RA3-6B2), Gr-1 (Ly6G, RB6-8C5), Cd11b (Mac1, M1/70), Ter119 (Ly76) and NK1.1 (Ly53, PK136), c-Kit (CD117, ACK2), and Sca-1 (D7) were all purchased from eBioscience. Glut1-FITC antibody was purchased from R&D Systems. These antibodies were used to sort HSCs and stain for leukocytes in peripheral blood and tissues.

BM harvest and treatment. Primary BM cells were resuspended in IMDM (Gibco) containing 10% FCS (STEMCELL Technologies) and cultured for 1 h in tissue culture flasks to remove adherent cells, including macrophages. Suspended cells were then cultured for 72 h in the presence of 6 ng/ml IL-3 (R&D Systems). In some experiments, the farnesyl transferase inhibitor (EMD Millipore) was used at the final concentration of 1 μM, fasentin (Sigma-Aldrich) at 50 μM, DL-AP3 (Tocris Bioscience) at 50 μM, myriocin (Sigma-Aldrich) at 10 μM, diglyceride acyltransferase inhibitor (EMD Millipore) at 40 μM, etomoxir (Sigma-Aldrich) at 40 μM, branched-chain amino acids (leucine, isoleucine, and valine; Sigma-Aldrich) at 1 mM, glutathione monoethyl ester (EMD Millipore) at 10 mM, tempol (EMD Millipore) at 4 mM, and carnitine (Sigma-Aldrich) at 1 mM. For proliferation assays, cells were pulsed for 2 h with 2 μCi/ml [^{3}H]thymidine, and the radioactivity incorporated into the cells was determined by standard procedures using a liquid scintillation counter. In one experiment (Fig. 4 F), cells were resuspended in 20 mM glucose DMEM (DMEM rich; Gibco) or low-glucose DMEM (DMEM poor; Gibco) supplemented with 20 mM glucose or 20 mM galactose (Sigma-Aldrich) and cultured for 48 h in the presence of 6 ng/ml IL-3. SDH activity was determined by an ELISA kit according to the manufacturer's instructions (MitoSciences). BM-derived macrophages were isolated and cultured in 10% FBS in DMEM supplemented with M-CSF for 5–10 d before the experiment. Where indicated, macrophages were incubated with 100 ng/ml LPS (*Escherichia coli* 0111:B4; Sigma-Aldrich).

Glucose metabolism experiments. Isolated BM cells were cultured for 24 h with or without 6 ng/ml IL-3 and 50 μM fasentin, a Glut1 inhibitor. Where indicated, BM cells were differentiated into macrophages as described above. Cells were next incubated with 5.5 mM [^{14}C]glucose in 2% BSA Krebs-Ringer bicarbonate buffer, pH 7.4. After 2 h, the generated $^{14}CO_2$ and the ^{14}C incorporation into lipids were quantified as previously described (Yvan-Charvet et al., 2005). In some experiments, cellular cholesterol was depleted by 5 mM cyclodextrin for 1 h before growth factor treatment as previously described (Yvan-Charvet et al., 2010).

Directed metabolomic experiments. Isolated BM cells (10^6 cells) were cultured with or without 6 ng/ml IL-3 for 24 h. The next day, suspended cells were centrifuged at 1,000 rpm for 5 min, and pellets were rapidly washed (less than 10 s) with a mass spectrometry–compatible buffer (150 mM ammonium acetate solution) to prevent the presence of sodium and phosphate in the residue and limit interference with LC-MS analyses. After a second step of centrifugation, pellets were immediately frozen in liquid nitrogen to quench metabolism according to the University of Michigan Molecular Phenotyping Core facility's instructions. Samples were shipped on dry ice to the Molecular Phenotyping Core facility where metabolites were extracted by exposing the cells to a chilled mixture of 80% methanol, 10% chloroform, and 10% water. Glycolytic and citric acid metabolites were then analyzed by the Molecular Phenotyping Core facility using LC-MS as previously described (Yuneva et al., 2012).

Western blot analysis. 2-h-fasted mice were administrated insulin i.p. (0.4 U/mouse). After 5 min, freshly isolated adipose tissue was homogenized as previously described (Yvan-Charvet et al., 2005), and cell extracts were either directly used to measure phospho-Akt (clone 587F11; Cell Signaling Technology) by Western blot analysis or fractionated by differential centrifugation to isolate plasma membranes and low-density microsomes (Yvan-Charvet et al., 2010) and quantify Glut4 expression (clone 1F8; R&D Systems).

RNA analysis. Total RNA extraction, cDNA synthesis, and real-time PCR were performed as described previously (Yvan-Charvet et al., 2005). Ribosomal 18S RNA expression was used to account for variability in the initial quantities of mRNA.

Statistical analysis. Statistical significance was performed by two-tailed parametric Student's *t* test or by one-way ANOVA (four-group comparisons) with a Bonferroni multiple comparison post test (GraphPad Software).

We thank Dr. Kristie Gordon for assistance with flow cytometry, Pr. Pascal Ferre for scientific discussion, and the French Cancer Research Association (ARC).

This work utilized Core Services supported by a National Institutes of Health (NIH) grant (DK089503) to the University of Michigan. This work was supported by grants to L. Yvan-Charvet from the American Heart Association (SDG2160053), to E.L. Gautier from the American Heart Association (10POST4160140), to M. Westerterp from the Netherlands Organization of Sciences (NWO VENI grant 916.11.072), to G.J. Randolph from the NIH (AI061741), and to A.R. Tall from the NIH (HL54591).

The authors have no financial conflict with these experiments.

Submitted: 22 June 2012
Accepted: 10 December 2012

REFERENCES

Argilés, J.M., S. Busquets, and F.J. López-Soriano. 2011. Anti-inflammatory therapies in cancer cachexia. *Eur. J. Pharmacol.* 668:S81–S86. http://dx.doi.org/10.1016/j.ejphar.2011.07.007

Blagih, J., and R.G. Jones. 2012. Polarizing macrophages through reprogramming of glucose metabolism. *Cell Metab.* 15:793–795. http://dx.doi.org/10.1016/j.cmet.2012.05.008

Bustamante, E., and P.L. Pedersen. 1977. High aerobic glycolysis of rat hepatoma cells in culture: role of mitochondrial hexokinase. *Proc. Natl. Acad. Sci. USA.* 74:3735–3739. http://dx.doi.org/10.1073/pnas.74.9.3735

Chang, F., J.T. Lee, P.M. Navolanic, L.S. Steelman, J.G. Shelton, W.L. Blalock, R.A. Franklin, and J.A. McCubrey. 2003. Involvement of PI3K/Akt pathway in cell cycle progression, apoptosis, and neoplastic transformation: a target for cancer chemotherapy. *Leukemia.* 17:590–603. http://dx.doi.org/10.1038/sj.leu.2402824

Das, S.K., S. Eder, S. Schauer, C. Diwoky, H. Temmel, B. Guertl, G. Gorkiewicz, K.P. Tamilarasan, P. Kumari, M. Trauner, et al. 2011. Adipose triglyceride lipase contributes to cancer-associated cachexia. *Science.* 333:233–238. http://dx.doi.org/10.1126/science.1198973

DeBerardinis, R.J., J.J. Lum, G. Hatzivassiliou, and C.B. Thompson. 2008. The biology of cancer: metabolic reprogramming fuels cell growth and proliferation. *Cell Metab.* 7:11–20. http://dx.doi.org/10.1016/j.cmet.2007.10.002

Delano, M.J., and L.L. Moldawer. 2006. The origins of cachexia in acute and chronic inflammatory diseases. *Nutr. Clin. Pract.* 21:68–81. http://dx.doi.org/10.1177/011542650602100168

Dingli, D., R.A. Mesa, and A. Tefferi. 2004. Myelofibrosis with myeloid metaplasia: new developments in pathogenesis and treatment. *Intern. Med.* 43:540–547. http://dx.doi.org/10.2169/internalmedicine.43.540

Fiorenza, A.M., A. Branchi, and D. Sommariva. 2000. Serum lipoprotein profile in patients with cancer. A comparison with non-cancer subjects. *Int. J. Clin. Lab. Res.* 30:141–145. http://dx.doi.org/10.1007/s005990070013

Flier, J.S., M.M. Mueckler, P. Usher, and H.F. Lodish. 1987. Elevated levels of glucose transport and transporter messenger RNA are induced by ras or src oncogenes. *Science.* 235:1492–1495. http://dx.doi.org/10.1126/science.3103217

Fukuzumi, M., H. Shinomiya, Y. Shimizu, K. Ohishi, and S. Utsumi. 1996. Endotoxin-induced enhancement of glucose influx into murine peritoneal macrophages via GLUT1. *Infect. Immun.* 64:108–112.

Gamelli, R.L., H. Liu, L.K. He, and C.A. Hofmann. 1996. Augmentations of glucose uptake and glucose transporter-1 in macrophages following thermal injury and sepsis in mice. *J. Leukoc. Biol.* 59:639–647.

Hansson, G.K., and M. Björkholm. 2010. Medicine. Tackling two diseases with HDL. *Science.* 328:1641–1642. http://dx.doi.org/10.1126/science.1191663

Hawkinson, J.E., M. Acosta-Burruel, and P.L. Wood. 1996. The metabotropic glutamate receptor antagonist L-2-amino-3-phosphonopropionic acid inhibits phosphoserine phosphatase. *Eur. J. Pharmacol.* 307:219–225. http://dx.doi.org/10.1016/0014-2999(96)00253-1

Herman, M.A., and B.B. Kahn. 2006. Glucose transport and sensing in the maintenance of glucose homeostasis and metabolic harmony. *J. Clin. Invest.* 116:1767–1775. http://dx.doi.org/10.1172/JCI29027

Jose, C., N. Bellance, and R. Rossignol. 2011. Choosing between glycolysis and oxidative phosphorylation: a tumor's dilemma? *Biochim. Biophys. Acta.* 1807:552–561. http://dx.doi.org/10.1016/j.bbabio.2010.10.012

Kelly, L.M., Q. Liu, J.L. Kutok, I.R. Williams, C.L. Boulton, and D.G. Gilliland. 2002. FLT3 internal tandem duplication mutations associated with human acute myeloid leukemias induce myeloproliferative disease in a murine bone marrow transplant model. *Blood.* 99:310–318. http://dx.doi.org/10.1182/blood.V99.1.310

Kumar, N.B., A. Kazi, T. Smith, T. Crocker, D. Yu, R.R. Reich, K. Reddy, S. Hastings, M. Exterman, L. Balducci, et al. 2010. Cancer cachexia: traditional therapies and novel molecular mechanism-based approaches to treatment. *Curr. Treat. Options Oncol.* 11:107–117. http://dx.doi.org/10.1007/s11864-010-0127-z

Lumeng, C.N., and A.R. Saltiel. 2011. Inflammatory links between obesity and metabolic disease. *J. Clin. Invest.* 121:2111–2117. http://dx.doi.org/10.1172/JCI57132

Lunt, S.Y., and M.G. Vander Heiden. 2011. Aerobic glycolysis: meeting the metabolic requirements of cell proliferation. *Annu. Rev. Cell Dev. Biol.* 27:441–464. http://dx.doi.org/10.1146/annurev-cellbio-092910-154237

Muoio, D.M., R.C. Noland, J.P. Kovalik, S.E. Seiler, M.N. Davies, K.L. DeBalsi, O.R. Ilkayeva, R.D. Stevens, I. Kheterpal, J. Zhang, et al. 2012. Muscle-specific deletion of carnitine acetyltransferase compromises glucose tolerance and metabolic flexibility. *Cell Metab.* 15:764–777. http://dx.doi.org/10.1016/j.cmet.2012.04.005

Odegaard, J.I., and A. Chawla. 2011. Alternative macrophage activation and metabolism. *Annu. Rev. Pathol.* 6:275–297. http://dx.doi.org/10.1146/annurev-pathol-011110-130138

Out, R., W. Jessup, W. Le Goff, M. Hoekstra, I.C. Gelissen, Y. Zhao, L. Kritharides, G. Chimini, J. Kuiper, M.J. Chapman, et al. 2008. Coexistence of foam cells and hypocholesterolemia in mice lacking the ABC transporters A1 and G1. *Circ. Res.* 102:113–120. http://dx.doi.org/10.1161/CIRCRESAHA.107.161711

Pikman, Y., B.H. Lee, T. Mercher, E. McDowell, B.L. Ebert, M. Gozo, A. Cuker, G. Wernig, S. Moore, I. Galinsky, et al. 2006. MPLW515L is a novel somatic activating mutation in myelofibrosis with myeloid metaplasia. *PLoS Med.* 3:e270. http://dx.doi.org/10.1371/journal.pmed.0030270

Rofe, A.M., C.S. Bourgeois, R. Bais, and R.A. Conyers. 1988. The effect of tumour-bearing on 2-deoxy[U-14C]glucose uptake in normal and neoplastic tissues in the rat. *Biochem. J.* 253:603–606.

Samudio, I., R. Harmancey, M. Fiegl, H. Kantarjian, M. Konopleva, B. Korchin, K. Kaluarachchi, W. Bornmann, S. Duvvuri, H. Taegtmeyer, and M. Andreeff. 2010. Pharmacologic inhibition of fatty acid oxidation sensitizes human leukemia cells to apoptosis induction. *J. Clin. Invest.* 120:142–156. http://dx.doi.org/10.1172/JCI38942

Vander Heiden, M.G., L.C. Cantley, and C.B. Thompson. 2009. Understanding the Warburg effect: the metabolic requirements of cell proliferation. *Science.* 324:1029–1033. http://dx.doi.org/10.1126/science.1160809

Wagers, A.J., R.I. Sherwood, J.L. Christensen, and I.L. Weissman. 2002. Little evidence for developmental plasticity of adult hematopoietic stem cells. *Science.* 297:2256–2259. http://dx.doi.org/10.1126/science.1074807

Westerterp, M., S. Gourion-Arsiquaud, A.J. Murphy, A. Shih, S. Cremers, R.L. Levine, A.R. Tall, and L. Yvan-Charvet. 2012. Regulation of hematopoietic stem and progenitor cell mobilization by cholesterol efflux pathways. *Cell Stem Cell.* 11:195–206. http://dx.doi.org/10.1016/j.stem.2012.04.024

Wood, T.E., S. Dalili, C.D. Simpson, R. Hurren, X. Mao, F.S. Saiz, M. Gronda, Y. Eberhard, M.D. Minden, P.J. Bilan, et al. 2008. A novel inhibitor of glucose uptake sensitizes cells to FAS-induced cell death. *Mol. Cancer Ther.* 7:3546–3555. http://dx.doi.org/10.1158/1535-7163.MCT-08-0569

Yuneva, M.O., T.W.M. Fan, T.D. Allen, R.M. Higashi, D.V. Ferraris, T. Tsukamoto, J.M. Matés, F.J. Alonso, C. Wang, Y. Seo, et al. 2012. The metabolic profile of tumors depends on both the responsible genetic lesion and tissue type. *Cell Metab.* 15:157–170. http://dx.doi.org/10.1016/j.cmet.2011.12.015

Yvan-Charvet, L., P. Even, M. Bloch-Faure, M. Guerre-Millo, N. Moustaid-Moussa, P. Ferre, and A. Quignard-Boulange. 2005. Deletion of the angiotensin type 2 receptor (AT2R) reduces adipose cell size and protects from diet-induced obesity and insulin resistance. *Diabetes.* 54:991–999. http://dx.doi.org/10.2337/diabetes.54.4.991

Yvan-Charvet, L., M. Ranalletta, N. Wang, S. Han, N. Terasaka, R. Li, C. Welch, and A.R. Tall. 2007. Combined deficiency of ABCA1 and ABCG1 promotes foam cell accumulation and accelerates atherosclerosis in mice. *J. Clin. Invest.* 117:3900–3908.

Yvan-Charvet, L., C. Welch, T.A. Pagler, M. Ranalletta, M. Lamkanfi, S. Han, M. Ishibashi, R. Li, N. Wang, and A.R. Tall. 2008. Increased inflammatory gene expression in ABC transporter-deficient macrophages: free cholesterol accumulation, increased signaling via toll-like receptors, and neutrophil infiltration of atherosclerotic lesions. *Circulation.* 118:1837–1847. http://dx.doi.org/10.1161/CIRCULATIONAHA.108.793869

Yvan-Charvet, L., T.A. Pagler, E.L. Gautier, S. Avagyan, R.L. Siry, S. Han, C.L. Welch, N. Wang, G.J. Randolph, H.W. Snoeck, and A.R. Tall. 2010. ATP-binding cassette transporters and HDL suppress hematopoietic stem cell proliferation. *Science.* 328:1689–1693. http://dx.doi.org/10.1126/science.1189731

Zou, C., Y. Wang, and Z. Shen. 2005. 2-NBDG as a fluorescent indicator for direct glucose uptake measurement. *J. Biochem. Biophys. Methods.* 64:207–215. http://dx.doi.org/10.1016/j.jbbm.2005.08.001

Regular Article

PHAGOCYTES, GRANULOCYTES, AND MYELOPOIESIS

Local apoptosis mediates clearance of macrophages from resolving inflammation in mice

Emmanuel L. Gautier,[1] Stoyan Ivanov,[1] Philippe Lesnik,[2] and Gwendalyn J. Randolph[1]

[1]Department of Pathology & Immunology, Washington University in St. Louis, St. Louis, MO; and [2]Institut National de la Santé et de la Recherche Médicale UMR-S 939, Hôpital de la Pitié, Pavillon Benjamin Delessert, Paris, France

Key Points

- Macrophage migration to lymph nodes during acute inflammation is quantitatively minor.
- Macrophages are cleared from acute inflammation by local death.

Chronic inflammatory diseases such as atherosclerosis are characterized by an accumulation of macrophages. To design therapies that would reduce macrophage burden during disease, understanding the cellular and molecular mechanisms that regulate macrophage removal from sites of resolving inflammation is critical. Although past studies have considered the local death of macrophages or the possibility that they emigrate out of inflammatory foci, methods to quantify death or emigration have never been employed. Here, we applied quantitative competition approaches and other methods to study resolution of thioglycollate-induced peritonitis, the model in which earlier work indicated that emigration to lymph nodes accounted for macrophage removal. We show that migration to lymph nodes occurred in a CC chemokine receptor 7–independent manner but, overall, had a quantitatively minor role in the removal of macrophages. Blocking migration did not significantly delay resolution. However, when macrophages resistant to death were competed against control macrophages, contraction of the macrophage pool was delayed in the apoptosis-resistant cells. These data refute the concept that macrophages are dominantly cleared through emigration and indicate that local death controls macrophage removal. This finding alters the emphasis on which cellular processes merit targeting in chronic diseases associated with accumulation of macrophages. (*Blood*. 2013;122(15):2714-2722)

Introduction

Resolution of acute inflammation is a crucial step toward return to tissue homeostasis after initiation of tissue injury.[1] In the case of infection, it is self-evident that clearance of the inciting microorganism or microorganisms would be necessary before resolution could be completed, but there are a growing list of health conditions not explicitly associated with infection in which low-grade chronic inflammation is observed, including metabolic diseases (obesity, atherosclerosis), neurodegenerative diseases, and cancers.[2-4] A better understanding of the mechanisms that support resolution of inflammation might facilitate new strategies aimed to combat these diseases.[5]

Initiation of inflammation is typically characterized by early neutrophil recruitment, followed by an influx of monocytes that develop into inflammatory macrophages. The neutrophils undergo death within hours and are cleared by macrophages,[6,7] with efferocytosis of neutrophils handled by neighboring macrophages. Efferocytosis triggers the production of mediators such as transforming growth factor β1, which in turn generate macrophages that facilitate resolution and tissue repair.[8,9] Novel lipid mediators participate critically in control of these steps.[7] Although there is consensus that the fate of neutrophils in acute inflammation is regulated through local death and efferocytosis,[6,7] with a small number of neutrophils emigrating to draining lymph nodes (LNs),[10] consensus is still lacking on the fate of monocyte-derived cells that become inflammatory macrophages. Two concepts are apparent in the literature: inflammatory macrophages die locally,[11-14] or alternatively, these cells are primarily cleared by emigration to draining LNs.[15] Although none of the studies is quantitative, the latter concept has received the most attention, cited as a classic in the field (www.nature.com/ni/focus/inflammation/classics/macrophages.html).

Accordingly, we earlier wondered whether the failure of resolution in atherosclerosis[16] might be linked to the failure of macrophages to acquire the appropriate emigratory phenotype.[17] However, although some evidence supports the link between atherosclerosis and emigration to LNs,[18-20] emigration from atherosclerotic plaques is not required to promote clearance of macrophages from plaques.[21] Instead, a combination of macrophage death and cessation of monocyte entry is sufficient for macrophage contraction during disease regression.[21] These observations and the overall qualitative nature of the previous studies[11-13,15] led us to reexamine the cellular mechanisms that underlie removal of macrophages from sites of resolving inflammation. We chose to use the model of thioglycollate-induced peritonitis that previously claimed a key role for emigration to LNs and added techniques to quantitatively evaluate emigration and death. We show that emigration to LNs plays only a minor quantitative role in the removal of macrophages relative to a dominant role for local death. Considering that the peritonitis model used in our study was the same as that used in the work claiming that emigration to LNs mediates macrophage removal, our findings indicate that the concept of emigration to LNs as a quantitatively

Submitted January 11, 2013; accepted August 14, 2013. Prepublished online as *Blood* First Edition paper, August 23, 2013; DOI 10.1182/blood-2013-01-478206.

The online version of this article contains a data supplement.

The publication costs of this article were defrayed in part by page charge payment. Therefore, and solely to indicate this fact, this article is hereby marked "advertisement" in accordance with 18 USC section 1734.

significant driver of macrophage clearance no longer holds experimental support.

Methods

Animals and treatments

C57BL/6J mice carrying the Ly5.1 allele (CD45.2) were purchased from The Jackson Laboratories or the National Cancer Institute. CD45.1 C57BL/6 mice were from the National Cancer Institute. CD45.2 and CD45.1 mice were bred to obtain CD45.1 × CD45.2 F1 mice. CC chemokine receptor (CCR)7$^{-/-}$, CCR2$^{-/-}$, and Bim$^{-/-}$ mice were obtained from The Jackson Laboratories. Bone marrow cells from CD68-hBcl2 (Mφ-hBcl2) mice[22] were used to transplant lethally irradiated mice, as described.[23]

Resolving acute peritonitis was induced by intraperitoneal injection of 1 mL sterile thioglycollate (Sigma-Aldrich; 3% weight/volume). Pertussis toxin (PTX; Sigma-Aldrich) was injected intraperitoneally (2.5 μg/mouse). PKH26 Red Fluorescent Cell Linker Kit for Phagocytic Cell Labeling was from Sigma-Aldrich; 200 μL of a 5-μM solution was injected intraperitoneally. Mice were housed in a specific pathogen-free environment and used in accordance with protocols approved by the Animal Care and Utilization Committees at Mount Sinai School of Medicine or Washington University.

Antibodies

Anti-mouse CD115 (AFS98), F4/80 (BM8), CD45 (30-F11), MHC-II (IA-IE, M5/114.15.2), CD45.2 (104), CD45.1 (A20), and CD11c (N418) were from eBiosciences. Anti-mouse Gr-1 (Ly-6C/G, RB6-8C5) and CD36 (HM36) were from Biolegend. Anti-mouse F4/80 (CI:A3-1) was from Serotec. Apoptosis was determined using annexin V after cell surface labeling by following the manufacturer's instructions (Miltenyi Biotec).

Microarray analysis

Male C57BL/6 mice at 6 weeks of age were used for gene expression analysis in macrophages. Inflammatory peritoneal macrophages were identified as CD115^{+} F4/80^{int} B220^{-} MHC-II^{+} or MHC-II^{-} and sorted using a BD FACSAria II cell sorter. Resident peritoneal macrophages, including CD115^{+} F4/80^{hi} MHC-II^{-} B220^{-} and CD115^{+} F4/80^{lo} MHC-II^{+} B220^{-} populations, were sorted at steady state and after thioglycollate injection. Microarrays were carried out as part of the Immunological Genome Project. Flow plots of sorted cells can be found on the Immunological Genome Project website (www.immgen.org). RNA was prepared from sorted populations from C57BL/6J mice after double sorting directly into TRIzol reagent (www.immgen.org/Protocols/Total RNA Extraction with Trizol.pdf). Then it was amplified and hybridized on the Affymetrix Mouse Gene 1.0 ST array. For data analysis, Immunological Genome Project data sets were used. Raw data were normalized using the RMA algorithm. Extensive quality control documents are available on the Immunological Genome Project website (www.immgen.org/Protocols/ImmGen QC Documentation_ALL-DataGeneration_0612.pdf). All data sets have been deposited at the National Center for Biotechnology Information/Gene Expression Omnibus under accession number GSE15907 (www.ncbi.nlm.nih.gov/geo/query/acc.cgi?acc=GSE15907). Data were analyzed with the GenePattern genomic platform (www.broadinstitute.org/cancer/software/genepattern/). A common threshold for positive expression at 95% confidence across the data set was determined to be 120 (www.immgen.org/Protocols/ImmGen QC Documentation_ALL-DataGeneration_0612.pdf). Differences in gene expression were identified and visualized with the Multiplot module of GenePattern. Clustering analysis considered the 15% most variable genes. Genes were clustered (centered on the mean) with the Hierarchical Clustering module of GenePattern, employing Pearson's correlation as a metric, and data were visualized with the Hierarchical Clustering Viewer heat-map module. Enrichment for gene ontology terms was done using List2Networks software.[24]

Tissue sample preparation for flow cytometry

Peritoneal exudates were collected in 4 mL cold Hanks' balanced saline solution supplemented with EDTA (0.3 μM final) and bovine serum albumin (0.06% final) into the peritoneal cavity. LN and omentum cell suspensions were obtained after digestion of the teased organ in collagenase D (Roche) for 30 minutes. Cell suspensions were then stained with appropriate antibodies for 30 minutes on ice. Data were acquired on a BD FACS Canto II or BD Fortessa Flow Cytometer (BD Biosciences) and analyzed with FlowJo software (Treestar).

Adoptive transfer and competition assay

Peritoneal macrophages were retrieved by lavage from donors injected with thioglycollate 5 days earlier. These macrophages were derived from CD45.1 wild-type (WT) mice, CD45.2 CCR7$^{-/-}$ mice, CD68-hBcl2 mice (human Bcl2 cDNA expression driven by the mouse CD68 promoter),[22] or CD45.2 Bim$^{-/-}$ mice. Mixtures composed of 1:1 CD45.1 WT macrophage and CD45.2 macrophages from one of the respective CD45.2 strains were made. These mixtures were injected in CD45.1 × CD45.2 F1 recipients that also received thioglycollate 5 days earlier, with a total of 2 to 5 million macrophages from the 1:1 mixture injected into each recipient. Ratios at the time of injection were assessed by flow cytometry on the mixture prepared for injection. At day 8, the peritoneal lavage or LN was analyzed for the presence and ratio of the transferred cells.

Efferocytosis assay

Freshly isolated thymocytes were labeled with carboxyfluorescein diacetate succinimidyl ester (10 μM) and then treated with UV light for 10 minutes, followed by a 3-hour incubation at 37°C. Apoptotic thymocytes (2.5 × 10^{7} per mouse, 40% annexin V^{+}) were then injected intraperitoneally in mice that had received thioglycollate 5 days earlier. Peritoneal lavage was performed 30 minutes after carboxyfluorescein diacetate succinimidyl ester–labeled apoptotic thymocyte injection, and uptake was determined by flow cytometry.

Statistical analysis

Data are expressed as mean ± SEM. Statistical differences were assessed using a 2-tailed *t* test or analysis of variance (with Tukey's posttest analysis), using GraphPad Prism software. A *P* value of less than .05 was considered statistically significant.

Results

Resident and inflammatory macrophages during onset and resolution of acute inflammation

On induction of peritonitis after thioglycollate administration intraperitoneally, a prominent recruitment of leukocytes into the peritoneal cavity occurred within 24 hours, as expected,[15] followed by gradual clearance to reach steady-state numbers 8 days later (Figure 1A). Peak leukocyte accumulation at 24 hours was associated with a massive influx of neutrophils (Gr-1^{+} CD115^{lo} F4/80^{-}) and eosinophils (Gr-1^{int} CD115^{lo} F4/80^{+}) (Figure 1B). Neutrophils were cleared completely within 5 days, whereas eosinophils remained longer (Figure 1B). Macrophages prominently expressed CD115 (Csf-1 receptor). We noted, as previously described,[25] that 2 resident macrophage populations were present in the steady-state peritoneum: CD115^{+} F4/80^{lo} CD11c^{lo} CD36^{-} MHC-II^{+} macrophages (5%-10% of all CD115^{+} macrophages) and CD115^{+} F4/80^{hi} CD11c^{-} MHC-II^{-} (90%-95% of all CD115^{+} macrophages; Figure 1C, day 0). These populations are macrophages, as evidenced from gene expression profiling.[26]

Inflammatory macrophages appeared in the peritoneal cavity after induction of inflammation (Figure 1C; day 1, 5, 8, and 14) and were distinguished from resident macrophage populations by intermediate cell surface levels of F4/80 (Figure 1C). In addition, these inflammatory macrophages (CD115^{+} F4/80^{int}) expressed CD11c and

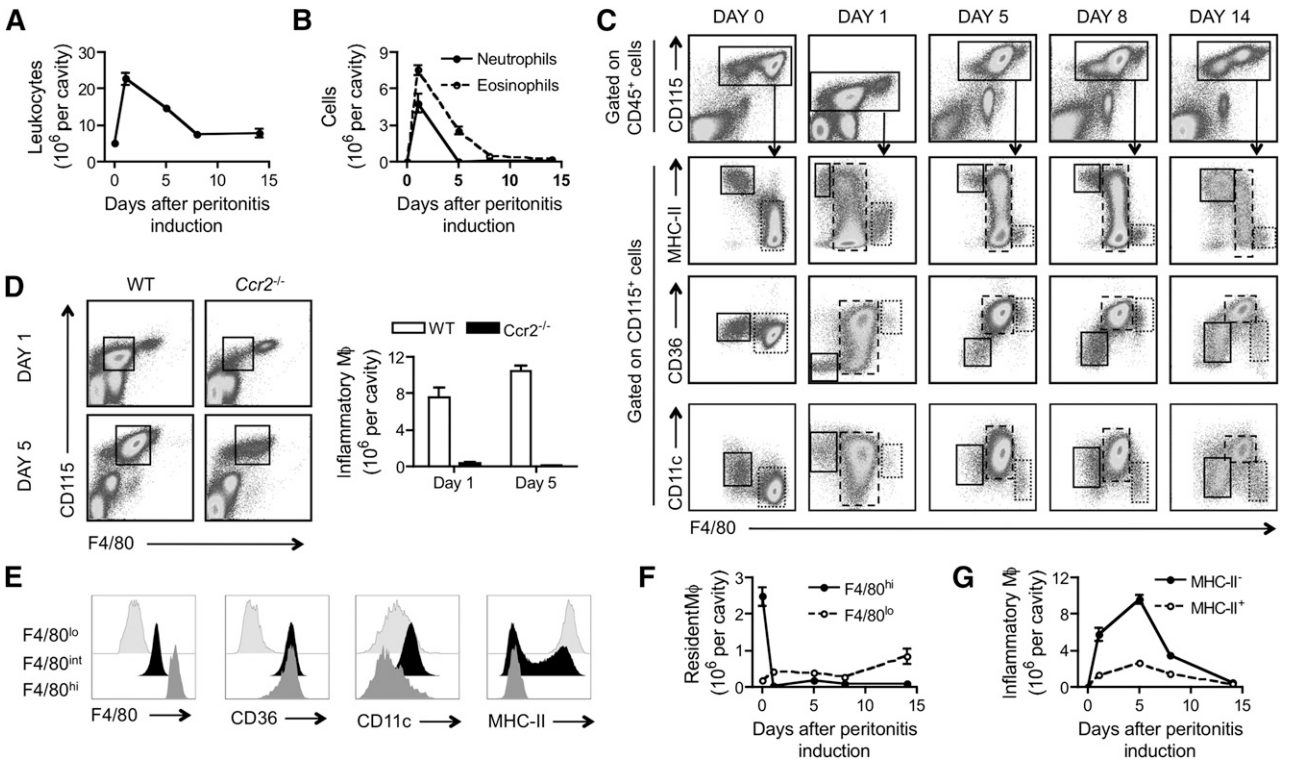

Figure 1. Phenotype and dynamics of resident and inflammatory macrophages during acute peritonitis. Quantification of total leukocytes (A) or granulocytes (neutrophils and eosinophils) (B) in the peritoneal cavity at the steady state and during a 14-day period after i.p. administration of thioglycollate. (C) Fluorescence-activated cell sorter (FACS) plots illustrating the gating strategy used for identification of macrophages at the steady state and during a 14-day period after i.p. administration of thioglycollate. Macrophages were found in CD115^{hi} gates (first row) at all times; CD115 expression on these cells was reduced at day 1. Three macrophage populations were discerned on the basis of F4/80 intensity, and these populations are depicted in the second through the fourth rows of the dot plots. F4/80^{low} macrophages (solid-line gates) and F4/80^{hi} macrophages (finely dotted gates) were resident macrophages, and inflammatory peritoneal macrophages (wide-dashed gates) appeared only in response to thioglycollate. (D) FACS plots illustrating the gating of inflammatory macrophages and corresponding cell counts in the peritoneum of CCR2-deficient mice and controls 1 and 5 days after initiation of peritonitis. (E) Comparison of F4/80, CD36, CD11c, and MHC-II cell surface expression levels between resident (F4/80^{low} and F4/80^{hi}) and inflammatory (F4/80^{int}) macrophages 5 days after initiation of peritonitis. (F) Quantification of resident macrophages and (G) inflammatory macrophages in the peritoneal cavity during the steady state and a 14-day period after i.p. administration of thioglycollate. Data are derived from at least 2 experiments performed with 5 replicates per experimental condition.

CD36. Approximately 20% to 30% of them displayed cell surface expression of MHC-II (Figure 1C). The gene expression profile of these inflammatory cells classified them as macrophages,[26] despite expression of CD11c and MHC-II that are also associated with dendritic cells (DCs) and despite their similar secretome to in vitro cultured granulocyte macrophage–CSF–derived DCs.[27] Inflammatory F4/80^{int} macrophages likely arose from circulating Ly-6C^{hi} monocytes, as their numbers were approximately 70-fold decreased 5 days after injection of thioglycollate in CCR2$^{-/-}$ mice with reduced circulating levels of Ly-6C^{hi} monocytes[28] and deficiency in monocyte trafficking into the inflamed peritoneum[29] (Figure 1D). Cell surface expression of CD36 and CD11c distinguished inflammatory macrophages (F4/80^{int}) from the 2 populations of resident macrophages (F4/80^{lo} and F4/80^{hi}) (Figure 1E). Thus, F4/80^{hi} and F4/80^{lo} cells represent tissue resident macrophage populations; whereas F4/80^{int} cells are Ly-6C^{hi} monocyte–derived inflammatory macrophages recruited after induction of peritonitis. As expected,[30] the dominant CD115^{+} F4/80^{hi} resident macrophages almost disappeared after initiation of inflammation (Figure 1F). Their numbers remained low at all times studied after thioglycollate was administered, including as long as days 8 to 14, when total leukocyte counts had returned to baseline (Figure 1F). In contrast, CD115^{+} F4/80^{low} resident macrophages were overall unchanged over time (Figure 1F). Both MHC-II^{+} and MHC-II^{-} inflammatory macrophages peaked in magnitude 5 days after injection of thioglycollate. Then they were cleared rapidly between day 5 and 8 (Figure 1G), as expected.[15,31] Thus, we chose the window of time between day 5 and 8 as the interval to study events associated with the clearance of inflammatory macrophages.

Gene expression signature of inflammatory macrophages

CD115^{+} F4/80^{int} MHC-II^{-} and CD115^{+} F4/80^{int} MHC-II^{+} cells were separately sorted from mice injected 5 days earlier with thioglycollate and further analyzed using microarray. In addition, gene expression profiles were carried out on resident CD115^{+} F4/80^{lo} MHC-II^{+} and CD115^{+} F4/80^{hi} MHC-II^{-} macrophages during the steady state and 5 days after thioglycollate injection. Clustering analysis of these populations revealed that CD115^{+} F4/80^{lo} macrophages clustered closely together with or without thioglycollate treatment (Figure 2A), and CD115^{+} F4/80^{hi} macrophages also clustered together with or without thioglycollate (Figure 2A). Furthermore, both MHC-II^{+} and MHC-II^{-} monocyte-derived inflammatory macrophages were more similar to each other than to the resident macrophages (Figure 2A). These clustering patterns confirm that cell surface levels of F4/80 for the different macrophage populations remain stable, and therefore are useful as means to track given populations after induction of inflammation with thioglycollate.

Focusing on the recruited inflammatory macrophages, the MHC-II^{+} and MHC-II^{-} populations were overall highly similar. Fewer than 200 genes were significantly different when the 2

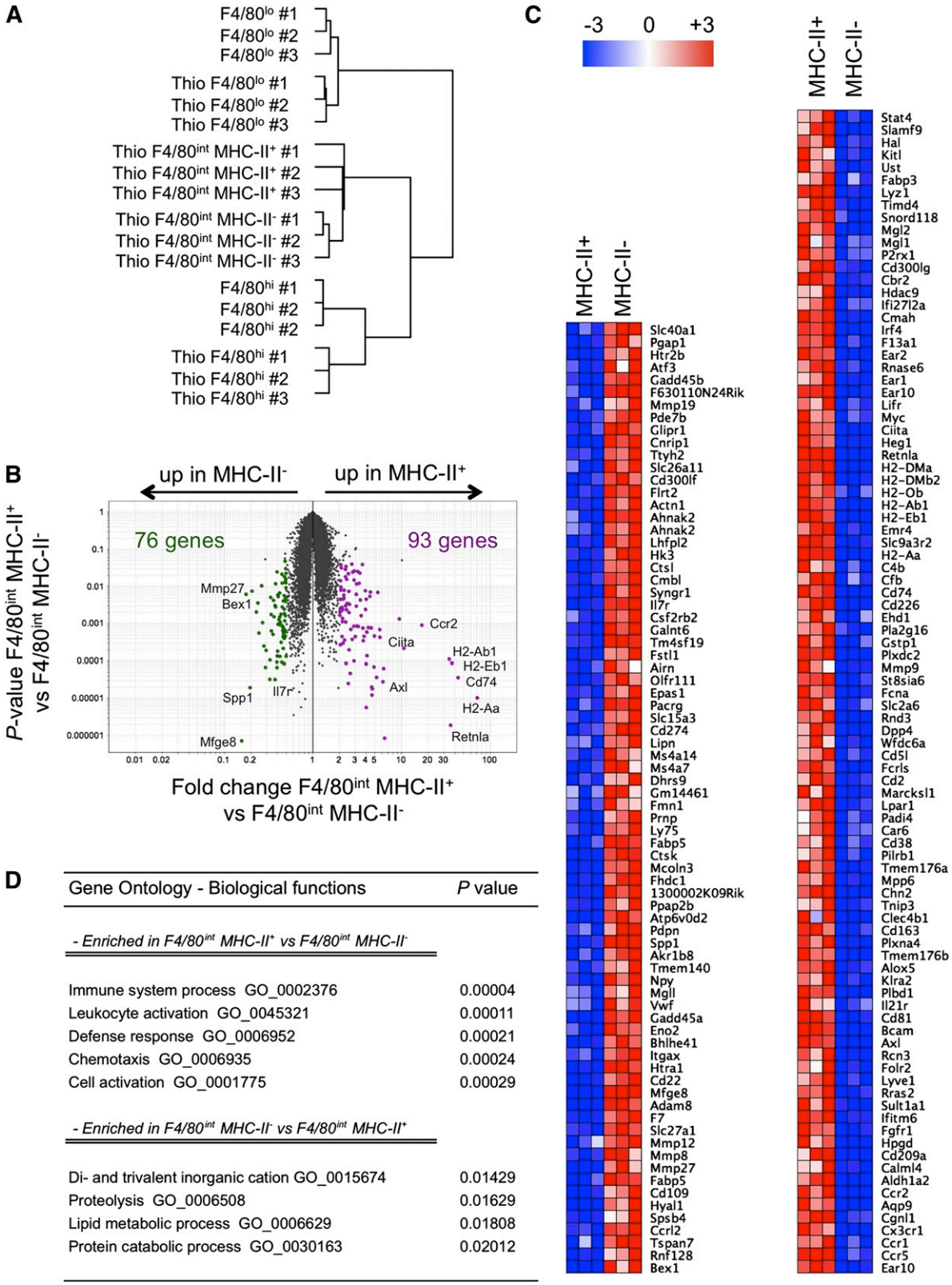

D

Gene Ontology - Biological functions	*P* value
- Enriched in F4/80^{int} MHC-II^{+} vs F4/80^{int} MHC-II^{-}	
Immune system process GO_0002376	0.00004
Leukocyte activation GO_0045321	0.00011
Defense response GO_0006952	0.00021
Chemotaxis GO_0006935	0.00024
Cell activation GO_0001775	0.00029
- Enriched in F4/80^{int} MHC-II^{-} vs F4/80^{int} MHC-II^{+}	
Di- and trivalent inorganic cation GO_0015674	0.01429
Proteolysis GO_0006508	0.01629
Lipid metabolic process GO_0006629	0.01808
Protein catabolic process GO_0030163	0.02012

Figure 2. Gene expression analysis of inflammatory macrophage populations. (A) Hierarchical clustering of steady-state and inflammatory macrophage populations (3 replicates for each populations) based on the 15% of genes with the greatest variability. (B) Volcano plot (*P* value vs fold change, with each dot representing 1 probe set), highlighting the 76 genes upregulated in MHC-II^{-} inflammatory macrophages (green) and the 93 genes upregulated in MHC-II^{+} inflammatory macrophages (purple). Some differentially expressed probe sets were tagged with the gene name they correspond to. (C) Heat map depicting genes differentially expressed ($P < .05$; fold > 2) between MHC-II^{-} and MHC-II^{+} inflammatory macrophages. (D) Pathways associated with differentially expressed genes between MHC-II^{-} and MHC-II^{+} inflammatory macrophages.

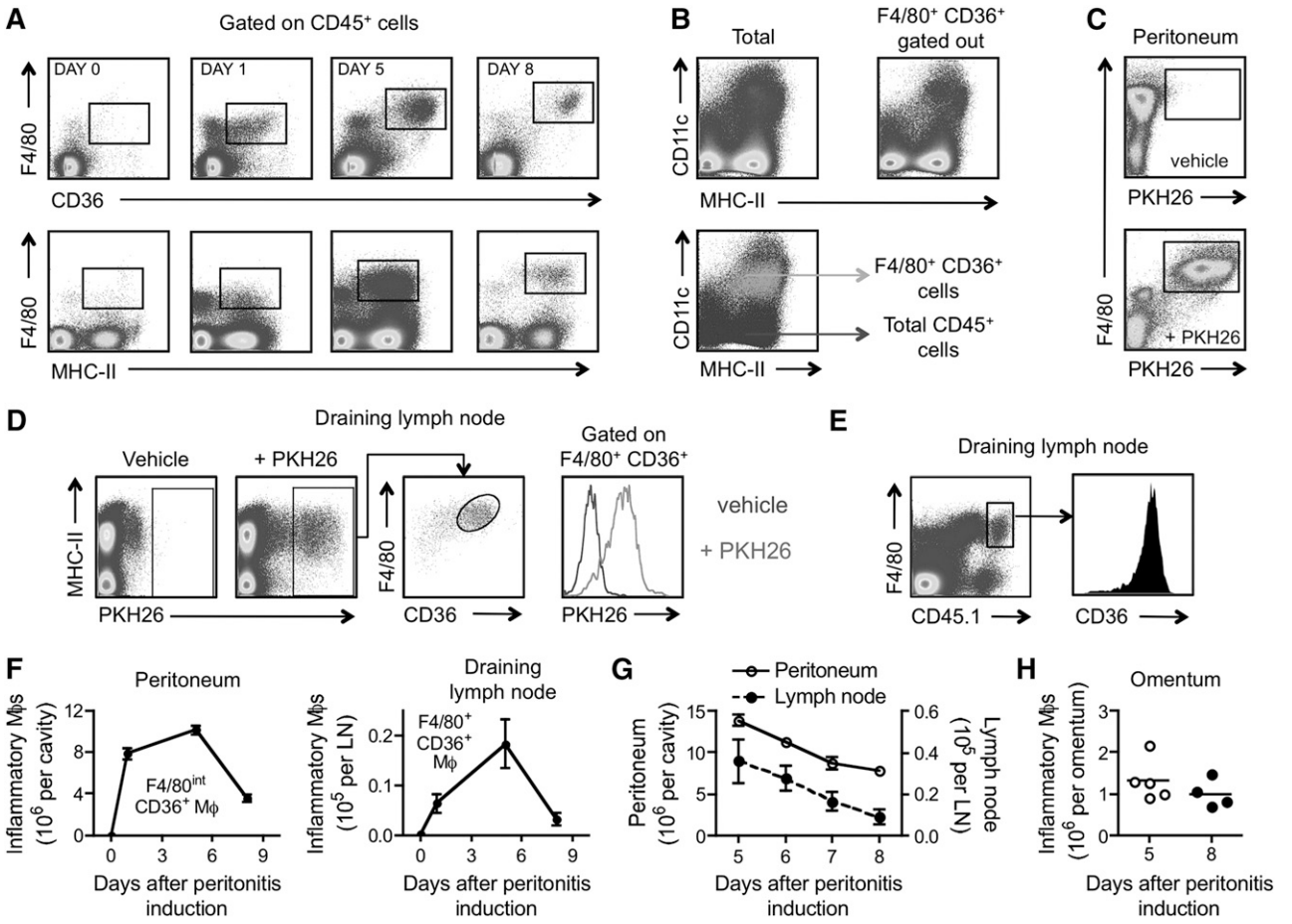

Figure 3. Kinetics of inflammatory macrophage migration to LNs. (A) FACS plots depicting the appearance of inflammatory macrophages ($F4/80^+CD36^+$ or $F4/80^+$ $MHC\text{-}II^+$) in the mediastinal LN over the course of 8 days after i.p. administration of thioglycollate. (B) Total LN cells (Left) or total cells with $F4/80^+$ $CD36^+$ cells gated out (Right) based on cell surface expression of CD11c and MHC-II. Bottom plot overlays $F4/80^+$ $CD36^+$ gated cells on total LN cells, plotted to show CD11c vs MHC-II. (C) Labeling of peritoneal inflammatory macrophages 24 hours after i.p. injection of the phagocytic tracer dye PKH26 in mice inflamed 2 days earlier by thioglycollate injection. (D) $PKH26^+$ cells were identified in the mediastinal LN 3 days after injection of PKH26 in the peritoneal cavity (5 days after inflammation was induced by thioglycollate) and analyzed for F4/80 and CD36 cell surface expression. Far-right plot shows PKH26 levels after gating on all $F4/80^+$ $CD36^+$ LN cells. (E) Inflammatory macrophages were retrieved from CD45.1 mice that had been injected 1 day earlier with thioglycollate. These macrophages were adoptively transferred into CD45.2 mice at the same stage of inflammation. $CD45.1^+$ inflammatory macrophages were gated in the mediastinal LN cell suspension (left FACS plot) 4 days later and analyzed for CD36 expression. (F-H) Inflammatory macrophages in the peritoneum, draining LN and omentum at different times after induction of peritonitis by thioglycollate (n = 4-6 mice per group per time point). Data are representative of at least 2 independent experiments.

populations were compared (≥twofold; $P < .05$; Figure 2B). The differentially regulated genes between the 2 populations are shown in Figure 2C, and included *Stat4*, *Mgl1* and *Mgl2*, *Irf4*, *Il21r*, and *Lyve1* upregulated in the $MHC\text{-}II^+$ macrophages (Figure 2C), whereas proteases were especially prominent in $MHC\text{-}II^-$ macrophages, including genes encoding cathepsins L and K and several metalloproteases (Figure 2C). Pathway analysis of the differentially expressed genes revealed pathways associated with proteolysis and lipid catabolic processes in $F4/80^{int}$ $MHC\text{-}II^-$ macrophages (Figure 2D), whereas pathways associated with T-cell activation and migratory behavior were enriched in $F4/80^{int}$ $MHC\text{-}II^+$ macrophages (Figure 2D). These data raised the possibility that $MHC\text{-}II^+$ inflammatory macrophages were poised to emigrate.

Emigration of macrophages to the LN peaks before the phase of clearance

We used flow cytometry to assess arrival of inflammatory macrophages in the mediastinal LN that drains the peritoneal cavity[15,32] after intraperitoneal thioglycollate administration. $F4/80^+$ $CD11c^+$ $CD36^+$ $MHC\text{-}II^+$ macrophages resembling the inflammatory $MHC\text{-}II^+$ macrophages from the peritoneum could be recovered from the inflamed, but not steady state, mediastinal LN (Figure 3A). The population was also absent from any other LNs tested (inguinal, mesenteric, and brachial) 5 days after induction of peritonitis. These cells fell into a typical DC gate with regard to their expression of CD11c and MHC-II (Figure 3B), but they expressed higher levels of F4/80 and CD36 compared with classical DCs. To confirm that these cells were from the inflamed peritoneal cavity, we injected the phagocytic tracer PKH26 into the thioglycollate-treated peritoneum (Figure 3C). Nearly all $PHK26^+$ cells in the mediastinal LN were $F4/80^+$ $CD36^+$ (and also $CD11c^+$ and $MHC\text{-}II^+$) (Figure 3D). Conversely, when we first gated on $F4/80^+$ $CD36^+$ cells in the LN, they were almost all $PKH26^+$ (Figure 3D). Transfer of peritoneal cells from thioglycollate-inflamed CD45.1 congenic mice into the peritoneum of thioglycollate-inflamed CD45.2 recipients also demonstrated that inflammatory CD45.1 macrophages migrated from the peritoneum to the mediastinal LN (Figure 3E), and all $F4/80^+CD45.1^+$ cells bore the $CD36^+$ phenotype (Figure 3E). Thus, $F4/80^+$ $CD36^+$ cells appearing in the mediastinal LN after thioglycollate injection in the peritoneum indeed originated from the peritoneum, and this phenotype included the majority of phagocytic cells that emigrated from the peritoneum.

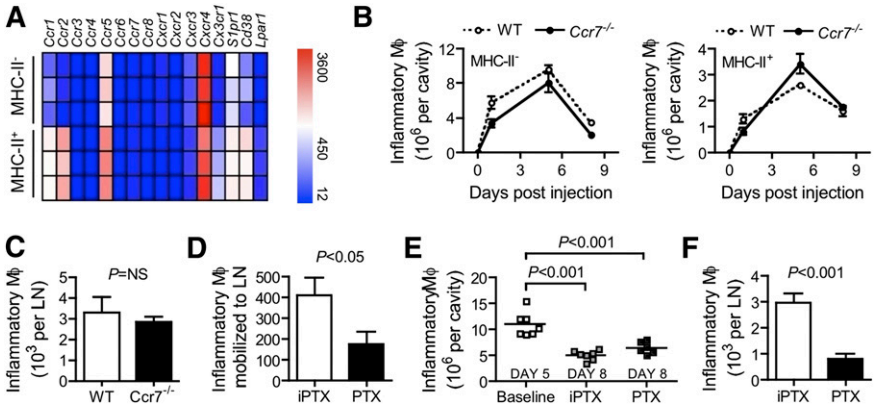

Figure 4. Blocking inflammatory macrophages migration marginally impaired their clearance during resolution. (A) Heat map showing the expression of chemotactic receptors in MHC-II$^-$ and MHC-II$^+$ inflammatory macrophages 5 days after intraperitoneal administration of thioglycollate (3 replicates were generated for each population). (B) Kinetics of MHC-II$^-$ and MHC-II$^+$ inflammatory macrophages during the course of thioglycollate-induced peritonitis in CCR7-deficient mice and controls (n = 5 mice per group per time). (C) Accumulation of inflammatory macrophage in the mediastinal LN of CCR7-deficient mice and controls 5 days after intraperitoneal administration of thioglycollate (n = 5 mice per group). (D) Mobilization to the mediastinal LN of adoptively transferred F4/80$^+$ CD36$^+$ CD45.1$^+$ inflammatory macrophages in CD45.2 mice injected with thioglycollate in the presence of PTX or iPTX (n = 5-7 per group). To maximize the recovery, cells and PTX or iPTX (single injection) were injected in the peritoneum at day 2, and LNs were analyzed at day 5. (E) Baseline number of inflammatory macrophage in the peritoneum at day 5 and numbers of macrophages recovered at day 8 after treatment with either active (PTX) or inactive (iPTX) pertussis toxin at day 5. Each symbol represents one mouse. (F) The number of F4/80$^+$CD36$^+$ macrophages recovered in the mediastinal LN at day 8 from the experiment in panel E, illustrating that active pertussis toxin prevented emigration to the LN.

When we used this strategy to identify and quantify macrophages in the mediastinal LN, the magnitude of inflammatory macrophage accumulation in the LN did not increase during the 5- to 8-day window when macrophages were clearing from the peritoneum, as would be expected if the LN were the major depot for the clearing cells. Instead, the accumulation of inflammatory macrophages in the LN roughly paralleled the kinetics of accumulated macrophages in the peritoneum, with a peak accumulation in the LN at day 5 before macrophage clearance from the peritoneum began (Figure 3F). A day-by-day analysis of inflammatory macrophages in the peritoneum and the LN from day 5 to day 8 further revealed a similar rate of decrease at both sites (Figure 3G). There was also no increase in macrophage numbers in the omentum during days 5 to 8, when macrophage numbers contracted (Figure 3H). Thus, macrophages emigrate to mediastinal LNs from the inflamed peritoneum, but the kinetics suggest that the LN is simply sampling a portion of the cells in the peritoneum, rather than serving as the target for removal of macrophages. If the latter were true, a transient increase in macrophages in the LN (or omentum) during the window from day 5 to day 8, when macrophages are lost from the peritoneum, would be expected.

Blocking CCR7-independent, Gαi-sensitive macrophage migration to the LN has a quantitatively minimal effect on macrophage contraction

LN-migrating macrophages were uniformly MHC-II$^+$. In the peritoneum, we observed a significant enrichment in genes involved in migratory behavior such as chemokine receptors (*Ccr2*, *Ccr5*, *Ccr1*, and *Cx3cr1*), the cyclic adenosine 5′-diphosphate-ribose hydrolase (*Cd38*), and sphingosine-1-phosphate receptor (*S1pr1*), selectively, in F4/80^{int} MHC-II$^+$ macrophages (Figures 2C and 4A). *Ccr7* mRNA was not detected in inflammatory macrophages in the peritoneum (Figure 4A). However, Ccr7 is, with little exception, universally associated with the migration of leukocytes to LNs through lymphatic vessels,[33,34] including the emigration of monocyte-derived cells from skin to draining LNs.[35] Discussion has argued that it would be essential for resolution of inflammation.[20] Thus, we tested whether CCR7 was needed for inflammatory macrophage migration to the mediastinal LN and resolution.

We injected CCR7-deficient animals with thioglycollate and followed the accumulation and clearance of inflammatory macrophages in the peritoneum. Other than a minor shift toward a slightly increased proportion of MHC-II$^+$ macrophages (Figure 4B), there was no difference in their accumulation or clearance during the resolution phase compared with WT controls (Figure 4B). The numbers of inflammatory macrophages that migrated to the LN at day 5 (peak macrophage accumulation) were similar between *Ccr7*$^{-/-}$ mice and WT controls (Figure 4C), illustrating that CCR7 is unnecessary for LN homing of macrophages. Chemokine receptors selectively expressed by MHC-II$^+$ inflammatory macrophages (Figure 4A) are all coupled to Gαi proteins, and are thus subject to inhibition by PTX. Thus, we adoptively transferred CD45.1$^+$ inflammatory macrophages in CD45.2$^+$ recipients and locally injected PTX or PTX inactivated by boiling (iPTX) simultaneously. PTX treatment substantially reduced migration of inflammatory macrophages to the mediastinal LN compared with treatment with iPTX (Figure 4D), revealing that emigration to the draining LN was dependent on Gαi-mediated signals. However, cohorts of mice injected with PTX (compared with iPTX) at the onset of resolution at day 5 had only a nonsignificant trend toward an increased number of inflammatory macrophages (+25%) that were retained in the peritoneum at day 8 (Figure 4E), even though we recovered few inflammatory macrophages from the LNs of the same PTX-treated mice (Figure 4F). PTX did not affect inflammatory macrophage survival, but it increased their proliferation (supplemental Figure 1A-B, available on the *Blood* Web site), although the percentage of proliferating cells was very low, which might explain the nonsignificant 25% increase in the number of inflammatory macrophages observed at day 8 in the PTX-treated group (Figure 4E). Thus, macrophage migration to LNs fails to account quantitatively for removal of macrophages during the phase of intense macrophage contraction observed during resolution.

Apoptosis of inflammatory macrophages promotes macrophage clearance during resolution

A key step necessary to allow for macrophage clearance is the shutdown in the recruitment of their precursors, circulating Ly-6C^{hi} monocytes.[31] The recruitment of neutrophils (gate ii, defined as Gr-1$^+$

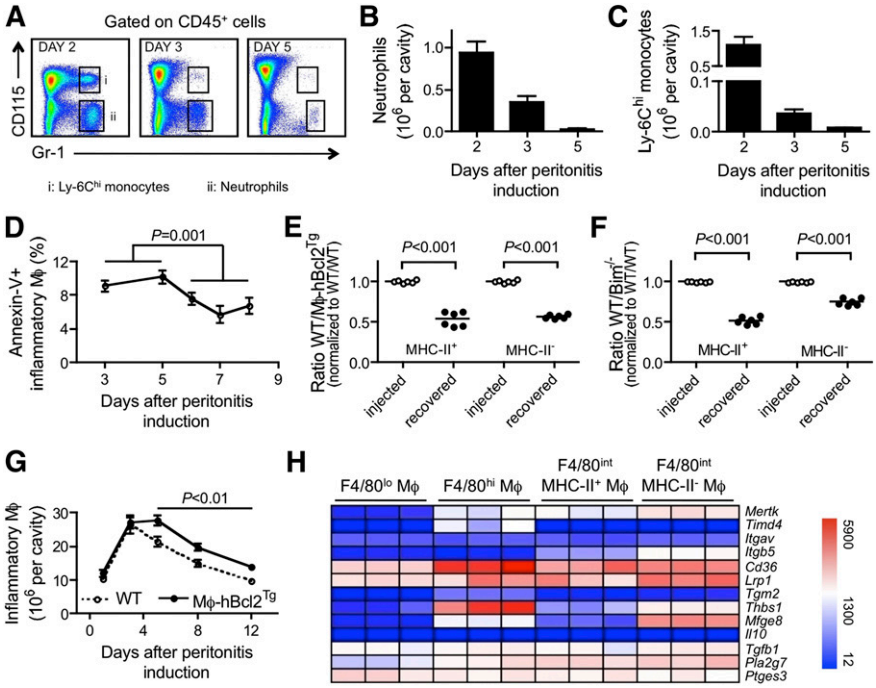

Figure 5. Inflammatory macrophages contraction during resolution is controlled by apoptotic cell death. (A) FACS plot illustrating the gating strategy used for neutrophils (ii, CD115$^-$ Gr-1$^+$) and Ly-6C^{hi} monocytes (i, CD115$^+$ Gr-1$^+$) in the inflamed peritoneal cavity. Quantification of neutrophils (B) as well as Ly-6C^{hi} monocytes (C) up to day 5 in mice injected with thioglycollate (n = 5 per time). (D) Quantification of annexin V staining in inflammatory macrophages from day 3 to 8 after intraperitoneal administration of thioglycollate (n = 5 per time). (E-F) Ratios of F4/80^{int} inflammatory macrophages competed after injection into thioglycollate-inflamed peritoneum at day 5 (injected) and recovered at day 8 (recovered). Two competitions are shown: between macrophages derived from WT and CD68-Bcl2 (Mϕ-hBcl2^{Tg}) transgenic mice and between macrophages derived from WT and Bim$^{-/-}$ mice. Each symbol represents data from 1 mouse. (G) Quantification of F4/80^{int} inflammatory macrophages in the peritoneal of irradiated recipient mice transplanted with bone marrow from CD68-Bcl2 (Mϕ-hBcl2^{Tg}) or WT mice during a 12-day period after i.p. administration of thioglycollate. (H) Heat maps depict gene expression patterns of mRNA transcripts that mediate or are induced in response to efferocytosis. Three replicates are shown for different macrophage populations.

CD115$^-$) and Ly-6C^{hi} monocytes (gate i, Gr-1$^+$ CD115$^+$) gradually and dramatically decreased before the onset of resolution (Figure 5B-C). However, cessation in recruitment alone could not account for a net reduction in macrophage numbers. Thus, we wondered whether concomitant local death would promote macrophage contraction between days 5 and 8 after intraperitoneal thioglycollate injection. F4/80^{int} inflammatory macrophages recovered from the peritoneum showed annexin V$^+$–positive cells, even as early as day 3 (Figure 5D). Annexin V–reactive macrophages were relatively more abundant, approaching 8% at early stages of resolution, and were present at all times studied (Figure 5D). To obtain a quantitative sense of the importance of apoptosis in macrophage clearance, we induced peritonitis using thioglycollate in 3 cohorts of mice, including CD45.1 WT mice, CD45.1 × CD45.2 F1 hybrid WT mice, and CD45.2 transgenic mice containing a transgene in which the CD68 promoter was used to drive expression of the antiapoptotic factor Bcl2.[22] In all cohorts of mice, we injected thioglycollate and maintained the mice until day 5. Macrophages from CD45.1 WT and CD45.2 CD68-Bcl2 transgenic mice were mixed 1:1 and then immediately transferred to the site of peritonitis in the CD45.1 × CD45.2 F1 WT mice. We then recovered cell suspensions of the peritoneal lavage at day 8. CD68-Bcl2 transgenic (Tg) macrophages cleared less efficiently from the peritoneum than nontransgenic WT cells, such that in the 3-day period of analysis, the Bcl2-overexpressing macrophages represented two-thirds of the transferred macrophages (Figure 5E). As expected, overexpression of Bcl2 reduced, although it did not eliminate, death by apoptosis (supplemental Figure 2A); it did not affect proliferation (supplemental Figure 2B).

When we repeated this experiment, substituting CD68-Bcl2 transgenic macrophages with macrophages from Bim$^{-/-}$ mice, the same outcome was observed, in which Bim$^{-/-}$ macrophages that are partially resistant to death[36] came to dominate over WT macrophages locally in the peritoneum during resolution of thioglycollate-induced peritonitis (Figure 5F).

Next we performed a detailed kinetic analysis of F4/80^{int} inflammatory macrophages in irradiated recipients mice repopulated with bone marrow from CD68-Bcl2 transgenic or WT mice during the course of thioglycollate-induced peritonitis. The appearance of inflammatory macrophages in the peritoneal cavity was comparable between both genotypes until day 3 (Figure 5G). However, macrophages from CD68-Bcl2 transgenic mice showed no contraction between days 3 and 5, whereas WT macrophages contracted (Figure 5G). Accumulation in draining LNs was comparable in both groups (supplemental Figure 2C). Together, these data indicate that local death accounts for macrophage contraction during inflammatory resolution and further suggest that efficient efferocytosis would be crucial to promote resolution. Using our microarray data, we probed the expression of key molecules involved in apoptotic cell clearance, as well as the response to efferocytosis (*Tgfb1, Pla2g7, Ptges3*) (Figure 5H). These data revealed that F4/80^{hi} resident and F4/80^{int} inflammatory macrophages seemed overall better-equipped than F4/80^{lo} resident macrophage for efferocytic function, as they expressed higher levels of *Mertk*, *Cd36*, and *Lrp1*, for example. This was confirmed experimentally after injecting exogenous apoptotic cells in vivo into the peritoneum of mice injected 5 days earlier with thioglycollate (supplemental Figure 3). Finally, all macrophages expressed *Tgfb1*, but not *Il10*, as well as the genes encoding the enzymes producing the lipid mediators PAF (*Pla2g7*) and PGE2 (*Ptges3*), all of which are induced in response to efferocytosis.[37]

Discussion

Resolution of inflammation is a key homeostatic response to injury critical to maintain tissue integrity. However, the fundamental mechanisms underlying the removal of infiltrated inflammatory macrophages are poorly understood. For decades, different studies have argued variably for local apoptosis,[11-13] akin to the mechanism removing neutrophils,[6,7] vs emigration to LNs[15] as the fundamental process governing macrophage removal. Although in fact only a single study, that of Bellingan and colleages,[15] concluded that emigration to LNs dominated, the conclusions of this single study have taken hold in the field. Others argued that CD36[38] and CD11b[39-41]

could modulate macrophage migration and thereby delay resolution, but they used a model of "resolution" that is triggered by lipopolysaccharide (LPS),[39] even though LPS promotes, rather than resolves, inflammation. The current study used the model of thioglycollate-induced peritoneal inflammation similarly to Bellingan and colleagues, although seemingly minor differences existed, including volume of injection and supplier. Local apoptosis can be difficult to appreciate because of the rapid and seemingly "invisible" clearance of apoptotic cells at the histological level. We got around this problem using a competitive approach that would allow us to quantity whether the ability to die (or emigrate) conferred a disadvantage to resolution. Although a low level of emigration of macrophages to LNs occurred during resolution of thioglycollate-induced inflammation, the concept that emigration is either required for or serves as the major mechanism in removing macrophages from resolving inflammatory lesions failed to stand. Instead, the fundamental mechanism most relevant to removal of macrophages is none other than local apoptosis. This revised concept will now need to be tested, using other models of inflammation in the peritoneum as well as in other tissues, but resolution of inflammation in the heart already appears to follow the paradigm we observe here.[42]

We argue that the straightforward body of work presented here is of fundamental importance with respect to how data in the literature are interpreted. Indeed, the Bellingan study has strongly influenced the interpretation and design of many studies. For example, a few years ago, we discussed how impaired macrophage emigration out of atherosclerotic vessels could negatively affect the course of atherosclerosis if this process were required for resolution.[17,43,44] However, when we observed that macrophage contraction from plaques did not depend on emigration out of the plaque environment,[21] we were prompted to return to studies of acute inflammation and reconsider how macrophages are cleared therein. We then recognized that the study of Bellingan and colleagues was generally qualitative and needed further investigation. Other studies have discussed their own findings with interpretations that reflect an assumption that the conclusions of Bellingan and colleagues are correct.[10,20] Indeed, lipid mediators that promote resolution, including resolvins and protectins, increase migration of macrophages to LNs,[10] but it remains unclear whether this is their dominant means for controlling macrophage burden. It would now be valuable to evaluate the role of resolvins and protectins, along with other mediators associated with macrophage removal, such as CD36[38] and netrin,[20] in monocyte recruitment and macrophage apoptosis. Although the implications of our work include the idea that macrophage apoptosis is beneficial to the resolution of inflammation, we recognize that in a context such as atherosclerosis, the failure to clear apoptotic bodies through efferocytosis can significantly diminish the benefits of macrophage death and even contribute to disease pathology.[45] Along these lines, developing mouse models that would allow for inducible and macrophage-specific alterations of efferocytic pathways would be useful to probe the requirement of this process in favoring silent inflammatory macrophage removal during resolution.

Even if the majority of macrophages are not cleared via emigration to LNs through lymphatic vessels, lymphatic transport is still a vital route for resolution of inflammation. For example, the decoy chemokine receptor D6 that sequesters and removes pro-inflammatory chemokines[46] is primarily expressed on lymphatic vessels.[47] Furthermore, removal of soluble mediators through the lymph is critical for resolution.[47] Indeed, in the context of atherosclerosis, our recent work revealed that cholesterol loaded onto high-density lipoproteins is cleared from tissues, including the artery wall, through the lymphatic vasculature, suggesting that intact lymphatic drainage would be important in the resolution of atherosclerosis.[48] Furthermore, although our data suggest that macrophage emigration to LNs during resolution of inflammation does not quantitatively prevail in the removal of macrophages and that the emigration is not otherwise essential for resolution (or else pertussis toxin would have delayed resolution), there is likely some relevance to the migration that does occur. For instance, emigratory macrophages may contribute to antigen presentation in the LN that, for pathogens, may be essential for mounting a response needed to ultimately eradicate the cause of the inflammatory response in the first place.[31] All emigratory macrophages in the LNs were MHC-II$^+$, and their MHC-II$^+$ counterparts in the peritoneum expressed many genes relevant to antigen presentation. Although they bore many features of dendritic cells, these cells could not be classified as dendritic cells by gene expression profiling[26,49]; instead, their expression profile is that of a macrophage. Genes associated with migration to LNs strongly cluster with dendritic cells, including CCR7, and did not appear to be induced in inflammatory macrophages. CCR7 also mediates the emigration of T cells[34] and neutrophils[50] to LNs from the skin, so we suspected it would govern the emigration of inflammatory macrophages from the peritoneum to the mediastinal LN. However, surprisingly, we found that CCR7 was not required for this step. This instance is one of only few documented cases in which emigration to LNs is CCR7-independent. Another example is found in chronic skin inflammation.[34] Thus, if CCR7 is a mediator of resolution, as recently proposed,[19,20] its role in resolution may not directly relate to a role in macrophage migration from the inflammatory environment.

In closing, this study revises the conclusions of an earlier influential body of work and, in so doing, alters the fundamental cellular pathways that merit strong consideration for therapeutics that seek to recapitulate the events that promote resolution of inflammation.

Acknowledgments

The authors thank Gerald Morris for help with mice irradiation. The authors thank the Immunological Genome Project for microarray and bioinformatics support associated with this work.

This work was funded by National Institutes of Health grants R01 AI049653 and R01 AI061741 (to G.J.R.). E.G. was supported in part by a postdoctoral fellowship from the American Heart Association, Heritage Affiliate (10POST4160140). The Immunological Genome Project is funded by R24 AI072073 to Christophe Benoist (Harvard Medical School). Earlier studies included in this body of work were carried out at the Mount Sinai School of Medicine before the laboratory relocated to the Washington University School of Medicine.

Authorship

Contribution: E.L.G. designed and conducted experiments and wrote the manuscript; S.I. conducted experiments; P.L. provided key reagents; and G.J.R. designed and supervised experiments and wrote the manuscript.

Conflict-of-interest disclosure: The authors declare no competing financial interests.

Correspondence: Gwendalyn J. Randolph, Department of Pathology & Immunology, Washington University School of Medicine, 660 South Euclid Ave, Campus Box 8118, St. Louis, MO 63110; email: grandolph@path.wustl.edu.

References

1. Buckley CD, Gilroy DW, Serhan CN, Stockinger B, Tak PP. The resolution of inflammation. *Nat Rev Immunol.* 2013;13(1):59-66.
2. Hotamisligil GS. Endoplasmic reticulum stress and the inflammatory basis of metabolic disease. *Cell.* 2010;140(6):900-917.
3. Grivennikov SI, Greten FR, Karin M. Immunity, inflammation, and cancer. *Cell.* 2010;140(6): 883-899.
4. Glass CK, Saijo K, Winner B, Marchetto MC, Gage FH. Mechanisms underlying inflammation in neurodegeneration. *Cell.* 2010;140(6):918-934.
5. Nathan C, Ding A. Nonresolving inflammation. *Cell.* 2010;140(6):871-882.
6. Lawrence T, Willoughby DA, Gilroy DW. Anti-inflammatory lipid mediators and insights into the resolution of inflammation. *Nat Rev Immunol.* 2002;2(10):787-795.
7. Serhan CN, Chiang N, Van Dyke TE. Resolving inflammation: dual anti-inflammatory and pro-resolution lipid mediators. *Nat Rev Immunol.* 2008;8(5):349-361.
8. Fadok VA, Bratton DL, Henson PM. Phagocyte receptors for apoptotic cells: recognition, uptake, and consequences. *J Clin Invest.* 2001;108(7): 957-962.
9. Huynh ML, Fadok VA, Henson PM. Phosphatidylserine-dependent ingestion of apoptotic cells promotes TGF-beta1 secretion and the resolution of inflammation. *J Clin Invest.* 2002; 109(1):41-50.
10. Schwab JM, Chiang N, Arita M, Serhan CN. Resolvin E1 and protectin D1 activate inflammation-resolution programmes. *Nature.* 2007;447(7146):869-874.
11. Tidball JG, St Pierre BA. Apoptosis of macrophages during the resulution of muscle inflammation. *J Leukoc Biol.* 1996;59(3):380-388.
12. Lan HY, Mitsuhashi H, Ng YY, Nikolic-Paterson DJ, Yang N, Mu W, Atkins RC. Macrophage apoptosis in rat crescentic glomerulonephritis. *Am J Pathol.* 1997;151(2):531-538.
13. Kuhlmann T, Bitsch A, Stadelmann C, Siebert H, Brück W. Macrophages are eliminated from the injured peripheral nerve via local apoptosis and circulation to regional lymph nodes and the spleen. *J Neurosci.* 2001;21(10):3401-3408.
14. Janssen WJ, Barthel L, Muldrow A, et al. Fas determines differential fates of resident and recruited macrophages during resolution of acute lung injury. *Am J Respir Crit Care Med.* 2011; 184(5):547-560.
15. Bellingan GJ, Caldwell H, Howie SE, Dransfield I, Haslett C. In vivo fate of the inflammatory macrophage during the resolution of inflammation: inflammatory macrophages do not die locally, but emigrate to the draining lymph nodes. *J Immunol.* 1996;157(6):2577-2585.
16. Merched AJ, Ko K, Gotlinger KH, Serhan CN, Chan L. Atherosclerosis: evidence for impairment of resolution of vascular inflammation governed by specific lipid mediators. *FASEB J.* 2008; 22(10):3595-3606.
17. Randolph GJ. Emigration of monocyte-derived cells to lymph nodes during resolution of inflammation and its failure in atherosclerosis. *Curr Opin Lipidol.* 2008;19(5):462-468.
18. Llodrá J, Angeli V, Liu J, Trogan E, Fisher EA, Randolph GJ. Emigration of monocyte-derived cells from atherosclerotic lesions characterizes regressive, but not progressive, plaques. *Proc Natl Acad Sci USA.* 2004;101(32):11779-11784.
19. Trogan E, Feig JE, Dogan S, et al. Gene expression changes in foam cells and the role of chemokine receptor CCR7 during atherosclerosis regression in ApoE-deficient mice. *Proc Natl Acad Sci USA.* 2006;103(10):3781-3786.
20. van Gils JM, Derby MC, Fernandes LR, et al. The neuroimmune guidance cue netrin-1 promotes atherosclerosis by inhibiting the emigration of macrophages from plaques. *Nat Immunol.* 2012; 13(2):136-143.
21. Potteaux S, Gautier EL, Hutchison SB, et al. Suppressed monocyte recruitment drives macrophage removal from atherosclerotic plaques of Apoe-/- mice during disease regression. *J Clin Invest.* 2011;121(5):2025-2036.
22. Gautier EL, Huby T, Witztum JL, et al. Macrophage apoptosis exerts divergent effects on atherogenesis as a function of lesion stage. *Circulation.* 2009;119(13):1795-1804.
23. Gautier EL, Huby T, Ouzilleau B, et al. Enhanced immune system activation and arterial inflammation accelerates atherosclerosis in lupus-prone mice. *Arterioscler Thromb Vasc Biol.* 2007; 27(7):1625-1631.
24. Lachmann A, Ma'ayan A. Lists2Networks: integrated analysis of gene/protein lists. *BMC Bioinformatics.* 2010;11:87.
25. Ghosn EE, Cassado AA, Govoni GR, et al. Two physically, functionally, and developmentally distinct peritoneal macrophage subsets. *Proc Natl Acad Sci USA.* 2010;107(6):2568-2573.
26. Gautier EL, Shay T, Miller J, et al; Immunological Genome Consortium. Gene-expression profiles and transcriptional regulatory pathways that underlie the identity and diversity of mouse tissue macrophages. *Nat Immunol.* 2012;13(11): 1118-1128.
27. Becker L, Liu NC, Averill MM, et al. Unique proteomic signatures distinguish macrophages and dendritic cells. *PLoS ONE.* 2012;7(3):e33297.
28. Serbina NV, Pamer EG. Monocyte emigration from bone marrow during bacterial infection requires signals mediated by chemokine receptor CCR2. *Nat Immunol.* 2006;7(3):311-317.
29. Tsou CL, Peters W, Si Y, et al. Critical roles for CCR2 and MCP-3 in monocyte mobilization from bone marrow and recruitment to inflammatory sites. *J Clin Invest.* 2007;117(4):902-909.
30. Barth MW, Hendrzak JA, Melnicoff MJ, Morahan PS. Review of the macrophage disappearance reaction. *J Leukoc Biol.* 1995;57(3):361-367.
31. Gautier EL, Chow A, Spanbroek R, et al. Systemic analysis of PPARγ in mouse macrophage populations reveals marked diversity in expression with critical roles in resolution of inflammation and airway immunity. *J Immunol.* 2012;189(5):2614-2624.
32. Kool M, Soullié T, van Nimwegen M, et al. Alum adjuvant boosts adaptive immunity by inducing uric acid and activating inflammatory dendritic cells. *J Exp Med.* 2008;205(4):869-882.
33. Randolph GJ, Angeli V, Swartz MA. Dendritic-cell trafficking to lymph nodes through lymphatic vessels. *Nat Rev Immunol.* 2005;5(8):617-628.
34. Brown MN, Fintushel SR, Lee MH, et al. Chemoattractant receptors and lymphocyte egress from extralymphoid tissue: changing requirements during the course of inflammation. *J Immunol.* 2010;185(8):4873-4882.
35. Qu C, Edwards EW, Tacke F, et al. Role of CCR8 and other chemokine pathways in the migration of monocyte-derived dendritic cells to lymph nodes. *J Exp Med.* 2004;200(10):1231-1241.
36. Bouillet P, Metcalf D, Huang DC, et al. Proapoptotic Bcl-2 relative Bim required for certain apoptotic responses, leukocyte homeostasis, and to preclude autoimmunity. *Science.* 1999;286(5445):1735-1738.
37. Fadok VA, Bratton DL, Konowal A, Freed PW, Westcott JY, Henson PM. Macrophages that have ingested apoptotic cells in vitro inhibit proinflammatory cytokine production through autocrine/paracrine mechanisms involving TGF-beta, PGE2, and PAF. *J Clin Invest.* 1998;101(4): 890-898.
38. Park YM, Febbraio M, Silverstein RL. CD36 modulates migration of mouse and human macrophages in response to oxidized LDL and may contribute to macrophage trapping in the arterial intima. *J Clin Invest.* 2009;119(1):136-145.
39. Kataru RP, Jung K, Jang C, et al. Critical role of CD11b+ macrophages and VEGF in inflammatory lymphangiogenesis, antigen clearance, and inflammation resolution. *Blood.* 2009;113(22):5650-5659.
40. Gomez IG, Tang J, Wilson CL, et al. Metalloproteinase-mediated Shedding of Integrin β2 promotes macrophage efflux from inflammatory sites. *J Biol Chem.* 2012;287(7): 4581-4589.
41. Schif-Zuck S, Gross N, Assi S, Rostoker R, Serhan CN, Ariel A. Saturated-efferocytosis generates pro-resolving CD11b low macrophages: modulation by resolvins and glucocorticoids. *Eur J Immunol.* 2011;41(2): 366-379.
42. Leuschner F, Rauch PJ, Ueno T, et al. Rapid monocyte kinetics in acute myocardial infarction are sustained by extramedullary monocytopoiesis. *J Exp Med.* 2012;209(1): 123-137.
43. Qin C, Nagao T, Grosheva I, Maxfield FR, Pierini LM. Elevated plasma membrane cholesterol content alters macrophage signaling and function. *Arterioscler Thromb Vasc Biol.* 2006;26(2): 372-378.
44. Pagler TA, Wang M, Mondal M, et al. Deletion of ABCA1 and ABCG1 impairs macrophage migration because of increased Rac1 signaling. *Circ Res.* 2011;108(2):194-200.
45. Tabas I. Macrophage death and defective inflammation resolution in atherosclerosis. *Nat Rev Immunol.* 2010;10(1):36-46.
46. Fra AM, Locati M, Otero K, et al. Cutting edge: scavenging of inflammatory CC chemokines by the promiscuous putatively silent chemokine receptor D6. *J Immunol.* 2003;170(5):2279-2282.
47. Lee KM, Nibbs RJ, Graham GJ. D6: the 'crowd controller' at the immune gateway. *Trends Immunol.* 2013;34(1):7-12.
48. Martel C, Li W, Fulp B, et al. Lymphatic vasculature mediates macrophage reverse cholesterol transport in mice. *J Clin Invest.* 2013; 123(4):1571-1579.
49. Miller JC, Brown BD, Shay T, et al; Immunological Genome Consortium. Deciphering the transcriptional network of the dendritic cell lineage. *Nat Immunol.* 2012;13(9):888-899.
50. Beauvillain C, Cunin P, Doni A, et al. CCR7 is involved in the migration of neutrophils to lymph nodes. *Blood.* 2011;117(4):1196-1204.

Published July 14, 2014

JEM

Gata6 regulates aspartoacylase expression in resident peritoneal macrophages and controls their survival

Emmanuel L. Gautier,[1] Stoyan Ivanov,[1] Jesse W. Williams,[1] Stanley Ching-Cheng Huang,[1] Genevieve Marcelin,[3] Keke Fairfax,[1] Peter L. Wang,[1] Jeremy S. Francis,[4] Paola Leone,[4] David B. Wilson,[2] Maxim N. Artyomov,[1] Edward J. Pearce,[1] and Gwendalyn J. Randolph[1]

[1]Department of Pathology and Immunology and [2]Department of Pediatrics, Washington University School of Medicine, St. Louis, MO 63110
[3]Department of Medicine, Albert Einstein School of Medicine, Bronx, NY 10461
[4]Department of Cell Biology, Rowan University School of Osteopathic Medicine, Stratford, NJ 08084

The transcription factor Gata6 regulates proliferation and differentiation of epithelial and endocrine cells and cancers. Among hematopoietic cells, Gata6 is expressed selectively in resident peritoneal macrophages. We thus examined whether the loss of Gata6 in the macrophage compartment affected peritoneal macrophages, using Lyz2-Cre x Gata6$^{flox/flox}$ mice to tackle this issue. In Lyz2-Cre x Gata6$^{flox/flox}$ mice, the resident peritoneal macrophage compartment, but not macrophages in other organs, was contracted, with only a third the normal number of macrophages remaining. Heightened rates of death explained the marked decrease in peritoneal macrophage observed. The metabolism of the remaining macrophages was skewed to favor oxidative phosphorylation and alternative activation markers were spontaneously and selectively induced in Gata6-deficient macrophages. Gene expression profiling revealed perturbed metabolic regulators, including aspartoacylase (Aspa), which facilitates generation of acetyl CoA. Mutant mice lacking functional Aspa phenocopied the higher propensity to death and led to a contraction of resident peritoneal macrophages. Thus, Gata6 regulates differentiation, metabolism, and survival of resident peritoneal macrophages.

CORRESPONDENCE
Gwendalyn J. Randolph:
grandolph@path.wustl.edu

Abbreviations used: Aspa, aspartoacylase; Gata6$^{\Delta Mac}$, Lyz2-Cre x Gata6$^{flox/flox}$.

Implicated in both tissue damage and repair, resident macrophages regulate numerous homeostatic, developmental, and host defense responses, rendering them therapeutic targets (Davies et al., 2013) where it might be desirable to selectively impact discrete macrophage populations. Recent studies confirm resident macrophages in adult mice sustain their own homeostasis through local proliferation, rather than replenishment from blood monocytes (Schulz et al., 2012; Hashimoto et al., 2013; Yona et al., 2013). Marked diversity in gene expression among macrophages residing in different organs suggests that distinct transcriptional programs may affect the maintenance of only single macrophage populations. For example, Spi-C is selectively expressed by red pulp macrophages, and it is essential for sustenance of this population, apparently due to its role in coordinating gene expression that facilitates handling of iron in macrophages that recycle aged erythrocytes (Kohyama et al., 2009; Haldar et al., 2014). Recently, we found that Gata6 is selectively expressed by resident peritoneal macrophages and predicted a set of peritoneal macrophage-specific genes that may be controlled by Gata6 in this population (Gautier et al., 2012). Subsequently, two studies identified a role for Gata6 in controlling the peritoneal macrophage pool (Okabe and Medzhitov, 2014; Rosas et al., 2014), including evidence that the ability of macrophages

S. Ivanov and J.W. Williams contributed equally to this paper.

E.L. Gautier's present address is INSERM UMR_S 1166, Sorbonne Universités, UPMC Univ Paris 06, Hôpital de la Pitié, 75651.

The Rockefeller University Press $30.00
J. Exp. Med. 2014 Vol. 211 No. 8 1525-1531
www.jem.org/cgi/doi/10.1084/jem.20140570

Supplemental Material can be found at:
http://jem.rupress.org/content/suppl/2014/07/10/jem.20140570.DC1.html

Published July 14, 2014

to proliferate during an inflammatory challenge was compromised (Rosas et al., 2014) and identification of retinoic acid as a signal that induces Gata6 in peritoneal macrophages (Okabe and Medzhitov, 2014). However, neither study explained what cellular events caused contraction of the macrophage pool within the peritoneum under resting conditions. Here, we show that apoptosis is induced in peritoneal macrophages in the absence of Gata6, at least in part because Gata6 expression either directly or indirectly supported expression of aspartoacylase (Aspa) that deacetylates *N*-acetyl aspartate. Mice bearing mutations in Aspa likewise displayed reduced macrophage counts concomitant with increased death. However, only the more global Gata6 deficiency, but not single deficiency in Aspa, resulted in a selective and seemingly cell autonomous polarization of peritoneal macrophages toward an alternatively activated phenotype. Collectively, these data delineate a role for Gata6 in regulating macrophage survival and activation state.

RESULTS AND DISCUSSION

The transcription factor Gata6 was expressed only in F4/80^{hi} peritoneal macrophages, corresponding with ICAM-2^{+} peritoneal macrophages (Gautier et al., 2012), within the entire hematopoietic system (Fig. 1, A and B). Thus, we crossed mice expressing the Cre recombinase downstream of the Lyz2 promoter, active in myeloid cells including macrophages (Clausen et al., 1999), with mice bearing floxed Gata6 alleles (Sodhi et al., 2006), generating mice specifically lacking Gata6 in macrophages (Gata6$^{\Delta Mac}$) to be compared with controls bearing the floxed alleles in the absence of Cre recombinase (Gata6$^{flox/flox}$; Fig. 1 C). Total cell numbers from the peritoneum were reduced by 25 ± 13%. Moreover, the frequency of F4/80^{hi} ICAM-2^{+} was selectively reduced in Gata6$^{\Delta Mac}$ mice, to 54 ± 16% of control mice. Together, these changes led to a marked reduction in Gata6$^{\Delta Mac}$ peritoneal macrophages compared with control mice (Fig. 1 D). A second, minor CD115^{+} F4/80^{lo} ICAM-2^{lo} macrophage population residing in the peritoneum (Gautier et al., 2013), which did not express Gata6 (Fig. 1 B), was unaffected in Gata6$^{\Delta Mac}$ mice (Fig. 1 E). Macrophage frequency in other organs was unchanged (Fig. 1 E). Increased activated caspase 3 and Annexin V in Gata6$^{\Delta Mac}$ macrophages revealed augmented apoptosis (Fig. 1 F). Consistent with previous work (Jenkins et al., 2013), infection with the parasite *Heligmosomoides polygyrus* led to a greater than fivefold increase in peritoneal macrophages in control mice, as the ICAM-2^{+} resident macrophage population associated with Gata6 expression was induced to proliferate during infection (Fig. 1 G). Percentage of cycling macrophages was not significantly affected in Gata6$^{\Delta Mac}$ macrophages compared with controls before or after infection (Fig. 1 G). However, Gata6$^{\Delta Mac}$ macrophage numbers scarcely elevated above baseline numbers observed in uninfected control mice (Fig. 1 G) because of markedly elevated apoptosis (Fig. 1 G). Thus, F4/80^{hi} ICAM-2^{+} resident peritoneal macrophages survival was selectively impaired in resting and parasite-challenged Gata6$^{\Delta Mac}$ mice.

After flow cytometric cell sorting and gene expression analysis using whole mouse genome arrays, we found that notably elevated mRNA transcripts in Gata6$^{\Delta Mac}$ macrophages were those associated with alternative activation (Gordon and Martinez, 2010) of macrophages, including mRNA transcripts encoding CD163, LYVE-1, Arg1, Clec10a (CD301), Chi3L3, and CD206 (mannose receptor, Mrc1; Fig. 2 A and Table S1), as well as mRNA for MARCO, which is associated with innate macrophage activation (Mukhopadhyay et al., 2014). Increased cell surface levels of corresponding proteins were accordingly observed (Fig. 2 B). Functional evidence in support of alternative activation included a significant increase in peritoneal eosinophils (Fig. 2 B) associated with type 2 immune responses (Gause et al., 2013), along with expanded resident B1a lymphocytes, whereas T cell counts were unchanged (Fig. 2 C). Infiltrating monocytes and neutrophils were not found, ruling out generalized local inflammation. Gata6$^{\Delta Mac}$ macrophages metabolism was oriented to oxidative phosphorylation, another feature of alternative activation (Vats et al., 2006; Pearce and Pearce, 2013), as observed by increased oxygen consumption rates (OCR; Fig. 2 D). Profiling of metabolic intermediates from sorted control and Gata6$^{\Delta Mac}$ macrophages, respectively, revealed greater ADP (34 ± 3 vs. 58 ± 12 pmol/10^6 cells), citrate or isocitrate (CIT/ICIT; 76 ± 12 vs. 129 ± 46 pm/10^6 cells), NAD^{+} (1.1 ± 0.4 vs. 2.1 ± 0.5 pmol/10^6 cells), and malate (MAL; 120 ± 28 vs. 167 ± 23 pmol/10^6 cells) levels in Gata6$^{\Delta Mac}$ macrophages, with reduced amounts of FAD (6.9 ± 0.4 vs. 5.5 ± 0.5 pmol/10^6 cells), consistent with a more active citric acid cycle (Fig. 2 E).

Deletion of Gata6 correlated with decreased F4/80 expression (Fig. 1 D, events below blue line in Gata6$^{\Delta Mac}$ gate), but a minority of macrophages, i.e., 19.9 ± 10.2% of remaining ICAM-2^{+} macrophages, retained the originally high levels of F4/80 (Fig. 1 D) and only these cells immunostained with Gata6 mAb (Fig. 2 F). Among flow-sorted Gata6$^{\Delta Mac}$ macrophages with higher F4/80, only 26 ± 7% of nuclei had deleted Gata6, whereas 99 ± 0.4% had deleted Gata6 among Gata6$^{\Delta Mac}$ macrophages with reduced F4/80. Thus, the persistence of some resident macrophages that remained Gata6^{+}, clearly demarcated by the same high expression of surface F4/80 as in WT mice, allowed us to address whether alternative activation was confined to macrophages that lost Gata6. Indeed, resident peritoneal macrophages with efficient deletion of Gata6 (F4/80 reduced) expressed higher level of CD206, CD301, and Lyve-1 compared with F4/80^{high} macrophages or macrophages from control mice (Fig. 2 F). However, the population of macrophages that did not delete Gata6 (F4/80^{high}) were those that induced Marco (Fig. 2 F). Macrophages in the splenic red pulp, lung (Fig. 2 G), or brain (not depicted) did not increase alterative activation markers in Gata6$^{\Delta Mac}$ mice. These data, therefore, indicate that deletion of Gata6 renders peritoneal macrophages prone to alternative activation. They may be more sensitive to external stimuli that promote alternative activation or there may be a derepression of an alternative activation program in a cell autonomous manner.

Published July 14, 2014

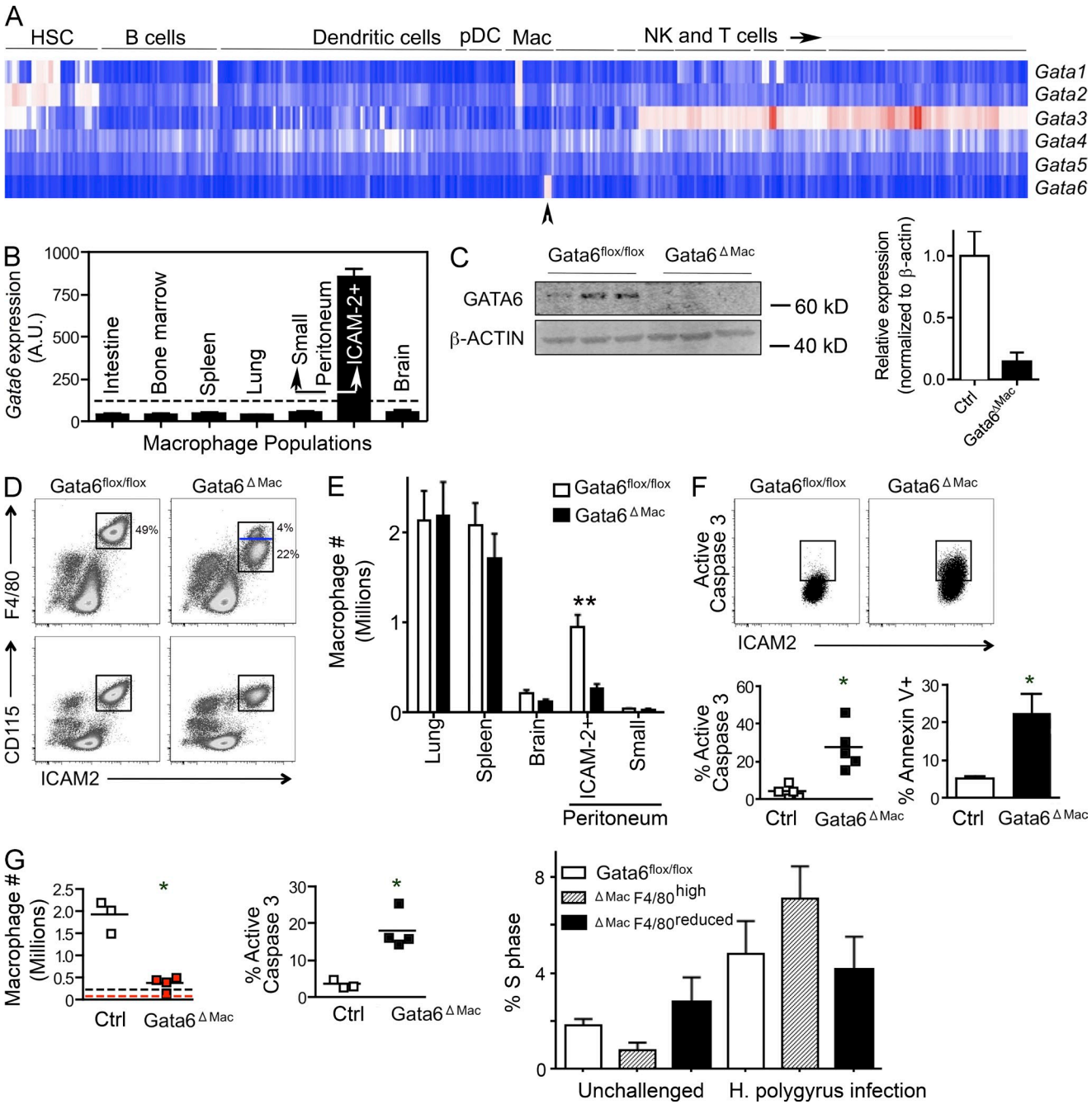

Figure 1. Gata6 deficiency decreases peritoneal macrophage density and induces apoptosis. (A) Expression of mRNA for the GATA family of transcription factors within the resting hematopoietic system profiled by the Immunological Genome Project. Arrowhead points to peritoneal macrophage. (B) Signal intensity of gene expression for Gata6 from array data comparing resident macrophages from multiple organs. Dotted line, cutoff representing positive expression after data normalization. (C) Immunoblot for Gata6 on sorted macrophages, in which all ICAM-2$^+$ macrophages were collected from each genotype. (D) Gata6$^+$ macrophages quantified after cell counts and gating during flow cytometric analysis on cells expressing F4/80, ICAM-2, and CD115. Blue line in gate delineates loss of F4/80 surface intensity in most Gata6$^{\Delta Mac}$ macrophages. (E) Macrophage counts in various organs are plotted. (F) Percent macrophages expressing active caspase 3 or Annexin V. (G) Peritoneal macrophages quantified in mice infected with *H. polygyrus*. Enumeration of these macrophages plotted in control Gata6$^{flox/flox}$ mice (black) or Gata6$^{\Delta Mac}$ mice (red); baselines for each strain shown as dotted line in same color. Percent macrophages positive for active caspase 3 after *H. polygyrus* infection are plotted, and S phase was analyzed in unchallenged and infected mice. Data are derived from 2–8 experiments, with 2–5 replicates per group, performed for each part of the figure. Means ± SEM are shown. *, $P < 0.05$; **, $P < 0.001$ relative to controls using two-tailed Student's *t* tests. Statistical significance in S phase analysis is not depicted, but all S phase analyses are statistically significant (one-way ANOVA) comparing unchallenged control mice to infected mice, $P < 0.05$, but differences between genotypes in the same condition are not significant.

Published July 14, 2014

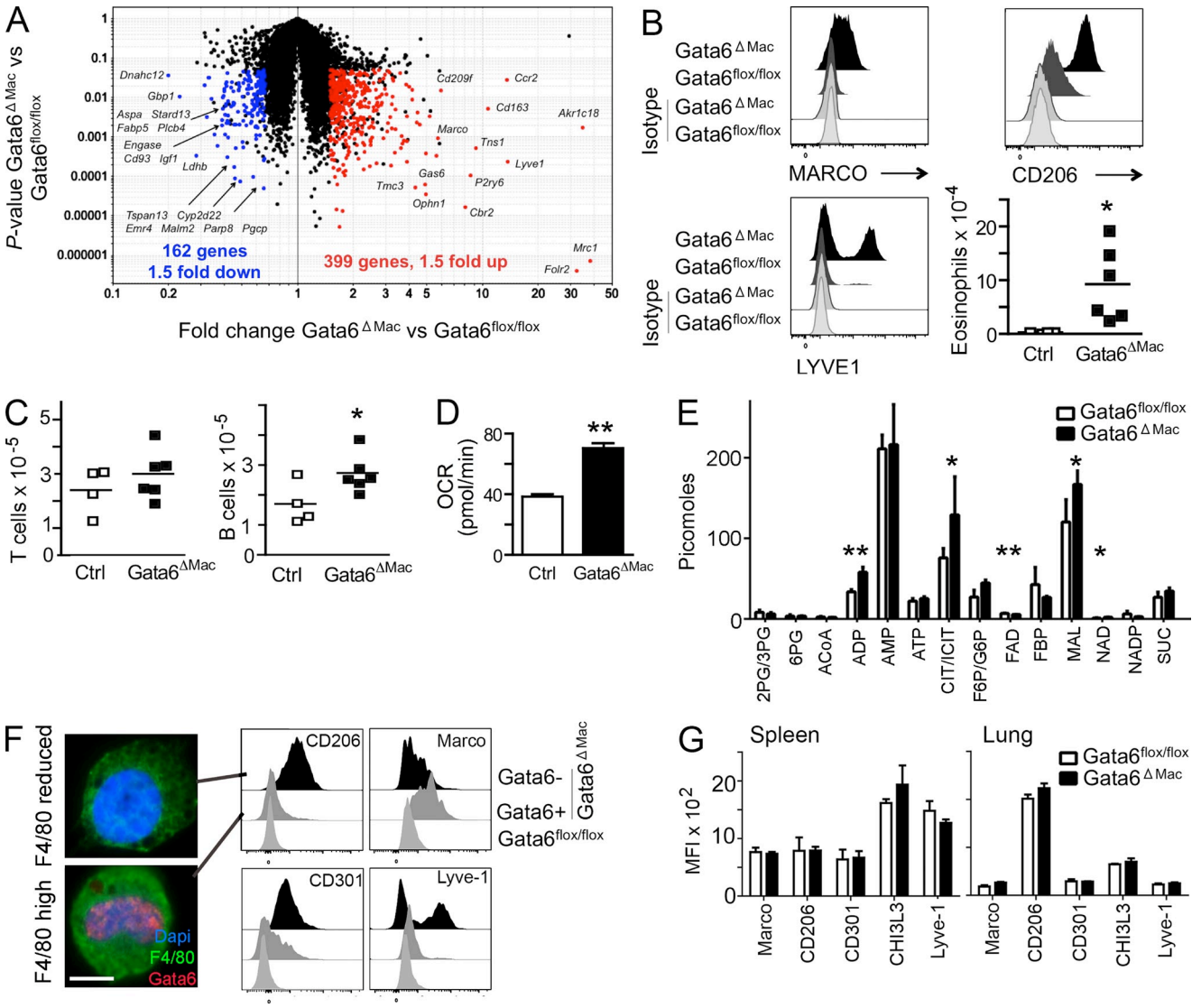

Figure 2. Gene expression changes and alternative activation of Gata6$^{\Delta Mac}$ macrophages. (A) Scatter plots depict mRNA transcripts significantly decreased (left, blue) or increased (right, red) in Gata6$^{flox/flox}$ (Ctrl) versus Gata6$^{\Delta Mac}$ mice. (B) Expression of macrophage polarization and activation markers and eosinophil counts in the peritoneum. (C) Peritoneal B1-a and T lymphocyte counts. (D) Oxygen consumption rates (OCR) of Gata6$^{flox/flox}$ and Gata6$^{\Delta Mac}$ mice. (E) Mass spectrometric analysis of metabolites. (F) As shown in Fig. 1 D (blue line in flow cytometry gate), Gata6$^{\Delta Mac}$ peritoneal macrophages were sorted into two populations based on a retention or reduction of the originally high levels of F4/80, then stained for nuclear Gata6. Bar, 5 µm. Various markers on Gata6$^{flox/flox}$ (light gray histograms) and Gata6$^{\Delta Mac}$ macrophages with preserved expression of Gata6 (Gata6^{+}, from F4/80^{high} gate; gray histograms) and Gata6$^{\Delta Mac}$ with efficient deletion of Gata6 (Gata6^{-} from F4/80^{reduced} gate; black histograms) were compared. (G) Analysis of similar markers on spleen or lung macrophages. Data in the figure summarize results from three or more independent experiments with two to five replicates per experimental group. Metabolic analysis was performed using five separate pools of sorted macrophages for each genotype. *, $P < 0.05$; **, $P < 0.001$ relative to controls, assessed using two-tailed Student's *t* tests.

As mentioned, alternative activation has been linked to changes in cellular metabolic orientation (Vats et al., 2006; Pearce and Pearce, 2013). Furthermore, mRNA transcripts that distinguish peritoneal macrophages from other macrophages were especially those associated with lipid synthesis and signaling (Gautier et al., 2012). Several such transcripts were among those that were confined to modules of genes predicted by the Ontogenet algorithm to be regulated in peritoneal macrophages by Gata6 (Gautier et al., 2012). Most mRNA transcripts that were peritoneal macrophage-specific within these modules were indeed down-regulated in Gata6-deficient macrophages (Fig. 3 A). Others in the same modules not originally identified to be specific for peritoneal macrophages were notably up-regulated, including Arg1, which encodes arginase-1, an enzyme associated with canonical alternative activation (Fig. 3 A). Thus, we examined the expression of genes involved in metabolism and lipid synthesis. Whereas many metabolic genes were up-regulated, Aspa mRNA encoding a key enzyme at an early step in the pathway leading to acetyl CoA synthesis, aspartoacylase, was among the most down-regulated genes (Fig. 3 B).

Published July 14, 2014

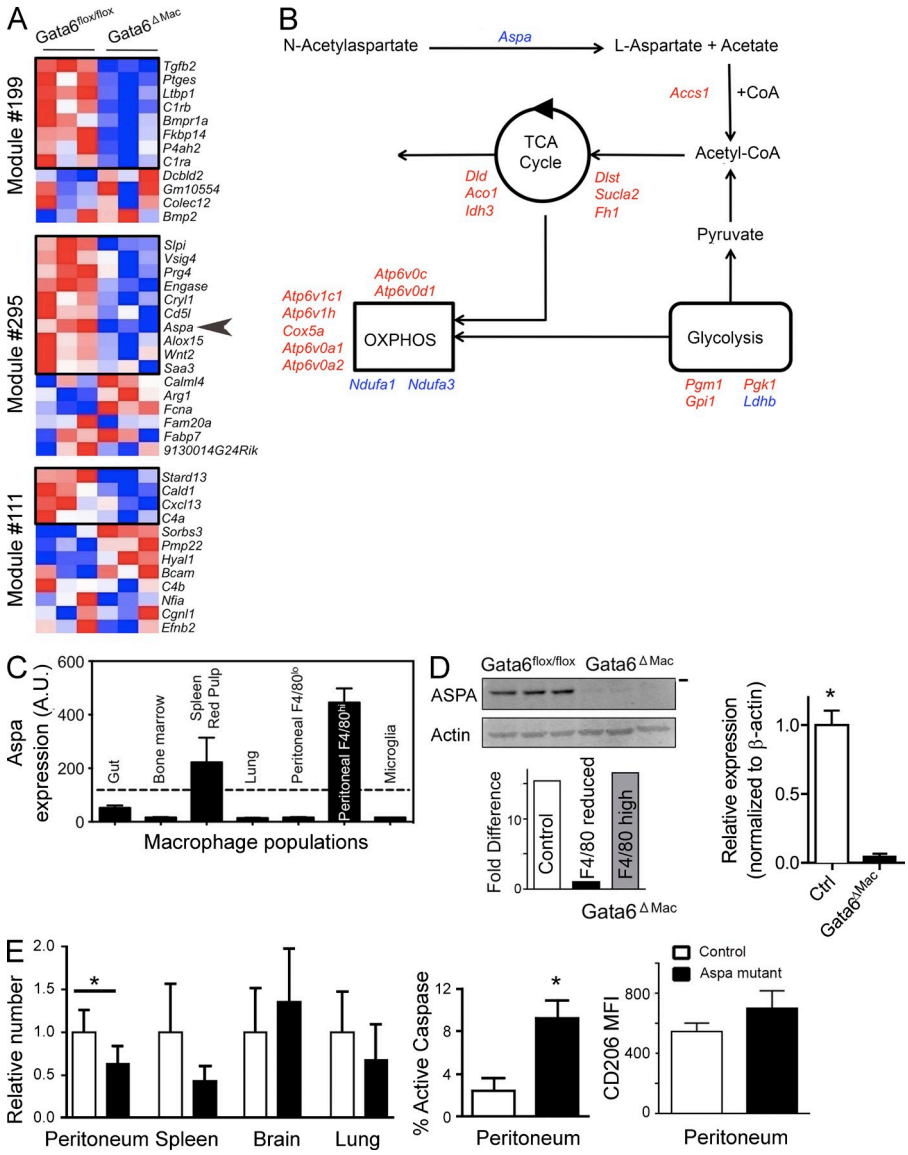

Figure 3. Gata6 regulates aspartylcyclase expression that in turn affects peritoneal macrophage survival. (A) Heat map depicts pattern of expression of mRNA transcripts within modules earlier predicted to be controlled by Gata6. Transcripts within black boxes indicate those that are selectively expressed in peritoneal macrophages relative to other macrophages (Gautier et al., 2012). Arrowhead delineates Aspa. Data are compiled from three independent experiments. (B) Generalized schematic image of metabolic pathways and the expression of various mRNA transcripts in the pathways by Gata6$^{\Delta Mac}$ peritoneal macrophages. Red color depicts mRNA transcripts significantly up-regulated and blue depicts those significantly down-regulated. (C) Signal intensity of gene expression for Aspa from array data comparing resident macrophages from multiple organs. Dotted line, cutoff representing positive expression after data normalization. (D) Immunoblot for aspartoacylase (ASPA) in control Gata6$^{flox/flox}$ versus Gata6$^{\Delta Mac}$ mice. Each lane represents a distinct experiment in which pooled macrophages of the depicted genotype were sorted, with acquisition of all ICAM-2^{+} macrophages sorted from the respective genotypes. Bar on right represents 37-kD molecular weight marker. Real-time quantitative PCR from a single experiment from sorted macrophages pooled from four to seven mice (control vs. Gata6-deficient, respectively) was used; Aspa mRNA transcripts are shown as fold differences between sorted macrophage groups. (E) Macrophage counts in different organs and percent active caspase 3 in control versus Aspa (Nur7) mutant peritoneal macrophages. Far right bar graph shows CD206 MFI in peritoneal macrophages. Two experiments were conducted, with $n = 9–10$ for peritoneal analyses and $n = 4–5$ for other organs. *, $P < 0.05$ relative to control, determined by two-tailed Student's *t* tests.

Furthermore, Aspa mRNA expression was highest in peritoneal macrophages and absent from other hematopoietic cells (http://www.immgen.org), including other macrophages, except for a more modest expression in red pulp macrophages (Fig. 3 C). Aspartoacylase is known to regulate lipid synthesis in the brain, and mutations in Aspa lead to Canavan disease characterized by defective synthesis of myelin (Traka et al., 2008). Its substrate N-acetylaspartate is the second-most abundant metabolite in the brain, being produced by neurons and used by oligodendrocytes to coordinate their differentiation, energy production, and lipid synthesis (Madhavarao and Namboodiri, 2006). We first confirmed that aspartoacylase protein was expressed by control peritoneal macrophages. It was reduced to nearly undetectable levels in Gata6$^{\Delta Mac}$ macrophages (Fig. 3 D), with its mRNA transcript selectively lost in the F4/80^{reduced} population of macrophages that corresponded to those that deleted Gata6 (Fig. 3 D). To test whether loss of Aspa might be relevant to the loss of viable macrophages in the peritoneum, we quantified peritoneal macrophages in Nur7 mutant mice that bear a nonsense mutation in the Aspa (Traka et al., 2008). These mutants showed a 37% reduction in resident peritoneal macrophages (Fig. 3 E), along with enhanced apoptosis indicated by increased active caspase 3 (Fig. 3 E), although the extent of the loss in overall macrophage numbers was not as large as observed in Gata6$^{\Delta Mac}$ macrophages. As the mutant mice lack aspartoacylase wherever it is expressed, we cannot be sure that the increased death of peritoneal macrophages is due to inherent lack of aspartoacylase expression. However, it is interesting to note that Aspa mutant mice trended to reduced red pulp macrophages ($P = 0.06$), whereas macrophages in lung and brain,

Published July 14, 2014

which do not express aspartoacylase, were not significantly decreased. Loss of expression of aspartoacylase did not lead to macrophage polarization, as shown by similar CD206 (Fig. 3 E) and other markers of alternative activation (not depicted) on the cell surface of peritoneal or other macrophages between mutant and control mice. We conclude that deficiency in Aspa increases peritoneal macrophage susceptibility to death, and partially accounts for the loss of peritoneal macrophages in Gata6$^{\Delta Mac}$ mice, but its loss is not sufficient to provoke alternative activation.

In conclusion, Gata6, selectively expressed in peritoneal macrophages, regulates peritoneal macrophage survival under homeostatic conditions. One of the underlying mechanisms supporting survival is the reliance of peritoneal macrophages on the enzyme aspartoacylase, but loss of this enzyme does not explain why surviving Gata6-deficient macrophages polarize themselves to an alternatively activated phenotype, whereas adjacent Gata6^{+} macrophages do not. Additional studies are needed to better understand the intrinsic regulation of polarization and tissue-specific macrophage differentiation. The Gata6-deficient peritoneal macrophage provides a compelling model system for such investigation.

MATERIALS AND METHODS

Mouse strains. Gata6$^{flox/flox}$ mice on a mixed 129S1/SvImJ and CD-1 background were bred with Lyz2-Cre$^{+/-}$ on a C57BL/6 background to yield Cre$^{+/-}$ Gata6$^{\Delta Mac}$ mice and Cre$^{-/-}$ Gata6$^{flox/flox}$ littermate control mice. Nur7 mice bearing mutant Aspa alleles were on a C57BL/6J background and compared with C57BL/6J mice. All experimental procedures were approved by the Animal Studies Committee at Washington University in St. Louis.

Gene expression analysis. RNA was amplified and hybridized on the Affymetrix Mouse Gene 1.0 ST array by the ImmGen Project consortium with double-sorted cell populations sorted directly into TRIzol (Life Technologies). These procedures followed a highly standardized protocol for data generation and documentation of quality control. A table listing QC data, replicate information, and batch information for each sample is also available on the ImmGen Project website. Data were analyzed with the GenePattern genomic analysis platform. Raw data were normalized with the robust multi-array algorithm, returning linear values between 10 and 20,000. A common threshold for positive expression at 95% confidence across the dataset was determined to be 120. Differences in gene expression signatures were identified and visualized with the Multiplot module of GenePattern. Probe sets were considered to have a difference in expression with a coefficient of variation of <0.5 and a p-value of ≥0.05 (Student's *t* test). Data were deposited into the Gene Expression Omnibus database under accession no. GSE37448 as part of the Immgen 2 dataset. Quantitative PCR was performed on ICAM-2^{+} peritoneal macrophages sorted from Gata6flox/flox or Gata6$^{\Delta Mac}$ mice in which F4/80^{high} and F4/80^{reduced} macrophages were distinctly sorted. 5′-TCCAAGGAATGAAAGTGGAGA-3′ was the sequence of the forward primer and 5′-TGCAATGGTTTCCAGTCTTG-3′ was the reverse primer.

Peritoneal macrophage quantification and characterization. Two methods were used to quantify peritoneal macrophages. Total peritoneal cells were counted in a hemacytometer or using an automated cell counter. Then this number was multiplied by the percent of macrophages stained for CD115 (AFS98; eBioscience), ICAM-2 (3C4; BioLegend) and F4/80 (BM8, eBioscience) by flow cytometry. These antibodies allow us to distinguish the minor and major peritoneal macrophage populations (Gautier et al., 2012), with only the major macrophage population expressing ICAM-2 (Gautier et al., 2012). Alternatively, peritoneal cells obtained by lavage were incubated with FITC-conjugated anti–ICAM-2 mAb, and then a manual count of the fraction of ICAM-2^{+} cells was made and multiplied by the total number of peritoneal cells. Both methods yielded similar results. Other reagents and mAbs used in flow cytometry were Annexin V (Miltenyi Biotec) and antibodies against Ki67 (B56; BD), active caspase 3 (C92-605; BD), pH3 (D2C8; Cell Signaling technology), TIMD4 (RMT4-54; eBioscience), CD206 (MR5D3; Serotec), LYVE-1 (Abcam), Siglec F (E50-2440; BD), CD11b (M1/70; eBioscience), CD5 (53–7.3; BD), B220 (RA3-6B2; eBioscience), ly 6C/G (RB6-8C5; eBioscience), Ly6-G (1A8; BD), TCRb (H57-597; eBioscience), MHC-II (M5/114.15.2; eBioscience), and MARCO (ED31; Serotec).

***H. polygyrus* infection.** Mice were infected orally with 200 infectious larvae of *H. polygyrus* and euthanized 8 d later for collection of peritoneal lavage and enumeration of macrophages.

Cell cycle analysis. Propidium iodide staining was used to analyze the cell cycle in peritoneal macrophages. A barcoding approach was used. Peritoneal cells stained for PE-conjugated CD11b were mixed 9:1 with a second collection of peritoneal cells from the same mouse separately stained with FITC-conjugated ICAM-2. Statistically doublets or larger aggregates could be CD11b^{+} ICAM-2^{-} or CD11b^{+} ICAM-2^{+}, but doublets that were ICAM-2^{+} CD11b^{-} would be a vast minority of doublets. Thus, ICAM-2^{+} CD11b^{-} macrophages from the mixture were gated and propidium iodide intensity was plotted on a linear scale.

Immunoblots. FACS-sorted cells were homogenized in lysis buffer containing protease inhibitors. Protein extracts were run on Criterion gels (Bio-Rad Laboratories) and blotted onto nitrocellulose membranes. After blocking, immunoblots were incubated with primary Abs against Gata6 (D61E4; Cell Signaling Technology) or aspartoacylase (GeneTex) and β-actin (Cell Signaling Technology). Blots were then incubated with fluorescent secondary Abs and proteins were detected using the fluorescence-based Odyssey Infrared Imaging System (LI-COR Biosciences).

Metabolomics. FACS-sorted macrophages (10^6 cells) were pelleted and rapidly washed (<10 s) with a mass spectrometry–compatible buffer (150 mM ammonium acetate solution) to prevent the presence of sodium and phosphate in the residue and limit interference with LC-MS analyses. After a second step of centrifugation, dry pellets were immediately frozen in liquid nitrogen to quench metabolism according to the University of Michigan Molecular Phenotyping Core facility's instructions. Samples were shipped on dry ice to the Molecular Phenotyping Core facility where metabolites were extracted by exposing the cells to a chilled mixture of 80% methanol, 10% chloroform, and 10% water. Glycolytic and citric acid metabolites were then analyzed by the Molecular Phenotyping Core facility using LC-MS.

Statistical analysis. The statistical significance of differences in mean values was analyzed with the unpaired, two-tailed Student's *t* test or ANOVA for multiple comparisons. P values < 0.05 were considered statistically significant. Errors shown in bar graphs and mentioned in text refer to standard deviations.

Supplemental material. Table S1 summarizes up-regulated mRNA transcripts in Gata6$^{\Delta Mac}$ macrophages compared to Gata6$^{flox/flox}$ macrophages. Table S2 summarizes down-regulated mRNA transcripts in Gata6$^{\Delta Mac}$ macrophages compared to Gata6$^{flox/flox}$ macrophages. Online supplemental material is available at http://www.jem.org/cgi/content/full/jem.20140570/DC1.

This work was supported by National Institutes of Health grant AI049653 to G. J. R. and utilized Core Services supported by a National Institutes of Health (NIH) grant (DK089503) to the University of Michigan. J.W.W. was supported by NIH training grant (T32DK007296).

The authors have no competing financial interests related to this work.

Submitted: 25 March 2014
Accepted: 24 June 2014

Published July 14, 2014

REFERENCES

Clausen, B.E., C. Burkhardt, W. Reith, R. Renkawitz, and I. Förster. 1999. Conditional gene targeting in macrophages and granulocytes using LysMcre mice. *Transgenic Res.* 8:265–277. http://dx.doi.org/10.1023/A:1008942828960

Davies, L.C., S.J. Jenkins, J.E. Allen, and P.R. Taylor. 2013. Tissue-resident macrophages. *Nat. Immunol.* 14:986–995. http://dx.doi.org/10.1038/ni.2705

Gause, W.C., T.A. Wynn, and J.E. Allen. 2013. Type 2 immunity and wound healing: evolutionary refinement of adaptive immunity by helminths. *Nat. Rev. Immunol.* 13:607–614. http://dx.doi.org/10.1038/nri3476

Gautier, E.L., T. Shay, J. Miller, M. Greter, C. Jakubzick, S. Ivanov, J. Helft, A. Chow, K.G. Elpek, S. Gordonov, et al. Immunological Genome Consortium. 2012. Gene-expression profiles and transcriptional regulatory pathways that underlie the identity and diversity of mouse tissue macrophages. *Nat. Immunol.* 13:1118–1128. http://dx.doi.org/10.1038/ni.2419

Gautier, E.L., S. Ivanov, P. Lesnik, and G.J. Randolph. 2013. Local apoptosis mediates clearance of macrophages from resolving inflammation in mice. *Blood.* 122:2714–2722. http://dx.doi.org/10.1182/blood-2013-01-478206

Gordon, S., and F.O. Martinez. 2010. Alternative activation of macrophages: mechanism and functions. *Immunity.* 32:593–604. http://dx.doi.org/10.1016/j.immuni.2010.05.007

Haldar, M., M. Kohyama, A.Y. So, W. Kc, X. Wu, C.G. Briseño, A.T. Satpathy, N.M. Kretzer, H. Arase, N.S. Rajasekaran, et al. 2014. Heme-mediated SPI-C induction promotes monocyte differentiation into iron-recycling macrophages. *Cell.* 156:1223–1234. http://dx.doi.org/10.1016/j.cell.2014.01.069

Hashimoto, D., A. Chow, C. Noizat, P. Teo, M.B. Beasley, M. Leboeuf, C.D. Becker, P. See, J. Price, D. Lucas, et al. 2013. Tissue-resident macrophages self-maintain locally throughout adult life with minimal contribution from circulating monocytes. *Immunity.* 38:792–804. http://dx.doi.org/10.1016/j.immuni.2013.04.004

Jenkins, S.J., D. Ruckerl, G.D. Thomas, J.P. Hewitson, S. Duncan, F. Brombacher, R.M. Maizels, D.A. Hume, and J.E. Allen. 2013. IL-4 directly signals tissue-resident macrophages to proliferate beyond homeostatic levels controlled by CSF-1. *J. Exp. Med.* 210:2477–2491. http://dx.doi.org/10.1084/jem.20121999

Kohyama, M., W. Ise, B.T. Edelson, P.R. Wilker, K. Hildner, C. Mejia, W.A. Frazier, T.L. Murphy, and K.M. Murphy. 2009. Role for Spi-C in the development of red pulp macrophages and splenic iron homeostasis. *Nature.* 457:318–321. http://dx.doi.org/10.1038/nature07472

Madhavarao, C.N., and A.M. Namboodiri. 2006. NAA synthesis and functional roles. *Adv. Exp. Med. Biol.* 576:49–66, discussion :361–363. http://dx.doi.org/10.1007/0-387-30172-0_4

Mukhopadhyay, S., A.S. Ramadass, A. Akoulitchev, and S. Gordon. 2014. Formation of distinct chromatin conformation signatures epigenetically regulate macrophage activation. *Int. Immunopharmacol.* 18:7–11. http://dx.doi.org/10.1016/j.intimp.2013.10.024

Okabe, Y., and R. Medzhitov. 2014. Tissue-specific signals control reversible program of localization and functional polarization of macrophages. *Cell.* 157:832–844. http://dx.doi.org/10.1016/j.cell.2014.04.016

Pearce, E.L., and E.J. Pearce. 2013. Metabolic pathways in immune cell activation and quiescence. *Immunity.* 38:633–643. http://dx.doi.org/10.1016/j.immuni.2013.04.005

Rosas, M., L.C. Davies, P.J. Giles, C.T. Liao, B. Kharfan, T.C. Stone, V.B. O'Donnell, D.J. Fraser, S.A. Jones, and P.R. Taylor. 2014. The transcription factor Gata6 links tissue macrophage phenotype and proliferative renewal. *Science.* 344:645–648. http://dx.doi.org/10.1126/science.1251414

Schulz, C., E. Gomez Perdiguero, L. Chorro, H. Szabo-Rogers, N. Cagnard, K. Kierdorf, M. Prinz, B. Wu, S.E. Jacobsen, J.W. Pollard, et al. 2012. A lineage of myeloid cells independent of Myb and hematopoietic stem cells. *Science.* 336:86–90. http://dx.doi.org/10.1126/science.1219179

Sodhi, C.P., J. Li, and S.A. Duncan. 2006. Generation of mice harbouring a conditional loss-of-function allele of Gata6. *BMC Dev. Biol.* 6:19. http://dx.doi.org/10.1186/1471-213X-6-19

Traka, M., R.L. Wollmann, S.R. Cerda, J. Dugas, B.A. Barres, and B. Popko. 2008. Nur7 is a nonsense mutation in the mouse aspartoacylase gene that causes spongy degeneration of the CNS. *J. Neurosci.* 28:11537–11549. http://dx.doi.org/10.1523/JNEUROSCI.1490-08.2008

Vats, D., L. Mukundan, J.I. Odegaard, L. Zhang, K.L. Smith, C.R. Morel, R.A. Wagner, D.R. Greaves, P.J. Murray, and A. Chawla. 2006. Oxidative metabolism and PGC-1beta attenuate macrophage-mediated inflammation. *Cell Metab.* 4:13–24. http://dx.doi.org/10.1016/j.cmet.2006.05.011

Yona, S., K.W. Kim, Y. Wolf, A. Mildner, D. Varol, M. Breker, D. Strauss-Ayali, S. Viukov, M. Guilliams, A. Misharin, et al. 2013. Fate mapping reveals origins and dynamics of monocytes and tissue macrophages under homeostasis. *Immunity.* 38:79–91. http://dx.doi.org/10.1016/j.immuni.2012.12.001